

BASIC COASTAL ENGINEERING

BASIC COASTAL ENGINEERING

Third Edition

ROBERT M. SORENSEN

*Department of Civil and
Environmental Engineering
Lehigh University, Bethlehem, Pennsylvania*



Springer

Library of Congress Cataloging-in-Publication Data

A C.I.P. Catalogue record for this book is available
from the Library of Congress

ISBN-10: 0-387-23332-6
ISBN-13: 9780387233321

ISBN-10: 0-387-23333-4 (e-book)
ISBN-13: 978038723338

Printed on acid-free paper.

©2006 Springer Science+Business Media, Inc.

All rights reserved. This work may not be translated or copied in whole or in part without the written permission of the publisher (Springer Science+Business Media, Inc. 233 Spring Street, New York, NY 10013, USA), except for brief excerpts in connection with reviews or scholarly analysis. Use in connection with any form of information storage and retrieval, electronic adaptation, computer software, or by similar or dissimilar methodology now known or hereafter developed is forbidden. The use in this publication of trade names, trademarks, service marks and similar terms, even if they are not identified as such, is not to be taken as an expression of opinion as to whether or not they are subject to proprietary rights.

Printed in the United States of America

10 9 8 7 6 5 4 3 2 1 (SPI/SBA)

springeronline.com

To
Rita, Jon, Jenny,
Mark, and John
With Love

Contents

Preface	xi
1. Coastal Engineering	1
1.1 The Coastal Environment	1
1.2 Coastal Engineering	3
1.3 Recent Trends	5
1.4 Coastal Engineering Literature	6
1.5 Summary	8
1.6 References	8
2. Two-Dimensional Wave Equations and Wave Characteristics	9
2.1 Surface Gravity Waves	9
2.2 Small-Amplitude Wave Theory	10
2.3 Wave Classification	15
2.4 Wave Kinematics and Pressure	18
2.5 Energy, Power, and Group Celerity	22
2.6 Radiation Stress and Wave Setup	30
2.7 Standing Waves, Wave Reflection	35
2.8 Wave Profile Asymmetry and Breaking	38
2.9 Wave Runup	44
2.10 Summary	47
2.11 References	48
2.12 Problems	49
3. Finite-Amplitude Waves	53
3.1 Finite-Amplitude Wave Theory Formulation	53
3.2 Stokes Waves	54
3.3 Cnoidal Waves	61
3.4 Solitary Waves	64
3.5 Stream Function Numerical Waves	68
3.6 Wave Theory Application	70
3.7 Summary	74
3.8 References	74
3.9 Problems	76
4. Wave Refraction, Diffraction, and Reflection	79
4.1 Three-Dimensional Wave Transformation	79
4.2 Wave Refraction	80

4.3	Manual Construction of Refraction Diagrams	82
4.4	Numerical Refraction Analysis	89
4.5	Refraction by Currents	91
4.6	Wave Diffraction	92
4.7	Combined Refraction and Diffraction	99
4.8	Wave Reflection	101
4.9	Vessel-Generated Waves	102
4.10	Summary	105
4.11	References	105
4.12	Problems	108
5.	Coastal Water Level Fluctuations	113
5.1	Long Wave Equations	114
5.2	Astronomical Tide Generation and Characteristics	117
5.3	Tide Datums and Tide Prediction	120
5.4	Tsunamis	124
5.5	Basin Oscillations	127
5.6	Resonant Motion in Two- and Three-Dimensional Basins	130
5.7	Resonance Analysis for Complex Basins	137
5.8	Storm Surge and Design Storms	138
5.9	Numerical Analysis of Storm Surge	141
5.10	Simplified Analysis of Storm Surge	144
5.11	Long-Term Sea Level Change	150
5.12	Summary	151
5.13	References	151
5.14	Problems	154
6.	Wind-Generated Waves	157
6.1	Waves at Sea	157
6.2	Wind-Wave Generation and Decay	158
6.3	Wave Record Analysis for Height and Period	161
6.4	Wave Spectral Characteristics	167
6.5	Wave Spectral Models	169
6.6	Wave Prediction—Early Methods	178
6.7	Wave Prediction—Spectral Models	183
6.8	Numerical Wave Prediction Models	185
6.9	Extreme Wave Analysis	187
6.10	Summary	190
6.11	References	190
6.12	Problems	193
7.	Coastal Structures	195
7.1	Hydrodynamic Forces in Unsteady Flow	196
7.2	Piles, Pipelines, and Cables	198

7.3	Large Submerged Structures	209
7.4	Floating Breakwaters	211
7.5	Rubble Mound Structures	214
7.6	Rigid Vertical-Faced Structures	227
7.7	Other Loadings on Coastal Structures	233
7.8	Wave–Structure Interaction	235
7.9	Selection of Design Waves	238
7.10	Summary	241
7.11	References	241
7.12	Problems	245
8.	Coastal Zone Processes	247
8.1	Beach Sediment Properties and Analysis	248
8.2	Beach Profiles and Profile Change	252
8.3	Nearshore Circulation	258
8.4	Alongshore Sediment Transport Processes and Rates	261
8.5	Shore Response to Coastal Structures	265
8.6	Numerical Models of Shoreline Change	269
8.7	Beach Nourishment and Sediment Bypassing	271
8.8	Wind Transport and Dune Stabilization	276
8.9	Sediment Budget Concept and Analysis	277
8.10	Coastal Entrances	280
8.11	Summary	282
8.12	References	282
8.13	Problems	285
9.	Field and Laboratory Investigations	287
9.1	Field Investigations	288
9.2	Wind-Wave Measurements	288
9.3	Other Hydrodynamic Measurements	291
9.4	Coastal Morphology and Sedimentary Processes	293
9.5	Coastal Structures	298
9.6	Laboratory Investigations	299
9.7	Wave Investigation Facilities	300
9.8	Scaling of Laboratory Investigations	302
9.9	Common Types of Investigations	304
9.10	Summary	305
9.11	References	305
	Appendices	309
A.	Notation and Dimensions	309
B.	Selected Conversion Factors	314
C.	Glossary of Selected Terms	315
	Index	321

Preface

The second edition (1997) of this text was a completely rewritten version of the original text *Basic Coastal Engineering* published in 1978. This third edition makes several corrections, improvements and additions to the second edition.

Basic Coastal Engineering is an introductory text on wave mechanics and coastal processes along with fundamentals that underline the practice of coastal engineering. This book was written for a senior or first postgraduate course in coastal engineering. It is also suitable for self study by anyone having a basic engineering or physical science background. The level of coverage does not require a math or fluid mechanics background beyond that presented in a typical undergraduate civil or mechanical engineering curriculum. The material presented in this text is based on the author's lecture notes from a one-semester course at Virginia Polytechnic Institute, Texas A&M University, and George Washington University, and a senior elective course at Lehigh University. The text contains examples to demonstrate the various analysis techniques that are presented and each chapter (except the first and last) has a collection of problems for the reader to solve that further demonstrate and expand upon the text material.

Chapter 1 briefly describes the coastal environment and introduces the relatively new field of coastal engineering. Chapter 2 describes the two-dimensional characteristics of surface waves and presents the small-amplitude wave theory to support this description. The third chapter presents the more complex nonlinear wave theories for two-dimensional waves, but only selected aspects of those theories that are most likely to be of interest to practicing coastal engineers. Wave refraction, diffraction, and reflection—the phenomena that control the three-dimensional transformation of waves as they approach the shore—are presented in Chapter 4. Besides the most common shorter period waves that have periods in the range generated by the wind, there are longer period coastal water level fluctuations that are important to coastal engineers. They are presented in Chapter 5.

Chapters 2 to 4 consider monochromatic waves—which are important for the analysis of both wind-generated waves and many of the longer period water level fluctuations. Chapter 6 then presents the behavior, analysis, and prediction of the more complex wind-generated waves—the “real” waves that confront the practicing coastal engineer.

The material presented in the first six chapters covers the primary controlling environmental factors for coastal engineering analysis and design. The next two

chapters—which deal with coastal structures and shoreline processes—are concerned with the effects of wave action on the shore and engineering responses to these effects. Chapter 7 focuses on determination of wave forces on coastal structures and related coastal structure stability requirements, as well as the interaction of waves with coastal structures and establishment of design wave conditions for coastal structures. Chapter 8 covers beach characteristics, their response to wave action, and the interaction of beach processes and coastal structures, as well as the design of stable beaches. The last chapter gives an overview of the types of field and laboratory investigations typically carried out to support coastal engineering analysis and design. Finally, there is an appendix that provides a tabulation of the notation used in the text, conversion factors for common dimensions used in the text, and a glossary of selected coastal engineering terms.

I wish to acknowledge the support provided by Mrs. Cathy Miller, who typed all of the equations in the original manuscript and Mrs. Sharon Balogh, who drafted the figures. I am indebted to the late J.W. Johnson and R.L. Wiegel, Emeritus Professors at the University of California at Berkeley, who introduced me to the subject of coastal engineering.

R.M. Sorensen
Lehigh University

BASIC COASTAL ENGINEERING

1

Coastal Engineering

The competent coastal engineer must develop a basic understanding of the characteristics and physical behavior of the coastal environment, as well as be able to apply engineering principles and concepts to developing opportunities and solving problems in this environment. Consequently, this book provides an introduction to those physical processes that are important in the coastal zone. It also introduces the analytical basis for and application of those methods required to support coastal engineering and design.

1.1 The Coastal Environment

We define the shoreline as the boundary between the land surface and the surface of a water body such as an ocean, sea, or lake. The coastal zone is that area of land and water that borders the shoreline and extends sufficiently landward and seaward to encompass the areas where processes important to the shore area are active.

The land portion of most of the world's coastal zone consists of sandy beaches. In some places the beach is covered with coarser stones known as shingle. Where wave and current action is relatively mild and a river provides large deposits of sediment a delta may form and extend seaward of the general trend of the shoreline. In some places there is a break in the shoreline to produce an estuary or inlet to a back bay area—the estuary or inlet being maintained by river and/or tide-induced flow. Also, some coasts may be fronted by steep cliffs that may or may not have a small beach at their toe. Since sandy beaches predominate and have very dynamic and interesting characteristics, this type of coastline will receive the greatest emphasis herein.

Waves are the dominant active phenomenon in the coastal zone. Most apparent and significant are the waves generated by the wind. Second in importance is the astronomical tide, which is a wave generated by the gravitational attraction of the sun and moon. Other waves, which on the whole are less important but

that may have important consequences in some places, are seismically generated surface waves (tsunamis) and waves generated by moving vessels.

The wind and related atmospheric pressure gradient will generate a storm surge—the piling up of water along the coast when the wind blows in an onshore direction. This raised water level can cause damage by flooding and it allows waves to attack the coast further inland. The wind will generate currents that move along the coast. Coastal currents are also generated by the tide as it propagates along the coast and alternately floods and ebbs through an inlet or into an estuary. Further, the wind has direct consequences on the shore by moving sand and causing structural damage.

Wind wave action causes the most significant changes to a beach. The shore-normal beach profile changes as sand is carried offshore and back onshore over a period of time. In many locations large volumes of sand are also carried along the shore by the action of waves that obliquely approach the shore. Current effects often dominate at the entrances to bays and estuaries where higher flow velocities develop.

When structures are built along the coast their design must anticipate the effects of this dynamic wave and beach environment. This is important insofar as the structures must remain stable and must not cause undesirable sand accumulation or erosion by interfering with on/offshore and alongshore sediment transport processes.

Understanding and being able to manage the coastal environment is of critical importance. About two-thirds of the world's population lives on or near the coast, and many others visit the coast periodically. This creates strong pressure for shore development for housing and recreation and for shore protection from storm-induced damage. Shore protection and stabilization problems often require regional solutions rather than a response by a single or small number of property owners. Much of our commerce is carried by ships that must cross the coastline to enter and exit ports. This requires the stabilization, maintenance, and protection of coastal navigation channels. Coastal waters are also used for power plant cooling water and as a receptacle for treated and untreated liquid wastes.

The importance of the coastal environment is demonstrated by events at Miami Beach, Florida. In the early 1970s the beach at Miami Beach was in poor shape—a narrow beach that was not very useful for recreation or effective for storm surge protection. In the late 1970s about 15 million cubic yards of sand were placed on the beach. Estimated annual beach attendance increased from 8 million in 1978 to 21 million in 1983 (Wiegel, 1992). This was twice the annual number of tourists who visited Yellowstone Park, the Grand Canyon, and Yosemite Park combined (Houston, 1995). Foreign visitors alone now spend more than 2 billion dollars a year at Miami Beach, largely because of the improved beach conditions. The expanded beach also has value because of the protection provided from potential storm surge and wave damage to the coast. The capitalized cost of the project is just 3 million dollars per year (Houston, 1995).

1.2 Coastal Engineering

Attempts to solve some coastal zone problems such as beach erosion and the functional and structural design of harbors date back many centuries. Bruun (1972) discusses early coastal erosion and flooding control activities in Holland, England, and Denmark in a review of coastal defense works as they have developed since the tenth century. Inman (1974), from a study of early harbors around the Mediterranean Sea, found that harbors demonstrating a “very superior ‘lay’ understanding of waves and currents, which led to development of remarkable concepts in working with natural forces” were constructed as early as 1000–2000 B.C.

Coastal works have historically been the concern of civil and military engineers. The term “coastal engineer” seems to have come into general use as a designation for a definable engineering field in 1950, with the meeting of the First Conference on Coastal Engineering in Long Beach, California. In the preface to the proceedings of that conference M.P. O’Brien wrote, “It (coastal engineering) is not a new or separate branch of engineering and there is no implication intended that a new breed of engineer, and a new society, is in the making. Coastal Engineering is primarily a branch of Civil Engineering which leans heavily on the sciences of oceanography, meteorology, fluid mechanics, electronics, structural mechanics, and others.” Among the others one could include geology and geomorphology, numerical and statistical analysis, chemistry, and material science.

This definition is still essentially correct. However, coastal engineering has dramatically grown in the past few decades. The Proceedings of the First Conference on Coastal Engineering contained 35 papers; the Proceedings of the 28th International Conference on Coastal Engineering held in 2002 contained 322 papers selected from over 600 abstracts presented to the conference. In addition to the biannual International Conferences on Coastal Engineering there are several specialty conferences held each year dealing with such subjects as ports, dredging, coastal sediment, the coastal zone, coastal structures, wave measurement and analysis, and coastal and port engineering in developing countries. The American Society of Civil Engineers has a Waterway, Port, Coastal, and Ocean Division which, along with magazines titled *Coastal Engineering* and *Shore and Beach* publish papers on all aspects of coastal engineering. In addition, a growing number of general and specialized textbooks on coastal engineering have been published.

Areas of concern to coastal engineers are demonstrated by the following list of typical coastal engineering activities:

- Development (through measurement and hindcasts) of nearshore wave, current, and water level design conditions

- Design of a variety of stable, effective, and economic coastal structures including breakwaters, jetties, groins, revetments, seawalls, piers, offshore towers, and marine pipelines
- Control of beach erosion by the design of coastal structures and/or by the artificial nourishment of beaches
- Stabilization of entrances for navigation and water exchange by dredging, construction of structures, and the mechanical bypassing of sediment trapped at the entrances
- Prediction of inlet and estuary currents and water levels and their effect on channel stability and water quality
- Development of works to protect coastal areas from inundation by storm surge and tsunamis
- Functional and structural design of harbors and marinas and their appurtenances including quays, bulkheads, dolphins, piers, and mooring systems
- Functional and structural design of offshore islands and dredge spoil disposal areas
- Monitoring various coastal projects through a variety of measurements in the field.

A major source of support for coastal engineers is the available literature on past coastal engineering works along with the design guidance published in textbooks; manuals from government agencies; and special studies conducted by university, government, and consulting firm personnel. Additional design tools generally fall into one of the following categories:

- Many aspects of coastal engineering analysis and design have a strong analytical foundation. This includes theories for the prediction of individual wave characteristics and the properties of wave spectra, for the calculation of wave-induced forces on structures, for the effect of structures on wave propagation, and for the prediction of tide-induced currents and water level changes.
- Many coastal engineering laboratories have two- and three-dimensional flumes in which monochromatic and spectral waves can be generated to study fundamental phenomena as well as the effects of waves in models of prototype situations. Examples of model studies include wave propagation toward the shore and into harbors, the stability of structures subjected to wave attack and the amount of wave overtopping and transmission that occurs at these structures, the response of beaches to wave attack, and the stability and morphological changes at coastal inlets owing to tidal flow and waves.

- Various computer models that numerically solve the basic wave, flow, and sediment transport equations have been developed. These include models for wind wave prediction, for the analysis of wave transformation from deep water to the nearshore zone, for the surge levels caused by hurricanes and other storms, for the resonant response of harbors and other water bodies to long period wave motion, and for the sediment transport and resulting shoreline change caused by a given set of incident wave conditions.
- An invaluable tool for coastal engineers is the collection of data in the field. This includes measurements of wave conditions, current patterns, water levels, shore plan and profile changes, and wave-induced damage to structures. There is a great need for more postconstruction monitoring of the performance of most types of coastal works. In addition, laboratory and numerical models require prototype data so that the models can be adequately calibrated and verified.

The wind wave and surge levels that most coastal works are ultimately exposed to are usually quite extreme. It is generally not economical to design for these conditions. The design often proceeds for some lesser wave and surge condition with the understanding that the structures will be repaired as needed.

Compared to most other areas of civil engineering (e.g., bridges, highways, water treatment facilities), coastal engineering design is less controlled by code requirements. This is because of the less predictable nature of the marine environment and the relative lack of an extensive experience base required to establish codes.

1.3 Recent Trends

Some of the recent important trends in coastal engineering practice should be noted.

With the explosion in the capabilities of computers there has been a parallel explosion in the types and sophistication of numerical models for analysis of coastal phenomena. In many, but not all, areas numerical models are supplementing and replacing physical models. Some areas such as storm surge prediction can be effectively handled only by a numerical model. On the other hand, some problems such as wave runup and overtopping of coastal structures or the stability of stone mound structures to wave attack are best handled in the laboratory.

There is a trend toward softer and less obtrusive coastal structures. For example, offshore breakwaters for shore protection and stabilization more commonly have their crest positioned just below the mean water level, where they still have an ability to control incident wave action but where they also have less

negative aesthetic impact. In some coastal areas coastal structures are discouraged.

There has been a significant increase in the capability and availability of instrumentation for field measurements. For example, three decades ago wave gages commonly measured only the water surface fluctuation at a point (i.e., the different directional components of the incident wave spectrum were not measured). Now directional spectral wave gages are commonly used in field studies.

Wave generation capabilities in laboratories have significantly improved. Prior to the 1960s only constant period and height (monochromatic) waves were generated. In the 1970s one-dimensional spectral wave generators became common-place. Now directional spectral wave generators are found at many laboratories.

1.4 Coastal Engineering Literature

This text presents an introduction to coastal engineering; it is not a coastal engineering design manual. For practical design guidance the reader should see, for example, the design manuals published by the U.S. Army Corps of Engineers including the Coastal Engineering Manual and the various Engineering Manuals dealing with coastal engineering topics.

A good source of detailed information on the various subjects encompassed by coastal engineering is the broad range of reports published by many government laboratories including the U.S. Army Coastal and Hydraulics Laboratory, the Delft Hydraulics Laboratory (Netherlands), Hydraulics Research Limited (Wallingford, England), the Danish Hydraulic Institute (Horsholm), and the National Research Council (Ottawa, Canada). Several universities conduct coastal engineering studies and publish reports on this work.

As mentioned previously, there are many general and specialty conferences dealing with various aspects of coastal engineering. The published proceedings of these conferences are an important source of information on the basic and applied aspects of coastal engineering.

Many senior coastal engineers were introduced to coastal engineering by two texts published in the 1960s: *Oceanographical Engineering* by R.L. Wiegel (Prentice-Hall, Englewood Cliffs, NJ, 1964) and *Estuary and Coastline Hydrodynamics* edited by A.T. Ippen (McGraw-Hill, New York, 1966). Since the 1960s a number of texts on coastal engineering or a specific facet of coastal engineering have been published. A selective list of these texts follows:

Abbott, M. B. and Price, W.A., Editors (1994), *Coastal, Estuarial and Harbor Engineers' Reference Book*, E & FN Spon, London.

- Bruun, P., Editor (1985), *Design and Construction of Mounds for Breakwaters and Coastal Protection*, Elsevier, Amsterdam.
- Bruun, P. (1989), *Port Engineering*, Fourth Edition, 2 Vols., Gulf Publishing, Houston.
- Dean, R.G. and Dalrymple, R.A. (1984), *Water Wave Mechanics for Engineers and Scientists*, Prentice-Hall, Englewood Cliffs, NJ.
- Dean, R.G. and Dalrymple, R.A. (2002), *Coastal Processes with Engineering Applications*, Cambridge University Press, Cambridge.
- Dean, R.G. (2003) *Beach Nourishment: Theory and Practice*, World Scientific, Singapore.
- Fredsoé, J. and Deigaard, R. (1992), *Mechanics of Coastal Sediment Transport*, World Scientific, Singapore.
- Goda, Y. (1985), *Random Seas and Design of Maritime Structures*, University of Tokyo Press, Tokyo.
- Herbich, J.B., Editor (1990), *Handbook of Coastal and Ocean Engineering*, 3 Vols., Gulf Publishing, Houston.
- Horikawa, K., Editor, (1988), *Nearshore Dynamics and Coastal Processes—Theory; Measurement and Predictive Models*, University of Tokyo Press, Tokyo.
- Hughes, S.A. (1993), *Physical Models and Laboratory Techniques in Coastal Engineering*, World Scientific, Singapore.
- Kamphius, J.W. (2000), *Introduction to Coastal Engineering and Management*, World Scientific, Singapore.
- Komar, P.D. (1998), *Beach Processes and Sedimentation*, Second Edition, Prentice Hall, Englewood Cliffs, NJ.
- Pilarczyk, K.W., Editor (1990), *Coastal Protection*, A.A. Balkema, Rotterdam.
- Sarpkaya, T. and Isaacson, M. (1981), *Mechanics of Wave Forces on Offshore Structures*, Van Nostrand Reinhold, New York.
- Sawaragi, T., Editor (1995), *Coastal Engineering—Waves, Beaches, Wave-Structure Interactions*, Elsevier, Amsterdam.
- Sorensen, R.M. (1993), *Basic Wave Mechanics for Coastal and Ocean Engineers*, John Wiley, New York.
- Tucker, M.J. (1991), *Waves in Ocean Engineering—Measurement, Analysis, Interpretation*, Ellis Horwood, New York.
- Thorne, C.R., Abt, S.R., Barends, F.B.J., Maynard, S.T., and Pilarczyk, K.W., Editors (1995), *River, Coastal and Shoreline Protection*, John Wiley, New York.

An increasing amount of field data and a number of useful publications and software packages are becoming available over the internet. Two useful sites are noaa.gov and bigfoot.wes.army.mil.

1.5 Summary

Coastal engineering is a unique branch of civil engineering that has undergone significant development in recent decades. Practitioners of this branch of engineering must be knowledgeable in a number of special subjects, one of which is the mechanics of surface gravity waves. Basic two-dimensional wave theory and the characteristics of these waves are the starting points for this text.

1.6 References

- Bruun, P. (1972), "The History and Philosophy of Coastal Protection," in *Proceedings, 13th Conference on Coastal Engineering*, American Society of Civil Engineers, Vancouver, pp. 33–74.
- Houston, J.R. (1995), "The Economic Value of Beaches," *The Circular*, U.S. Army Coastal Engineering Research Center, Vicksburg, MS, December, pp. 1–3.
- Inman, D.L. (1974), "Ancient and Modern Harbors: A Repeating Phylogeny," in *Proceedings, 14th Conference on Coastal Engineering*, American Society of Civil Engineers, Copenhagen, pp. 2049–2067.
- U.S. Army Coastal Engineering Research Center (1984), *Shore Protection Manual*, Fourth Edition, 2 Vols., U.S. Government Printing Office, Washington DC.
- Wiegel, R.L. (1992), "Dade County, Florida, Beach Nourishment and Hurricane Surge Protection Project," *Shore and Beach*, October, pp. 2–26.

2

Two-Dimensional Wave Equations and Wave Characteristics

A practicing coastal engineer must have a basic and relatively easy to use theory that defines the important characteristics of two-dimensional waves. This theory is required in order to analyze changes in the characteristics of a wave as it propagates from the deep sea to the shore. Also, this theory will be used as a building block to describe more complex sea wave spectra. Such a theory—the small amplitude wave theory—is presented in this chapter along with related material needed to adequately describe the characteristics and behavior of two-dimensional waves.

2.1 Surface Gravity Waves

When the surface of a body of water is disturbed in the vertical direction, the force of gravity will act to return the surface to its equilibrium position. The returning surface water has inertia that causes it to pass its equilibrium position and establish a surface oscillation. This oscillation disturbs the adjacent water surface, causing the forward propagation of a wave.

A wave on the water surface is thus generated by some disturbing force which may typically be caused by the wind, a moving vessel, a seismic disturbance of the shallow sea floor, or the gravitational attraction of the sun and moon. These forces impart energy to the wave which, in turn, transmits the energy across the water surface until it reaches some obstacle such as a structure or the shoreline which causes the energy to be reflected and dissipated. The wave also transmits a signal in the form of the oscillating surface time history at a point.

As a wave propagates, the oscillatory water motion in the wave continues because of the interaction of gravity and inertia. Since water particles in the wave are continuously accelerating and decelerating as the wave propagates, dynamic pressure gradients develop in the water column. These dynamic pressure gradients are superimposed on the vertical hydrostatic pressure gradient. As the wave

propagates energy is dissipated, primarily at the air–water boundary and, in shallower water, at the boundary between the water and the sea floor.

The different wave generating forces produce waves with different periods. Wind-generated waves have a range of periods from about 1 to 30 s with the dominant periods for ocean storm waves being between 5 and 15 s. Vessel-generated waves have shorter periods, typically between 1 and 3 s. Seismically generated waves (tsunamis) have longer periods from about 5 min to an hour and the dominant periods of the tide are around 12 and 24 hours.

Wind waves in the ocean have a height (vertical distance crest to trough) that is typically less than 10 ft, but it can exceed 20 ft during significant storms. Vessel waves rarely exceed 3 ft in height. At sea, tsunami waves are believed to have a height of 2 ft or less, but as the tsunami approaches the coast heights often increase to greater than 10 ft, depending on the nature of the nearshore topography. Similarly, tide wave heights (tide ranges) in the deep ocean are relatively low, but along the coast tide ranges in excess of 20 ft occur at a number of locations.

Wind-generated waves are complex, consisting of a superimposed multitude of components having different heights and periods. In this chapter we consider the simplest theory for the characteristics and behavior of a two-dimensional monochromatic wave propagating in water of constant depth. This will be useful in later chapters as a component of the spectrum of waves found at sea. It is also useful for first-order design calculations where the height and period of this monochromatic wave are selected to be representative of a more complex wave spectrum. Also, much laboratory research has used, and will continue to use, monochromatic waves for basic studies of wave characteristics and behavior such as the wave-induced force on a structure or the nature of breaking waves.

The simplest and often most useful theory (considering the effort required in its use) is the two-dimensional small-amplitude or linear wave theory first presented by Airy (1845). This theory provides equations that define most of the kinematic and dynamic properties of surface gravity waves and predicts these properties within useful limits for most practical circumstances. The assumptions required to derive the small-amplitude theory, an outline of its derivation, the pertinent equations that result, and the important characteristics of waves described by these equations are presented in this chapter. More detail on the small-amplitude wave theory can be found in Wiegel (1964), Ippen (1966), Dean and Dalrymple (1984), U.S. Army Coastal Engineering Research Center (1984), and Sorensen (1993).

2.2 Small-Amplitude Wave Theory

The small-amplitude theory for two-dimensional, freely propagating, periodic gravity waves is developed by linearizing the equations that define the free surface boundary conditions. With these and the bottom boundary condition,

a periodic velocity potential is sought that satisfies the requirements for irrotational flow. This velocity potential, which is essentially valid throughout the water column except at the thin boundary layers at the air–water interface and at the bottom, is then used to derive the equations that define the various wave characteristics (e.g., surface profile, wave celerity, pressure field, and particle kinematics). Specifically, the required assumptions are:

1. The water is homogeneous and incompressible, and surface tension forces are negligible. Thus, there are no internal pressure or gravity waves affecting the flow, and the surface waves are longer than the length where surface tension effects are important (i.e., wave lengths are greater than about 3 cm).
2. Flow is irrotational. Thus there is no shear stress at the air–sea interface or at the bottom. Waves under the effects of wind (being generated or diminished) are not considered and the fluid slips freely at the bottom and other solid fixed surfaces. Thus the velocity potential ϕ must satisfy the Laplace equation for two-dimensional flow:

$$\frac{\partial^2 \phi}{\partial x^2} + \frac{\partial^2 \phi}{\partial z^2} = 0 \quad (2.1)$$

where x and z are the horizontal and vertical coordinates, respectively.

3. The bottom is stationary, impermeable, and horizontal. Thus, the bottom is not adding or removing energy from the flow or reflecting wave energy. Waves propagating over a sloping bottom, as for example when waves propagate toward the shore in the nearshore region, can generally be accommodated by the assumption of a horizontal bottom if the slope is not too steep.
4. The pressure along the air–sea interface is constant. Thus, no pressure is exerted by the wind and the aerostatic pressure difference between the wave crest and trough is negligible.
5. The wave height is small compared to the wave length and water depth. Since particle velocities are proportional to the wave height, and wave celerity (phase velocity) is related to the water depth and the wave length, this requires that particle velocities be small compared to the wave celerity. This assumption allows one to linearize the higher order free surface boundary conditions and to apply these boundary conditions at the still water line rather than at the water surface, to obtain an easier solution. This assumption means that the small-amplitude wave theory is most limited for high waves in deep water and in shallow water and near wave breaking where the waves peak and wave crest particle velocities approach the wave phase celerity. Given this, the small-amplitude theory is still remarkably useful and extensively used for wave analysis.

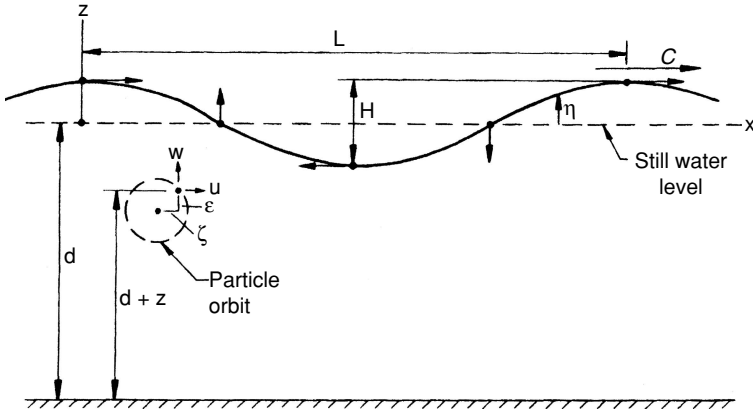


Figure 2.1. Definition of progressive surface wave parameters.

Figure 2.1 depicts a monochromatic wave traveling at a phase celerity C on water of depth d in an x, z coordinate system. The x axis is the still water position and the bottom is at $z = -d$. The wave surface profile is defined by $z = \eta$, where η is a function of x and time t . The wave length L and height H are as shown in the figure. Since the wave travels a distance L in one period T ,

$$C = L/T \quad (2.2)$$

The arrows at the wave crest, trough, and still water positions indicate the directions of water particle motion at the surface. As the wave propagates from left to right these motions cause a water particle to move in a clockwise orbit. The water particle velocities and orbit dimensions decrease in size with increasing depth below the still water line. Particle orbits are circular only under certain conditions as defined in Section 2.4.

The horizontal and vertical components of the water particle velocity at any instant are u and w , respectively. The horizontal and vertical coordinates of a water particle at any instant are given by ζ and ε , respectively. The coordinates are referenced to the center of the orbital path that the particle follows. At any instant, the water particle is located a distance $d - (-z) = d + z$ above the bottom.

The following dimensionless parameters are often used:

$$k = 2\pi/L (\text{wave number})$$

$$\sigma = 2\pi/T (\text{wave angular frequency})$$

We also use the terms “wave steepness” defined as the wave height divided by the wave length (i.e., H/L) and “relative depth” defined as the water depth divided by the wave length (i.e., d/L) in discussions of wave conditions.

The small-amplitude wave theory is developed by solving Eq. (2.1) for the domain depicted in Figure 2.1, with the appropriate boundary conditions for the free surface (2) and the bottom (1).

At the bottom there is no flow perpendicular to the bottom which yields the bottom boundary condition (BBC):

$$w = \frac{\partial \phi}{\partial z} = 0 \text{ at } z = -d \quad (2.3)$$

At the free surface there is a kinematic boundary condition (KSBC) that relates the vertical component of the water particle velocity at the surface to the surface position:

$$w = \frac{\partial \eta}{\partial t} + u \frac{\partial \eta}{\partial x} \text{ at } z = \eta \quad (2.4)$$

The Bernoulli equation for unsteady irrotational flow may be written

$$\frac{1}{2}(u^2 + w^2) + \frac{p}{\rho} + gz + \frac{\partial \phi}{\partial t} = 0 \quad (2.5)$$

where g is the acceleration of gravity, p is the pressure, and ρ is the fluid density. At the surface where the pressure is zero the dynamic boundary condition (DSBC) becomes

$$\frac{1}{2}(u^2 + w^2) + gz + \frac{\partial \phi}{\partial t} = 0 \text{ at } z = \eta \quad (2.6)$$

The KSBC and the DSBC have to be linearized and applied at the still water line rather than at the a priori unknown water surface. This yields for the KSBC

$$w = \frac{\partial \eta}{\partial t} \text{ at } z = 0 \quad (2.7)$$

and for the DSBC

$$g\eta + \frac{\partial \phi}{\partial t} = 0 \text{ at } z = 0 \quad (2.8)$$

Employing the Laplace equation, the BBC, and the linearized DSBC, we can derive the velocity potential for the small-amplitude wave theory (see Ippen, 1966; Sorensen, 1978; or Dean and Dalrymple, 1984). The most useful form of this velocity potential is

$$\phi = \frac{gH}{2\sigma} \frac{\cosh k(d+z)}{\cosh kd} \sin(kx - \sigma t) \quad (2.9)$$

The velocity potential demonstrates an important point. Since the wave length or wave number ($k = 2\pi/L$) depends on the wave period and water depth [see Eq. (2.14)], when the wave height and period plus the water depth are known the wave is fully defined and all of its characteristics can be calculated.

We can insert the velocity potential into the linearized DSBC with $z = 0$ to directly determine the equation for the wave surface profile:

$$\eta = \frac{H}{2} \cos(kx - \sigma t) \quad (2.10)$$

which can also be written

$$\eta = \frac{H}{2} \cos 2\pi \left(\frac{x}{L} - \frac{t}{T} \right) \quad (2.11)$$

by inserting the wave number and wave angular frequency. Thus, the small-amplitude wave theory yields a cosine surface profile. This is reasonable for low-amplitude waves, but with increasing wave amplitude the surface profile becomes vertically asymmetric with a more peaked wave crest and a flatter wave trough (as will be shown in Chapter 3).

Combining the KSBC and the DSBC by eliminating the water surface elevation yields

$$\frac{\partial^2 \phi}{\partial t^2} + g \frac{\partial \phi}{\partial z} = 0 \text{ at } z = 0$$

Then, inserting the velocity potential, differentiating, and rearranging we have

$$\sigma^2 = gk \tanh kd$$

or

$$C = \frac{\sigma}{k} = \sqrt{\frac{g}{k} \tanh kd}$$

and

$$C = \sqrt{\frac{gL}{2\pi} \tanh \frac{2\pi d}{L}} \quad (2.12)$$

Equation (2.12) indicates that for small-amplitude waves, the wave celerity is independent of the wave height. As the wave height increases there is a small but growing dependence of the wave celerity on the wave height (see Chapter 3). Equation (2.12) can also be written [by inserting Eq. (2.2)]

$$C = \frac{gT}{2\pi} \tanh \frac{2\pi d}{L} \quad (2.13)$$

$$L = \frac{gT^2}{2\pi} \tanh \frac{2\pi d}{L} \quad (2.14)$$

From Eq. (2.14), if the water depth and the wave period are known, the wave length can be calculated by trial and error. Then the celerity can be determined from $C = L/T$. Tables are available (U.S. Army Coastal Engineering Research Center, 1984) for the direct determination of L given the water depth and wave period.

Equations (2.12) to (2.14) collectively are commonly known as the dispersion equation. For a spectrum of waves having different periods (or lengths), the longer waves will propagate at a higher celerity and move ahead while the shorter waves will lag behind.

It can be demonstrated (see Ippen, 1966) that as a wave propagates from deep water in to the shore, the wave period will remain constant because the number of waves passing sequential points in a given interval of time must be constant. Other wave characteristics including the celerity, length, height, surface profile, particle velocity and acceleration, pressure field, and energy will all vary during passage from deep water to the nearshore area.

2.3 Wave Classification

An important classification of surface waves is based on the relative depth (d/L). When a wave propagates from deep water offshore in to shallower water nearshore the wave length decreases [see Eq. (2.14)], but at a slower rate than that at which the depth decreases. Thus, the relative depth decreases as a wave approaches the shore. When d/L is greater than approximately 0.5, $\tanh (2\pi d/L)$ is essentially unity and Eqs. (2.12) to (2.14) reduce to

$$C_o = \sqrt{\frac{gL_o}{2\pi}} \quad (2.15)$$

$$C_o = \frac{gT}{2\pi} \quad (2.16)$$

and

$$L_o = \frac{gT^2}{2\pi} \quad (2.17)$$

respectively. Waves in this region are called deep water waves and this condition is commonly denoted by the subscript zero (except for the wave period which is

not depth dependent and thus does not change as the relative depth decreases). Wave particle velocities and orbit dimensions decrease with increasing distance below the free surface. In deep water at a depth of $-z/L > 0.5$ the particle velocities and orbit dimensions are close to zero. Since for $d/L > 0.5$ the waves do not interact with the bottom, wave characteristics are thus independent of the water depth [e.g., see Eqs. (2.15) to (2.17)].

Example 2.3-1

A wave in water 100 m deep has a period of 10 s and a height of 2 m. Determine the wave celerity, length, and steepness. What is the water particle speed at the wave crest?

Solution:

Assume that this is a deep water wave. Then, from Eq. (2.17)

$$L_o = \frac{9.81(10)^2}{2\pi} = 156 \text{ m}$$

Since the depth is greater than half of the calculated wave length, the wave is in deep water and the wave length is 156 m. [Otherwise, Eq. (2.14) would have to be used to calculate the wave length.] The wave celerity is from Eq. (2.2)

$$C_o = \frac{156}{10} = 15.6 \text{ m/s}$$

and the steepness is

$$\frac{H_o}{L_o} = \frac{2}{156} = 0.013$$

For deep water the particle orbits are circular having a diameter at the surface equal to the wave height. Since a particle completes one orbit in one wave period, the particle speed at the crest would be the orbit circumference divided by the period or

$$u_c = \frac{\pi H_o}{T} = \frac{3.14(2)}{10} = 0.63 \text{ m/s}$$

Note that this is much less than C_o .

When the relative depth is less than 0.5 the waves interact with the bottom. Wave characteristics depend on both the water depth and the wave period, and

continually change as the depth decreases. The full dispersion equations must be used to calculate wave celerity or length for any given water depth and wave period. Dividing Eq. (2.13) by Eq. (2.16) or Eq. (2.14) by Eq. (2.17) yields

$$\frac{C}{C_o} = \frac{L}{L_o} = \tanh \frac{2\pi d}{L} \quad (2.18)$$

which is a useful relationship that will be employed in a later chapter. Waves propagating in the range of relative depths from 0.5 to 0.05 are called intermediate or transitional water waves.

When the relative depth is less than approximately 0.05, $\tanh (2\pi d/L)$ approximately equals $2\pi d/L$ and the dispersion equation yields

$$C = \sqrt{gd} \quad (2.19)$$

or

$$L = \sqrt{gd}T \quad (2.20)$$

Waves in this region of relative depths are called shallow water waves. In shallow water the small-amplitude wave theory gives a wave celerity that is independent of wave period and dependent only on the water depth (i.e., the waves are not period dispersive). The finite-amplitude wave theories presented in the next chapter show that the shallow water wave celerity is a function of the water depth and the wave height so that in shallow water waves are amplitude dispersive. Remember that it is the relative depth, not the actual depth alone, that defines deep, intermediate, and shallow water conditions. For example, the tide is a very long wave that behaves as a shallow water wave in the deepest parts of the ocean.

Example 2.3-2

Consider the wave from Example 2.3-1 when it has propagated in to a nearshore depth of 2.3 m. Calculate the wave celerity and length.

Solution:

Assuming this is a shallow water wave, Eq. (2.19) yields

$$C = \sqrt{9.81(2.3)} = 4.75 \text{ m/s}$$

and Eq. (2.2) yields

$$L = 4.75(10) = 47.5 \text{ m}$$

So $d/L = 2.3/47.5 = 0.048 < 0.05$ and the assumption of shallow water was correct. Compare these values to the results from Example 2.3-1

2.4 Wave Kinematics and Pressure

Calculation of the wave conditions that will cause the initiation of bottom sediment motion, for example, requires a method for calculating water particle velocities in a wave. The water particle velocity and acceleration as well as the pressure field in a wave are all needed to determine wave-induced forces on various types of coastal structures.

Wave Kinematics

The horizontal and vertical components of water particle velocity (u and w , respectively) can be determined from the velocity potential where

$$u = \frac{\partial \phi}{\partial x}, \quad w = \frac{\partial \phi}{\partial z}$$

This yields, after inserting the dispersion relationship and some algebraic manipulation

$$u = \frac{\pi H}{T} \left[\frac{\cosh k(d+z)}{\sinh kd} \right] \cos(kx - \sigma t) \quad (2.21)$$

and

$$w = \frac{\pi H}{T} \left[\frac{\sinh k(d+z)}{\sinh kd} \right] \sin(kx - \sigma t) \quad (2.22)$$

Equations (2.21) and (2.22) give the velocity components at the point $(x, -z)$ as a function of time as different water particles pass through this point.

Note that each velocity component consists of three parts: (1) the surface deep water particle speed $\pi H/T$, (2) the term in brackets which accounts for particle velocity variation over the vertical water column at a given location and for particle velocity variation caused by the wave moving from deep to shallow water, and (3) a phasing term dependent on position in the wave and time. Note that $d+z$ is the distance measured up from the bottom as demonstrated in Figure 2.1. Also, as would be expected, the horizontal and vertical velocity components are 90° out of phase.

The horizontal component of particle acceleration a_x may be written

$$a_x = u \frac{\partial u}{\partial x} + w \frac{\partial u}{\partial z} + \frac{\partial u}{\partial t}$$

where the first two terms on the righthand side are the convective acceleration and the third term is the local acceleration. The magnitude of the convective

acceleration for a small-amplitude wave is of the order of the wave steepness (H/L) squared while the magnitude of the local acceleration is of the order of the wave steepness. Since the wave steepness is much smaller than unity, we can usually neglect the higher order convective acceleration term in determining the particle acceleration. This yields

$$a_x = \frac{2\pi^2 H}{T^2} \left[\frac{\cosh k(d+z)}{\sinh kd} \right] \sin(kx - \sigma t) \quad (2.23)$$

for the horizontal component and

$$a_z = -\frac{2\pi^2 H}{T^2} \left[\frac{\sinh k(d+z)}{\sinh kd} \right] \cos(kx - \sigma t) \quad (2.24)$$

for the vertical component of acceleration. The terms in brackets are the same for both the particle velocity and acceleration components. The cosine/sine terms indicate that the particle velocity components are 90° out of phase with the acceleration components. This is easily seen by considering a particle following a circular orbit. The velocity is tangent to the circle and the acceleration is toward the center of the circle or normal to the velocity.

As water particles orbit around a mean position (see Figure 2.1) the horizontal and vertical coordinates of the particle position relative to the mean position are given by ζ and ε , respectively. These components can be found by integrating the particle velocity components with time. This yields

$$\zeta = \frac{-H}{2} \left[\frac{\cosh k(d+z)}{\sinh kd} \right] \sin(kx - \sigma t) \quad (2.25)$$

and

$$\varepsilon = \frac{H}{2} \left[\frac{\sinh k(d+z)}{\sinh kd} \right] \cos(kx - \sigma t) \quad (2.26)$$

where $H/2$ is the orbit radius for a particle at the surface of a deep water wave. The position coordinates are evaluated for the orbit of the particle that is passing through the point $x, -z$ at that instant, but the small-amplitude assumptions allow us to assume that these coordinates [given by Eqs. (2.25) and (2.26)] apply to the orbit mean position.

As a wave propagates from deep water into shallow water, the particle orbit geometries undergo the transformation depicted in Figure 2.2. In deep water the orbits are circular throughout the water column but decrease in diameter with increasing distance below the water surface, to approximately die out at a distance

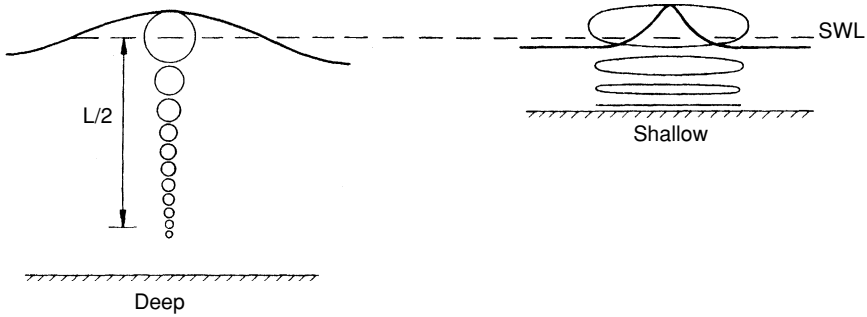


Figure 2.2. Deep and shallow water surface profiles and particle orbits.

of $L/2$. In transitional to shallow water, the orbits reach the bottom and become elliptical—with the ellipses becoming flatter near the bottom. At the bottom the particles follow a reversing horizontal path. (This is for the assumed irrotational motion—for real conditions a bottom boundary layer develops and the horizontal dimension of the particle orbit reduces to zero at the bottom.) Since the terms in brackets are the same for the respective velocity, acceleration, and displacement equations, the particle velocity and acceleration component magnitudes demonstrate the same spatial change as do the displacement coordinates.

According to the small-amplitude theory surface waves have a sinusoidal surface profile. This is reasonable for low steepness waves in deep water. But, for steeper deep water waves or as waves propagate into transitional and shallow water the surface profile becomes trochoidal, having long flat troughs and shorter peaked crests (see Figure 2.2). The amplitude of the crest increases while the amplitude of the trough decreases. In transitional and shallow water, particles still move in essentially closed orbits. Since they must travel the same distance forward under the crest in less time (owing to the trochoidal profile) as they travel back under the trough in more time, peak velocities under the wave crest will exceed those under the trough. As with the profile asymmetry, this velocity asymmetry is not predicted by the small amplitude wave theory.

It is useful to consider the deep and shallow water limits for the term in brackets in the particle velocity, acceleration, and orbit displacement equations. At these limits we have:

$$\text{Deep water: } \frac{\cosh k(d+z)}{\sinh kd} = \frac{\sinh k(d+z)}{\sinh kd} = e^{kz} \quad (2.27)$$

$$\text{Shallow water: } \frac{\cosh k(d+z)}{\sinh(kd)} = \frac{1}{kd} \quad (2.28)$$

$$\frac{\sinh k(d+z)}{\sinh kd} = 1 + \frac{z}{d} \quad (2.29)$$

Substitution of Eq. (2.27) into Eqs. (2.21) to (2.26) indicates that, in deep water, the particle velocity, acceleration, and orbit displacement decay exponentially with increasing distance below the still water line. At $z = -L/2$ they are reduced to 4.3% of their value at the surface.

Substitution of Eqs. (2.28) and (2.29) into Eqs. (2.21) and (2.22) respectively yields (after some algebraic manipulation) the following equations for water particle velocity in shallow water:

$$u = \frac{H}{2} \sqrt{\frac{g}{d}} \cos(kx - \sigma t) \quad (2.30)$$

$$w = \frac{\pi H}{T} \left(1 + \frac{z}{d}\right) \sin(kx - \sigma t) \quad (2.31)$$

Equation (2.30) indicates that, in shallow water, the horizontal component of water particle velocity is constant from the water surface to the bottom. The vertical component of particle velocity can be seen from Eq. (2.31) to decrease linearly from a maximum at the water surface to zero at the bottom. Similar statements can be made for the particle acceleration and orbit dimensions.

Pressure Field

Substitution of the velocity potential into the linearized form of the equation of motion [Eq. (2.5) without the velocity squared terms] yields the following equation for the pressure field in a wave:

$$p = -\rho g z + \frac{\rho g H}{2} \left[\frac{\cosh k(d+z)}{\cosh kd} \right] \cos(kx - \sigma t) \quad (2.32)$$

The first term on the right gives the normal hydrostatic pressure variation and the second term is the dynamic pressure variation owing to the wave-induced particle acceleration. These components are plotted in Figure 2.3 for vertical sections through the wave crest and trough. Since particles under the crest are accelerating downward, a downward dynamic pressure gradient is required. The reverse is true under a wave trough. Halfway between the crest and trough the acceleration is horizontal so the vertical pressure distribution is hydrostatic. Equation (2.32) is not valid above the still water line owing to the linearization of the DSBC and its application at the still water line. Above the still water line the pressure must regularly decrease to zero at the water surface.

In deep water, the dynamic pressure reduces to near zero at $z = -L/2$. A pressure gage at this depth would essentially measure the static pressure for the given depth below the still water line. A pressure gage (located above $-L/2$) can be used as a wave gage. The period of the pressure fluctuation is the wave period which can be used to calculate the wave length from the dispersion equation. The

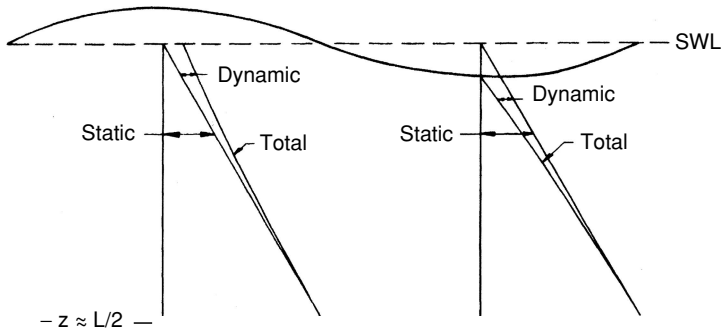


Figure 2.3. Deep water wave vertical pressure distributions.

wave height can then be calculated from Eq. (2.32), assuming the position of the gage, the wave period and length, and the water depth are known.

Note that the term in brackets differs from the terms in brackets for the particle velocity, acceleration, and orbit displacement equations. At the deep and shallow water limits we have,

$$\frac{\cosh k(d+z)}{\cosh kd} = e^{kz} \text{ (deep water)} \quad (2.33)$$

$$= 1 \text{ (shallow water)}$$

Thus, from the small-amplitude wave theory, in deep water there is also an exponential decay in the dynamic pressure with distance below the still water line. In shallow water the total pressure distribution is given by

$$p = \rho g(\eta - z) \quad (2.34)$$

2.5 Energy, Power, and Group Celerity

An important characteristic of gravity waves is that they have mechanical energy and that this energy is transmitted forward as they propagate. It is important to be able to quantify this energy level and the rate of energy transmission (energy flux or power) for a given wave height and period and water depth.

Wave Energy

The total mechanical energy in a surface gravity wave is the sum of the kinetic and potential energies. Equations for each may be derived by considering Figure 2.4. The kinetic energy for a unit width of wave crest and for one wave length E_k

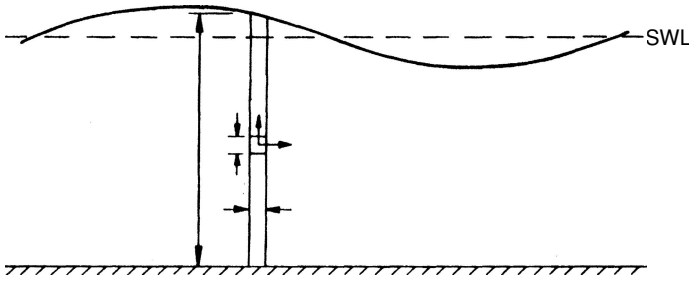


Figure 2.4. Definition sketch for wave energy derivation.

is equal to the integral over one wave length and the water depth of one-half times the mass of a differential element times the velocity of that element squared. Thus

$$E_k = \int_0^L \int_{-d}^0 \frac{1}{2} \rho dx dz (u^2 + w^2)$$

where the upper limit of the vertical integral is taken as zero in accord with the assumptions of the small-amplitude wave theory. Inserting the velocity terms [Eqs. (2.21) and (2.22)], integrating, and performing the required algebraic manipulation yields the kinetic energy

$$E_k = \frac{\rho g H^2 L}{16}$$

If we subtract the potential energy of a mass of still water (with respect to the bottom) from the potential energy of the wave form shown in Figure 2.4 we will have the potential energy due solely to the wave form. This gives the potential energy per unit wave crest width and for one wave length E_p as

$$E_p = \int_0^L \rho g (d + \eta) \left(\frac{d + \eta}{2} \right) dx - \rho g L d \left(\frac{d}{2} \right)$$

The surface elevation as a function of x is given by Eq. (2.10) with $t = 0$. Performing the integration and simplifying yields

$$E_p = \frac{\rho g H^2 L}{16}$$

Thus, the kinetic and potential energies are equal and the total energy in a wave per unit crest width E is

$$E = E_k + E_p = \frac{\rho g H^2 L}{8} \quad (2.35)$$

A wave propagating through a porous structure, for example, where the water depth is the same on both sides of the structure, will have the same period and wave length on both sides. Thus, a reduction of wave energy because of reflection from the structure and viscous dissipation within the structure will result in a decrease in the wave height. A 50% reduction in wave energy would result in only a 29% decrease in the wave height because the wave energy is proportional to the wave height squared.

Both the kinetic and potential energies are variable from point to point along a wave length. However, a useful concept is the average energy per unit surface area given by

$$\bar{E} = \frac{E}{L(1)} = \frac{\rho g H^2}{8} \quad (2.36)$$

This is usually known as the energy density or specific energy of a wave. Equations (2.35) and (2.36) apply for deep to shallow water within the limits of the small-amplitude wave theory.

Wave Power

Wave power P is the wave energy per unit time transmitted in the direction of wave propagation. Wave power can be written as the product of the force acting on a vertical plane normal to the direction of wave propagation times the particle flow velocity across this plane. The wave-induced force is provided by the dynamic pressure (total pressure minus hydrostatic pressure) and the flow velocity is the horizontal component of the particle velocity. Thus

$$P = \frac{1}{T} \int_0^T \int_{-d}^0 (p + \rho g z) u dz dt$$

where the term in parentheses is the dynamic pressure. Inserting the dynamic pressure from Eq. (2.32) and the horizontal component of velocity from Eq. (2.21) and integrating leads to

$$P = \frac{\rho g H^2 L}{16T} \left(1 + \frac{2kd}{\sinh 2kd} \right)$$

or

$$P = \frac{E}{2T} \left(1 + \frac{2kd}{\sinh 2kd} \right) \quad (2.37)$$

Letting

$$n = \frac{1}{2} \left(1 + \frac{2kd}{\sinh 2kd} \right) \quad (2.38)$$

Equation (2.37) becomes

$$P = \frac{nE}{T} \quad (2.39)$$

The value of n increases as a wave propagates toward the shore from 0.5 in deep water to 1.0 in shallow water. Equation (2.39) indicates that n can be interpreted as the fraction of the mechanical energy in a wave that is transmitted forward each wave period.

As a train of waves propagates forward the power at one point must equal the power at a subsequent point minus the energy added, and plus the energy dissipated and reflected per unit time between the two points. For first-order engineering analysis of waves propagating over reasonably short distances it is common to neglect the energy added, dissipated, or reflected, giving

$$P = \left(\frac{nE}{T} \right)_1 = \left(\frac{nE}{T} \right)_2 = \text{constant} \quad (2.40)$$

Equation (2.40) indicates that, for the assumptions made, as a two-dimensional wave travels from deep water to the nearshore the energy in the wave train decreases at a rate inversely proportional to the increase in n since the wave period is constant.

As waves approach the shore at an angle and propagate over irregular hydrography they vary three-dimensionally owing to refraction. (See Chapter 4 for further discussion and analysis of wave refraction.) If we construct lines that are normal or orthogonal to the wave crests as a wave advances and assume that no energy propagates along the wave crest (i.e., across orthogonal lines) the energy flux between orthogonals can be assumed to be constant. If the orthogonal spacing is denoted by B , Eq. (2.40) can be written

$$\left(\frac{BnE}{T} \right)_1 = \left(\frac{BnE}{T} \right)_2 = \text{constant}$$

Inserting the wave energy from Eq. (2.35) yields

$$\frac{H_1}{H_2} = \sqrt{\frac{n_2 L_2}{n_1 L_1}} \sqrt{\frac{B_2}{B_1}} \quad (2.41)$$

The first term on the right represents the effects of shoaling and the second term represents the effects of orthogonal line convergence or divergence owing to refraction. These are commonly called the coefficient of shoaling K_s and the coefficient of refraction K_r , respectively.

Equation (2.41) allows us to calculate the change in wave height as a wave propagates from one water depth to another depth. Commonly, waves are

predicted for some deep water location and then must be transformed to some intermediate or shallow water depth nearshore using Eq. (2.41). For this, Eq. (2.41) becomes

$$\frac{H}{H_o} = \sqrt{\frac{L_o}{2nL}} \sqrt{\frac{B_o}{B}} \quad (2.42)$$

or

$$\frac{H}{H_o} = \frac{H}{H'_o} \sqrt{\frac{B_o}{B}}$$

where the prime denotes the change in wave height from deep water to the point of interest considering only two-dimensional shoaling effects.

Figure 2.5 is a plot of H/H'_o versus d/L and d/L_o from deep to shallow water. Initially, as a wave enters intermediate water depths the wave height decreases because n increases at a faster rate than L decreases [see Eq. (2.42)]. H/H'_o reaches a minimum value of 0.913 at $d/L = 0.189$ ($d/L_o = 0.157$). Shoreward of this point the wave height grows at an ever-increasing rate until the wave becomes unstable and breaks.

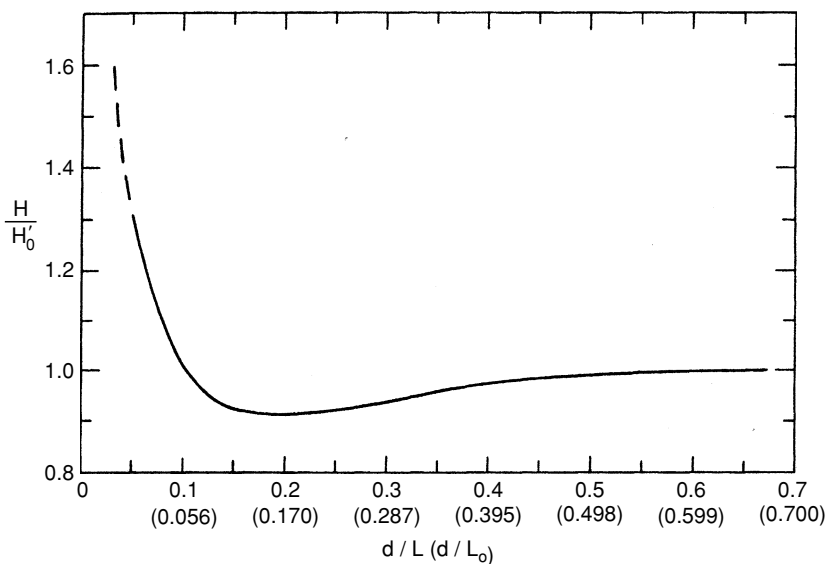


Figure 2.5. Dimensionless wave height versus relative depth for two-dimensional wave transformation.

Example 2.5-1

Consider the wave from Example 2.3–1 when it has propagated into a water depth of 10 m without refracting and assuming energy gains and losses can be ignored. Determine the wave height and the water particle velocity and pressure at a point 1 m below the still water level under the wave crest. (Assume fresh water.)

Solution:

From Example 2.3–1 we have $L_o = 156$ m and Eq. (2.14) gives

$$L = \frac{9.81(10)^2}{2\pi} \tanh \frac{2\pi(10)}{L}$$

which can be solved by trial to yield $L = 93.3$ m. Then, $k = 2\pi/93.3 = 0.0673 \text{ m}^{-1}$ and from Eq. (2.38)

$$n = \frac{1}{2} \left(1 + \frac{2(0.0673)(10)}{\sinh(2(0.0673)(10))} \right) = 0.874$$

With $K_r = 1$, Eq. (2.42) yields

$$H = 2\sqrt{\frac{156}{2(0.874)(93.3)}} = 1.97 \text{ m}$$

At the crest of the wave $\cos(kx - \sigma t) = 1$, and $z = -1$, so Eq. (2.21) gives

$$u = \frac{\pi(1.97)}{10} \left[\frac{\cosh(0.0673)(9)}{\sinh(0.0673)(10)} \right] = 1.01 \text{ m/s}$$

which is the total particle velocity since $w = 0$ under the wave crest. Equation (2.32) gives

$$\begin{aligned} P &= -1000(9.81)(-1) + \frac{1000(9.81)(1.97)}{2} \left[\frac{\cosh(0.0673)9}{\cosh(0.0673)10} \right] \\ &= 19,113 \text{ N/m}^2 \end{aligned}$$

Remember, Eqs. (2.40) to (2.42) neglect energy transfer to and from waves by surface and bottom effects. The nature of these effects is discussed briefly below. Bottom effects, of course, require that the water depth be sufficiently shallow for a strong interaction between the wave train and the bottom.

Wave Reflection

If the bottom is other than horizontal, a portion of the incident wave energy will be reflected seaward. This reflection is generally negligible for wind wave periods on typical nearshore slopes. However, for longer period waves and steeper bottom slopes wave reflection would not be negligible. Any sharp bottom irregularity such as a submerged structure of sufficient size will also reflect a significant portion of the incident wave energy.

Wind Effects

Nominally, if the wind has a velocity component in the direction of wave propagation that exceeds the wave celerity the wind will add energy to the waves. If the velocity component is less than the wave celerity or the wind blows opposite to the direction of wave propagation the wind will remove energy from the waves. For typical nonstormy wind conditions and the distances from deep water to the nearshore zone found in most coastal locations, the wind effect can be neglected in the analysis of wave conditions nearshore.

Bottom Friction

As the water particle motion in a wave interacts with a still bottom, an unsteady oscillatory boundary layer develops near the bottom. For long period waves in relatively shallow water this boundary layer can extend up through much of the water column. But, for typical wind waves the boundary layer is quite thin relative to the water depth, and if propagation distances are not too long and the bottom is not too rough, bottom friction energy losses can be neglected.

Bottom Percolation

If the bottom is permeable to a sufficient depth, the wave-induced fluctuating pressure distribution on the bottom will cause water to percolate in and out of the bottom and thus dissipate wave energy.

Bottom Movement

When a wave train propagates over a bottom consisting of soft viscous material (such as the mud deposited at the Mississippi River Delta) the fluctuating pressure on the bottom can set the bottom in motion. Viscous stresses in the soft bottom dissipate energy provided by the waves.

Wave Group Celerity

Consider a long constant-depth wave tank in which a small group of deep water waves is generated. As the waves travel along the tank, waves in the front of the group will gradually decrease in height and, if the tank is long enough, disappear

in sequence starting with the first wave in the group. As the waves in the front diminish in height, new waves will appear at the rear of the group and commence to grow. One new wave will appear each wave period so the total number of waves in the group will continually increase. This phenomenon causes the wave group to have a celerity that is less than the celerity of the individual waves in the group. Since the total energy in the group is constant (neglecting dissipation) the average height of the waves in the group will continually decrease.

An explanation for this phenomenon can be found in the fact that only a fraction $[n; \text{ see Eq. (2.39)}]$ of the wave energy goes forward with the wave as it advances each wave length. Thus, the first wave in the group is diminished in height by the square root of n during the advance of one wave length. Waves in the group lose energy to the wave immediately behind and gain energy from the wave in front. The last wave in the group leaves energy behind so, relative to the group, a new wave appears each T seconds and gains additional energy as time passes.

A practical consequence of the deep water group celerity being less than the phase celerity of individual waves is that when waves are generated by a storm, prediction of their arrival time at a point of interest must be based on the group celerity.

To develop an equation for calculating the group celerity C_g consider two trains of monochromatic waves having slightly different periods and propagating in the same direction. Figure 2.6 shows the wave trains separately (above) and superimposed (below) when propagating in the same area. The superimposition of the two wave trains results in a beating effect in which the waves are alternately in and out of phase. This produces the highest waves when the two components are in phase, with heights diminishing in the forward and backward directions to zero height where the waves are exactly out of phase. The result is a group of waves advancing at a celerity C_g . If you follow an individual wave in the wave group its amplitude increases to a peak and then diminishes as it passes through the group and disappears at the front of the group.

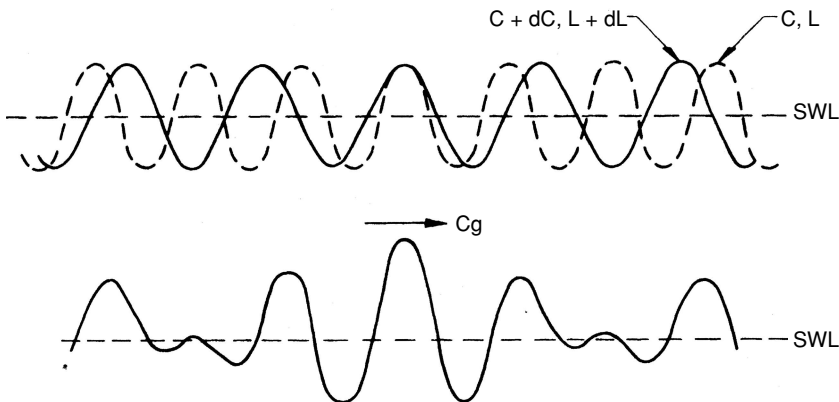


Figure 2.6. Two wave trains shown separately and superimposed.

Referring to Figure 2.6, the time required for the lag between the two components dL to be made up is dt , where dt equals the difference in component lengths divided by dC , the difference in component celerities, i.e., $dt = dL/dC$. The group advances a distance dx in the time dt , where dx is the distance traveled by the group in the time interval dt minus the one wave length that the peak wave dropped back (as the in-phase wave drops back one wave length each period). This can be written

$$dx = \left[\frac{(C + dC) + C}{2} \right] dt - \frac{(L + dL) + L}{2} \approx Cdt - L.$$

if dL and dC are very small compared to L and C . Then,

$$C_g = \frac{dx}{dt} = \frac{Cdt - L}{dt} = C - \frac{L}{dt}$$

since $dt = dL/dC$ this leads to

$$C_g = C - L \left(\frac{dC}{dL} \right) \quad (2.43)$$

In shallow water, small-amplitude waves are not dispersive ($dC/dL = 0$) so $C_g = C$. In deep water $dC/dL = C/2L$ [from Eq. (2.15)] so the group celerity is half of the phase celerity. For a general relationship for the group celerity, employing the dispersion relationship with Eq. (2.43) yields

$$C_g = \frac{C}{2} \left(1 + \frac{2kd}{\sinh 2kd} \right) \quad (2.44)$$

Thus, with n as defined in Eq. (2.38)

$$C_g = nC \quad (2.45)$$

So n is also the ratio of the wave group celerity to the phase celerity. Another way to look at this is that the wave energy is propagated forward at the group celerity.

2.6 Radiation Stress and Wave Setup

In fluid flow problems, some analyses are best carried out by energy considerations (e.g., head loss along a length of pipe) and some by momentum considerations (e.g., force exerted by a water jet hitting a wall). Similarly, for waves it is

better to consider the flux of momentum for some problem analyses. For wave analyses, the flux of momentum is commonly referred to as the wave “radiation stress” which may be defined as “the excess flow of momentum due to the presence of waves” (Longuet-Higgins and Stewart, 1964). Problems commonly addressed by the application of radiation stress include the lowering (setdown) and raising (setup) of the mean water level that is induced by waves as they propagate into the nearshore zone, the interaction of waves and currents, and the alongshore current in the surf zone induced by waves obliquely approaching the shore.

Radiation Stress

The horizontal flux of momentum at a given location consists of the pressure force acting on a vertical plane normal to the flow plus the transfer of momentum through that vertical plane. The latter is the product of the momentum in the flow and the flow rate across the plane. From classical fluid mechanics, the momentum flux from one location to another will remain constant unless there is a force acting on the fluid in the flow direction to change the flux of momentum.

If we divide the momentum flux by the area of the vertical plane through which flow passes, we have for the x direction

$$p + \rho u^2$$

For a wave, we want the excess momentum flux owing to the wave, so the radiation stress S_{xx} for a wave propagating in the x direction becomes

$$S_{xx} = \int_{-d}^{\eta} \overline{(p + \rho u^2)} dz - \int_{-d}^0 \rho g dz \quad (2.46)$$

where the subscript xx denotes the x -directed momentum flux across a plane defined by $x = \text{constant}$. In Eq. (2.46) p is the total pressure given by Eq. (2.32) so the static pressure must be subtracted to obtain the radiation stress for only the wave. The overbar denotes that the first term on the right must be averaged over the wave period. Inserting the pressure and the particle velocity from Eq. (2.21) leads to (Longuet-Higgins and Stewart, 1964)

$$S_{xx} = \frac{\rho g H^2}{8} \left(\frac{1}{2} + \frac{2kd}{\sinh 2kd} \right) = \bar{E} \left(2n - \frac{1}{2} \right) \quad (2.47)$$

For a wave traveling in the x -direction there also is a y -directed momentum flux across a plane defined by $y = \text{constant}$. This is

$$S_{yy} = \frac{\rho g H^2}{8} \left(\frac{kd}{\sinh kd} \right) = \bar{E} (n - 1/2) \quad (2.48)$$

The radiation stress components S_{xy} and S_{yx} are both zero. Note that in deep water Eqs. (2.47) and (2.48) become

$$S_{xx} = \frac{\bar{E}}{2}, S_{yy} = 0 \quad (2.49)$$

And in shallow water they become

$$S_{xx} = \frac{3\bar{E}}{2}, S_{yy} = \frac{\bar{E}}{2} \quad (2.50)$$

so, like wave energy, the radiation stress changes as a wave propagates through water of changing depth (as well as when a force is applied).

If a wave is propagating in a direction that is situated at an angle to the specified x direction, the radiation stress components become

$$\begin{aligned} S_{xx} &= \bar{E} [n(\cos^2 \theta + 1) - 1/2] \\ S_{yy} &= \bar{E} [n(\sin^2 \theta + 1) - 1/2] \\ S_{xy} &= \frac{\bar{E}}{2} n \sin^2 \theta = \bar{E} n \sin \theta \cos \theta \end{aligned} \quad (2.51)$$

where θ is the angle between the direction of wave propagation and the specified x direction.

Wave Setup

When a train of waves propagates toward the shore, at some point, depending on the wave characteristics and nearshore bottom slope, the waves will break. Landward of the point of wave breaking a surf zone will form where the waves dissipate their energy as they decay across the surf zone.

As the waves approach the breaking point there will be a small progressive set down of the mean water level below the still water level. This setdown is caused by an increase in the radiation stress owing to the decreasing water depth as the waves propagate toward the shore. The setdown is maximum just seaward of the breaking point. In the surf zone, there is a decrease in radiation stress as wave energy is dissipated. This effect is stronger than the radiation stress increase owing to continued decrease in the water depth. The result is a progressive increase or setup of the mean water level above the still water level in the direction of the shore. This surf zone setup typically is significantly larger than the setdown that occurs seaward of the breaking point.

The equations that predict the wave-induced nearshore setdown and setup can be developed by considering the horizontal momentum balance for two-dimensional waves approaching the shore (Longuet-Higgins and Stewart, 1964). The

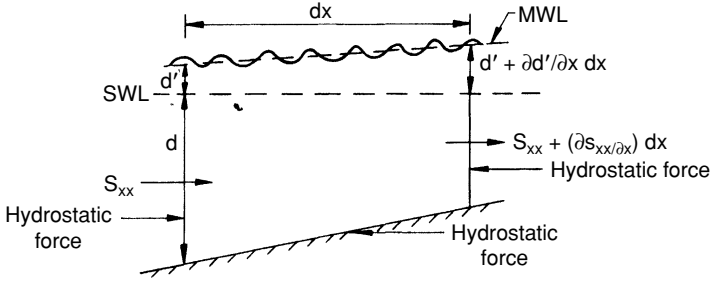


Figure 2.7. Force balance for wave-induced setup analysis.

net force caused by the cyclic bottom shear stress is reasonably neglected. Consider Figure 2.7 which shows a shore-normal segment of length dx with a setup d' . The forces and related change in the radiation stress at the boundaries are as shown. Writing the force-momentum flux balance for a segment of unit width parallel to the shore yields

$$\frac{\rho g}{2} (d + d')^2 - \frac{\rho g}{2} \left(d + d' + \frac{\partial d'}{\partial x} dx \right)^2 = \frac{\partial S_{xx}}{\partial x} dx$$

where the two terms on the left are the fore and aft hydrostatic forces and the term on the right is the resulting change in radiation stress. Assuming $d \gg d'$ and neglecting higher order terms this leads to

$$\frac{dS_{xx}}{dx} + \rho g d \frac{dd'}{dx} = 0 \quad (2.52)$$

Equation (2.52) basically relates the change in radiation stress (caused either by a depth change and/or wave energy dissipation) to the resulting slope of the mean water level. This equation applies to the regions before and after the breaking point.

For the region just seaward of the breaking point assume that the wave power is constant and employ Eq. (2.47) to integrate Eq. (2.52). This leads to the setdown of the mean water level given by

$$d' = -\frac{1}{8} \frac{H^2 k}{\sinh 2kd} \quad (2.53)$$

For deep water, Eq. (2.53) shows that the setdown is zero irrespective of the wave height because the \sinh term is very large. In shallow water, which may be used as an estimate of the conditions just prior to breaking, $d' = -H^2/16d$.

In the surf zone, the rate of energy dissipation by wave breaking will depend on the type of breaker that occurs. This rate of energy dissipation is complex and typically nonuniform. However, to reasonably develop an equation for wave setup, we will assume that the wave height across the surf zone is proportional to the depth below the local mean water level, i.e., $H = \gamma(d + d')$. A reasonable value for γ is 0.9 (see Section 2.8). Also, we will assume that shallow water wave conditions exist so $S_{xx} = 3E/2$. These assumptions lead to a solution to Eq. (2.52) given by

$$\frac{dd'}{dx} = \left(1 + \frac{8}{3\gamma^2}\right)^{-1} \frac{dd}{dx} \quad (2.54)$$

which gives the slope of the mean water level as a function of the bottom slope in the surf zone.

Example 2.6-1

Consider a wave that has a height of 2 m in water 2.2 m deep (below the mean water level) as it is about to break. The nearshore bottom slope through the surf zone is 0.02. Find the setdown at the breaker point and the setup (above the still water line) at the still water line contour of the shore. Assume shallow water wave conditions throughout.

Solution:

The setdown at the breaker line is

$$d' = -\frac{(2)^2}{16(2.2)} = -0.11 \text{ m}$$

The slope of the rising mean water level through the surf zone is

$$\frac{dd'}{dx} = \left(1 + \frac{8}{3(.9)^2}\right)^{-1} (0.02) = 0.0047$$

For a bottom slope of 0.02 the still water line at the beach will be $(2.2 + 0.11)/(0.02) = 115.5$ m shoreward of the breaker line. At this point the mean water level will be $-0.11 + (115.5)(0.0047) = 0.43$ m above the still water level.

Equations (2.53) and (2.54) indicate that the setdown is a function of the incident wave height but the slope of the mean water level through the surf zone is not. However, higher incident waves will break further seaward so the same mean water level slope will yield a higher mean water level throughout the surf zone.

It should be kept in mind that the development of Eqs. (2.53) and (2.54) employed the small-amplitude wave theory, which is less accurate in the near-shore zone. However, experiments conducted by Saville (1961) in a large two-dimensional wave tank yielded results that favorably agree with predictions from these equations. Also, the equations apply to waves approaching normal to the shore. If the waves approach obliquely to the shore, only the shore normal component of radiation stress will induce setdown and setup.

2.7 Standing Waves, Wave Reflection

A solid structure such as a vertical wall will reflect an incident wave, the amplitude of the reflected wave depending on the wave and wall characteristics. When the reflected wave passes through the incident wave a standing wave will develop. It is worthwhile to investigate the nature of wave reflection and standing waves, particularly the resulting surface profile and particle kinematics of the resulting wave motion as well as the dependence of the reflected wave characteristics on the reflecting structure makeup.

Standing Waves

Consider two waves having the same height and period but propagating in opposite (+/−) directions along the x axis. When these two waves are superimposed the resulting motion is a standing wave as depicted in Figure 2.8a. The water surface oscillates from one position to the other and back to the original position in one wave period. The arrows indicate the paths of water particle oscillation. Under a nodal point particles oscillate in a horizontal plane while under an antinodal point they oscillate in a vertical plane. When the surface is at one of the two envelope positions shown, water particles instantaneously come to rest and all of the wave energy is potential. Halfway between the envelope positions the water surface is horizontal and all wave energy is kinetic. The net energy flux (if the two component waves are identical) is zero.

The velocity potential for a standing wave can be obtained by adding the velocity potentials for the two component waves that move in opposite directions. This yields

$$\phi = \frac{gH}{\sigma} \left[\frac{\cosh k(d+z)}{\cosh kd} \right] \cos kx \sin \sigma t \quad (2.55)$$

With the velocity potential given by Eq. (2.55), we can derive the various standing wave characteristics in the same way as for a progressive wave. This yields a surface profile given by

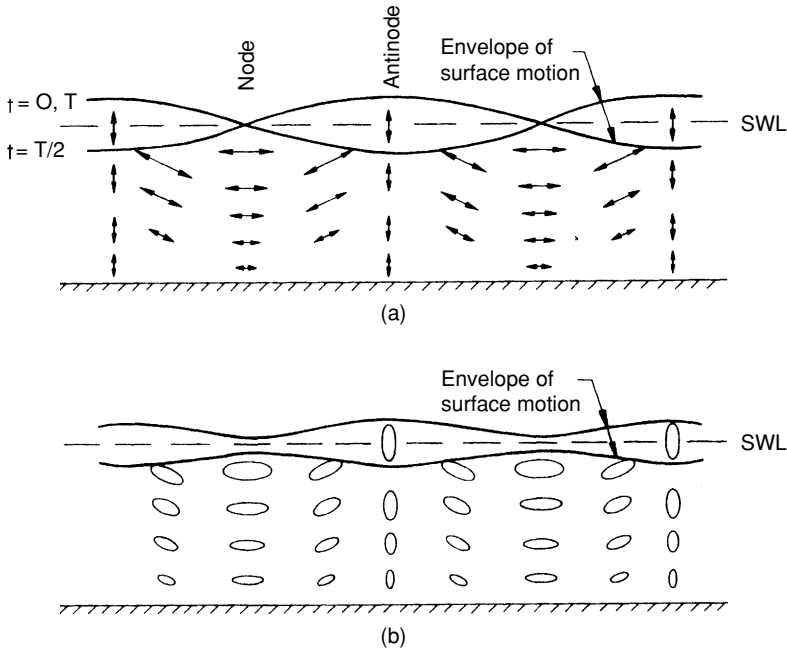


Figure 2.8. Standing wave particle motion and surface profile envelope. (a) $C_r = 1.0$, (b) $C_r < 1.0$.

$$\eta = H \cos kx \sin \sigma t; \quad (2.56)$$

horizontal and vertical velocity components given by

$$u = \frac{\pi H}{T} \left[\frac{\cosh k(d+z)}{\sinh kd} \right] \sin kx \sin \sigma t \quad (2.57)$$

and

$$w = \frac{\pi H}{T} \left[\frac{\sinh k(d+z)}{\sinh kd} \right] \cos kx \sin \sigma t; \quad (2.58)$$

a pressure field given by

$$p = -\rho g z + \rho g H \left[\frac{\cosh k(d+z)}{\cosh kd} \right] \cos kx \cos \sigma t; \quad (2.59)$$

and horizontal and vertical particle displacements given by

$$\zeta = -H \left[\frac{\cosh k(d+z)}{\sinh kd} \right] \sin kx \cos \sigma t \quad (2.60)$$

and

$$\varepsilon = H \left[\frac{\sinh k(d+z)}{\sinh kd} \right] \cos kx \cos \sigma t \quad (2.61)$$

Equations (2.56) through (2.61) demonstrate some interesting features of a standing wave. If the component progressive wave heights are H , the standing wave height is $2H$. The terms in brackets that define wave decay/shoaling effects are the same as for the equivalent progressive wave characteristic. However, at a given point $(x, -z)$ the horizontal and vertical velocity and displacement components are in phase, rather than being 90° out of phase as is the case for progressive waves. The pressure is hydrostatic under a node where particle acceleration is horizontal; but under an antinode there is a fluctuating vertical component of dynamic pressure.

The energy in a standing wave per unit crest width and for one wave length is

$$E = \frac{\rho g H^2 L}{4} \quad (2.62)$$

where, again, H is the height of a component progressive wave. This consists of potential and kinetic energy components given by

$$E_p = \frac{\rho g H^2 L}{4} \cos^2 \sigma t \quad (2.63)$$

and

$$E_k = \frac{\rho g H^2 L}{4} \sin^2 \sigma t \quad (2.64)$$

Equations (2.63) and (2.64) demonstrate, as discussed above, that at $t = 0, T/2, \dots E = E_p$ and at $T = T/4, 3T/4, \dots E = E_k$.

Wave Reflection

In a standing wave, the particle velocity under an antinode is always vertical. If a frictionless, rigid, vertical, impermeable wall were placed at the antinode the water particle motion would be unaffected. Thus, we would have a standing wave caused by the reflection of a progressive wave from the wall. The particle velocity and the pressure distribution along the wall would be given by Eqs. (2.58) and (2.59), respectively with $\cos kx = 1$.

As the wall slope decreases, the wall becomes elastic and/or the wall surface becomes rough and permeable, the reflected wave height becomes less than the incident height. The surface profile and the particle motion in this standing wave are depicted in Figure 2.8b. We can define a reflection coefficient C_r as

$$C_r = \frac{H_r}{H_i} \quad (2.65)$$

where H_r is the reflected wave height and H_i is the incident wave height (i.e., the reflection coefficient will be equal to or less than unity). Considering Figure 2.8, as the reflection coefficient decreases from unity to zero the particle trajectories transition from those for a pure standing wave to those of the orbital pattern for a pure progressive wave.

The envelope height at the antinode for a standing wave is $H_i + H_r$ and the nodal envelope height is $H_i - H_r$ (Ippen, 1966). It can also be shown the reflection coefficient equals the difference between the two envelope heights divided by the sum of the two envelope heights. When wave tank tests are being run with monochromatic waves and a reflecting structure, the wet mark on the side of the tank displays the upper envelope shown in Figure 2.8b and is an indicator of the amount of wave reflection from the structure. A wave gage mounted on a carriage and slowly moved at least one wave length along the wave tank will measure the node and antinode envelope heights which can be used to calculate the reflection coefficient for a monochromatic wave.

2.8 Wave Profile Asymmetry and Breaking

As a wave propagates into intermediate and shallow water an initial profile asymmetry develops around the horizontal axis as the wave crest steepens and the wave trough flattens. Further on an asymmetry also develops around a vertical axis through the wave crest (neither asymmetry is defined by the small amplitude wave theory). These asymmetries ultimately lead to wave instability and breaking.

Profile Asymmetry

Figure 2.9 shows a typical asymmetric wave profile as a wave propagates through relatively shallow water prior to breaking. Besides the vertical asymmetry resulting in a crest amplitude that exceeds half the wave height, the front face of the wave becomes steeper than the back face and the distance (in the direction of wave propagation) from crest to trough is less than the distance from trough to crest. These asymmetries increase as the wave moves into shallower and shallower water. They also contribute to increased particle velocities at the wave crest and ultimately to crest instability and wave breaking.

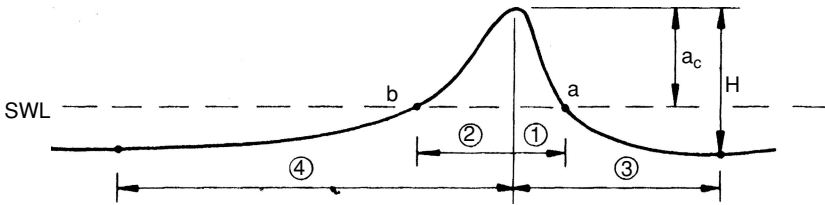


Figure 2.9. Definition of profile asymmetry terms.

Wave tank experiments were conducted by Adeyemo (1968) for intermediate depth waves shoaling on slopes from 1:18 to 1:4. These slopes are somewhat steeper than found in most nearshore areas. He presented his data in terms of four values defined as follows (see Figure 2.9):

$$\text{Vertical asymmetry} = a_c/H$$

$$\text{Slope asymmetry} = 0.5(\text{slope } a + \text{slope } b)$$

$$\text{Horizontal asymmetry (1)} = \text{distance 1}/\text{distance 2}$$

$$\text{Horizontal asymmetry (2)} = \text{distance 3}/\text{distance 4}$$

The slopes were stated in radians with slope b being a positive value and slope a being a negative value.

The experiments showed the vertical asymmetry continuously increased as the wave shoaled, reaching a maximum of between 0.62 and 0.74 at breaking. In shallower depths ($d/L < 0.10$) wave vertical asymmetry was greater for flatter slopes. Flatter slopes mean that the wave has more travel time for the asymmetry to develop. Thus, for natural beach slopes that are flatter than the experimental slopes one might expect vertical asymmetries greater than the 0.62 to 0.74 values reported. The slope and horizontal asymmetries also continuously increased as the wave shoaled; but, as opposed to vertical asymmetries steeper bottom slopes caused greater slope and horizontal asymmetries.

Wave Breaking

If a wave has sufficient height in any water depth it will break. In deep water, for a given wave period, the crest particle velocity is proportional to the wave height. From the small-amplitude wave theory, the wave celerity is independent of the wave height. So, as the wave height increases the crest particle velocity will eventually equal the wave celerity and the wave will break. In shallow water, as the water depth decreases the crest particle velocity increases and the wave celerity decreases, leading to instability and breaking.

Miche (1944) developed a simple equation for wave breaking in any water depth given by

$$\left(\frac{H}{L}\right)_{\max} = \frac{1}{7} \tanh \frac{2\pi d}{L} \quad (2.66)$$

This equation ignores the bottom slope which, as discussed above, affects development of wave asymmetry and breaking as a wave shoals. As a consequence, Eq. (2.66) gives a good indication of deep water breaking limits on wave height but only an approximate rule of thumb for shallow water breaking conditions. For deep water Eq. (2.66) reduces to

$$\left(\frac{H_o}{L_o}\right)_{\max} = \frac{1}{7} \quad (2.67)$$

indicating that the maximum wave height in deep water is limited to one-seventh of the wave length. In shallow water we have

$$\left(\frac{H}{L}\right)_{\max} = \frac{1}{7} \left(\frac{2\pi d}{L}\right)$$

or

$$\left(\frac{H}{d}\right)_{\max} = 0.9 \quad (2.68)$$

Thus, in shallow water wave heights are limited by the water depth. This is often an important consideration in the design of structures built seaward of the water's edge. No matter how high the deep water wind generated waves are, the highest wave that can reach the structure is dependent primarily on the water depth in front of the structure. Thus, as structures are extended further seaward they tend to be exposed to higher, more damaging waves.

Waves breaking on a beach are commonly classified into three categories (U.S. Army Coastal Engineering Research Center, 1984) depicted in Figure 2.10. These three breaker classes are:

Spilling. As breaking commences, turbulence and foam appear at the wave crest and then spread down the front face of the wave as it propagates toward the shore. The turbulence is steadily dissipating energy, resulting in a relatively uniform decrease in wave height as the wave propagates forward across the surf zone.

Plunging. The wave crest develops a tongue that curls forward over the front face and plunges at the base of the wave face. The breaking action and

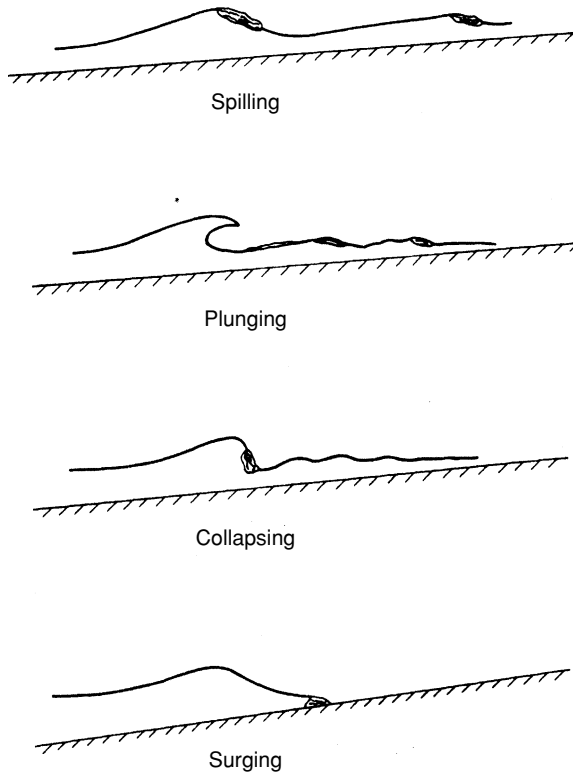


Figure 2.10. Wave breaker classification.

energy dissipation are more confined to the point of breaking than is the case for a spilling wave. The plunging tongue of water may regenerate lower more irregular waves that propagate forward and break close to the shore.

Surging. The crest and front face of the wave approximately keep their asymmetric shape as they surge across the beach slope. This form of breaking is a progression toward a standing or reflecting wave form.

While the above three classes are relatively distinct, for gradually changing incident wave steepnesses and bottom slopes there is a gradual transition from one form to the next. (Some investigators add a transitional class—collapsing breakers—between plunging and surging.) Only spilling and plunging breakers occur in deep water and they are the most common types of breakers in shallow water. Spilling breakers, accompanied by “whitecapping” if there is a strong wind, are most common in deep water. The type of breaker is important, for example, to the stability of a stone mound structure exposed to breaking waves.

It will also affect the amount of energy reflected from a slope and the elevation of wave runoff on a slope.

As discussed above, Eq. (2.68) only gives an approximate rule of thumb for wave breaking in shallow water. A number of experimenters have investigated nearshore breaking conditions in the laboratory and presented procedures for predicting the breaking height H_b and water depth at breaking d_b as a function of incident wave characteristics and bottom slope m . Figures 2.11 and 2.12, modified slightly from the U.S. Army Coastal Engineering Research Center (1984) and based on studies by Goda (1970) and Weggel (1972), are commonly used for estimating breaking conditions.

Given the beach slope, the unrefracted deep water wave height, and the wave period one can calculate the deep water wave steepness and then determine the breaker height from Figure 2.11. The regions for the three classes of wave breaker types are also denoted on this figure. With the breaker height one can then determine the water depth at breaking from Figure 2.12. Note the range of d_b/H_b values in Figure 2.12 versus the guidance given by Eq. (2.68). If a wave refracts as it propagates toward the shore, the equivalent unrefracted wave height given by

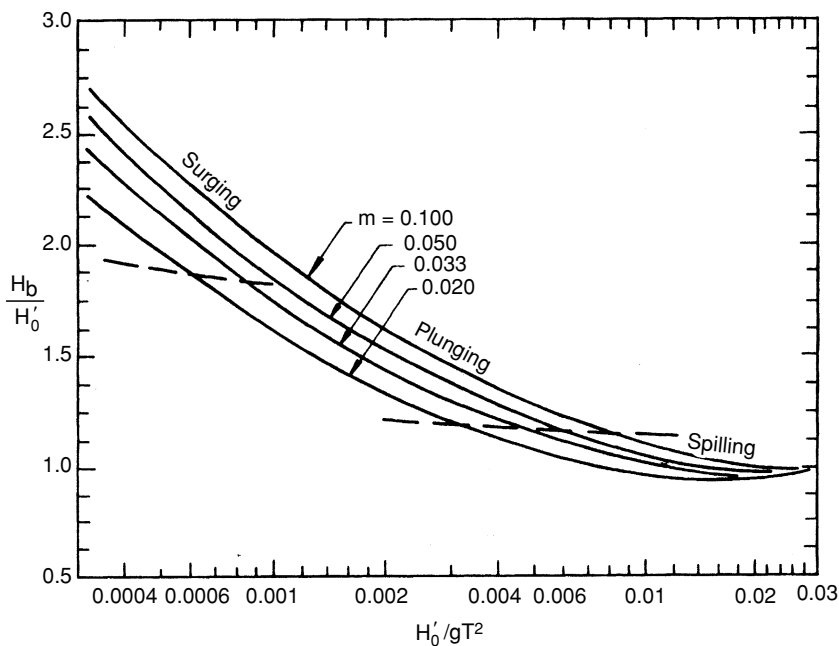


Figure 2.11. Dimensionless breaker height and class versus bottom slope and deep water steepness. (Modified from U.S. Army Coastal Engineering Research Center, 1984.)

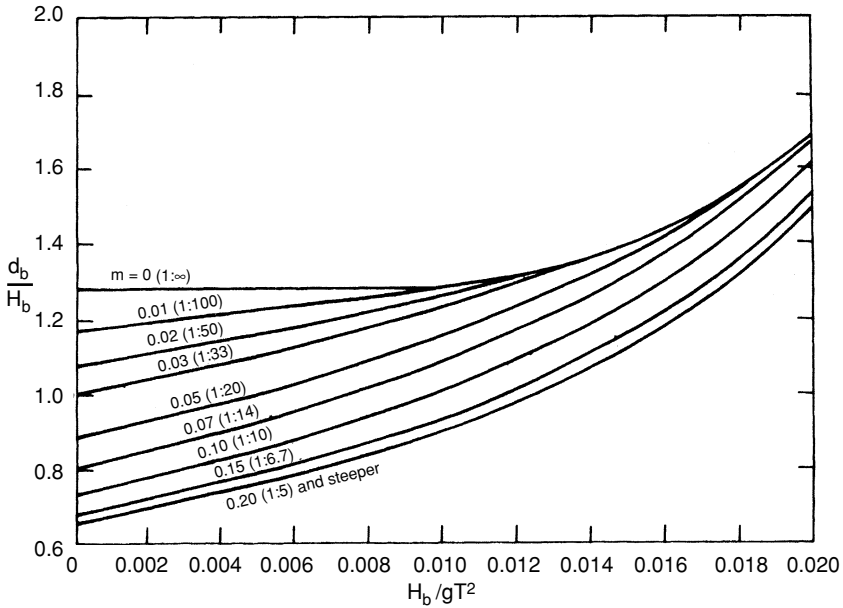


Figure 2.12. Dimensionless breaker depth versus bottom slope and breaker steepness. (Modified from U.S. Army Coastal Engineering Research Center, 1984.)

$$H'_o = K_r H_o \quad (2.69)$$

should be used in Figure 2.11.

Figures 2.11 and 2.12 do not consider the effects of wind on wave breaking. Douglass (1990) conducted limited laboratory tests on the effect of inline following and opposing winds on nearshore wave breaking. He found that offshore directed winds retarded the growth of wave height toward the shore and consequently caused the waves to break in shallower water than for the no wind condition. Onshore winds had the opposite effect but to a lesser extent. However, H_b/d_b was greater for offshore winds than for onshore winds, given the same incident wave conditions and beach slope. For the same incident waves, offshore winds caused plunging breakers when onshore winds caused waves to spill.

The design of some coastal structures is dependent on the higher wave that breaks somewhat seaward of the structure and plunges forward to hit the structure. Thus, when designing a structure for breaking wave conditions, the critical breaking depth is some point seaward of the structure that is related to the breaker plunge distance X_p as depicted in Figure 2.13. Smith and Kraus (1991), based on experiments with plane slopes and slopes having a submerged

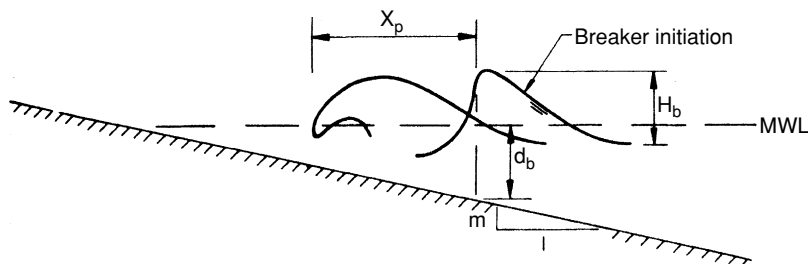


Figure 2.13. Definition sketch for breaker plunge distance.

bar that trips wave breaking, found the following relationships for the plunge distance. For plane slopes,

$$\frac{X_p}{H_b} = 3.95 \left(\frac{\sqrt{H_o/L_o}}{m} \right)^{0.25} \quad (2.70)$$

and, for slopes with a submerged bar

$$\frac{X_p}{H_b} = 0.63 \left(\frac{\sqrt{H_o/L_o}}{m} \right) + 1.81 \quad (2.71)$$

For structure design one might typically use the wave that breaks at $0.5X_p$ seaward of the structure.

2.9 Wave Runup

After a wave breaks, a portion of the remaining energy will energize a bore that will run up the face of a beach or sloped shore structure. Figure 2.14 depicts this

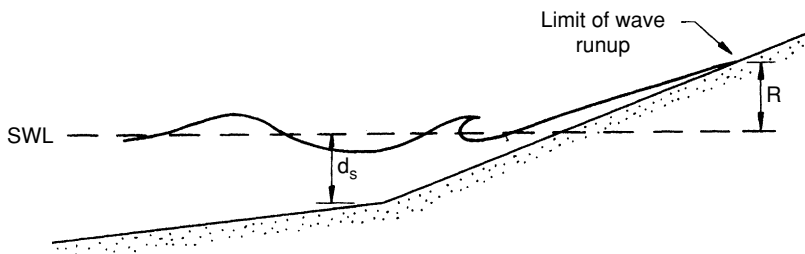


Figure 2.14. Definition sketch for wave runup.

process where the runup R is the maximum vertical elevation above the still water level to which the water rises on the beach or structure. Prediction of the wave runup is important, for example, for the determination of the required crest elevation for a sloping coastal structure or to establish a beach setback line for limiting coastal construction.

The runup depends on the incident deep water wave height and period, the surface slope and profile form if not planar, the depth d_s fronting the slope (see Figure 2.14), and the roughness and permeability of the slope face. Dimensional analysis leads to

$$\frac{R}{H'_o} = fcn\left(\alpha, \frac{H'_o}{gT^2}, \frac{d_s}{H'_o}\right) \quad (2.72)$$

for a given surface shape and condition (where $\cot \alpha = 1/m$).

Figure 2.15 is a typical plot of experimental data from a laboratory wave runup study with monochromatic waves. These data are for a smooth, planar, impermeable slope with d_s/H'_o between 1 and 3. (See U.S. Army Coastal Engineering Research Center, 1984 for similar plots for other slope conditions.) Figure 2.15 indicates that, for a given structure slope, steeper waves (higher H'_o/gT^2) have a lower relative runup (R/H'_o). Also, for most beach and revetment slopes (which are flatter than 1 on 2), the wave runup increases as the slope becomes steeper.

Table 2.1, developed from a number of laboratory experiments, gives an indication of the effect of slope surface condition on wave runup. The factor r is the ratio of the runup on the given surface to that on a smooth impermeable surface and may be multiplied by the runup determined from figures such as Figure 2.15 to predict the wave runup.

Example 2.9-1

Consider the deep water wave in Example 2.3-1 propagating toward the shore without refracting. The wave breaks and runs up on a 1:10 grass covered slope having a toe depth of 4 m. Determine the breaking wave height and the wave runup elevation on the grass-covered slope.

Solution:

For a deep water unrefracted wave height of 2 m and a period of 10 s we have

$$\frac{H'_o}{gT^2} = \frac{2}{(9.81)(10)^2} = 0.002$$

From Figure 2.11 for $m = 0.1$

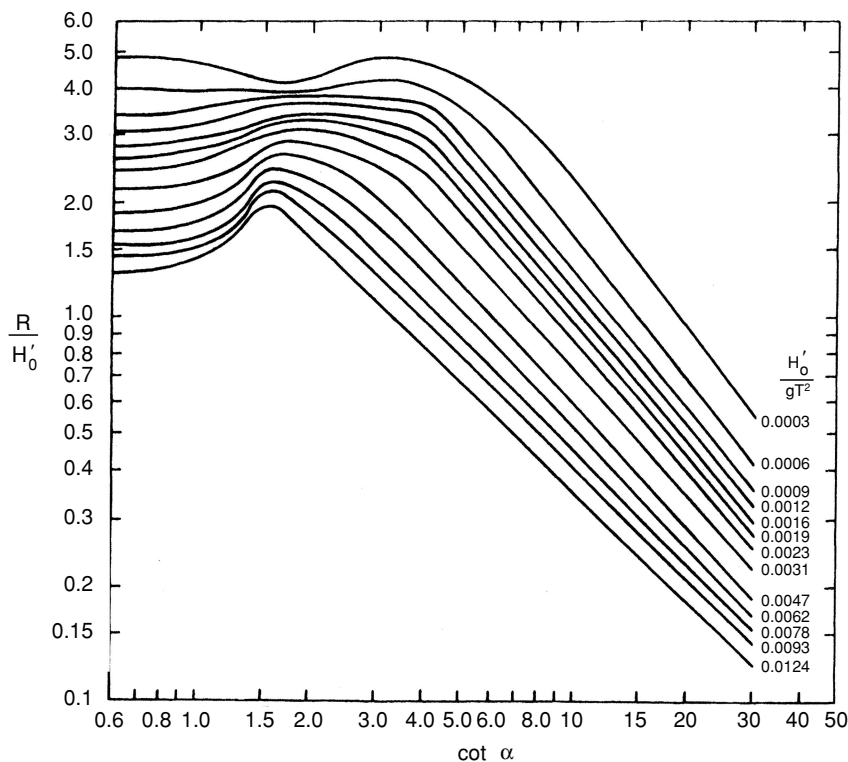


Figure 2.15. Dimensionless runup on smooth impermeable slopes versus bottom slope and incident deep water wave steepness; $1 < d_s/H'_0 < 3$. (Modified from U.S. Army Coastal Engineering Research Center, 1984.)

Table 2.1. Runup Factors for Various Slope Conditions

Slope facing	r
Concrete slabs	0.9
Placed basalt blocks	0.85–0.9
Grass	0.85–0.9
One layer of riprap on an impermeable base	0.8
Placed stones	0.75–0.8
Round stones	0.6–0.65
Dumped stones	0.5–0.6
Two or more layers of riprap	0.5
Tetrapods, etc.	0.5

From Battjes, 1970.

$$\frac{H_b}{H'_o} = 1.6$$

or

$$H_b = 1.6(2) = 3.2 \text{ m}$$

The wave would form a plunging breaker. From Figure 2.15, since $d_s/H'_o = 4/2 = 2$, at $\cot \alpha = 10$

$$\frac{R}{H'_o} = 0.85$$

or the uncorrected smooth slope runup is

$$R = 0.85(2) = 1.7 \text{ m}$$

Using $r = 0.875$ from Table 2.1 gives a runup of

$$R = 0.875(1.7) = 1.5 \text{ m}$$

on the grass-covered slope.

2.10 Summary

Experiments conducted in wave tanks (Wiegel, 1950; Eagleson, 1956; LeMehaute et al., 1968) give some indication of the accuracy of small-amplitude wave theory in predicting the transformation of monochromatic two-dimensional waves as they travel into intermediate and shallow water depths, and of the accuracy in predicting particle kinematics given the wave height and period and the water depth. A summary follows:

1. For most typical bottom slopes the dispersion equation is satisfactory for predicting the wave celerity and length up to the breaker zone.
2. For increasing beach slopes and wave steepnesses, the wave height predictions given by Eq. (2.42) will be lower than the real wave heights. This discrepancy increases as the relative depth decreases. As an example, on a 1:10 slope, for a relative depth of 0.1 and a deep water wave steepness of 0.02, the experimental wave height exceeded the calculated wave height by 15%.
3. For waves on a relatively flat slope and having a relative depth greater than about 0.1, the small-amplitude theory is satisfactory for predicting horizontal

water particle velocities. At lesser relative depths the small-amplitude theory still predicts reasonably good values for horizontal velocity near the bottom, but results are poorer (up to 50% errors on the low side) near the surface.

Limitations of the small-amplitude theory in shallow water and for high waves in deep water suggest a need to consider nonlinear or finite-amplitude wave theories for some engineering applications. The next chapter presents an overview of selected aspects of the more useful finite-amplitude wave theories, as well as their application and the improved understanding of wave characteristics that they provide.

2.11 References

- Adeyemo, M.D. (1968), "Effect of Beach Slope and Shoaling on Wave Asymmetry," in *Proceedings, 11th Conference on Coastal Engineering*, American Society of Civil Engineers, London, pp. 145–172.
- Airy, G.B. (1845), "On Tides and Waves," in *Encyclopedia Metropolitana*, London, pp. 241–396.
- Battjes, J.A. (1970), Discussion of "The Runup of Waves on Sloping Faces—A Review of the Present State of Knowledge," by N.B. Webber and G.N. Bullock, *Proceedings, Conference on Wave Dynamics in Civil Engineering*, John Wiley, New York, pp. 293–314.
- Dean, R.G. and Dalrymple, R.A. (1984), *Water Wave Mechanics for Engineers and Scientists*, Prentice-Hall, Englewood Cliffs, NJ.
- Douglass, S.L. (1990), "Influence of Wind on Breaking Waves," *Journal, Waterways, Port, Coastal and Ocean Engineering Division, American Society of Civil Engineers*, November, pp. 651–663.
- Eagleson, P.S. (1956), "Properties of Shoaling Waves by Theory and Experiment," *Transactions, American Geophysical Union*, Vol. 37, pp. 565–572.
- Goda, Y. (1970), "A Synthesis of Breaker Indices," *Transactions, Japan Society of Civil Engineers*, Vol. 2, Tokyo, pp. 227–230.
- Ippen, A.T. (1966), *Estuary and Coastline Hydrodynamics*, McGraw-Hill, New York.
- LeMehaute, B., Divoky, D., and Lin, A. (1968), "Shallow Water Waves: A Comparison of Theories and Experiments," in *Proceedings, 11th Conference on Coastal Engineering*, American Society of Civil Engineers, London, pp. 86–107.
- Longuet-Higgins, M.S. and Stewart, R.W. (1964), "Radiation Stress in Water Waves: A Physical Discussion, with Applications," *Deep Sea Research*, Vol. 11, pp. 529–549.
- Miche, M. (1944), "Movements Ondulatoires des Mers en Profondeur Constante ou Decroissante," *Annales des Ponts et Chaussees*, pp. 25–78, 131–164, 270–292, 369–406.
- Saville, T., Jr. (1961), "Experimental Determination of Wave Setup," in *Proceedings, 2nd Conference on Hurricanes*, U.S. Department of Commerce National Hurricane Project, Report 50, pp. 242–252.

- Smith, E.R. and Kraus, N.C. (1991), "Laboratory Study of Wave Breaking Over Bars and Artificial Reefs," *Journal, Waterway, Port, Coastal and Ocean Engineering Division, American Society of Civil Engineers*, July/August, pp. 307–325.
- Sorensen, R.M. (1978), *Basic Coastal Engineering*, John Wiley, New York.
- Sorensen, R.M. (1993), *Basic Wave Mechanics for Coastal and Ocean Engineers*, John Wiley, New York.
- U.S. Army Coastal Engineering Research Center (1984), *Shore Protection Manual*, U.S. Government Printing Office, Washington, DC.
- Weggel, J.R. (1972), "Maximum Breaker Height," *Journal, Waterway, Port, Coastal and Ocean Engineering Division, American Society of Civil Engineers*, November, pp. 529–548.
- Wiegel, R.L. (1950), "Experimental Study of Surface Waves in Shoaling Water," *Transactions, American Geophysical Union*, Vol. 31, pp. 377–385.
- Wiegel, R.L. (1964), *Oceanographical Engineering*, Prentice-Hall, Englewood Cliffs, NJ.

2.12 Problems

1. A two-dimensional wave tank has a still water depth of 1.9 m and a 1:20 plane slope installed with its toe at the tank midpoint. The tank is 1 m wide. A wave generator produces monochromatic waves that, when measured at a wave gage installed before the toe of the slope, have a height of 0.5 m and a period of 2.8 s.
 - (a) Determine the wave length, celerity, group celerity, energy, and energy density at the wave gage.
 - (b) At the instant that a wave crest passes the wave gage, determine the water particle velocity and acceleration below the gage at mid depth.
 - (c) Is the wave passing the gage a deep water wave? If not, what would the equivalent deep water length, celerity, group celerity, energy, and energy density be? Compare these values to those in part a.
 - (d) Calculate the wave height as a function of distance along the slope from the toe to the point at which the wave breaks.
2. An ocean bottom-mounted pressure sensor measures a reversing pressure as a train of swells propagates past the sensor toward the shore. The pressure fluctuations have a 5.5 s period and vary from a maximum of 54.3 kN/m^2 to a minimum of 41.2 kN/m^2 .
 - (a) How deep is the pressure sensor (and bottom) below the still water level?
 - (b) Determine the wave height, celerity, group celerity, energy, and power as it passes the sensor.
 - (c) As a wave crest is passing the sensor determine the water particle velocity and acceleration at a point 1.5 m above the bottom.

- (d) Calculate the deep water wave celerity, length, group celerity, energy, and power if the wave propagates along a line perpendicular to the shore without refracting.
- (e) The nearshore bottom slope is 1:30. Calculate and plot the wave height as a function of position from deep water into the point at which the wave breaks.
3. Offshore, in deep water, a wave gage measures the height and period of a train of waves to be 2 m and 7.5 s, respectively. The wave train propagates toward the shore in a normal direction without refracting and the nearshore bottom slope is 1:40. It passes the outer end of a pier located in water 4.5 m deep.
 - (a) Determine the wave length, celerity, group celerity, energy density, and power in deep water.
 - (b) Determine the wave length, height, celerity, group celerity, energy density, and power at the end of the pier. Is this a deep, transitional or shallow water wave at the end of the pier?
 - (c) At the instant that a wave crest passes the end of the pier, what is the pressure at a point 2 m below the still water level?
 - (d) Calculate the horizontal components of the water particle velocity and acceleration at this point 2 m below the still water level 1 s before the wave crest passes the end of the pier.
 - (e) At what water depth will the wave break? What will the wave height be as the wave breaks? What type of breaker will it be?
4. A wave gage mounted on the seaward end of a pier where the water depth is 6 m, measures a wave having $H = 2.3$ m and $T = 7.1$ s. This wave is one of a train of waves that is traveling normal to the shore without refracting. The bottom slope is 1:30.
 - (a) Determine the deep water wave height and energy.
 - (b) Determine the wave height and water depth where the wave breaks.
 - (c) What are the water particle pressure, velocity and acceleration 1.7 m above the bottom 1.3 seconds after the wave crest passes the gage?
5. A wave has a height of 1.5 m in water 5 m deep and a wave period of 6 s. Plot the horizontal component of velocity, the vertical component of acceleration, and the dynamic pressure at a point 2 m below the still water level versus time for a 6-s interval. Plot the three values on the same diagram and comment on the results.
6. Estimate the maximum height wave that can be generated in a wave tank having water 1.8 m deep if the wave period is 1 s and if the period is 3 s.
7. A wave has a measured height of 1.4 m in water 5.6 m deep. If it shoals on a 1:50 slope how wide will the surf zone be? Assume the wave propagates normal to the shore without refracting.
8. A pressure gage located 1 m off the bottom in water 10 m deep measures an average maximum pressure of 100 kN/m^2 having an average fluctuation period of 12 s. Determine the height and period of the wave causing the measured pressure fluctuation.

9. Derive an equation for the horizontal component of particle convective acceleration in a wave. Compare the horizontal components of convective and local acceleration versus time for a time interval of one wave period, at a distance of 2 m below the still water level and for a 1 m high 6 s wave in water 5 m deep.

10. Demonstrate, using Eq. (2.43), that $C_g = C/2$ in deep water and $C_g = C$ in shallow water.

11. Calculate and plot n and L nondimensionalized by dividing by the deep water values for n and L , as a function of d/L for d/L from 0.5 to 0.05.

12. Derive the equations for the horizontal and vertical components of particle acceleration in a standing wave, starting from the velocity potential [Eq. (2.55)].

13. As the tide enters a river and propagates upstream, the water depth at a given location is 3.7 m. At this location the tide range is 1 m. If the dominant tidal component has a period of 12.4 hours, estimate the peak flood tidal flow velocity at this location in the river.

14. Consider the conditions given in Problem 13. At a location in the river where the water depth is 5.1 m estimate the tide range and peak flood tidal flow velocity.

15. The first wave of a group of waves advancing into still water is 0.30 m high. The water depth is 4.5 m and the wave period is 2 s. How high is this wave 8 s later?

16. Consider a 1 m high, 4 s wave in water 5 m deep. Plot sufficient velocity potential lines to define their pattern and then sketch in orthogonal streamlines.

17. Consider a deep water wave having a height of 2.1 m and a period of 9 s shoaling on a 1:50 slope without refraction. Calculate, for comparison, the crest particle velocity in deep water, at $d = 20$ m, and just prior to breaking. Calculate the wave celerity just prior to breaking and compare it to the crest particle velocity. Comment on the reason for any discrepancies.

18. A 12 s, 2 m high wave in deep water shoals without refracting. Calculate the maximum horizontal velocity component and the maximum horizontal displacement from the mean position for a particle 5 m below the still water level in deep water and where the water depth is 6 m.

19. As the wave given in Problem 4 propagates toward the shore determine the mean water level setdown at the breaker line and the setup 40 m landward of the breaker line.

20. Equation (2.56) defines the surface profile as a function of time for a standing wave. From this, derive the potential energy per wave length and the potential energy density, both as a function of time. Realizing that at the instant a standing wave has zero particle velocity throughout, all energy is potential energy, determine the total and kinetic energies per wave length and the total and kinetic energy densities.

21. For the conditions in Example 2.6-1, calculate and plot (to a 10:1 vertical scale distortion) the bottom, still water line, and the mean water line from a point 20 m seaward of the breaker point to the shoreline.

22. A wave having a height of 2.4 m and a period of 8 s in deep water is propagating toward the shore without refracting. A water particle velocity of 0.25 m/s on the bottom is required to initiate movement of the sand on the sea floor. At what water depth will sand movement commence as the wave shoals?

23. Using shallow water wave equations for celerity and water particle velocity and the criteria that at incipient breaking the crest particle velocity equals the wave celerity, derive a criterion for wave breaking. Comment on the result of this derivation.

24. To an observer moving in the direction of a monochromatic wave train at the wave celerity, the wave motion appears to be steady. The surface particle velocity at the wave crest $U_c = C_o - \pi H/T$ and at the trough $U_t = C_o + \pi H/T$ for a deep water wave. Apply the Bernoulli equation between these two points to derive Eq. (2.16).

25. For a given wave height and period and water depth which of the following wave parameters depend on the water density: celerity, length, energy density, particle pressure, and particle velocity at a given depth? Explain each answer.

26. How does increased water viscosity affect a wave train as it propagates toward the shore?

27. Waves with a period of 10 s and a deep water height of 1 m arrive normal to the shore without refracting. A 100-m long device that converts wave motion to electric power is installed parallel to the shore in water 6 m deep. If the device is 45% efficient what power is generated?

28. Demonstrate that the velocity potential defined by Eq. (2.9) does represent irrotational flow.

29. A wave with a period of 7 s propagates toward the shore from deep water. Using the limit presented in this chapter, at what water depth does it become a shallow water wave? If the deep water wave height is 1 m would this wave break before reaching the shallow water depth? Assume that no refraction occurs and that the nearshore slope is 1:30.

3

Finite-Amplitude Waves

The small-amplitude wave theory was formulated as a solution to the Laplace equation with the required surface (two) and bottom (one) boundary conditions [Eqs. (2.1), (2.3), (2.4), and (2.6)]. But the two surface boundary conditions had to be linearized and then applied at the still water level rather than at the water surface. This requires that H/d and H/L be small compared to unity. Consequently, the small-amplitude wave theory can be applied over the complete range of relative water depths (d/L), but it is limited to waves of relatively small amplitude relative to the water depth (for shallow water waves) and wave length (for deep water waves).

There is no general solution to the Laplace equation and three gravity wave boundary conditions. All wave theories require some form of approximation or another. Typically, the finite-amplitude wave theories relax the requirement that either H/d or H/L be small to produce a theory that is applicable for finite-amplitude waves over some specific range of wave conditions. A finite H/d yields a theory useful in shallow water whereas a finite H/L yields a theory more appropriate for deep water.

The intent of this chapter is to provide a brief overview of selected useful finite-amplitude wave theories and to employ these theories to provide additional insight into the characteristics of two-dimensional waves. A discussion of the application of these finite-amplitude theories to engineering analysis will also be presented.

3.1 Finite-Amplitude Wave Theory Formulation

Finite-amplitude wave theories are generally of two types. There are numerical theories that employ a finite difference, finite element, or boundary integral method to solve the Laplace and boundary condition equations. There are also analytical theories in which the velocity potential (and other parameters such as the surface amplitude and wave celerity) is written as a power series that is solved by successive approximations or by the perturbation approach.

For numerical theories a computer solution of the numerical equations yields tabulated values of the desired wave characteristics such as the surface profile, particle velocity and acceleration, dynamic pressure, energy and momentum flux, etc. as a function of selected values of wave height and period and water depth. On the other hand, the analytical theories produce specific equations for the various wave characteristics which are given in terms of the wave height and period and the water depth. Both numerical and analytical theories are not complete solutions of the wave boundary value problem, but infinite series solutions that must be truncated at some point (e.g., truncation of a series after the third term yields a third-order solution).

In this chapter we briefly consider four finite-amplitude wave theories. The Stokes theory for deep water waves and the cnoidal and solitary theories for shallow water waves are useful analytical theories. Dean's stream function numerical wave theory is a commonly used numerical theory applicable to finite-amplitude waves throughout the range of relative water depths. For a more detailed presentation of these and other finite-amplitude wave theories see Wiegel (1964), Ippen (1966), Sarpkaya and Isaacson (1981), and Dean and Dalrymple (1984).

If any of the finite-amplitude wave theories are to be used in practice, two important considerations arise. The first is the choice of which theory to use to calculate wave characteristics for a given combination of wave height and period and water depth. As indicated above, most finite-amplitude theories are developed for a specific range of relative depths and the higher order solutions for a particular theory are often more appropriate for higher steepness waves. In some cases, one characteristic may be best predicted by one theory and another by a different theory. The finite-amplitude theories are generally much more complex and difficult to apply than the small-amplitude theory, but generally yield better results. Is the increased effort justified given the accuracy of analysis desired and the accuracy to which the input wave conditions are known?

A second consideration is the difficulty of employing finite-amplitude wave theories to calculate wave transformations over a wide range of water depths, since these theories are commonly developed for specific ranges of relative water depth. (In practice, wave conditions are typically forecast for an offshore deep water location and then must be transformed to some nearshore point for coastal design analysis.) This factor, plus the ease in applying the theory, generally induces the coastal engineer to apply the small-amplitude wave theory for most analyses.

These two considerations are addressed further in Section 3.6.

3.2 Stokes Waves

Stokes (1847), employing perturbation techniques to solve the wave boundary value problem, developed a theory for finite-amplitude waves that he carried to the second order. In this theory all the wave characteristics (velocity potential,

celerity, surface profile, particle kinetics, etc.) are formulated in terms of a power series in successively higher orders of the wave steepness H/L . A condition of this theory is that H/d be small so the theory is applicable only in deep water and a portion of the intermediate depth range.

As the deep water wave steepness increases improved accuracy can generally be achieved (at the price of more onerous equations to work with) if the Stokes theory is carried out to higher orders. Various higher order approximations to the Stokes theory have been developed. For example, see Skjelbreia (1959) for a third-order theory, Skjelbreia and Hendrickson (1961) for a fifth-order theory, and Schwartz (1974) for much higher order solutions based on calculations using a powerful computer. We will present selected elements of the second-order and third-order theories that demonstrate some of the interesting characteristics of finite amplitude waves (vis-à-vis small-amplitude waves). For engineering applications the second-order and possibly the fifth-order theories are most commonly used.

For the Stokes theory second-order solution the velocity potential is given by

$$\begin{aligned}\Phi = & \frac{gH}{2\sigma} \frac{\cosh k(d+z)}{\cosh kd} \sin(kx - \sigma t) \\ & + \frac{3\pi CH}{16} \left(\frac{H}{L}\right) \frac{\cosh 2k(d+z)}{\sinh^4(kd)} \sin 2(kx - \sigma t)\end{aligned}\quad (3.1)$$

Inspection of Eq. (3.1) reveals a number of important features of the second-order theory. Comparison of Eq. (3.1) with Eq. (2.9) shows that the first term on the right is the small-amplitude theory velocity potential. The magnitude of the second term on the right is dependent on the wave steepness, a ratio that has a numerical value that is significantly less than unity but that increases as the wave amplitude increases for a given wave period. The second term on the right also has a frequency that is twice that of the small-amplitude term.

The surface profile is given by

$$\begin{aligned}\eta = & \frac{H}{2} \cos(kx - \sigma t) \\ & + \frac{\pi H}{8} \left(\frac{H}{L}\right) \frac{\cosh kd(2 + \cosh 2kd)}{\sinh^3 kd} \cos 2(kx - \sigma t)\end{aligned}\quad (3.2)$$

for which the same comments can be made as were made above for the velocity potential. The effect of the second-order term having twice the frequency of the small-amplitude or first-order term is that the two components of surface amplitude reinforce (i.e., are in phase) each other at the wave crest and oppose each other at the wave trough. This yields a surface profile vertical asymmetry (more peaked wave crest and flatter wave trough than a cosine profile given by the small-amplitude theory) that grows as the wave steepness increases.

In the second-order Stokes theory, the wave celerity is the same as for the small-amplitude wave theory [given by Eq. (2.12)]. Thus, to the second order, waves are still period dispersive but not amplitude dispersive. For the Stokes third-order theory the dispersion relationship becomes

$$C^2 = \frac{g}{k} \tanh kd \left[1 + \left(\frac{\pi H}{L} \right)^2 \left(\frac{9 + 8 \cosh^4(kd) - 8 \cosh^2(kd)}{8 \sinh^4(kd)} \right) \right] \quad (3.3)$$

[It should be noted that small variations on Eq. (3.3) for the third-order celerity have been given by various authors, e.g., see Wiegel (1964) and Ippen (1966).] Thus, to the third order, wave celerity is amplitude as well as period dispersive. For the same wave period higher waves travel faster than lower waves. For the limiting steepness in deep water ($H_0/L_0 = 1/7$) the third-order theory yields a wave celerity that is about 10% greater than the celerity given by the small-amplitude theory. A greater celerity for the same wave period means that the wave length would also be 10% larger (since $L = CT$).

For deep water, Eq. (3.2) becomes

$$\eta = \frac{H_0}{2} \cos(kx - \sigma t) + \frac{\pi H_0}{4} \left(\frac{H_0}{L_0} \right) \cos 2(kx - \sigma t) \quad (3.4)$$

which yields the following relationships for the amplitude of the wave crest a_c and wave trough a_t :

$$\begin{aligned} a_c &= \frac{H_0}{2} + \frac{\pi H_0^2}{4L_0} \\ a_t &= \frac{H_0}{2} - \frac{\pi H_0^2}{4L_0} \end{aligned} \quad (3.5)$$

From Eq. (3.5) for the limiting wave steepness in deep water (1/7) we have $a_c = 0.611H$ and $a_t = 0.389H$. Equation (3.2) shows that as a wave enters intermediate water depths the asymmetry will increase over its equivalent deep water value.

Example 3.2-1

A 6 m high, 7 s period wave is propagating over a water depth that is just at the deep water limit. Using the equations presented above, calculate the wave celerity and length. Also, determine the wave crest and trough amplitudes. Compare the results to those from the small-amplitude wave theory.

Solution:

For deep water Eq. (3.3) reduces to

$$C_0 = \sqrt{\frac{gL_0}{2\pi} \left(1 + \left(\frac{\pi H_0}{L_0} \right)^2 \right)}$$

Inserting $L_0 = C_0 T$ yields

$$C_0 = \sqrt{\frac{gC_0 T}{2\pi} \left(1 + \left(\frac{\pi H_0}{C_0 T} \right)^2 \right)}$$

which can be solved ($T = 7$ s and $H_0 = 6$ m) by trial to yield

$$C_0 = 11.54 \text{ m/s}$$

$$L_0 = 80.78 \text{ m}$$

For the small-amplitude theory, Eq (2.16) yields $C_0 = 10.93$ m/s and Eq (2.2) yields $L_0 = 76.50$ m. The Stokes theory values are both 5.5% higher. The steepness of this wave is $6/80.78 = 0.074$ or about half the limiting steepness of $1/7$.

From Eq. (3.5) we have

$$a_c = \frac{6}{2} + \frac{\pi(6)^2}{4(80.78)} = 3.35^{\text{m}}$$

$$a_t = \frac{6}{2} - \frac{\pi(6)^2}{4(80.78)} = 2.65^{\text{m}}$$

With increasing wave steepness the second-order term in Eq. (3.2) increases in size relative to the first-order term. This causes an accelerated “peaking” at the wave crest where the two terms are in phase; but at the wave trough the first- and second-order terms are out of phase, causing the trough to become increasingly flat. A point is reached where the trough surface becomes horizontal. Increases in wave steepness beyond this point cause a hump to form and grow at the wave trough. This hump is not a real wave phenomenon and its appearance is an indication that the theory is being used beyond its appropriate limit. If we set a limit of applicability at the point where the trough becomes horizontal, the maximum wave steepness for application of the second-order Stokes theory would be

$$\frac{H}{L} = \frac{\sinh^3 kd}{\pi \cosh kd(2 + \cosh 2kd)} \quad (3.6)$$

In deep water the steepness value given by Eq. (3.6) is greater than 1/7 so the limit has no practical meaning. For a relative depth (d/L) as small as 0.1 the limiting steepness from Eq. (3.6) is 0.021. This puts a significant restriction on the use of the second-order theory as the wave propagates into shallower water.

The Stokes second-order equations for particle velocity and acceleration follow:

$$u = \frac{\pi H}{T} \frac{\cosh k(d+z)}{\sinh kd} \cos(kx - \sigma t) + \frac{3(\pi H)^2}{4TL} \frac{\cosh 2k(d+z)}{\sinh^4(kd)} \cos 2(kx - \sigma t) \quad (3.7)$$

$$w = \frac{\pi H}{T} \frac{\sinh k(d+z)}{\sinh kd} \sin(kx - \sigma t) + \frac{3(\pi H)^2}{4TL} \frac{\sinh 2k(d+z)}{\sinh^4(kd)} \sin 2(kx - \sigma t) \quad (3.8)$$

$$a_x = \frac{2\pi^2 H}{T^2} \frac{\cosh k(d+z)}{\sinh kd} \sin(kx - \sigma t) + \frac{3\pi^3 H^2}{T^2 L} \frac{\cosh 2k(d+z)}{\sinh^4 kd} \sin 2(kx - \sigma t) \quad (3.9)$$

$$a_z = -\frac{2\pi^2 H}{T^2} \frac{\sinh k(d+z)}{\sinh kd} \cos(kx - \sigma t) - \frac{3\pi^3 H^2}{T^2 L} \frac{\sinh 2k(d+z)}{\sinh kd} \cos 2(kx - \sigma t) \quad (3.10)$$

The second-order terms in Eqs. (3.7) to (3.10) also have twice the frequency of the first-order terms, leading to asymmetries in the particle velocity and acceleration as a particle completes its orbit. The particle velocity and acceleration are increased under the wave crest and diminished under the wave trough. Again, these asymmetries increase as the wave steepness increases.

Since the horizontal component of particle velocity is maximum at the wave crest and trough (and zero at the still water positions), this crest/trough asymmetry in velocity causes particle orbits that are not closed and results in a small drift of the water particles in the direction of wave propagation. This mass transport is also evident in the second-order particle displacement equations.

$$\begin{aligned}
\zeta = & -\frac{H}{2} \frac{\cosh k(d+z)}{\sinh kd} \sin(kx - \sigma t) \\
& + \frac{\pi H^2}{8L \sinh^2(kd)} \left(1 - \frac{3 \cosh 2k(d+z)}{2 \sinh^2(kd)} \right) \sin 2(kx - \sigma t) \\
& + \frac{\pi H^2}{4L} \frac{\cosh 2k(d+z)}{\sinh^2(kd)} \sigma t
\end{aligned} \tag{3.11}$$

$$\begin{aligned}
\varepsilon = & \frac{H}{2} \frac{\sinh k(d+z)}{\sinh kd} \cos(kx - \sigma t) \\
& + \frac{3\pi H^2}{16L} \frac{\sinh 2k(d+z)}{\sinh^4(kd)} \cos 2(kx - \sigma t)
\end{aligned} \tag{3.12}$$

Note that the last term in Eq. (3.11) is not periodic but continually increases with time, indicating a net forward transport of water particles as the wave propagates. If we divide the last term in Eq. (3.11) by time we have the second-order equation for the mass transport velocity

$$\bar{u} = \frac{\pi^2 H^2}{2TL} \frac{\cosh 2k(d+z)}{\sinh^2(kd)} \tag{3.13}$$

Since the surface particle velocity at the crest of a wave in deep water is $\pi H/T$ to the first order, Eq. (3.13) indicates that the surface mass transport velocity is of the order of the crest particle velocity times the wave steepness and thus generally much smaller than the crest particle velocity.

Example 3.2-2

Consider the wave discussed in Example 3.2-1. Calculate the mass transport velocity versus distance below the water surface level for $z = 0, -0.1, -0.2, -0.3, -0.4$, and -0.5 times the wave length. Compare this to the wave celerity and crest particle velocity.

Solution:

For the first or second order, the wave length is given by Eq. (2.17) or

$$L_0 = \frac{9.81(7)^2}{2\pi} = 76.5 \text{ m}$$

Thus, the water depth is $76.5/2 = 38.25 \text{ m}$ and $k = 2\pi/76.5 = 0.0821$. Then, the mass transport velocity, given by Eq. (3.13), becomes

$$\begin{aligned}\bar{u} &= \frac{\pi^2(6)^2}{2(7)(76.5)} \frac{\cosh 2(0.0821)(d+z)}{\sinh^2(\pi)} \\ &= 0.0025 \cosh 0.164(d+z)\end{aligned}$$

where $d+z$ is the distance up from the bottom. Proceeding with the calculations yields:

z (m)	$d+z$ (m)	\bar{u} (m/s)
0	38.25	0.665
-7.65	30.60	0.189
-15.30	22.95	0.053
-22.95	15.30	0.015
-30.60	7.65	0.004
-38.25	0	0.002

Note the rapid decay in the mass transport velocity with distance below the still water level. From Eq. (2.16) the wave celerity is

$$C_0 = \frac{9.81(7)}{2\pi} = 10.93 \text{ m/s}$$

for both the first and second order. Using the first-order crest particle velocity as sufficient for comparison purposes we have

$$u_c = \frac{\pi(6)}{7} = 2.69 \text{ m/s}$$

Thus, the celerity, crest particle velocity, and mass transport velocity at the water surface are 10.93 m/s, 2.69 m/s and 0.665 m/s respectively for this wave.

The pressure field in a wave according to the Stokes second order is

$$\begin{aligned}p &= \rho g z + \frac{\rho g H}{2} \frac{\cosh k(d+z)}{\cosh kd} \cos(kx - \sigma t) \\ &+ \frac{3\pi\rho g H^2}{4L \sinh 2kd} \left[\frac{\cosh 2k(d+z)}{\sinh^2(kd)} - \frac{1}{3} \right] \cos 2(kx - \sigma t) \\ &- \frac{\pi\rho g H^2}{4L \sinh 2kd} (\cosh 2k(d+z) - 1)\end{aligned} \quad (3.14)$$

Besides the usual higher frequency second-order term, there is a noncyclic last term on the righthand side. This noncyclic term has a zero value at the bottom which is in keeping with the requirement that if there is no vertical velocity component at the

bottom boundary there can be no vertical momentum flux so the time average pressure must balance the time average weight of water above. Away from the bottom there is a time average vertical momentum flux owing to the crest to trough asymmetry in the vertical velocity component. This produces the above-zero time average dynamic pressure given by this last term on the right in Eq. (3.14).

3.3 Cnoidal Waves

The applicability of Stokes theory diminishes as a wave propagates across decreasing intermediate/shallow water depths. Keulegan (1950) recommended a range for Stokes theory application extending from deep water to the point where the relative depth is approximately 0.1. However, the actual Stokes theory cutoff point in intermediate water depths depends on the wave steepness as well as the relative depth. For steeper waves, the higher order terms in the Stokes theory begin to unrealistically distort results at deeper relative depths. For shallower water, a finite-amplitude theory that is based on the relative depth is required. Cnoidal wave theory and in very shallow water, solitary wave theory, are the analytical theories most commonly used for shallower water.

Cnoidal wave theory is based on equations developed by Korteweg and de Vries (1895). The resulting equations contain Jacobian elliptical functions, commonly designated cn , so the name cnoidal is used to designate this wave theory. The most commonly used versions of this theory are to the first order, but these theories are still capable of describing finite-amplitude waves. The deep water limit of cnoidal theory is the small-amplitude wave theory and the shallow water limit is the solitary wave theory. Owing to the extreme complexity of applying the cnoidal theory, most authors recommend extending the use of the small-amplitude, Stokes higher order, and solitary wave theories to cover as much as possible of the range where cnoidal theory is applicable.

The most commonly used presentation of the cnoidal wave theory is from Wiegel (1960), who synthesized the work of earlier writers and presented results in as practical a form as possible. Elements of this material, including slight modifications presented by the U.S. Army Coastal Engineering Research Center (1984), are presented herein. The reader should consult Wiegel (1960, 1964) for more detail and the information necessary to make more extensive cnoidal wave calculations.

Some of the basic wave characteristics from cnoidal theory, such as the surface profile and the wave celerity, can be presented by diagrams that are based on two parameters, namely k^2 and U_r . The parameter k^2 is a function of the water depth, the wave length, and the vertical distance up from the bottom to the water surface at the wave crest and trough. It varies from 0 for the small-amplitude limit to 1.0 for the solitary wave limit as the ratio of the crest amplitude to wave height varies from 0 to 1.0 for the two wave theories. U_r , which is known as the

Ursell number (Ursell, 1953), is a dimensionless parameter given as $L^2 H / d^3$ that is also useful for defining the range of application for various wave theories. From Hardy and Kraus (1987) the Stokes theory is generally applicable for $U_r < 10$ and the cnoidal theory for $U_r > 25$. The theories are equally applicable in the range $U_r = 10$ to 25.

Figures 3.1 and 3.2, which are taken from Wiegel (1960) with slight modification, allow us to determine the cnoidal wave length, celerity, and surface profile, given the wave period and height and the water depth. From Figure 3.1 $T(g/d)^{0.5}$ and H/d yield the value of k^2 which then yields (using the dashed line) a value for the Ursell number. The Ursell number indicates how appropriate cnoidal theory is for our application and allows the wave length to be calculated if the wave height and water depth are known. This then gives the wave celerity from $C = L/T$.

Figure 3.2 is a plot of the water surface amplitude with reference to the elevation of the wave trough ($-\eta_t$) as a function of dimensionless horizontal distance x/L . Thus, $\eta - (-\eta_t) = \eta + \eta_t$. From Figure 3.2, with the value of k^2 we can define the complete surface profile relative to the still water line. Note that when k^2 is near zero the surface profile is nearly sinusoidal, whereas when k^2 is close to unity the profile has a very steep crest and a very flat trough with the ratio of crest amplitude to wave height approaching unity.

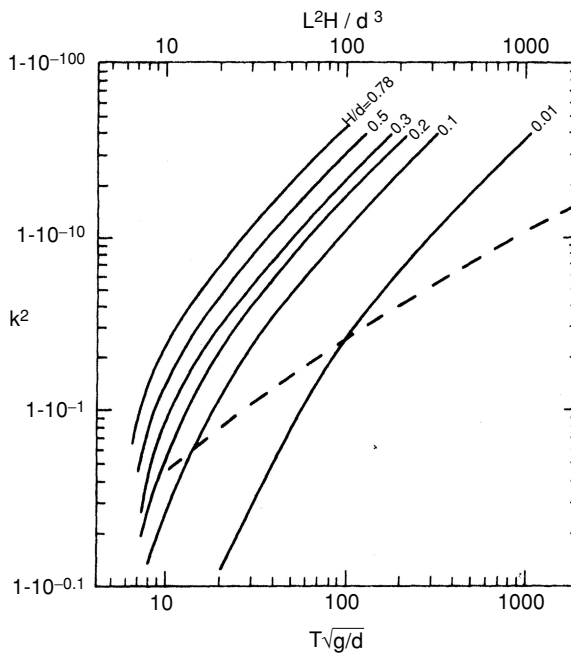


Figure 3.1. Solution for basic parameters of cnoidal wave theory. (Modified from Wiegel, 1964.)

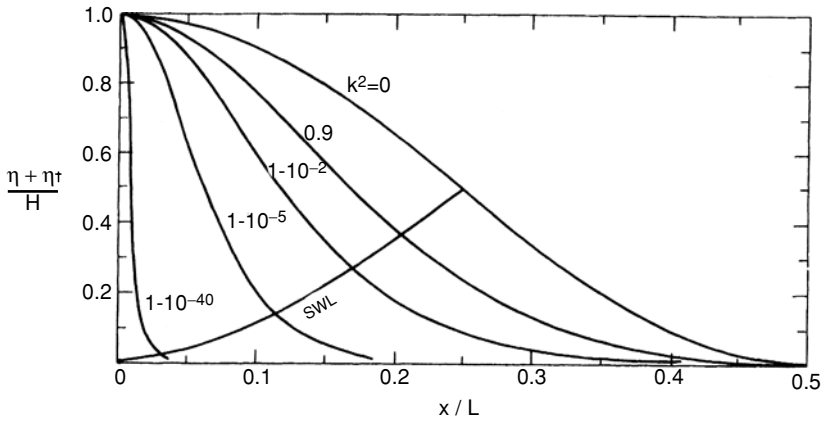


Figure 3.2. Cnoidal wave theory surface profiles. (Modified from U.S. Army Coastal Engineering Research Center, 1984.)

Example 3.3-1

A wave having a period of 14 s and a height of 2 m is propagating in water 4 m deep. Using cnoidal wave theory determine the wave length and celerity and compare the results to the small-amplitude theory. Also plot the wave surface profile.

Solution:

To employ Figure 3.1 we need

$$\frac{H}{d} = \frac{2}{4} = 0.5$$

and

$$T\sqrt{g/d} = 14\sqrt{9.81/4} = 21.9$$

This gives

$$k^2 = 1 - 10^{-5.3}$$

and

$$U_r = 300$$

So the cnoidal theory is quite appropriate for this wave condition. From the Ursell number the wave length is

$$L = \sqrt{\frac{(4)^3 300}{2}} = 98.0 \text{ m}$$

and

$$C = 98.0/14 = 7.0 \text{ m/s}$$

Since $d/L = 4/98$ this is a shallow water wave. Using the procedure demonstrated in Example 2.3–2 for the small-amplitude wave theory we have

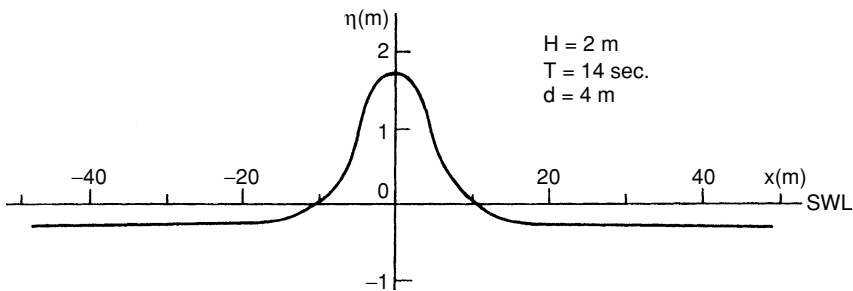
$$C = \sqrt{9.81(4)} = 6.26 \text{ m/s}$$

and

$$L = 6.26(14) = 87.6 \text{ m}$$

The difference between the results of the two theories is 11.7% with the small amplitude theory yielding smaller values of C and L for a given H , T , and d .

With the value of k^2 and the wave length and height, the surface profile can be determined from Figure 3.2. A plot of the surface profile (with a 10:1 vertical scale exaggeration) is:



Note that the ratio of the crest amplitude to the wave height for this wave is 0.86.

For cnoidal theory to the first order the pressure distribution is essentially hydrostatic with distance below the water surface, i.e.,

$$p = \rho g (\eta - z) \quad (3.15)$$

Equations are available to calculate the water particle velocity and acceleration components [see Wiegel (1960,1964)] but they are very complex, involving Jacobian elliptical functions.

3.4 Solitary Waves

A solitary wave has a crest that is completely above the still water level, and no trough. It is the wave that would be generated in a wave flume by a vertical paddle that is pushed forward and stopped without returning to the starting

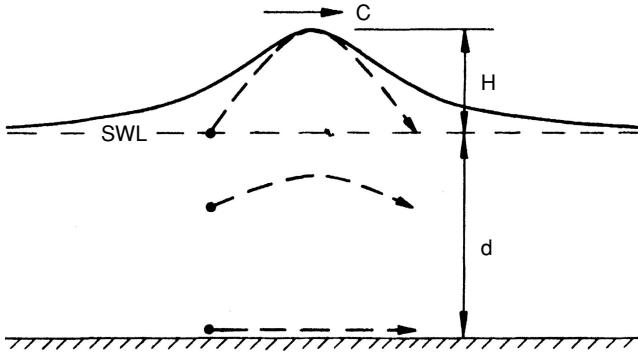


Figure 3.3. Surface profile and particle paths for a solitary wave.

position. The water particles move forward as depicted in Figure 3.3 and then come to rest without returning to complete an orbit. Thus, it is a translatory rather than an oscillatory wave. It has an infinite wave length and period. The surface profile is depicted by Figure 3.2 as the limit as k^2 approaches unity.

As a long period oscillatory wave propagates in very shallow water of decreasing depth, the surface profile approaches the solitary wave form. But the wave will break before a true solitary form is reached. The cnoidal wave theory would still be most appropriate for these very long oscillatory waves in shallow water. However, owing to the complexity of cnoidal theory, solitary wave theory has been used by some investigators to calculate wave characteristics in very shallow relative water depths. Munk (1949) and Wiegel (1964) present good summaries of the most common forms of solitary wave theory.

As k^2 approaches unity the cnoidal theory surface profile becomes

$$\eta = H \operatorname{sech}^2 \left[\sqrt{\frac{3H}{4d^3}} (x - Ct) \right] \quad (3.16)$$

which defines the profile of a solitary wave. The wave celerity is commonly given by

$$C = \sqrt{gd} \left(1 + \frac{H}{2d} \right) \quad (3.17)$$

but slight variations on Eq. (3.17) have also been developed for solitary wave celerity.

Thus, at incipient wave breaking (say $H/d = 0.9$; see Chapter 2) the solitary wave theory celerity will be 45% greater than the small-amplitude wave theory celerity assuming shallow water conditions.

As a solitary wave approaches, water particles begin to move forward and upward as depicted in Figure 3.3. As the wave crest passes the particle velocity is horizontal throughout the water column and reaches its highest value. Then the particles move downward and forward at decreasing speed until the wave passes. The most commonly used equations for the horizontal and vertical components of water particle velocity in a solitary wave are from McCowan (1891). They are

$$u = NC \frac{1 + \cos\left(M \frac{z+d}{d}\right) \cosh\left(\frac{Mx}{d}\right)}{\left[\cos\left(M \frac{z+d}{d}\right) + \cosh\left(\frac{Mx}{d}\right)\right]^2} \quad (3.18)$$

$$w = NC \frac{\sin\left(M \frac{z+d}{d}\right) \sinh\left(\frac{Mx}{d}\right)}{\left[\cos\left(M \frac{z+d}{d}\right) + \cosh\left(\frac{Mx}{d}\right)\right]^2} \quad (3.19)$$

where the coefficients N and M are defined by

$$\begin{aligned} \frac{H}{d} &= \frac{N}{M} \tan \frac{1}{2} \left[M \left(1 + \frac{H}{d} \right) \right] \\ N &= \frac{2}{3} \sin^2 \left[M \left(1 + \frac{2}{3} \frac{H}{d} \right) \right] \end{aligned} \quad (3.20)$$

As a solitary wave passes a point the mass of water transported past that point is simply the integral of the water surface elevation above the still water level from $x = \text{minus to plus infinity}$ (letting $t = 0$). For a unit width along the wave crest this yields the following volume of water:

$$V = \left(\frac{16}{3} d^3 H \right)^{1/2} \quad (3.21)$$

Since the period of a solitary wave is infinite it is not possible to determine a mass transport in terms of a mass per unit time. Using the solitary wave theory, however, the mass transport can be estimated by dividing the water mass represented by Eq. (3.21) by the period of the wave in question.

A solitary wave also has its energy divided approximately half as potential energy and half as kinetic energy. The total energy for a unit crest width is given by

$$E = \frac{8}{3\sqrt{3}} \rho g (Hd)^{3/2} \quad (3.22)$$

Since the length is infinite it is not possible to determine an energy density for a solitary wave. Since all of the energy in a solitary wave moves forward with the wave, the wave power is equal to the product of the wave energy and wave celerity.

Example 3.4-1

Consider the same wave as in Example 3.3-1 (i.e., $T = 14$ s, $H = 2$ m, and $d = 4$ m). Using solitary wave theory calculate the wave celerity and compare it to the results from that example. Also, calculate the crest particle velocity and compare it with the results from the small-amplitude wave theory.

Solution:

From Eq. (3.17) the wave celerity is

$$C = \sqrt{9.81(4)} (1 + 2/4 (2)) = 7.8 \text{ m/s}$$

which compares to 6.3 m/s and 7.0 m/s for the small-amplitude and cnoidal wave theories, respectively.

Given $H = 2$ m and $d = 4$ m, Eqs. (3.20) can be solved simultaneously by trial and error to yield

$$M = 0.88$$

$$N = 0.57$$

Then, with $C = 7.8$ m/s, $z = 2$ m, $x = 0$ we have for the particle velocity at the wave crest

$$u_c = 0.57(7.8) \frac{1 + [\cos(0.88)6/4] \cosh(0.88) (0)/4}{[\cos(0.88)6/4 + \cosh(0.88) (0)/4]^2}$$

or

$$u_c = 1.98 \text{ m/s}$$

From Eq. (2.30), for the small-amplitude wave theory in shallow water

$$u_c = \frac{2}{2} \sqrt{\frac{9.81}{4}} (1) = 1.6 \text{ m/s}$$

Thus, in shallow water there is a significant difference between the results from the two theories. For this wave the true value lies between the two results, but is probably closer to the result given by the solitary wave theory.

Using the concept of the crest particle velocity being equal to the wave celerity at breaking, one can derive a limiting value of H/d for wave breaking in shallow water. This has produced values ranging from 0.73 to 0.83 with a most common value of 0.78 (see Galvin, 1972). Thus, neglecting the bottom slope because solitary wave theory is developed for a horizontal bottom, the relationship $H/d = 0.78$ should well define shallow water breaking conditions. Note that this is the limit used in Fig. 3.4.

3.5 Stream Function Numerical Waves

The foregoing finite-amplitude analytical wave theories are somewhat deficient in satisfactorily defining wave characteristics for waves of large steepness. In addition, they are generally limited to a range of relative water depths. The use of numerical techniques with a computer has provided wave theories that have overcome these difficulties. Another limitation is introduced, however. Rather than producing equations (however complex) that can be used to calculate wave characteristic for any H , T , and d condition, the numerical theories directly produce and tabulate solutions for selected H , T , and d values. Application of

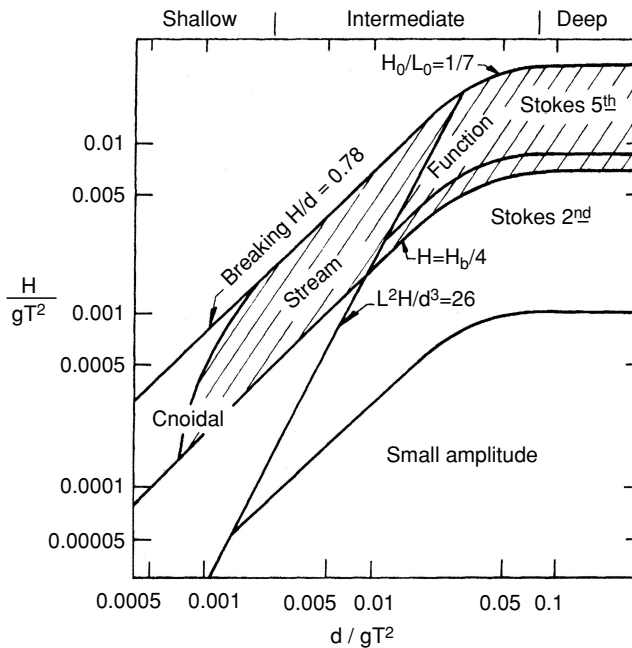


Figure 3.4. Recommended wave theory selection. (Based on LeMehaute, 1969.)

these results for conditions other than those selected by the practicing engineer requires interpolation between tabulated results.

The numerical wave theory most used in practice is the stream function theory developed by Dean (1965). Use of this wave theory is greatly facilitated by a set of broadly tabulated results (Dean, 1974) published by the U.S. Army Corps of Engineers. Some other numerical theories, which employ different approaches, have been presented by Chappellear (1961), Schwartz (1974), and Williams (1985).

Dean uses the stream function ψ rather than the velocity potential function to define the wave field in his numerical theory. Wave motion is first converted to steady flow by subtracting the wave celerity from the horizontal motion in the wave. Thus, the free surface profile and the bottom become steady-state stream lines and the stream function becomes constant along these two surfaces.

The boundary value problem is to seek a solution of the Laplace equation

$$\frac{\partial^2 \psi}{\partial x^2} + \frac{\partial^2 \psi}{\partial z^2} = 0 \quad (3.23)$$

for the steady-state surface and bottom boundary conditions written in terms of the stream function. These become

$$\frac{\partial \psi}{\partial x} = 0 \text{ at } z = -d \quad (3.24)$$

$$\frac{\partial \psi}{\partial x} = \left(\frac{\partial \psi}{\partial z} - C \right) \frac{\partial \eta}{\partial x} \text{ at } z = \eta \quad (3.25)$$

$$\frac{1}{2} \left[\left(\frac{\partial \psi}{\partial z} - C \right)^2 + \left(\frac{\partial \psi}{\partial x} \right)^2 \right] + g\eta = Q \text{ at } z = \eta \quad (3.26)$$

where Q is the total energy with respect to the still water surface elevation, $u = \delta\psi/\delta z$, and $w = \delta\psi/\delta x$.

The stream function for the small-amplitude wave theory is

$$\psi = \frac{gH}{2\sigma} \frac{\sinh k(d+z)}{\cosh kd} \cos(kx - \sigma t) \quad (3.27)$$

which defines the streamline pattern in a wave with respect to both position and time. If a steady uniform horizontal flow is added we have

$$\psi = Cz + \frac{gH}{2\sigma} \frac{\sinh k(d+z)}{\cosh kd} \cos kx \quad (3.28)$$

which is the steady flow streamline pattern.

Since the surface profile is a streamline, with Dean's theory the measured surface profile for a nonlinear wave can be used to calculate the related wave characteristics. Also, the classic wave problem of calculating the wave characteristics given the wave height and period and the water depth can be solved. The latter approach is discussed below.

Using the form of (Eq. 3.28) and the form of the Stokes higher order equations, Dean proposed a boundary value solution to the N th order that had the following form:

$$\psi = Cz + \sum_{n=1}^N X_n \sinh nk(d+z) \cos nkx \quad (3.29)$$

for the stream line pattern in a wave. From Eq. (3.29), the streamline at the surface ψ_s would be

$$\psi_s = C\eta + \sum_{n=1}^N X_n \sinh nk(d+\eta) \cos nkx \quad (3.30)$$

Since the surface is a streamline, Eq. (3.30) exactly satisfies the Laplace equation, the BBC [Eq. (3.24)], and the KSBC [Eq. (3.25)]. The basic problem is to evaluate the coefficient X_n to the order desired, the wave number k , and the value of ψ_s so that they best satisfy the DSBC [Eq. (3.26)]. This is accomplished by evaluating the constant Q in the DSBC at a number of points along the wave. Then, by trial, the square of the difference of each Q value from the average Q value for these points is minimized. The volumes of water above and below the still water level [using Eq. (3.30)] must also be equal.

The result is a value for k that defines the wave length, the value of X_n that defines the stream function to the desired order, and a value for ψ_s that gives the surface profile using Eq. (3.30). With the stream function defined, all the other wave characteristics can be determined using standard potential flow analysis.

The tabulated results presented by Dean (1974) are for 40 dimensionless combinations of H , $L_o (= gT^2/2\pi)$, and d . Specifically, these include 10 values of d/L_o from deep water (2.0) to shallow water (0.002) and $H/H_b = 0.25, 0.50, 0.75$, and 1.0 for each d/L_o value. The tabulated results include the wave length, surface profile, particle velocity and acceleration fields, dynamic pressure field, group celerity, energy, and momentum flux all in dimensionless form. Interpolation is required if the desired d/L_o and H/H_b values are not included in the 40 sets of tabulated information.

3.6 Wave Theory Application

When the various wave theories are to be applied in engineering practice two important concerns must be addressed. The first is which theory to use for a particular application. The second is how to apply one or more theories over a

range of relative water depths to analyze the change in wave characteristics as a wave propagates from one water depth to another.

Range of Application

Selection of the appropriate wave theory to be used for a particular coastal engineering application depends on several factors. A general guide can be given in terms of the wave steepness (H/gT^2) and the relative depth (d/gT^2), but this must be tempered by conditions of the actual application.

If one is calculating wave characteristics for a given set of input conditions (H , T , and d), these input conditions may be only generally specified or they may be specified for a range of values. This may be due to the fact that these input conditions are only approximately known from wave hindcasts and a shoaling/refraction analysis for a given return period storm. A very sophisticated wave calculation may not be justified so the easier-to-apply small amplitude theory may be adequate.

Even if the input values of H , T , and d are fairly precisely known, the calculated wave characteristics may only need to be approximately known—thus the advantage of small-amplitude wave theory again. However, if it were necessary to calculate the surface profile of a wave in relatively shallow water, say to determine the loading on the underside of a pier deck, cnoidal or stream function wave theory would be more appropriate. Or, if the surface profile of a wave was being measured in a field experiment on wave forces on a pile structure, the stream function theory might be more appropriate for calculating the wave particle velocity and acceleration fields for that surface profile.

Another factor that compounds the choice of a wave theory for a particular application is that a particular theory may be better at defining some characteristics than others. For example, in fairly shallow water, the small-amplitude wave theory does well at predicting bottom particle velocities, but does not do well at predicting particle velocities near the surface or the surface profile itself.

A number of authors including Muir Wood (1969), LeMehaute (1969), and Komar (1976) have recommended ranges of application of the various wave theories. These recommendations are based on several factors including the range of conditions for which the theory was derived, results of experiments on the efficacy of the various theories in predicting certain wave characteristics, ease of application of the theories, and some personal judgment.

Figure 3.4, based on a diagram originally presented by LeMehaute (1969) but with slight modification by the author, can be used as a starting point in selecting a wave theory for an engineering application. It is a plot of wave steepness versus relative depth with breaking wave cutoff limits in deep and shallow water. The general areas for use of each theory are denoted with the stream function theory application range defined by the cross-hatched area. The application range for small-amplitude wave theory is extended as far as reasonable owing to its ease of

application. The Stokes fifth-order theory is specified where LeMehaute recommends the third- and fourth-order theories for increasing wave steepnesses. The solitary wave theory is not shown but, depending on the wave characteristics to be calculated, it may be used in place of the cnoidal theory for very steep waves in shallow water.

Shoaling Calculations

By equating the wave power from one depth to another Eqs. (2.41) and (2.42) were developed from the small-amplitude wave theory to predict the resulting change in wave height as a wave shoals. This change in wave height is dependent only on the relative depth change, i.e., just the change in depth for a given wave period. If the wave steepness is not too large this affords an easy way to calculate the change in wave height from one water depth to another. Given the new wave height along with the known wave period and water depth, all of the other wave characteristics can be calculated from the small-amplitude or some finite-amplitude wave theory.

For steeper waves the small-amplitude wave theory is generally less valid. Finite-amplitude wave theories should be used to calculate changes in wave height as a wave propagates from one water depth to another. However, most finite-amplitude wave theories are valid only for a limited range of relative depths. So, to carry out the analysis two theories would have to be coupled at some intermediate point. This can cause difficulties to arise. Given the same value of wave power at the coupling point, two different finite-amplitude theories often yield a different value of wave height (and other characteristics) at the intersection point. Or, if wave heights are matched at the intersection point there would be a power discontinuity. For finite-amplitude wave theories the change in wave height depends on the initial wave steepness as well as the change in relative depth. For numerical wave theories that may be valid over a wide range of relative depths it is not easy to relate wave power values at two depths and calculate the resulting wave height change.

Nevertheless, a number of efforts have been made to employ finite-amplitude theories for wave shoaling analysis. See LeMehaute and Webb (1964), Koh and LeMehaute (1966), Iwagaki (1968), Svendsen and Brink-Kjaer (1972), Svendsen and Buhr-Hansen (1977), and LeMehaute and Wang (1980) for some of these efforts. Walker and Headland (1982) evaluated these various finite-amplitude theory approaches to shoaling analysis along with the available experimental data on wave shoaling and breaking to develop Figure 3.5. The lowest solid line in this figure is the shoaling curve (H/H'_o versus d/L_o) from the small-amplitude wave theory (i.e., for H'_o/L_o near zero). The other solid lines give the shoaling curves for increasing deep water wave steepnesses. The dashed lines indicate the breaker point as the waves shoal, for various beach slopes (i.e., $m = 0.05$ is a slope of 1:20).

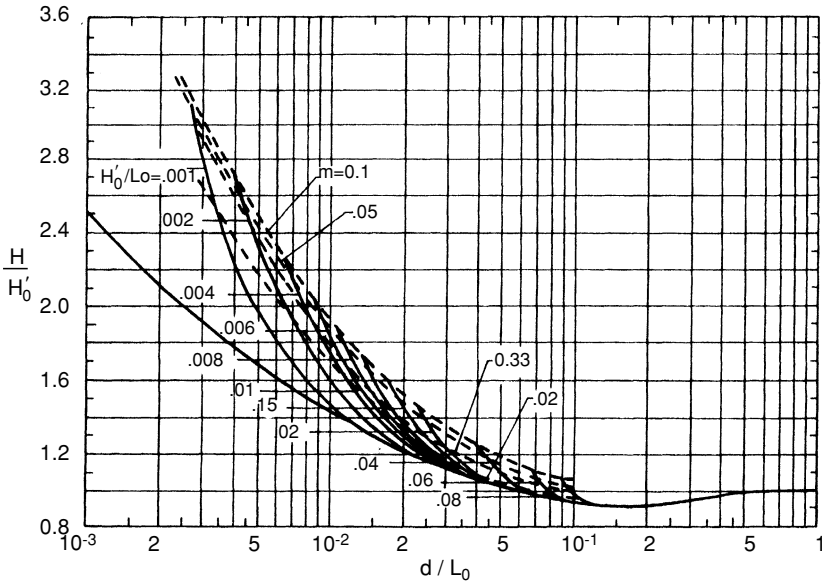


Figure 3.5. Wave shoaling and breaking characteristics. (Walker and Headland, 1982.)

Example 3.6-1

A wave having a deep water height of 4 m and a period of 11 s shoals with negligible refraction and breaks on a beach slope of 1:20. Determine the wave height and water depth just before the wave breaks.

Solution:

From the small-amplitude wave theory

$$L_0 = \frac{9.81(11)^2}{2\pi} = 188.9 \text{ m}$$

So

$$\frac{H'_0}{L_0} \frac{4}{188.9} = 0.021$$

Figure 3.5 then yields (for $m = 0.05$ and $H'_0/L_0 = 0.021$)

$$\frac{H}{H'_0} = 1.4$$

$$\frac{d}{L_0} = 0.024$$

Thus, the wave height at breaking

$$H_b = 1.4 (4) = 5.6 \text{ m}$$

and the water depth at breaking

$$d_b = 0.024 (188.9) = 4.5 \text{ m}$$

The solitary wave theory could then be used to estimate some of the other characteristics of this wave just before it breaks.

3.7 Summary

Chapters 2 and 3 together present the characteristics and analysis of changes in the characteristics as a wave propagates from deep water into the point of breaking and runup on a slope. This is done only for the two-dimensional (x , z) plane as waves propagate along a nearshore profile. For a complete analysis of wave propagation to the shore the three-dimensional effects of wave refraction, diffraction, and reflection must also be considered.

3.8 References

- Chappelear, J.E. (1961), "Direct Numerical Calculation of Wave Properties," *Journal of Geophysical Research*, Vol. 66, pp. 501–508.
- Dean, R.G. (1965), "Stream Function Representation of Nonlinear Ocean Waves," *Journal of Geophysical Research*, Vol. 70, pp. 4561–4572.
- Dean, R.G. (1974), "Evaluation and Development of Water Wave Theories for Engineering Application," Special Report No. 1, U.S. Army Coastal Engineering Research Center, Ft. Belvoir, VA.
- Dean, R.F. and Dalrymple, R.A. (1984), *Water Wave Mechanics for Engineers and Scientists*, Prentice-Hall, Englewood Cliffs, NJ.
- Galvin, C.J. (1972), "Wave Breaking in Shallow Water," in *Waves on Beaches and Resulting Sediment Transport* (R.E. Myers, Editor) Academic Press, New York, pp. 413–451.
- Hardy, T.A. and Kraus, N.C. (1987), "A Numerical Model for Shoaling and Refraction of Second Order Cnoidal Waves Over an Irregular Bottom," Miscellaneous Paper CERC 87–9, U.S. Army Waterways Experiment Station, Vicksburg, MS.
- Ippen, A.T. (1966), *Estuary and Coastline Hydrodynamics*, McGraw-Hill, New York.
- Iwagaki, Y. (1968), "Hyperbolic Waves and Their Shoaling," in *Proceedings, 11th Conference on Coastal Engineering*, American Society of Civil Engineers, London, pp. 124–144.

- Keulegan, G.H. (1950), "Wave Motion," in *Engineering Hydraulics*, (H. Rouse, Editor) John Wiley, New York, Chapter 11.
- Koh, R.C.Y. and LeMehaute, B. (1966), "Wave Shoaling," *Journal of Geophysical Research*, Vol. 71, pp. 2005–2012.
- Komar, P.D. (1976), *Beach Processes and Sedimentation*, Prentice-Hall, Englewood Cliffs, NJ.
- Korteweg, D.J. and de Vries, G. (1985), "On the Change of Form of Long Waves Advancing in a Rectangular Canal, and on a New Type of Long Stationary Waves," *Philosophical Magazine*, Series 5, Vol. 39, pp. 422–443.
- LeMehaute, B. (1969), "An Introduction to Hydrodynamics and Water Waves," Technical Report ERL 118-POL-3-2, U.S. Department of Commerce, Washington, DC.
- LeMehaute, B. and Wang, J.D. (1980), "Transformation of Monochromatic Waves from Deep to Shallow Water," Technical Report 80-2, U.S. Army Coastal Engineering Research Center, Ft. Belvoir, VA.
- LeMehaute, B. and Webb, L.M. (1964), "Periodic Gravity Waves over a Gentle Slope at a Third Order Approximation," in *Proceedings, 9th Conference on Coastal Engineering*, American Society of Civil Engineers, Lisbon, pp. 23–40.
- McGowan, J. (1891), "On the Solitary Wave," *London, Edinburgh and Dublin Magazine and Journal of Science*, Vol. 32, pp. 45–58.
- Muir Wood, A.M. (1969), *Coastal Hydraulics*, Gordon and Breach, New York.
- Munk, H.W. (1949), "Solitary Wave and Its Application to Surf Problems," *Annals, New York Academy of Science*, Vol. 51, pp. 376–424.
- Sarpkaya, T. and Isaacson, M. (1981), *Mechanics of Wave Forces on Offshore Structures*, Van Nostrand Reinhold, New York.
- Schwartz, L.W. (1974), "Computer Extension and Analytical Continuation of Stokes' Expansion for Gravity Waves," *Journal of Fluid Mechanics*, Vol. 62, pp. 552–578.
- Skjelbreia, L. (1959), "Gravity Waves, Stokes Third Order Approximations, Tables of Functions," Council on Wave Research, Engineering Foundation, University of California, Berkeley.
- Skjelbreia, L. and Hendrickson, J.A. (1961), "Fifth Order Gravity Wave Theory," in *Proceedings, 7th Conference on Coastal Engineering*, Council on Wave Research, Engineering Foundation, University of California, Berkeley, pp. 184–196.
- Stokes, G.G. (1847), "On the Theory of Oscillatory Waves," *Transactions, Cambridge Philosophical Society*, Vol. 8, pp. 441–455.
- Svendsen, I.A. and Brink-Kjaer, O. (1972), "Shoaling of Cnoidal Waves," in *Proceedings, 13th International Conference on Coastal Engineering*, American Society of Civil Engineers, Vancouver, pp. 365–383.
- Svendsen, I.A. and Buhr-Hansen, J. (1977), "The Wave Height Variation for Regular Waves in Shoaling Water," *Coastal Engineering*, Vol. 1, pp. 261–284.
- Ursell, F. (1953), "The Long Wave Paradox in the Theory of Gravity Waves," *Proceedings, Cambridge Philosophical Society*, Vol. 49, pp. 685–694.

- U.S. Army Coastal Engineering Research Center (1984), *Shore Protection Manual*, U.S. Government Printing Office, Washington, DC.
- Walker, J. and Headland, J. (1982), "Engineering Approach to Nonlinear Wave Shoaling," in *Proceedings, 18th International Conference on Coastal Engineering*, American Society of Civil Engineers, Cape Town, pp. 523–542.
- Wiegel, R.L. (1960), "A Presentation of Cnoidal Wave Theory for Practical Application," *Journal of Fluid Mechanics*, Vol. 7, pp. 273–286.
- Wiegel, R.L. (1964), *Oceanographical Engineering*, Prentice-Hall, Englewood Cliffs, NJ.
- Williams, J.M. (1985), *Tables of Progressive Gravity Waves*, Pitman, London.

3.9 Problems

1. A 8.5 m high, 8 s period wave is propagating in water 30 m deep. Calculate and plot the water surface profile over one wave length using the small-amplitude and Stokes second-order wave theories. Plot the two profiles superimposed and comment on the difference.
2. For the wave given in Problem 1, calculate the water particle velocity at the still water level under the wave crest using the small-amplitude and Stokes second-order wave theories.
3. For the wave given in Problem 1, calculate and plot the mass transport velocity as a function of position along a vertical line from the bottom up to the still water level.
4. For the wave given in Problem 1, calculate the wave celerity employing both the second- and the third-order Stokes theories.
5. For the wave given in Problem 1, calculate and plot the pressure distribution along a vertical line under the wave crest from the bottom up to the still water level.
6. A wave having a height of 2.4 m and a period of 5 s is propagating in water 8 m deep. Is it more appropriate to use the Stokes second-order wave theory or the cnoidal wave theory to calculate characteristics of this wave?
7. A wave having a deep water height of 5 m and a period of 8 s propagates toward the shore. Calculate and plot the ratio of a_c to a_l from deep water into a depth where $U_r = 10$. For this plot estimate H and L from the small-amplitude wave theory. Comment on the results.
8. A 7 s period wave having a height of 1.5 m is propagating in water 5.3 m deep. Plot the surface profile using the most appropriate theory.
9. A 9 s period wave having a height of 2.1 m is propagating in water 4.5 m deep. Calculate and plot the surface profile using the small-amplitude, Stokes second-order, cnoidal, and solitary wave theories. Plot the four profiles superimposed and comment on the results.

10. For the wave in Problem 9, calculate the wave celerity and length by each of the four mentioned theories and comment on the results.

11. A wave has a length of 50 m and a height of 1.9 m in water 7 m deep. Using the cnoidal wave theory determine the period of this wave. What wave period would the small-amplitude wave theory yield?

12. Plot the surface profile of the wave given in Problem 10, using the cnoidal wave theory.

13. Consider a wave having a period of 12.5 s and a height of 2.1 m in water 3.8 m deep. Using the solitary wave theory calculate the wave celerity, length, crest particle velocity, and energy. Compare these with the results given by the small-amplitude wave theory.

14. A section of a beach has a bottom surface layer of shingle (stones with a diameter of around 100 mm). The water depth is 1.8 m in the vicinity of the shingle. If the required velocity to initiate movement of these shingle units is 1.5 m/s, will a 1.3 m high wave initiate movement?

15. Show that the maximum water particle velocity in a solitary wave is given by:

$$u = \frac{CN}{1 + \cos\left(1 + \frac{H}{d}\right)}$$

16. Demonstrate that the stream function given by Eq. (3.27) represents irrotational flow.

17. For the wave given in Example 3.6–1 determine the wave height when the wave is propagating in water 6 m deep.

18. A 2.5 m high, 12 s period wave in deep water propagates toward the shore on a 1:30 slope. Determine the wave height, length, and celerity just prior to breaking by the best procedures available from Chapter 3. Compare the results of this analysis to results using the small-amplitude wave theory from Chapter 2.

19. A wave having a period of 10 s and a deep water height of 3.5 m propagates to the shore in a normal direction. The nearshore beach profile has a 1:20 slope. Estimate the width of the surf zone.

20. Considering the material presented in this chapter, are waves dispersive in shallow water? Explain your answer.

21. List three significant ocean wave characteristics that are demonstrated by finite amplitude wave theories, but not by the small amplitude wave theory.

4

Wave Refraction, Diffraction, and Reflection

Consider the design of a protective breakwater for a small marina that is located on the open coast. A typical design concern would be to predict wave conditions at interior points in the marina (where vessels will be moored) for a given deep water design wave height, period, and direction. There must be an analysis of the change in wave height owing to the change in relative depth from deep water to the marina interior (as discussed in Chapters 2 and 3). We must also evaluate the effects of refraction on wave height and crest orientation as the wave propagates over the nearshore bottom contours from deep water to the vicinity of the marina. Then the effects of diffraction and possibly further refraction as the wave propagates into the lee of the marina breakwater must be evaluated. The combined effects of shoaling, refraction, and diffraction will yield the resulting wave height and direction of propagation pattern within the marina. If any of the interior borders of the marina (e.g., vertical bulkheads and quay walls) have a high reflection coefficient, reflected waves may also be active at the points of interest.

4.1 Three-Dimensional Wave Transformation

Wave refraction occurs in transitional and shallow water depths because wave celerity decreases with decreasing water depths to cause the portion of the wave crest that is in shallower water to propagate forward at a slower speed than the portion that is in deeper water. The result is a bending of the wave crests so that they approach the orientation of the bottom contours. Wave orthogonals, to remain normal to the wave crest, will also bend so that orthogonals that are parallel in deep water may converge or diverge as wave refraction occurs. This convergence or divergence of wave orthogonals will cause local increases or decreases in wave energy and consequently wave height.

Wave celerity relative to the fixed sea floor will also depend on the possible existence of an ocean current. If a train of waves crosses a region where there is a

horizontal gradient in the current velocity the waves will be refracted. This phenomenon is common, for example, when deep water waves from the Atlantic Ocean cross the Gulf Stream near the U.S. coastline or when waves propagating toward the coast interact with the tide-induced ebb current at a coastal entrance.

Diffraction will occur when the height of a wave is greater at one point along a wave crest than at an adjacent point. This causes a flow of energy along the crest in the direction of decreasing height and a consequent adjustment of wave height along the crest as the wave propagates forward. This is particularly important, for example, when a wave crest is truncated as it passes the end of a structure that extends out into the water. Diffraction will then cause a flow of wave energy into the shadow region in the lee of the structure. Diffraction also occurs whenever wave refraction causes wave height differences along a wave crest. However, for many (but not all) wave refraction analyses the effect of diffraction on wave height changes is a second-order effect that may be neglected. In this chapter, we will consider refraction and diffraction separately and then look at the techniques available to evaluate the combined effects of refraction and diffraction where they are important and can be evaluated.

The two-dimensional aspects of wave reflection were discussed in Section 2.7. When the incident wave crest is not completely parallel to a reflecting structure the reflected wave crest will have a changed orientation from that of the incident wave.

The effects of wave shoaling, refraction, and diffraction all depend on the period of the wave being considered. Also, the effects of wave refraction and diffraction depend on the incident direction of the wave. Thus, for a spectrum of wind-generated waves having a range of component periods and directions, the different components of the spectrum will be affected differently as they propagate from deep water to the point of interest. The components of a wave spectrum can be analyzed separately and then regrouped to approximate the nearshore characteristics of the spectrum. An easier approach, commonly used for many engineering analyses, is to select a single representative wave height, period, and direction to represent the spectrum of waves and to analyze the behavior of this wave as it propagates toward the shore.

A related phenomenon that involves the planform transformation of waves is vessel-generated waves. The generation, resulting wave crest patterns, and behavior of vessel-generated waves will be presented in Section 4.9.

4.2 Wave Refraction

Figure 4.1 shows a hypothetical shoreline and nearshore bottom contours. A wave train with a deep water wave length L_o is approaching the shore with a crest orientation in deep water that is parallel to the average shoreline position. Bottom contour depths are given in terms of the deep water wave length. As

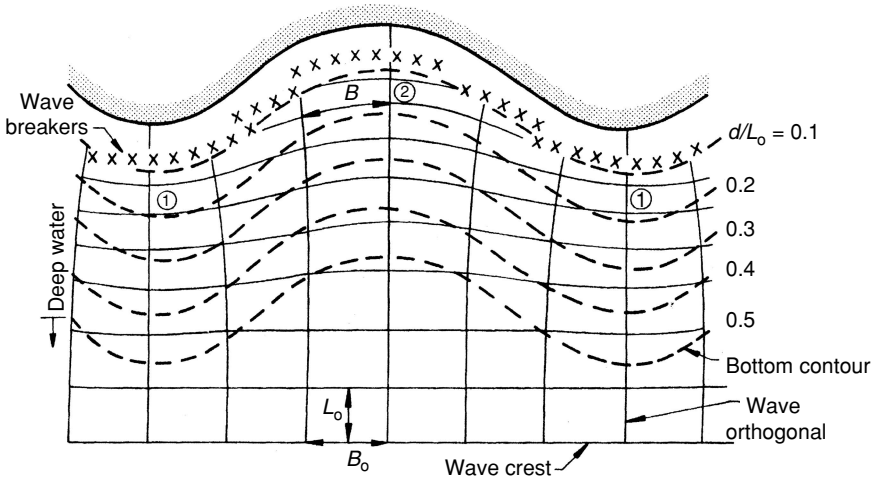


Figure 4.1. Wave refraction pattern.

portions of the wave crest enter the region where $d/L_o < 0.5$ the wave length and celerity commence to decrease [as given by Eqs. (2.13) and (2.14)]. The result is the refraction of the wave train with the wave crest orientations approaching the orientation of the bottom contours as the waves propagate shoreward. If one constructs equally spaced orthogonal lines along the deep water wave crests and extends these lines toward the shore, being sure that they remain normal to the wave crests, one can see the pattern of energy distribution at any point along a wave crest. Where orthogonals converge there is an increase in the energy per unit crest length, and vice versa.

The wave refraction diagram shown in Figure 4.1 defines the wave crest orientation as the wave propagates forward and allows one to determine the change in wave height owing to wave refraction. The convergence and divergence of the wave orthogonals along with the effects of wave shoaling cause the wave height variation from deep water defined by

$$\frac{H}{H_o} = \sqrt{\frac{L_o}{2nL}} \sqrt{\frac{B_o}{B}} = \frac{H}{H'_o} \sqrt{\frac{B_o}{B}} \quad (2.42)$$

In Eq. (2.42), the shoaling coefficient ($K_s = H/H'_o$) is only a function of d/L_o . The orthogonal spacing ratio ($B_o/B = K_r^2$) for a nearshore point of interest must be determined from a refraction analysis. The calculated change in wave height employing Eq. (2.42) yields a wave height value that is the average over the orthogonal spacing B . This may require the use of smaller orthogonal spacings in deep water to sufficiently define the wave height at a desired nearshore location, especially if the hydrography is complex.

Note in Figure 4.1 that refraction causes a convergence of orthogonals over the submerged ridge (point 1), resulting in higher waves that break further offshore. Over the submerged trough (point 2), wave heights are lower than they would be over the ridge and can actually be much lower than the deep water height if the effect of refraction in lowering the wave height is greater than the increase in wave height owing to shoaling.

Since wave celerity depends on the wave period, waves with different periods will refract differently as they approach the shore. Longer period waves begin to feel bottom and refract in deeper water and consequently may undergo greater refraction as they approach the shore. The resulting wave refraction pattern will also be different for each different deep water approach direction. For a typical wave analysis at a coastal site refraction patterns must be investigated for a representative range of wave periods and deep water directions to determine the most critical wave height/direction combinations at the site.

It should be noted that some empirical data for wave processes are presented in terms of the unrefracted deep water wave height H'_o (e.g., see Figures 2.11 and 2.15). If a wave having a deep water height H_o refracts into a nearshore location where the refraction coefficient is K_r , then the unrefracted deep water height to be used in these diagrams is $H'_o = K_r H_o$.

Refraction analyses were initially done by the manual construction of refraction diagrams. Now they are mostly done by numerical/computer analysis, except for situations that only involve a limited number of wave conditions for a specific location when manual construction of a refraction diagram may reasonably be carried out. We will present the common procedures used for both manual and numerical refraction analysis.

4.3 Manual Construction of Refraction Diagrams

The first method used for the construction of refraction diagrams is known as the wave crest method (Johnson et al., 1948). Working on a hydrographic chart of the study area, a wave crest having the proper orientation is constructed in deep water. Then, points along the wave crest are advanced normal to the crest by an integral number of wave lengths and the new crest position is drawn. This process is continued until the crest pattern from deep water into the shore is constructed. Given the deep water wave length and the local average water depth over which the wave will advance, the advancing wave length (or an integral number of wave lengths) can be calculated from Eq. (2.18). A template that graphically solves Eq. (2.18) (see Wiegel, 1964) may be constructed to simplify the plotting of crest positions. After all of the crest positions for the advancing wave train are drawn, orthogonal lines are constructed normal to the wave crests at desired intervals.

The wave crest method is presented because it is of historic interest and it provides a simple explanation of the wave refraction process. However, for

engineering analysis it is most important to produce an accurate depiction of the wave orthogonal pattern, so satisfactory computation of wave height patterns can be accomplished. The orthogonal lines also depict the local direction of wave propagation. Thus, a procedure that directly produces the orthogonal pattern is preferable to the wave crest method where the orthogonal lines are less accurately constructed. After the orthogonal pattern is constructed wave crests can be drawn if so desired.

A second graphical method for constructing refraction diagrams, known as the orthogonal method, is based on Snell's Law which may be derived by considering Figure 4.2. Consider a train of waves propagating over a step where the water depth instantaneously decreases from d_1 to d_2 (ignore wave reflection by the step). This causes the wave celerity and length to decrease from C_1 and L_1 to C_2 and L_2 , respectively. For an orthogonal spacing x and a time interval T , $\sin \alpha_1 = C_1 T/x$ and $\sin \alpha_2 = C_2 T/x$. Dividing yields

$$\frac{\sin \alpha_1}{\sin \alpha_2} = \frac{C_1}{C_2} = \frac{L_1}{L_2} \quad (4.1)$$

which is Snell's Law for wave refraction. Applying Eq. (4.1) to wave refraction over a gradually varying bottom slope, α_1 and α_2 become the angles between the wave crest and bottom contour line at successive points along an orthogonal as a wave propagates forward, and L_1 and L_2 become the wave lengths at the points where α_1 and α_2 are measured.

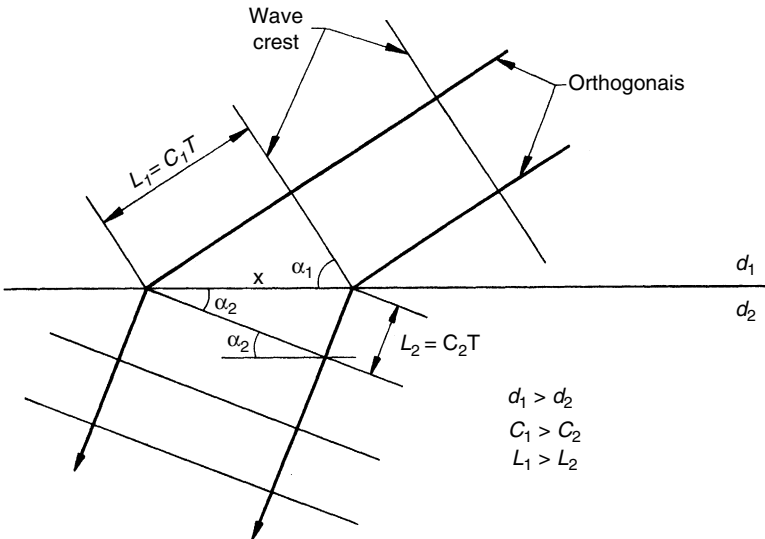


Figure 4.2. Definition sketch for Snell's law derivation.

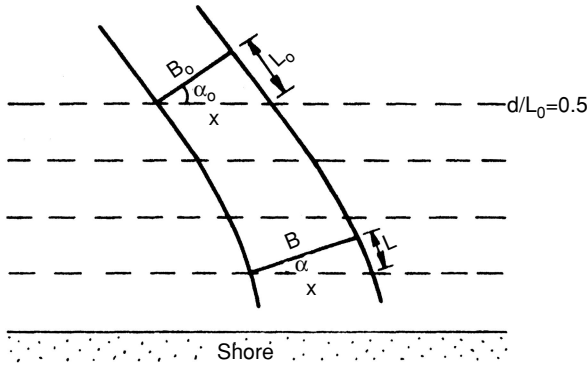


Figure 4.3. Wave refraction over straight parallel bottom contours.

When waves propagate shoreward over bottom contours that are essentially straight and parallel as shown in Figure 4.3

$$\frac{\sin \alpha_o}{L_o} = \frac{\sin \alpha}{L} = \frac{1}{x}$$

if we choose B_o and B so that the orthogonal lengths equal L_o and L as shown. Then,

$$\frac{B_o}{\cos \alpha_o} = x = \frac{B}{\cos \alpha}$$

or

$$K_r = \sqrt{\frac{B_o}{B}} = \sqrt{\frac{\cos \alpha_o}{\cos \alpha}} \quad (4.2)$$

where

$$\alpha = \sin^{-1} \left(\frac{C}{C_o} \sin \alpha_o \right) \quad (4.3)$$

Equations (4.2) and (4.3) allow one to determine the refracted wave height [also using Eq. (2.42)] and wave crest orientation or orthogonal direction when waves refract over essentially uniform nearshore hydrography. Note that the nearshore bottom slope does not enter the analysis as long as the bottom contours are essentially straight and parallel. Wiegel and Arnold (1957) conducted wave tank tests on uniform slopes and found Snell's Law valid for deep water incident wave angles between 10° and 70° and bottom slopes ranging from 1:10 to vertical (step).

Example 4.3-1

Consider the wave from Examples 2.3-1 and 2.3-2 which has a deep water height of 2 m and a period of 10 s. Assume the wave crests in deep water are oriented at an angle of 35° with the shoreline and that the nearshore bottom contours are essentially straight and parallel to the shoreline. Determine the wave height and crest orientation with respect to the shoreline when the wave propagates into water 2.3 m deep.

Solution:

From Examples 2.3-1 and 2.3-2 respectively, $C_o = 15.6$ m/s and at $d = 2.3$ m, $C = 4.75$ m/s.

Then for an offshore angle of 35° , Eq. (4.3) yields

$$\alpha = \sin^{-1} \left(\frac{4.75}{15.6} \sin 35^\circ \right) = 9.5^\circ$$

which is the angle between the wave crest and the shoreline at the water depth of 2.3 m.

From Eq. (4.2)

$$K_r = \sqrt{\frac{\cos 35^\circ}{\cos 9.5^\circ}} = 0.91$$

which is the refraction coefficient from deep water to the 2.3 m water depth.

Since $C_o/C = L_o/L$ and $n = 1.0$ for the shallow water depth of 2.3 m, Eq. (2.42) yields

$$\frac{H}{H_o} = \sqrt{\frac{15.6}{2(1)(4.75)}} (0.91) = 1.166$$

or

$$H = 2(1.166) = 2.33 \text{ m}$$

Thus, wave refraction decreases the wave height but the height increase caused by wave shoaling is greater, so there is a net increase in the wave height from deep water to the point where the depth is 2.3 m.

The commonly used orthogonal method for manual construction of wave refraction diagrams for irregular hydrography is based on Arthur et al. (1952). Essentially, as one progresses shoreward it is assumed that the bottom

topography is horizontal from a contour line to the midpoint to the next contour line where the bottom is stepped up to the depth represented by that next contour line. Snell's Law is applied at this midpoint step to predict the change in orthogonal line direction that would gradually occur over the particular contour interval being traversed.

To assist this graphical procedure for laying out orthogonal lines on a hydrographic chart, the template shown in Figure 4.4 has been developed. For practical use, a template scaled so that the distance from the turning point to the orthogonal line is about 15 cm and printed on a transparent sheet should be employed for refraction diagram construction on most hydrographic charts. A pin is placed through the turning point and the ratio of the wave celerities at the two contour lines defining the interval being crossed controls the change in orthogonal direction.

The procedure for constructing an orthogonal line on a hydrographic chart is as follows:

1. Locate the depth contour represented by $d/L_o = 0.5$ on the hydrographic chart for the area of interest. Then label each of the shallower contours in terms of the relative depth d/L_o . Bottom contour irregularities that are smaller than about one wave length do not appreciably affect wave behavior and may be smoothed out.
2. For each contour line and the one landward of it calculate the ratio of wave celerities C_1/C_2 where C_1 is the celerity at the deeper contour. From Eq. (2.13)

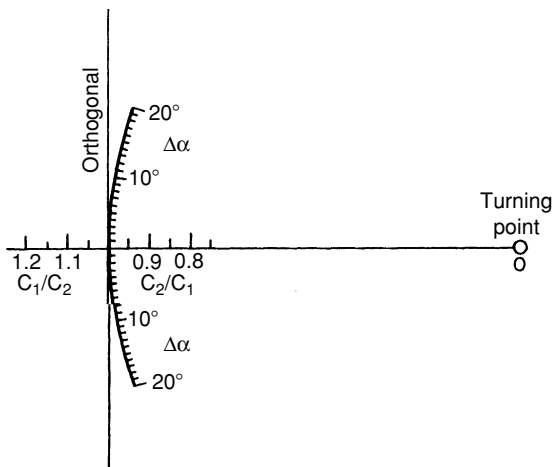


Figure 4.4. Template for orthogonal refraction analysis.

$$\frac{C_1}{C_2} = \frac{\tanh\left(\frac{2\pi d_1}{L_1}\right)}{\tanh\left(\frac{2\pi d_2}{L_2}\right)}$$

where d/L can be determined by trial and error from Eq. (2.18) reorganized as

$$\frac{d}{L_o} = \frac{d}{L} \tanh\left(\frac{2\pi d}{L}\right)$$

3. Starting at the two most seaward contours, construct a line that is a midcontour halfway between these two contours; extend the incoming deep water orthogonal straight to the midcontour, and construct a line tangent to the midcontour at the intersection of the midcontour and the incoming orthogonal.
4. Lay the template (Figure 4.4) with the line marked orthogonal over the incoming orthogonal and $C_1/C_2 = 1.0$ at the intersection of the midcontour and the orthogonal.
5. Rotate the template around the turning point until the calculated value of C_1/C_2 intersects the tangent to the midcontour line. The line on the template labeled orthogonal now lies in the direction of the outgoing orthogonal. However, it is not at the correct position for the outgoing orthogonal.
6. With a pair of triangles, move the outgoing orthogonal to a parallel position such that the incoming and outgoing orthogonals connect and the lengths of these two orthogonal lines are equal (thus the two orthogonals may not cross exactly at the midcontour line).
7. Repeat the above procedure at successive contour intervals to extend the orthogonal line forward toward the shore.
8. Repeat the above procedure for additional orthogonal lines as needed.

The usual objective in constructing a refraction diagram is to evaluate wave height and direction at a particular point or points nearshore. To do this, at least two orthogonal lines are needed and they should arrive at the shore bracketing the point of interest with not too large of a spread. Experience and some forethought are necessary to start the orthogonals in deep water at a point that will lead to the desired location on shore.

Orthogonals may be constructed from shallow to deep water using the above procedure except that C_2/C_1 values are used where C_1 is still the wave celerity at the deeper contour line. For example, selecting a range of seaward projecting directions at a nearshore point and constructing orthogonals seaward from these initial directions would demonstrate the range of offshore directions from which waves will reach the shoreline site.

To obtain sufficient accuracy, Arthur et al. (1952) recommend a contour spacing such that the absolute value of $\Delta C/C_1 < 0.2$ and $\Delta\alpha < 15^\circ$. If the angle between the wave crest and the bottom contour exceeds 80° , the above procedure is not sufficiently accurate. A modified procedure presented by the U.S. Army Coastal Engineering Research Center (1984) should be used.

Figure 4.5 is a refraction diagram constructed by the above procedure. It shows the orthogonal pattern for 7 s waves approaching the shore from S 30° E. Note how refraction concentrates wave energy at the breakwater dogleg ($B_o/B > 4$) and spreads energy at the breakwater head ($B_o/B < 1$). Additional orthogonal lines might be constructed for this wave condition to better define the variation of wave height along the breakwater and the wave height and direction of propagation at the breakwater head. The former is desirable for the structural design of the breakwater and the latter (as will be seen later) is desirable for predicting wave conditions in the lee of the breakwater.

Occasionally, when refraction diagrams are constructed a pair of orthogonals will cross, forming a caustic point. As the orthogonal lines approach the caustic

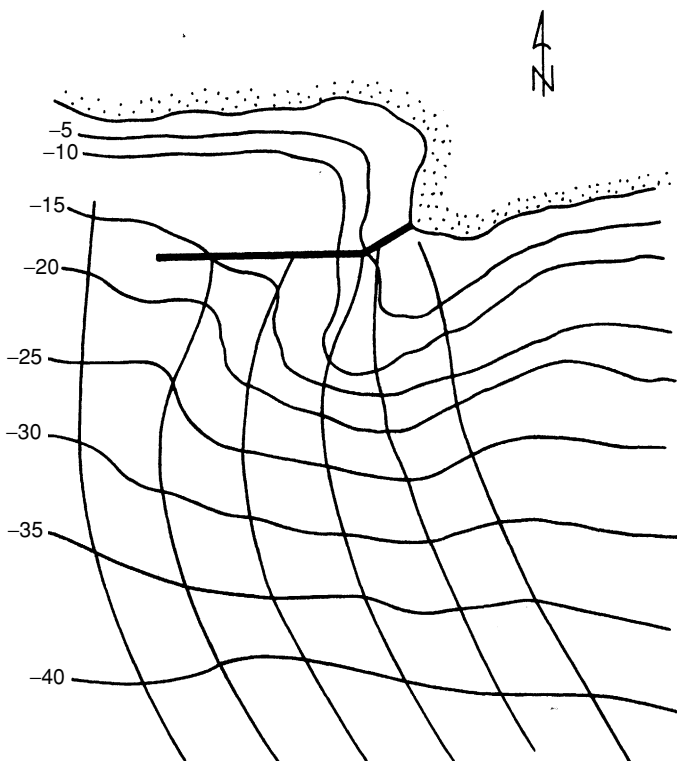


Figure 4.5. Wave refraction diagram for 7 s wave from S 30° E. (Sorensen, 1993.)

point their spacing approaches zero so the wave height would approach infinity. In reality, before the orthogonals cross there would be wave breaking and reformation. The wave conditions in the lee of the caustic would then not be well defined by the refraction diagram.

4.4 Numerical Refraction Analysis

Numerical refraction analysis by computer requires that the equations for wave orthogonal position and spacing be developed for a wave propagating through water of changing depth. These equations, presented by Arthur et al. (1952), are summarized below.

Figure 4.6 depicts a wave orthogonal crossing a bottom contour where the orthogonal position is given in an horizontal x, y coordinate system. Define θ as the angle between the x axis and a tangent to the wave orthogonal, and s and n as the distances along the orthogonal and wave crest from their point of crossing. Then, from the geometry of the system, an equation defining the redirection of the orthogonal is

$$\frac{d\theta}{ds} = -\frac{1}{C} \frac{dC}{dn} \quad (4.4)$$

Equation (4.4) states that the curvature of the wave orthogonal depends on the gradient of the wave celerity normal to the direction of wave propagation (i.e., along the wave crest) and that the wave orthogonal bends toward the region of lower wave celerity. This is a general statement of the wave refraction process. By the chain rule we can write Eq. (4.4) as

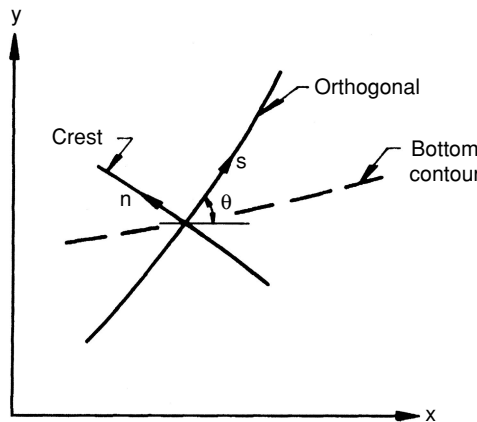


Figure 4.6. Definition sketch for Eq. (4.4).

$$\frac{d\theta}{ds} = \frac{1}{C} \left[\sin \theta \frac{dC}{dx} - \cos \theta \frac{dC}{dy} \right] \quad (4.5)$$

Equation (4.5) must be solved to define the progressive positions of a wave orthogonal as the wave propagates forward. Given the incoming orthogonal direction in the x, y coordinate system, and determining the wave celerity and x and y component gradients of the celerity at a point in the x, y coordinate system one can determine the change in the orthogonal direction at that point. The celerity, from the small-amplitude wave theory, depends on the wave period and water depth at the point of interest. The component gradients of the celerity can be determined in finite difference form from the celerity at two adjacent points separated by a distance x or y . The computed change in orthogonal direction at a point ($d\theta/ds$) is employed to extend the orthogonal a finite distance to a new point where the new orthogonal direction change is computed, etc. This allows the orthogonal line to be advanced in steps toward the shore. The nearshore hydrography is set up on an x, y grid system and an interpolation scheme is established to compute values of dC/dx , dC/dy , and C at intermediate points reached by the extended orthogonal. Smaller grids improve accuracy at the cost of greatly increased computer time.

See Griswold (1963), Wilson (1966), Jen (1969), Keulegan and Harrison (1970), Crowley et al. (1982), Headland and Chiu (1984) and Oh and Grosch (1985) for applications of these refraction analysis techniques including the use of finite-amplitude wave theory, different interpolation schemes, and variable forward step distances to provide increased accuracy in shallower water. The orthogonal spacing can be computed as two orthogonals are extended shoreward to yield values of the refraction coefficient along the wave orthogonals. As an alternative, Munk and Arthur (1951) developed a set of equations that predict the spacing of a pair of closely spaced orthogonals (and thus K_r) at any point along a wave orthogonal. These equations can be employed along with the computation of the path of a single orthogonal propagating toward the shore.

An alternative to the above procedure is to use the conservation of waves equation which equates the number of waves entering and leaving a two-dimensional (x, y) region. This equation can be written (see Dean and Dalrymple, 1984)

$$k \cos \theta \frac{\partial \theta}{\partial x} + k \sin \theta \frac{\partial \theta}{\partial y} = \cos \theta \frac{\partial k}{\partial y} - \sin \theta \frac{\partial k}{\partial x} \quad (4.6)$$

where k is the wave number equal to $2\pi/L$. Equation (4.6) would be solved numerically over an x, y grid to determine values of θ for the points on that grid. Given the deep water direction of the wave orthogonal, the orthogonal can be extended shoreward using interpolated values of θ as the orthogonal is extended forward. See Noda et al. (1974) and Perlin and Dean (1983) for examples of this

approach. The latter coupled their solution with a conservation of energy flux equation which could incorporate energy dissipation as the wave propagated forward to more realistically calculate wave heights. Hardy and Krauss (1987) and Cialone and Krauss (1987) used both the conservation of waves and conservation of energy flux equations with finite-amplitude wave theory to carry out wave refraction and shoaling analyses.

4.5 Refraction by Currents

When a wave train propagates in a region where there is a current of varying velocity, the wave celerity relative to the fixed sea floor will change, causing the wave to refract. Johnson (1947) presented an analysis of this phenomenon assuming deep water waves. A similar analysis can be carried out for intermediate and shallow water waves. The results would be similar but with much more complex equations.

Consider Figure 4.7, which depicts a wave propagating from still water to water having a current velocity U . The orthogonal direction relative to the current interface changes from α to α_c and the wave crest and orthogonal pattern change as shown. From the geometry of this figure Johnson showed that

$$\sin \alpha_c = \frac{\sin \alpha}{\left(1 - \frac{U}{C} \sin \alpha\right)^2} \quad (4.7)$$

where U/C would be negative when the current opposes the wave direction and vice versa. From the conservation of energy flux between two orthogonals Johnson found the following relationship for wave height change:

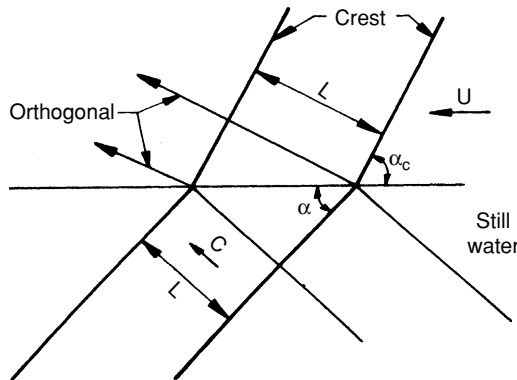


Figure 4.7. Definition sketch for wave refraction by a current.

$$\left(\frac{H_c}{L_c}\right)^2 = \left(\frac{H}{L}\right)^2 \frac{\cos \alpha}{\cos \alpha_c} \left[\frac{(1 - \frac{U}{C} \sin \alpha)^6}{1 + \frac{U}{C} \sin \alpha} \right] \quad (4.8)$$

where

$$L_c = L \frac{\sin \alpha_c}{\sin \alpha}$$

When waves enter a navigation channel where the current is ebbing, the current will cause the waves to decrease in length and increase in height, possibly to the point of breaking. This can have serious negative consequences on navigation, particularly for small vessels. Perigrine (1976) found that if the ebb current is about 0.3 times the celerity that the approaching wave has offshore in still water, waves will break in the channel no matter what the approaching wave steepness may be. For waves entering a channel with a flood current the wave steepness is decreased, which would have a positive effect of vessel navigation.

The creation of an opposing current, for example by a surface water jet or by rising air bubbles, has been used to dissipate wave energy, particularly by steepening and breaking the waves. This would be more effective for shorter steeper waves than for the longer components of a wave spectrum, and one would have to evaluate the cost of the energy required to operate the system versus the effect achieved.

4.6 Wave Diffraction

Consider a train of waves approaching a barrier as shown in Figure 4.8. The portion of the wave that hits the barrier will be reflected and dissipated, with the possible transmission of some wave energy through or over the barrier depending

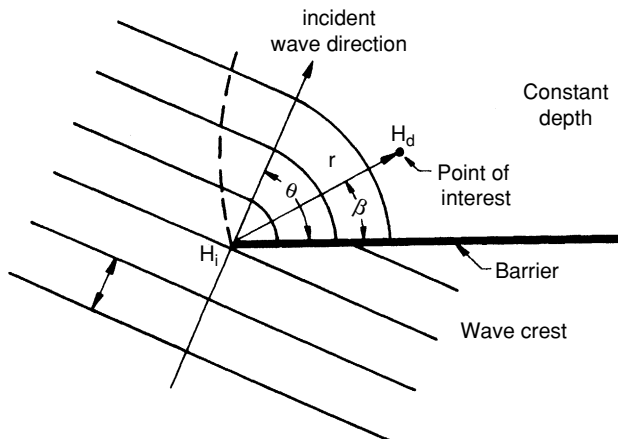


Figure 4.8. Definition sketch for wave diffraction in the lee of a barrier.

on the cross-section geometry and composition of the barrier. The portion of the wave passing the end of the barrier will have a lateral transfer of wave energy along the wave crest into the lee of the barrier. The diffracted wave crests in the lee of the barrier will form approximately concentric circular arcs with the wave height decreasing exponentially along the crests. The shadow region out to the dashed line will have a wave height that is less than the incident wave height at the end of the barrier. Note that the water depth in Figure 4.8 is constant; otherwise the wave crest pattern and wave heights would also be affected by refraction.

If H_i is the incident wave height at the end of the barrier and H_d is the diffracted wave height at a point of interest in the lee of the barrier, we can define a diffraction coefficient $K_d = H_d/H_i$. The value of K_d depends on the location behind the barrier defined by r and β , and the incident wave direction defined by θ ; or in dimensionless form $K_d = f(\theta, \beta, r/L)$ where L is the wave length in the lee of the barrier. Since the wave length is a function of the wave period and water depth, the resulting diffraction coefficient for each component of the wave spectrum would depend on the incident direction and period of that component.

Water wave diffraction is analogous to the diffraction of light. The two most common diffraction problems encountered in coastal engineering design are diffraction past the end of a semi-infinite barrier as depicted in Figure 4.8 and diffraction through a relatively small gap in a barrier. Penny and Price (1952) showed that the mathematical solution for the diffraction of light can be used to predict the wave crest pattern and height variation for these two wave diffraction problems.

Semi-infinite Barrier

A summary of the diffraction solution for a semi-infinite barrier is presented by Wiegel (1964) and by Putnam and Arthur (1948), who also conducted some wave tank experiments to verify results. Wiegel (1962) used the Penny and Price (1952) solution to calculate and tabulate values of K_d for selected values of θ , β , and r/L . His results are tabulated in Table 4.1. Graphic plots of the tabulated results are also presented in Wiegel (1962, 1964) and the U.S. Army Coastal Engineering Research Center (1984). Figure 4.9 is an example of these diagrams for the incident wave approach angle (θ) of 90° . The horizontal position of the point of interest in Figure 4.9 is given in the usual x, y coordinate system nondimensionalized by dividing by the wave length.

A curious result depicted in Figure 4.9 and common to other wave approach directions as shown in Table 4.1 is that the value of K_d along a line extending back from the end of the barrier in the direction of the incident wave is about 0.5. It should also be noted in Figure 4.9 and in Table 4.1 that regions outside of the lee of the barrier have K_d values in excess of unity. These values develop because the theoretical solution assumes a perfectly reflecting barrier and a small portion of the reflected wave energy diffracts to add to the energy of the incident wave in

Table 4.1. K_d versus θ , β , r/L for Semi-Infinite Breakwater

	β (Degrees)													
r/L	0	15	30	45	60	75	90	105	120	135	150	165	180	
$\theta = 15^\circ$														
1/2	0.49	0.79	0.83	0.90	0.97	1.01	1.03	1.02	1.01	0.99	0.99	1.00	1.00	
1	0.38	0.73	0.83	0.95	1.04	1.04	0.99	0.98	1.01	1.01	1.00	1.00	1.00	
2	0.21	0.68	0.86	1.05	1.03	0.97	1.02	0.99	1.00	1.00	1.00	1.00	1.00	
5	0.13	0.63	0.99	1.04	1.03	1.02	0.99	0.99	1.00	1.01	1.00	1.00	1.00	
10	0.35	0.58	1.10	1.05	0.98	0.99	1.01	1.00	1.00	1.00	1.00	1.00	1.00	
$\theta = 30^\circ$														
1/2	0.61	0.63	0.68	0.76	0.87	0.97	1.03	1.05	1.03	1.01	0.99	0.95	1.00	
1	0.50	0.53	0.63	0.78	0.95	1.06	1.05	0.98	0.98	1.01	1.01	0.97	1.00	
2	0.40	0.44	0.59	0.84	1.07	1.03	0.96	1.02	0.98	1.01	0.99	0.95	1.00	
5	0.27	0.32	0.55	1.00	1.04	1.04	1.02	0.99	0.99	1.00	1.01	0.97	1.00	
10	0.20	0.24	0.54	1.12	1.06	0.97	0.99	1.01	1.00	1.00	1.00	0.98	1.00	
$\theta = 45^\circ$														
1/2	0.49	0.50	0.55	0.63	0.73	0.85	0.96	1.04	1.06	1.04	1.00	0.99	1.00	
1	0.38	0.40	0.47	0.59	0.76	0.95	1.07	1.06	0.98	0.97	1.01	1.01	1.00	
2	0.29	0.31	0.39	0.56	0.83	1.08	1.04	0.96	1.03	0.98	1.01	1.00	1.00	
5	0.18	0.20	0.29	0.54	1.01	1.04	1.05	1.03	1.00	0.99	1.01	1.00	1.00	
10	0.13	0.15	0.22	0.53	1.13	1.07	0.96	0.98	1.02	0.99	1.00	1.00	1.00	

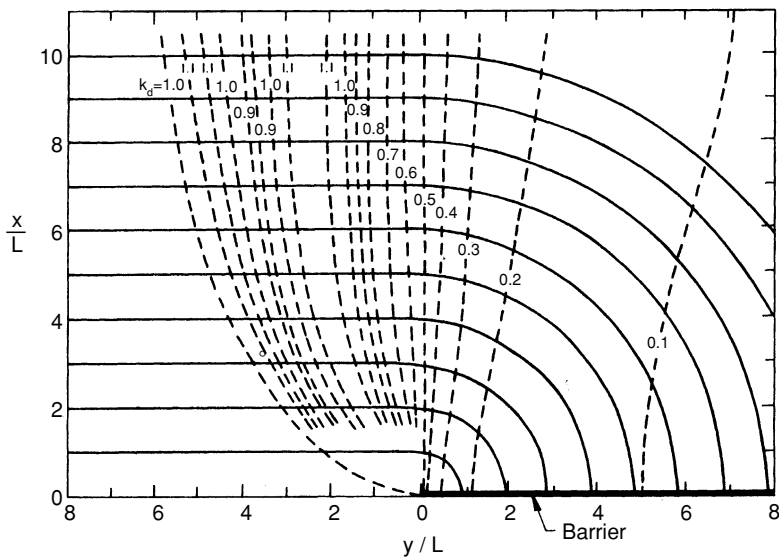


Figure 4.9. Wave crest pattern and related K_d values for normal wave incidence. (Wiegel, 1962.)

(Table 4.1. continued.)

r/L	β (Degrees)												
	0	15	30	45	60	75	90	105	120	135	150	165	180
$\theta = 60^\circ$													
1/2	0.40	0.41	0.45	0.52	0.60	0.72	0.85	1.13	1.04	1.06	1.03	1.01	1.00
1	0.31	0.32	0.36	0.44	0.57	0.75	0.96	1.08	1.06	0.98	0.98	1.01	1.00
2	0.22	0.23	0.28	0.37	0.55	0.83	1.08	1.04	0.96	1.03	0.98	1.01	1.00
5	0.14	0.15	0.18	0.28	0.53	1.01	1.04	1.05	1.03	0.99	0.99	1.00	1.00
10	0.10	0.11	0.13	0.21	0.52	1.14	1.07	0.96	0.98	1.01	1.00	1.00	1.00
$\theta = 75^\circ$													
1/2	0.34	0.35	0.38	0.42	0.50	0.59	0.71	0.85	0.97	1.04	1.05	1.02	1.00
1	0.25	0.26	0.29	0.34	0.43	0.56	0.75	0.95	1.02	1.06	0.98	0.98	1.00
2	0.18	0.19	0.22	0.26	0.36	0.54	0.83	1.09	1.04	0.96	1.03	0.99	1.00
5	0.12	0.12	0.13	0.17	0.27	0.52	1.01	1.04	1.05	1.03	0.99	0.99	1.00
10	0.08	0.08	0.10	0.13	0.20	0.52	1.14	1.07	0.96	0.98	1.01	1.00	1.00
$\theta = 90^\circ$													
1/2	0.31	0.31	0.33	0.36	0.41	0.49	0.59	0.71	0.85	0.96	1.03	1.03	1.00
1	0.22	0.23	0.24	0.28	0.33	0.42	0.56	0.75	0.96	1.07	1.05	0.99	1.00
2	0.16	0.16	0.18	0.20	0.26	0.35	0.54	0.69	1.08	1.04	0.96	1.02	1.00
5	0.10	0.10	0.11	0.13	0.16	0.27	0.53	1.01	1.04	1.05	1.02	0.99	1.00
10	0.07	0.07	0.08	0.09	0.13	0.20	0.52	1.14	1.07	0.96	0.99	1.01	1.00
$\theta = 105^\circ$													
1/2	0.28	0.28	0.29	0.32	0.35	0.41	0.49	0.59	0.72	0.85	0.97	1.01	1.00
1	0.20	0.20	0.24	0.23	0.27	0.33	0.42	0.56	0.75	0.95	1.06	1.04	1.00
2	0.14	0.14	0.13	0.17	0.20	0.25	0.35	0.54	0.83	1.08	1.03	0.97	1.00
5	0.09	0.09	0.10	0.11	0.13	0.17	0.27	0.52	1.02	1.04	1.04	1.02	1.00
10	0.07	0.06	0.08	0.08	0.09	0.12	0.20	0.52	1.14	1.07	0.97	0.99	1.00
$\theta = 120^\circ$													
1/2	0.25	0.26	0.27	0.28	0.31	0.35	0.41	0.50	0.60	0.73	0.87	0.97	1.00
1	0.18	0.19	0.19	0.21	0.23	0.27	0.33	0.43	0.57	0.76	0.95	1.04	1.00
2	0.13	0.13	0.14	0.14	0.17	0.20	0.26	0.16	0.55	0.83	1.07	1.03	1.00
5	0.08	0.08	0.08	0.09	0.11	0.13	0.16	0.27	0.53	1.01	1.04	1.03	1.00
10	0.06	0.06	0.06	0.07	0.07	0.09	0.13	0.20	0.52	1.13	1.06	0.98	1.00
$\theta = 135^\circ$													
1/2	0.24	0.24	0.25	0.26	0.28	0.32	0.36	0.42	0.52	0.63	0.76	0.90	1.00
1	0.18	0.17	0.18	0.19	0.21	0.23	0.28	0.34	0.44	0.59	0.78	0.95	1.00
2	0.12	0.12	0.13	0.14	0.14	0.17	0.20	0.26	0.37	0.56	0.84	1.05	1.00
5	0.08	0.07	0.08	0.08	0.09	0.11	0.13	0.17	0.28	0.54	1.00	1.04	1.00
10	0.05	0.06	0.06	0.06	0.07	0.08	0.09	0.13	0.21	0.53	1.12	1.05	1.00
$\theta = 150^\circ$													
1/2	0.23	0.23	0.24	0.25	0.27	0.29	0.33	0.38	0.45	0.55	0.68	0.83	1.00
1	0.16	0.17	0.17	0.18	0.19	0.22	0.24	0.29	0.36	0.47	0.63	0.83	1.00

(Table 4.1. continued.)

	β (Degrees)												
r/L	0	15	30	45	60	75	90	105	120	135	150	165	180
2	0.12	0.12	0.12	0.13	0.14	0.15	0.18	0.22	0.28	0.39	0.59	0.86	1.00
5	0.07	0.07	0.08	0.08	0.08	0.10	0.11	0.13	0.18	0.29	0.55	0.99	1.00
10	0.05	0.05	0.05	0.06	0.06	0.07	0.08	0.10	0.13	0.22	0.54	1.10	1.00
$\theta = 165^\circ$													
1/2	0.23	0.23	0.23	0.24	0.26	0.28	0.31	0.35	0.41	0.50	0.63	0.79	1.00
1	0.16	0.16	0.17	0.17	0.19	0.20	0.23	0.26	0.32	0.40	0.53	0.73	1.00
2	0.11	0.11	0.12	0.12	0.13	0.14	0.16	0.19	0.23	0.31	0.44	0.68	1.00
5	0.07	0.07	0.07	0.07	0.08	0.09	0.10	0.12	0.15	0.20	0.32	0.63	1.00
10	0.05	0.05	0.05	0.06	0.06	0.06	0.07	0.08	0.11	0.11	0.21	0.58	1.00
$\theta = 180^\circ$													
1/2	0.20	0.25	0.23	0.24	0.25	0.28	0.31	0.34	0.40	0.49	0.61	0.78	1.00
1	0.10	0.17	0.16	0.18	0.18	0.23	0.22	0.25	0.31	0.38	0.50	0.70	1.00
2	0.02	0.09	0.12	0.12	0.13	0.18	0.16	0.18	0.22	0.29	0.40	0.60	1.00
5	0.02	0.06	0.07	0.07	0.07	0.08	0.10	0.12	0.14	0.18	0.27	0.46	1.00
10	0.01	0.05	0.05	0.06	0.06	0.07	0.07	0.08	0.10	0.13	0.20	0.36	1.00

From Wiegel, 1962.

this region. For a real barrier with a low reflection coefficient it is not likely that these values in excess of unity would occur.

Example 4.6-1

Consider a train of 6 s period waves approaching a breakwater so that the angle of approach at the breakwater head (θ) is 60° . The water depth in the lee of the breakwater is 10 m. Determine the wave height at an angle (β) of 30° from the breakwater and a distance of 96.6 m from the breakwater head if the incident wave height at the head is 2.2 m.

Solution:

For a wave period of 6 s and a water depth of 10 m we can calculate the wave length in the lee of the breakwater [by trial using Eq. (2.14)], $L = 48.3$ m.

From Table 4.1 for $r/L = 2.0$, $\theta = 60^\circ$, and $\beta = 30^\circ$ we have $K_d = 0.28$.

Thus, the wave height at the point of interest is $0.28(2.2) = 0.62$ m. At the point of interest the wave would be propagating in the direction of the 30° radial line.

Note from Table 4.1 that a spectrum of waves all coming from the same direction will experience a greater percentage decrease in wave height at successively lower periods (i.e., higher values of r/L for the same point). Thus, the energy density concentration in the wave spectrum will shift toward the higher

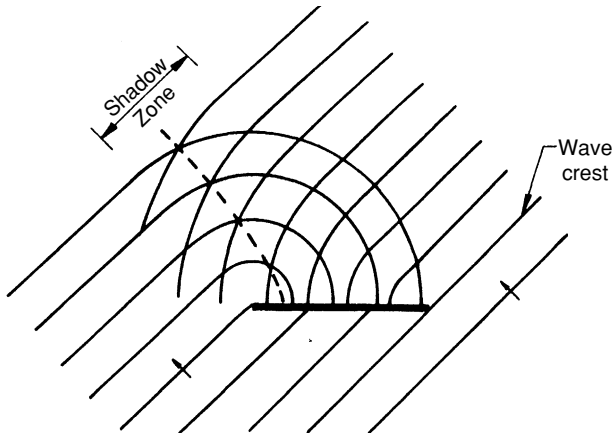


Figure 4.10. Diffraction in the lee of a barrier of finite length. (U.S. Army Coastal Engineering Research Center, 1984.)

wave periods in the spectrum. For a spectrum of waves having a range of periods and directions one can evaluate on a component-by-component basis the modified characteristics for a diffracted wave spectrum at a particular point of interest (e.g., see Goda, 1985).

When waves approach a barrier of finite length and wave diffraction occurs at both ends, a wave crest pattern similar to that shown in Figure 4.10 will develop. It can be constructed by combining the patterns for semi-infinite barrier diffraction at each end. The wave crests combine along lines like the dashed line to form the higher amplitudes which may be estimated (assuming linear waves) by combining the heights from the two separate patterns. Harms (1979) has presented an analytical solution for the wave weight pattern in the lee of the barrier and performed laboratory experiments to evaluate his analysis.

Barrier Gap

Penny and Price (1952) also presented a solution for the diffraction of waves passing through a gap in a barrier. These solutions were in agreement with the results of wave tank studies conducted by Blue and Johnson (1949). Johnson (1952) presented plots of diffraction coefficient versus nondimensional horizontal position similar to Figure 4.11 for normally incident waves penetrating barrier gaps having a range of dimensions from one to five wave lengths.

Johnson (1952) demonstrated that these diffraction diagrams could also be used if the angle of wave approach is other than 90° by using a projected imaginary gap width as shown in Figure 4.12. When the gap width is about five times the incident wave length or greater, the diffraction zones caused by

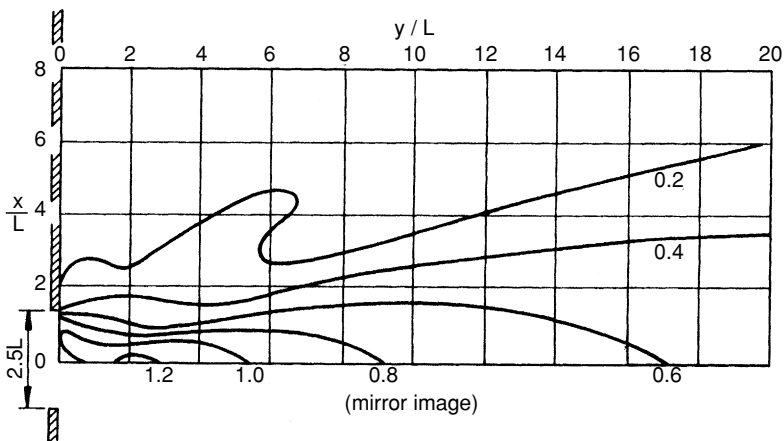


Figure 4.11. K_d values for the lee of a barrier gap 2.5 wave lengths wide, with normally incident waves. (Johnson, 1952.)

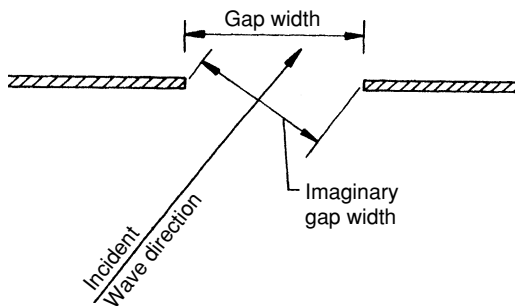


Figure 4.12. Oblique wave incident to a barrier gap.

the barrier on each end of the gap are essentially independent. Then, the diffraction analyses for the two separate semi-infinite barriers may be combined.

Johnson (1952), using analytical results from Carr and Stelzreide (1952), also presented a series of diffraction diagrams for a range of incident wave directions passing through a single gap width equal to one wave length. A compilation of all of the barrier gap diffraction diagrams discussed above is presented by the U.S. Army Coastal Engineering Research Center (1984). Often, the barrier geometries encountered in practice will not be the same as the specific geometries for which solutions are presented. However, approximate but useful results can still be achieved by employing these solutions with some ingenuity to approximate the effect of the actual barrier geometry. If the project is of sufficient

importance, these approximate results can also be coupled with limited physical model tests to achieve better results.

Wave Action in Harbors

A major design concern for typical marinas or small craft harbors is to limit the wave height in the interior of the harbor at the points where vessels are docked. This limit would be established for a given design wave condition or conditions having a specified probability of occurrence. A typical criteria for marinas where recreational vessels and small working vessels are docked is to limit the wave height to 0.3 m under “normal” conditions but to allow up to a 0.6 m wave height during “extreme storm events” (Cox and Clark, 1992). Normal conditions would be a wave event that is exceeded only once a year and extreme storm events might be an event that is exceeded once in fifty years. It is preferable that the waves approach a moored vessel head on; for beam seas the allowable wave heights might be reduced. For large vessels (e.g. tankers and bulk carriers) the allowable wave heights would be significantly higher.

Typically, the water depth in a marina or harbor is dredged to one or more constant depths so that as a wave enters the harbor, diffraction dominates in establishing the wave height variation throughout the harbor. The design wave or waves will typically be specified (height and direction) in deep water offshore of the harbor. Shoaling and refraction analyses (e.g. see Figure 4.5) would determine the height and direction of the incident wave at the tip of the breakwater that protects the harbor. This might be a single breakwater as depicted in Figures 4.5 and 4.9 or a pair of breakwaters having a gap as depicted in Figures 4.11 and 4.12.

The harbor designer can then adjust the length of the single breakwater or the gap width between the breakwater pair to control the wave height at points of interest within the harbor. A minimum gap width might be dictated by other considerations such as the width of the channel required for vessels to navigate through the harbor entrance. The possibility that wave energy can penetrate the harbor by wave transmission through or over the breakwater must also be considered. Also, the wave reflection characteristics of the harbor interior boundaries (see Section 4.8) must be considered.

4.7 Combined Refraction and Diffraction

Whenever the wave height is not constant along a wave crest wave diffraction will occur to diminish the wave height variation. For the example depicted in Figure 4.5 a refraction/shoaling analysis from deep water to the breakwater would be adequate for most design purposes. One should realize, however, that in some areas such as where the orthogonals converge at the breakwater

dogleg the wave height may be lower than predicted because of the lateral spread of energy caused by wave diffraction.

Immediately in the lee of the breakwater in Figure 4.5 wave diffraction would dominate, owing to the cutting of the wave crest by the breakwater head and to the fact that the bottom is relatively flat in the lee of the breakwater. As the wave moves further shoreward to where the bottom contours commence to change significantly (i.e., inside the -10 m contour) both refraction and diffraction might be significant. The significance of refraction would depend both on the bottom slope and on how large of an angle is formed between the wave crests and the bottom contours. For cases like this, the U.S. Army Coastal Engineering Research Center (1984) recommends carrying the diffraction process forward for three or four wave lengths in the lee of the breakwater and then continuing with the wave refraction analysis as a way to account for the combined effects of refraction and diffraction. After three or four wave lengths the diffractive effects are well established so the refraction of the wave with this wave crest pattern and height distribution can now be carried forward. The actual number of wave lengths for which the diffraction analysis should proceed before the refraction analysis should take over would depend on the actual bottom conditions as discussed above.

Mobarek (1962) conducted experiments in a wave basin that had a single barrier oriented parallel to the wave generator and extending part of the way across the basin. There was an opening from the barrier tip to the opposite basin wall. In the lee of the barrier there was a 1:12 sloped bottom with straight bottom contours situated normal to the barrier. For an incident wave with $d/L = 0.14$ at the barrier tip the experimental wave heights on the slope generally agreed with the heights determined by the suggested procedure, which was applied by constructing a diffraction diagram for one wave length in the lee of the barrier and then conducting the refraction analysis to the point of interest on the slope.

In practice, there may be some situations where an adequate analysis cannot be conducted by the alternate application of diffraction and refraction analyses. Such problems may be studied by a physical model. The cost and time requirements for a physical model study may make it of limited value, particularly for small projects or projects with time constraints on completion of the design. Also, there are some physical constraints on combined refraction-diffraction model studies. If the model does not require a vertical to horizontal scale distortion then both refraction and diffraction can be studied simultaneously. But, space limitations, viscous and surface tension scale effects, and difficulties in adequately measuring wave heights in a small vertical scale model may require that the model be distorted. Then, both refraction and diffraction cannot simultaneously be modeled if intermediate depth water waves are being studied (see Chapter 9 and Sorensen, 1993).

Recently, numerical model analyses of wave propagation where refraction and diffraction are both important have been developed using the mild slope equation

first presented by Berkhoff (1972). These analyses are successful where refraction/diffraction are not strong over a large lateral extent. For example, this approach would be useful to give a better analysis of wave height variation seaward of the breakwater in Figure 4.5 than the classic refraction/shoaling analysis alone. For some examples see Berkhoff et al. (1982), Ebersole (1985), Houston (1981), Kirby and Dalrymple (1983), Lozano and Liu (1980), and Tsay and Liu (1983).

4.8 Wave Reflection

The reflection of two-dimensional waves, where a reflection coefficient $C_r = H_r/H_i$ was defined, was covered in Section 2.7. When waves in a three-dimensional domain obliquely approach a reflecting barrier a method is required to predict the shape and orientation of the reflected wave crests. This, along with the reflection coefficient allows one to determine the wave height along the reflected wave crest.

Consider Figure 4.13, which shows an incident wave crest, which may be curved as a result of previous diffraction, and is undergoing refraction as it approaches a reflecting barrier. To construct the reflected wave crest pattern, first construct imaginary mirror image bottom contours in the lee of the reflecting barrier. Then extend the incident wave crest into this imaginary domain, refracting and diffracting it as necessary. Then construct a mirror image of this wave crest that was constructed in the imaginary domain. This will be the pattern of the reflected wave crest. The wave height at any point along the reflected wave crest will be the wave height at the equivalent point in the imaginary domain times the reflection coefficient of the barrier.

An example that further demonstrates this process is depicted in Figure 4.14, where a straight crested wave passes a barrier, diffracts into the lee of that barrier, and then reflects off a second barrier. The water depth is constant so the wave only undergoes diffraction and reflection. The imaginary diffracted wave crest pattern is carried to point A' where the imaginary wave height can

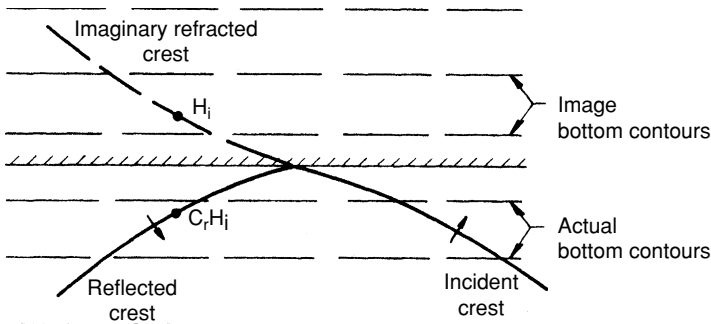


Figure 4.13. Wave reflection analysis.

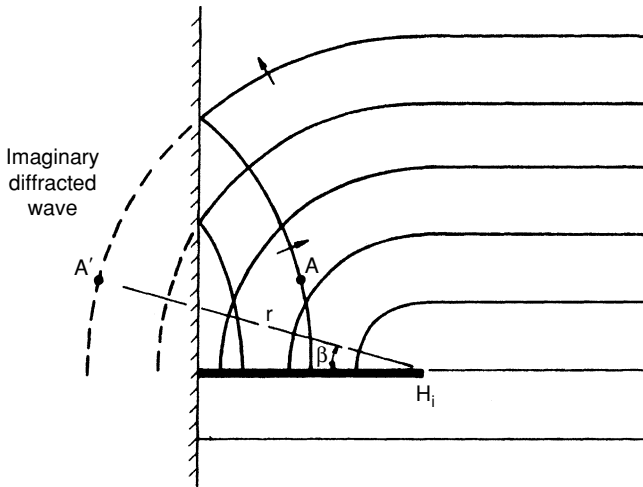


Figure 4.14. Combined wave diffraction and reflection.

be determined from the incident height and direction along with the values of r and β as previously discussed. The reflected wave height at point A would equal the imaginary diffracted height at point A' times the reflection coefficient. Remember, the wave crests are continually moving forward, the patterns depicted in Figures 4.13 and 4.14 are only a “snapshot” in time showing one view of the advancing wave crests. The total vertical displacement of the water surface at any point would equal the sum of the displacements of the incident wave and reflected wave at that point and instant of time.

As the waves continue to propagate forward they may be reflected again and again to produce complex patterns, particularly inside of harbors where most of the boundaries have relatively high reflection coefficients. An analysis of the reflection patterns and related reflected wave heights may indicate potential “trouble spots” in a harbor. Inspection of the pattern of reflected waves will indicate possible desired changes in the harbor boundaries (e.g., lowering the reflection coefficient of a segment of the harbor boundary by changing it from a vertical bulkhead to a sloping stone revetment). Ippen (1966) discusses this in greater detail and presents suggestions for applying these concepts to the study of wave reflection in harbors.

4.9 Vessel-Generated Waves

In restricted areas, owing to the relatively short expanse of water over which the wind can generate waves, the waves generated by a moving vessel often are the dominant waves for design.

As a vessel moves across the water surface, the flow of water back across the vessel hull causes a varying pressure distribution over the hull surface. The magnitudes of these dynamic pressures depend on the vessel speed, the water depth (if sufficiently shallow), the vessel hull geometry and draft, and the channel cross-section shape if the channel is relatively narrow. For vessels moving in a confined channel the resulting pressure gradients will be greater than if the vessel is moving across a wide and deep body of water.

For common vessel hull shapes, the pressure will rise in the vicinity of the vessel bow, fall below the free stream pressure along the midsection of the hull, and rise again at the vessel stern. The water surface profile along the hull responds to this pressure variation, rising at the bow and stern and falling along the midsection. Owing to flow separation that is common at the vessel stern, the pressure and resulting water surface rise will be less there than at the bow. The inertia of the rising and falling water causes the water to lag behind its equilibrium position and to produce a surface oscillation which, in turn, produces the pattern of free waves that propagate out from the vessel. The amplitude of the waves will depend on the magnitude of the pressure variation (i.e. on the vessel speed, hull geometry and draft, and the water depth). The period (length) and direction of propagation of the waves depends only on the vessel speed and water depth.

For some lighter vessels moving at higher speeds, the hydrodynamic forces on the hull will lift the vessel (planing) so it “skims” the water surface. When a vessel planes, the generated wave heights are lower than they otherwise would be and do not noticeably increase with increasing vessel speed. Sorensen (1973)

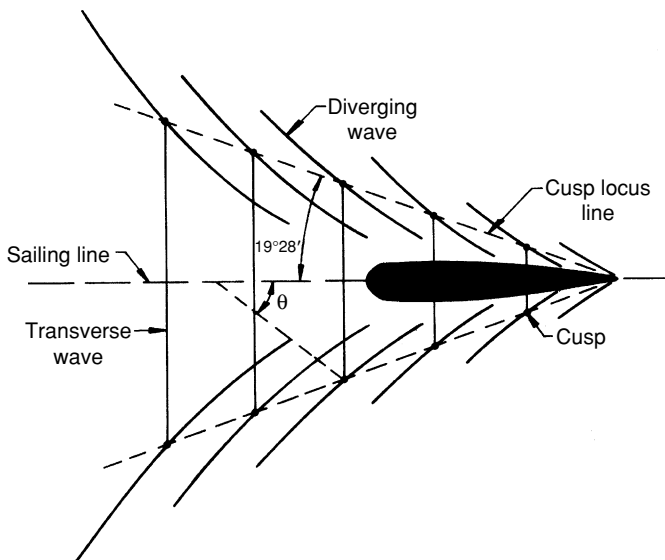


Figure 4.15. Deep water wave crest pattern generated by the bow of a moving vessel.

gives a more thorough review of the generation and resulting characteristics of vessel generated waves.

Figure 4.15 shows the wave crest pattern generated by the bow of a vessel moving across deep water. Only the crests in the vicinity of the vessel are shown. The pattern of waves would extend back from the vessel with decreasing wave amplitudes until the wave crests are no longer discernable.

The wave pattern consists of symmetrical pairs of diverging waves that move obliquely out from the vessel sailing line and a single set of transverse waves that move forward in the direction of the sailing line. The transverse and diverging waves meet to form cusps which are located along lines that are $19^{\circ}28'$ out from the sailing line. The largest wave amplitudes are at the cusps. A similar wave pattern, but usually with lower amplitudes would be generated at the stern. If the vessel speed is increased, the wave lengths would accordingly increase, but the overall pattern (including the $19^{\circ}28'$ angle) would retain the same form.

Since the wave pattern remains steady relative to the vessel, the celerity C of all of the waves in the pattern must be related to the vessel speed V by

$$C = V \cos \Theta$$

Where Θ is the angle between the sailing line and the direction of wave propagation as depicted in Figure 4.15. For diverging waves in deep water the theoretical value of Θ is $35^{\circ} 16'$. Consequently, the diverging wave crests form an angle of $54^{\circ} 44'$ with the sailing line at the cusp point (i.e. $180^{\circ} - 90^{\circ} - 35^{\circ}16' = 54^{\circ}44'$).

Owing to wave diffraction, successive transverse and diverging waves aft of the vessel have increasing crest lengths and commensurate energy densities and wave amplitudes. It can be shown (Havelock, 1908) that the diverging wave heights at the cusp points should decrease at a rate that is inversely proportional to the cube root of the distance from the sailing line. Transverse wave heights at the sailing line decrease at a rate that is inversely proportional to the square root of the distance from the vessel bow. Thus, at a greater distance from the vessel, the diverging waves become relatively higher than the transverse waves.

Note that the diverging waves are propagating away from the sailing line; however, the wave pattern does not change if the vessel maintains a constant speed. This apparent anomaly is explained by considering the group celerity (Section 2.5) for deep water waves. As a diverging wave propagates forward one wave length (refer to Figure 4.15), half of its energy remains behind. The outer portion of the diverging wave receives no energy from the wave in front of it, but the inner portion of the wave does. Thus, as the diverging waves propagate forward, they diminish at the outer end and grow at the inner end, allowing them to remain stationary relative to the vessel. Also, by this process, the total wave system adds one wave at the distant point for each wave length that the vessel advances.

The total drag on a moving vessel consists of the fluid friction and form drag owing to flow past the hull, plus the vessel wave drag as it is energy from the

vessel that produces the vessel wave system. As a vessel's speed is increased, wave amplitudes and wave drag increase exponentially.

Also, as the vessel speed increases causing the generated wave lengths to increase, the waves may become long enough to "feel" the bottom ($d/L < 0.5$). This occurs when the Froude number F (where $F = V/(gd)^{0.5}$) exceed approximately 0.7. As the Froude number increases from 0.7 to 1.0, the transverse wave heights increase faster than the diverging wave heights, becoming more prominent toward $F = 1$. Concurrently, the cusp locus angle increases from $19^\circ 18'$ to 90° at $F = 1$. At $F = 1$, with the cusp locus angle equal to 90° , the diverging and transverse waves have coalesced with their crests oriented perpendicular to the sailing line. Also, most of the energy in the wave system is concentrated in the first wave at the bow.

For Froude numbers in excess of unity, since the greatest wave celerity can only equal $(gd)^{0.5}$, no transverse waves can exist. Diverging waves extend back from the vessel and form an angle equal to $\arcsin(F^{-1})$ with the sailing line (similar to the Mach angle in aerodynamics).

In addition to the vessel speed and the water depth, the generated wave heights depend on the vessel bow geometry and draft. Consequently, most wave height prediction schemes are semi-empirical. Sorensen (1989, 1997) summarizes field and laboratory vessel-generated wave height measurements, as well as most of the available wave height prediction schemes. For the range of vessel speeds between 5 and 15 knots the maximum wave heights generated by a vessel (near the vessel at the cusp point) typically range between 0.2 and 0.9 m. Common wave periods range between 1 and 2.5s.

4.10 Summary

The basic material on surface waves covered to this point can generally be applied to the full range of wave periods from the shorter wind generated waves to long period waves such as the astronomical tide. But the applications of this material that were presented have focused on the characteristics and behavior of the wind wave portion of the wide spectrum of waves that occur at sea. Next, we must turn our attention to the longer period fluctuations of coastal water levels, which includes wave phenomena such as the tide and seismically generated tsunamis as well as phenomena such as storm surge which does not primarily involve wave action.

4.11 References

Arthur, R.S., Munk, W.H., and Isaacs, J.D. (1952), "The Direct Construction of Wave Rays," *Transactions, American Geophysical Union*, Vol. 33, pp. 855–865.

- Berkhoff, J.C.W. (1972), "Computation of Combined Refraction-Diffraction," in *Proceedings, 13th International Conference on Coastal Engineering*, American Society of Civil Engineers, Vancouver, pp. 471-490.
- Berkhoff, J.C.W., Booij, N., and Radder, A.C. (1982), "Verification of Numerical Wave Propagation Models for Simple Harmonic Linear Water Waves," *Coastal Engineering*, Vol. 6, pp. 255-279.
- Blue, F.L. and Johnson, J.W. (1949), "Diffraction of Water Waves Passing Through a Breakwater Gap," *Transactions, American Geophysical Union*, Vol. 33, pp. 705-718.
- Carr, J.H. and Stelzreide, M.E. (1952), "Diffraction of Water Waves by Breakwaters," *Gravity Waves*, Circular 521, National Bureau of Standards, Washington, DC, pp. 109-125.
- Cialone, M.A. and Kraus, N.C. (1987), "A Numerical Model for Shoaling and Refraction of Third-Order Stokes Waves Over an Irregular Bottom," Miscellaneous Paper CERC 87-10, U.S. Army Waterways Experiment Station, Vicksburg, MS.
- Crowley, J.B., Fleming, C.A., and Cooper, C.K. (1982), "Computer Model for the Refraction of Nonlinear Waves," in *Proceedings, 18th International Conference on Coastal Engineering*, American Society of Civil Engineers, Cape Town, pp. 384-403.
- Cox, J.C. and Clark, G.R. (1992), "Design Development of a Tandem Breakwater System for Hammond Indiana," in *Proceedings, Coastal Structures and Breakwaters Conference*, Thomas Telford, London, pp. 111-121.
- Dean, R.G. and Dalrymple, R.A. (1984), *Water Wave Mechanics for Engineers and Scientists*, Prentice-Hall, Englewood Cliffs, NJ.
- Ebersole, B.A. (1985), "Refraction-Diffraction Model for Linear Water Waves," *Journal, Waterway, Port, Coastal and Ocean Engineering Division, American Society of Civil Engineers*, November, pp. 939-953.
- Goda, Y. (1985), *Random Seas and the Design of Maritime Structures*, University of Tokyo Press, Tokyo.
- Griswold, G.M. (1963), "Numerical Calculation of Wave Refraction," *Journal of Geophysical Research*, Vol. 68, pp. 1715-1723.
- Hardy, T.A. and Krauss, N.C. (1987), "A Numerical Model for Shoaling and Refraction of Second Order Cnoidal Waves Over an Irregular Bottom," Miscellaneous Paper CERC 87-9, U.S. Army Waterways Experiment Station, Vicksburg, MS.
- Harms, V.W. (1979), "Diffraction of Water Waves by Isolated Structures," *Journal, Waterway, Port, Coastal and Ocean Engineering Division, American Society of Civil Engineers*, May, pp. 131-147.
- Havelock, T.H. (1908), "The Propagation of Groups of Waves in Dispersive Media, with Application to Waves on Water Produced by a Travelling Disturbance," *Proceedings Royal Society of London Series A*, pp. 398-430.
- Headland, J.R. and Chiu, H.-L. (1984), "A Numerical Model for Refraction of Linear and Cnoidal Waves," in *Proceedings, 19th International Conference on Coastal Engineering*, American Society of Civil Engineers, Houston, pp. 1118-1131.

- Houston, J.R. (1981), "Combined Refraction and Diffraction of Short Waves Using the Finite Element Method," *Applied Ocean Research*, Vol. 3, pp. 163–170.
- Ippen, A.T. (1966), *Estuary and Coastline Hydrodynamics*, McGraw-Hill, New York.
- Jen, Y. (1969), "Wave Refraction Near San Pedro Bay, California," *Journal, Waterways and Harbors Division, American Society of Civil Engineers*, August, pp. 379–393.
- Johnson, J.W. (1947), "The Refraction of Surface Waves by Currents," *Transactions, American Geophysical Union*, Vol. 28, pp. 867–874.
- Johnson, J.W. (1952), "Generalized Wave Diffraction Diagrams," in *Proceedings, 2nd Conference on Coastal Engineering*, Council on Wave Research, Berkeley, pp. 6–23.
- Johnson, J.W., O'Brien, M.P., and Isaacs, J.D. (1948), "Graphical Construction of Wave Refraction Diagrams," Navy Hydrographic Office Publication Number 605, Washington, DC.
- Keulegan, G.H. and Harrison, J. (1970), "Tsunami Refraction Diagrams by Digital Computer," *Journal, Waterways and Harbors Division, American Society of Civil Engineers*, May, pp. 219–233.
- Kirby, J.T. and Dalrymple, R.A. (1983), "A Parabolic Equation for the Combined Refraction–Diffraction of Stokes Waves by Mildly Varying Topography," *Journal of Fluid Mechanics* Vol. 136, pp. 453–466.
- Lozano, C.J. and Liu, P.L.-F. (1980), "Refraction–Diffraction Model for Linear Surface Water Waves," *Journal of Fluid Mechanics*, Vol. 101, pp. 705–720.
- Mobarek, I. (1962), "Effect of Bottom Slope on Wave Diffraction," Report HEL 1-1, Hydraulic Engineering Laboratory, University of California, Berkeley.
- Munk, W.H. and Arthur, R.S. (1951), "Wave Intensity Along a Refracted Ray," *Gravity Waves*, Circular 521, National Bureau of Standards, Washington, DC, pp. 95–108.
- Noda, E.K., Sonu, C.J., Rupert, V.C., and Collins, J.I. (1974), "Nearshore Circulation Under Sea Breeze Conditions and Wave Current Interaction in the Surf Zone," Tetra Tech Report P-72–149–4, Pasadena, CA.
- Oh, I.S. and Grosch, C.E. (1985), "Numerical Study of Finite Amplitude Wave Refraction," *Journal, Waterway, Port, Coastal and Ocean Engineering Division, American Society of Civil Engineers*, January, pp. 78–95.
- Penny, W.G. and A.T. Price (1952), "The Diffraction Theory of Sea Waves by Breakwaters and the Shelter Afforded by Breakwaters," *Philosophical Transactions, Royal Society*, Series A, Vol. 244, London, pp. 236–253.
- Perigrine, D.H. (1976), "Interaction of Water Waves and Currents," *Advances in Applied Mathematics*, Vol. 16, Academic, New York, pp. 9–117.
- Perlin, M. and Dean, R.G. (1983), "An Efficient Algorithm for Wave Refraction/Shoaling Problems," in *Proceedings, Coastal Structures '83 Conference*, American Society of Civil Engineers, Arlington, VA, pp. 988–999.
- Putnam, J.A. and Arthur, R.S. (1948), "Diffraction of Water Waves by Breakwaters," *Transactions, American Geophysical Union*, Vol. 29, pp. 481–490.
- Sorensen, R.M. (1973), "Ship-Generated Waves," *Advances in Hydrosience* Academic Press, New York, Vol.9, pp. 49–83.

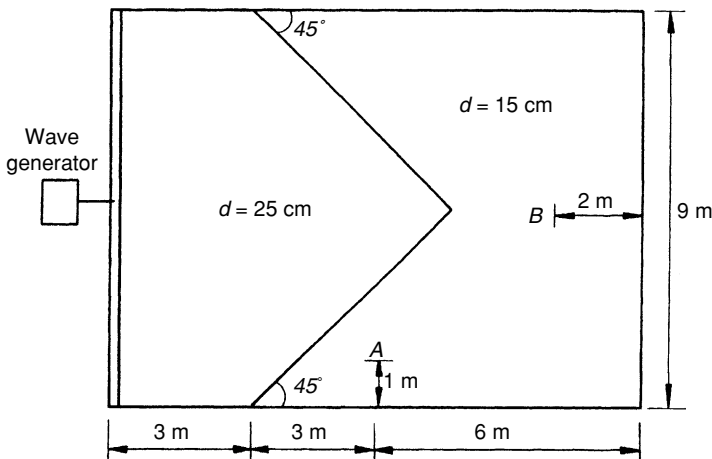
- Sorensen, R.M. (1993), *Basic Wave Mechanics for Coastal and Ocean Engineers*, John Wiley, New York.
- Sorensen, R.M. (1989), "Port and Channel Bank Protection from Ship Waves," *Proceedings, Ports '89 Conference*, American Society of Civil Engineers, Boston, pp. 393–401.
- Sorensen, R.M. (1997), "Prediction of Vessel-Generated Waves with Reference to Vessels Common to the Upper Mississippi River System," ENV Report 4, U.S. Army Corps of Engineers, Upper Mississippi River-Illinois Waterway System Navigation Study, Rock Island, Illinois.
- Tsay, T.-K. and Liu, P.L.-F. (1983), "A Finite Element Model for Refraction and Diffraction," *Applied Ocean Research*, Vol. 5, pp. 30–37.
- U.S. Army Coastal Engineering Research Center (1984), *Shore Protection Manual*, U.S. Government Printing Office, Washington, DC.
- Wiegel, R.L. (1962), "Diffraction of Waves by Semi-infinite Breakwater," *Journal, Hydraulics Division, American Society of Civil Engineers*, January, pp. 27–44.
- Wiegel, R.L. (1964), *Oceanographical Engineering*, Prentice-Hall, Englewood Cliffs, NJ.
- Wiegel, R.L. and Arnold, A.L. (1957), "Model Study of Wave Refraction," Technical Memorandum 103, U.S. Army Corps of Engineers Beach Erosion Board, Washington, DC.
- Wilson, W.S. (1966), "A Method for Calculating and Plotting Surface Wave Rays," Technical Memorandum 17, U.S. Army Coastal Engineering Research Center, Washington, DC.

4.12 Problems

1. A wave train is observed approaching a coast that has straight parallel nearshore bottom contours that are oriented in a north–south direction. Where the water depth is 5 m the wave crests are observed to form an angle of 9° with the shoreline (waves from the southwest) and the wave period is measured to be 7.3 s. What is the incident wave direction in deep water? If the measured wave height at the 5 m depth is 2.2 m, what is the deep water wave height?
2. A wave train approaches the same shore location as in Problem 1 but the deep water wave crests form an angle with the shoreline of 50° . If the wave period is 11 s and the deep water height is 2 m what is the wave height and angle between the wave crest and shoreline where the water depth is 8 m? At what depth will the wave break?
3. A wave train has a period of 8.6 s and propagates toward the shore over straight shore-parallel bottom contours. Plot the wave crest angle (with respect to the shoreline orientation) in deep water versus the wave crest angle at a water depth of 5 m for deep water angles ranging from zero to 80° . How would this curve differ if the incident wave period were 6 s?

4. The wave refracted in Figure 4.5 has a deep water height of 2.1 m. Determine its height at the breakwater dogleg and at the head of the breakwater.

5. A train of waves having a 1 s period and a height of 5 cm is generated in a wave basin having the dimensions and water depths shown. The side walls of the basin have a reflection coefficient of zero and the step has a reflection coefficient of 0.2 (assume no energy dissipated at the step). Construct the refraction diagram, indicate regions where wave diffraction effects would be significant, sketch the wave crest pattern in the diffraction region, and calculate the wave height at point *A*.



6. Draw 10 parallel lines 3 cm apart and assign depths of 105, 85, 70, 58, 48, 38, 28, 18, 10, and 5 m. Construct a pair of orthogonals for a 11.5 s wave approaching the contours at a 45° angle and determine the refraction coefficient at the 5 m depth. Calculate the refraction coefficient using Eqs. (4.2) and (4.3) and compare the result from that for the refraction diagram analysis.

7. Given the hydrography in Problem 6 construct a pair of orthogonals for a 10 s period wave train approaching with deep water wave crests forming a 40° angle with the bottom contours. If the wave has a height of 6 m in deep water, determine the wave height, water depth, and angle between the wave crest and bottom contours just prior to breaking.

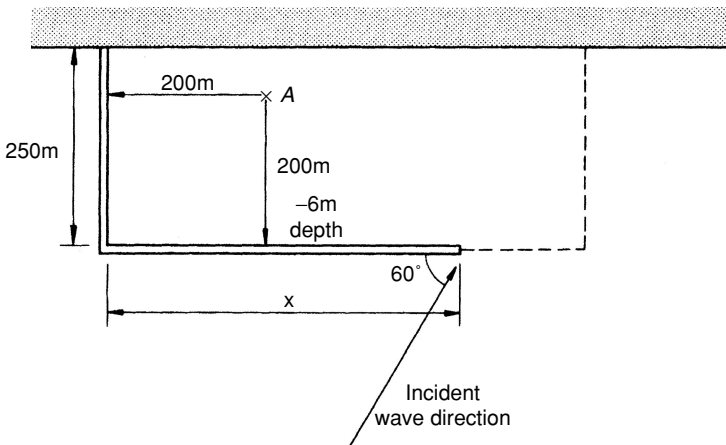
8. The Gulf Stream flows generally to the northeast offshore of the eastern seaboard of the United States. At a point where this current is flowing directly to the northeast at 1.8 m/s, it is approached by waves from the east having a period of 8 s and a height of 2.1 m. Assuming the ocean east of the Gulf stream has a

negligible current, what is the effect on the celerity, height, and direction of the approaching waves as they enter the Gulf Stream?

9. An ocean current flows directly to the east. Describe the effect of this current on a train of waves approaching from still water and a northeast direction. From still water and a northwest direction? Be specific.

10. Considering the effects of wave diffraction, what is the wave height at point *B* along the centerline in Problem 5?

11. Consider the L-shaped breakwater that protects a small harbor dredged to a uniform depth of 6 m. For a 2 m high, 10 s period incident wave at the head of the breakwater having the direction shown, what length x must the seaward arm of the breakwater have to diminish the wave height to 0.5 m at point *A*?



12. With $x = 300$ m in Problem 11 and the same incident wave direction, what are the values of K_d at point *A* for a 2, 4, 6, 8 and 10 s wave? From this, discuss the effect of wave diffraction on a spectrum of waves all arriving from the same direction and diffracting to the lee of a breakwater.

13. A 7 s, 2.5 m high deep water wave approaches the shore in a normal direction. At a distance of 300 m from the shore a 700 m long breakwater is constructed parallel to the shore and the area leeward of the breakwater is dredged to a depth of 5 m, which is the natural depth at the breakwater. What is the maximum wave height that will occur at the center of the breakwater on the leeward side?

14. If the deep water incident wave direction in Problem 13 is 30° off a line normal to the breakwater axis and the nearshore bottom contours are all straight and parallel to the shore, what is the maximum wave height at the center of the

breakwater on the leeward side? Draw the wave crest pattern in the vicinity of the breakwater. Assume the breakwater has a reflection coefficient of zero.

15. In Problem 11, for the same incident wave height, period, and direction and a breakwater length of $x = 400$ m, what is the wave height at point A if the water depth in the lee of the breakwater decreases linearly from -6 m at the offshore arm to -2 m at point A ?

16. In Problem 11, for the same incident wave height, period, and direction and a breakwater length of $x = 300$ m draw the diffracted and reflected wave crest pattern in the harbor. Assume that the shoreline is a bulkhead with a reflection coefficient of 0.8 and that the interior sides of the breakwater are stone mound with a reflection coefficient that is essentially zero. What will the reflected wave height be at point A ?

17. Consider the situation depicted in Figure 4.14 and assume the water depth throughout is 5 m. If the incident wave height and period are 2.2 m and 4 s, respectively, what is the reflected wave height at point A which is 20 m from each of the barriers? The barrier that reflects the wave has a $C_r = 0.75$.

18. The offshore arm of the breakwater in Problem 11 has a reflection coefficient of 0.65 on the seaward side. Consider the incident wave period, height, and incident direction given in Problem 11 and assume that the water depth immediately seaward of the breakwater is also 6 m. What is the reflected wave height at a point 100 m from the head of the breakwater along a line that extends out from the axis of the offshore arm? Show the reflected wave crest pattern out to this point.

19. A vessel is traveling at 10 knots over deep water. Determine the transverse and diverging wave lengths and periods. How deep must the water be to be deep water?

5

Coastal Water Level Fluctuations

This chapter is concerned with coastal water level fluctuations caused by waves having longer periods than those generated directly by the wind, and other nonwave fluctuations in coastal water levels. In particular, these may be classified as:

1. Astronomical tide—periodic fluctuations caused by the interaction of gravitational and centrifugal forces primarily between the earth, sun, and moon
2. Tsunamis—surface waves generated by underwater disturbances primarily of seismic origin
3. Basin oscillations—resonant response of water bodies to long period wave and nonwave excitations
4. Storm surge—setup and setdown of coastal water levels caused by meteorological forces
5. Climatological/geological effects—long-term changes in relative sea level owing to atmospheric warming coupled with coastal uplift or subsidence.

Figure 5.1 is a schematic depiction of a common type of gage that can be used to measure the coastal water level fluctuations that are discussed in this chapter. Water surface fluctuations cause the water level and float inside the stilling well to rise and fall. The stilling well water level is recorded on a chart to provide a time-history of the coastal water level fluctuations. The small orifice in the stilling well is designed to filter out oscillations having periods typically smaller than a minute or so. This is accomplished through frictional dissipation at the orifice and by the large ratio of stilling well cross-sectional area to orifice area. Gages of this type and other types of gages that make similar measurements are located at numerous places around the coastline and in bays and estuaries. They provide an excellent long-term record of the coastal water level conditions at a site as well as general insight as to the nature of shorter term fluctuations. Also,

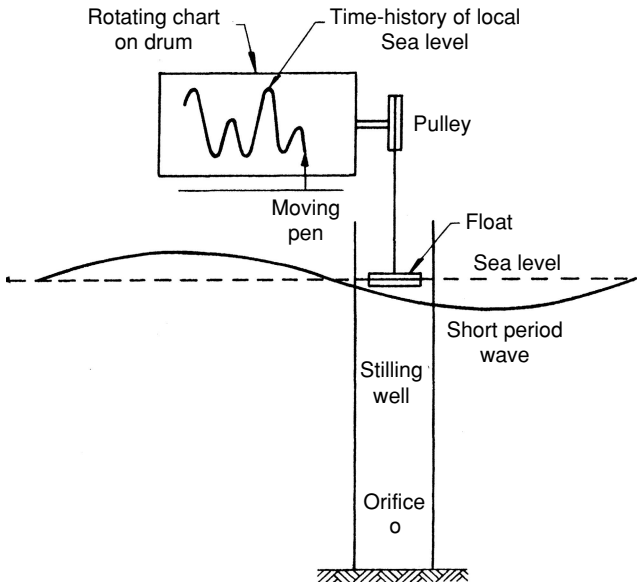


Figure 5.1. Float-stilling well water level gage.

our predictive procedures for most coastal water level fluctuations require calibration data provided by these gages.

Figure 5.2 is a plot that schematically shows the spectrum of wave energy typically found on the ocean and large bays and lakes. The actual energy level any spectral component has will vary with location and time. Also indicated on the figure are the primary generating forces for the various components of the spectrum. The portion of the spectrum from about 1 to 30 s covers the wind-generated waves one typically sees when visiting the coast. Surf beat consists of oscillations in the surf zone caused by wind wave induced setup and setdown (see Section 2.6) as groups of higher and lower waves reach the coast. Tsunami waves can have periods from 5 to 60 min while the dominant tidal periods are around 12 and 24 hours. Basin oscillations commonly occur in response to the portion of the spectrum from surf beat up to the astronomical tide, the specific periods responded to depending on the geometry of the basin and the periods of the spectrum that are active at the basin location.

5.1 Long Wave Equations

The waves considered in this chapter have relatively long periods and thus tend to have low d/L values so that they usually are shallow water waves even in the deeper ocean. Employing the small-amplitude wave theory, the wave celerity would be

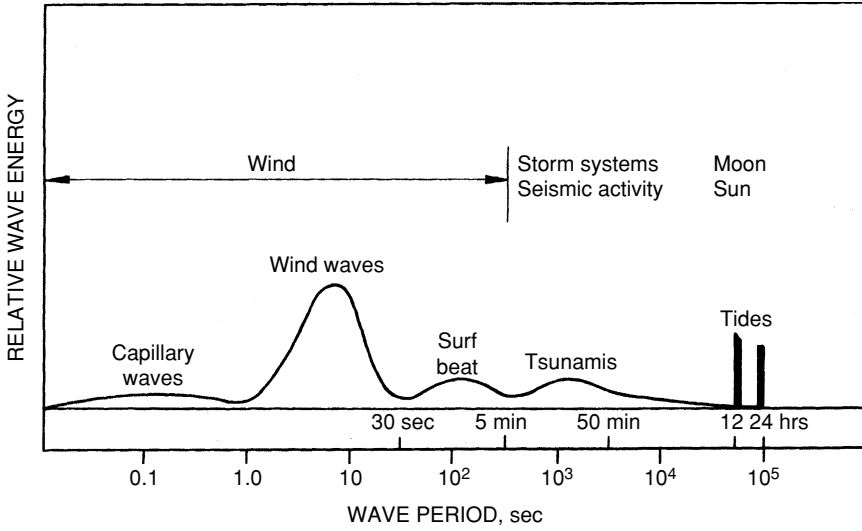


Figure 5.2. Typical ocean wave energy spectrum.

given by Eq. (2.19), the particle velocities by Eqs. (2.30) and (2.31), and the pressure distribution by Eq. (2.34). As an alternative, we can start with the known physical characteristics of shallow water waves and directly develop the relevant form of the equations of continuity and motion. These equations are commonly known as the long wave equations. Owing to the typical applications of the long wave equations for the phenomena discussed in this chapter, these equations will be presented in three-dimensional cartesian form (x, y horizontal coordinates; z vertical coordinate) and the equations of motion will include the effects of surface and bottom stress as well as Coriolis acceleration. For a more thorough discussion of the long wave equations see Dean and Dalrymple (1984) and Sorensen (1993).

In the long wave equations, vertical flow velocities are assumed negligible. Horizontal flows are considered in terms of the average velocity over the vertical water column. This is done in terms of the volumetric flow rate per unit width of vertical section q_x and q_y for the two coordinate directions. Thus

$$q_x = \int_{-d}^{\eta} u \, dz$$

and

$$q_y = \int_{-d}^{\eta} v \, dz$$

where d is the bottom depth below the still water level and η is the water surface elevation above the still water level. Considering a mass balance where the net

sum of the horizontal flow rates into and out of a control volume equals the net change in volume per unit time of the control volume represented by a rise or fall of the water surface leads to the equation of continuity which can be written:

$$\frac{\partial q_x}{\partial x} + \frac{\partial q_y}{\partial y} + \frac{\partial \eta}{\partial t} = 0 \quad (5.1)$$

To present the equations of motion for the two horizontal directions we must introduce the bottom stresses in the x and y directions (τ_{bx} and τ_{by}) and the surface stresses in the x and y directions (τ_{sx} and τ_{sy}). These might typically represent bottom friction and the surface stress due to wind shear on the water. Also we must introduce the Coriolis parameter f where

$$f = 2\omega \sin \phi \quad (5.2)$$

In Eq. (5.2) ω is the earth's rotational speed (7.27×10^{-5} rad/s) and ϕ is the latitude of the point on the earth's surface where the equations are being applied. This parameter would be zero at the equator and maximum at the poles. The product of f times a horizontal component of the flow velocity yields the horizontal Coriolis force per unit mass or acceleration which acts at right angles to that flow velocity component (to the right in the Northern hemisphere and to the left in the Southern hemisphere). The Coriolis acceleration is relatively small, but can be important in some long wave analyses where large masses of water are involved.

Integrating the equations of motion from the bottom to the water surface yields a common form for the horizontal components of the equations of motion

$$-g(d + \eta) \frac{\partial \eta}{\partial x} + f q_y + \frac{1}{\rho} (\tau_{sx} - \tau_{bx}) = \frac{\partial}{\partial x} \left(\frac{q_x^2}{d + \eta} \right) + \frac{\partial}{\partial y} \left(\frac{q_x q_y}{d + \eta} \right) + \frac{\partial q_x}{\partial t} \quad (5.3a)$$

$$-g(d + \eta) \frac{\partial \eta}{\partial y} + f q_x + \frac{1}{\rho} (\tau_{sy} - \tau_{by}) = \frac{\partial}{\partial x} \left(\frac{q_x q_y}{d + \eta} \right) + \frac{\partial}{\partial y} \left(\frac{q_y^2}{d + \eta} \right) + \frac{\partial q_y}{\partial t} \quad (5.3b)$$

where ρ is the density of the water. In Eqs. (5.3) the first term on the lefthand side represents the gravitational force per unit mass exerted through the slope of the water surface in that component direction; the second term is the Coriolis acceleration component; and the last term on the left represents the net horizontal stress per unit mass in that component direction. The three terms on the right represent the resulting convective and local acceleration components for the water. As will be seen, in some physical situations certain terms in Eqs. (5.3) are negligible and may be excluded. Also, if the water surface fluctuations are small compared to the depth, the total water depth can be represented by d . The effects of a pressure gradient acting across the water surface are not included in

the force summation on the lefthand side. If this force is significant in practical problems its effect is usually evaluated separately.

5.2 Astronomical Tide Generation and Characteristics

A coastal engineer's ability to predict the astronomical tide at a given location is important for a number of practical reasons. Nearshore coastal hydrographic work from a floating vessel may be referenced to the instantaneous tide level. Planning for field work may be keyed to the need to work at high or low tide or related periods of ebb or flood current at an estuary. The range of tides indicates the range of water levels at which waves and currents will act on coastal works. At places where the tide range is large, the importance of an impending storm may be very dependent on whether it arrives at high or low tide. In addition, analysis of the reversing currents and related stability of a coastal inlet is primarily dependent on the tide characteristics at the entrance to that inlet. Astronomical tide theory is presented in great detail in specialized texts such as Macmillan (1966), Harris (1981), and Pugh (1987). This section concentrates on those aspects of the tide that are of particular interest to coastal engineers.

The gravitational attraction of the sun and moon on the oceans and the equal and opposite centrifugal forces owing to the rotation of the earth–sun–moon system are the primary tide generating forces. Although the sun's mass is approximately 2.7×10^7 times that of the moon, the closer proximity of the moon to the earth results in the moon having about twice the sun's gravitational force on the oceans. The resulting tide is a long period wave generated by these gravitational and centrifugal forces. Consequently, even in the deepest areas of the ocean the tide is a shallow water wave. As the tide wave propagates onto the continental shelf and into bays and estuaries it is significantly affected by nearshore hydrography, bottom friction, Coriolis acceleration, and resonant effects.

The range of the tide and the arrival time of high or low tide at a given location are dependent on the above mentioned factors. Converging or diverging estuary shorelines cause the amplitude of the tide to increase or decrease respectively owing to the concentration or spreading of the tide wave's energy. Decreasing water depths as a tide wave propagates up an estuary will increase the tidal range. Bottom friction, which dissipates wave energy, will cause the tide range to decrease at successive points along an estuary.

The tide is a wave that has a very low steepness and thus relatively high reflectivity. At some locations such as the Bay of Fundy, Nova Scotia, reflection causes resonance and resulting amplification of the tidal range in the bay. Reflection of the tide wave also increases the complexity of the tide in some coastal regions.

In the Northern hemisphere, Coriolis acceleration will deflect flowing water to the right as one looks in the direction of the flow (left in the Southern hemisphere). Thus, as the tide propagates up an estuary causing flow into the

estuary, the water level will be relatively higher on the righthand side. On the ebb tide, this will cause a relatively higher water level on the other side of the estuary.

Further insight into the nature of the tide can be gained from an elementary description of the way the tide is generated. Consider an idealized earth-moon system with the earth covered by a uniform layer of water and the two bodies revolving around a common axis that is about 2900 miles from the earth's axis (Figure 5.3). The gravitational forces F_g and the centrifugal forces F_c are in balance at the center of mass of each body. But an element of water located on the side of the earth farthest from the moon would have $F_c > F_g$ and a resulting net outward force. On the half of the earth closest to the moon $F_g > F_c$, which also causes a net outward force. The result is two bulges as shown or two high and two low tides each day as the earth rotates. These bulges are the tide waves that propagate as shallow water waves.

While the earth rotates once (relative to the position of the sun), the moon makes $1/29.5$ th of a revolution (a lunar month is 29.5 solar days). Thus, the principal lunar tidal period $M_2 = 12.0(1 + 1/29.5) = 12.42$ hours. The principal solar tidal period $S_2 = 12.0$ hours. Since the lunar force dominates, high and low tides progress 0.84 hours (about 50 min) each day.

The planes of the moon's and sun's rotation relative to the earth are not in line and change with regard to each other as time passes. Also, the orbits of the sun and moon are elliptical rather than circular. These plus other factors make the

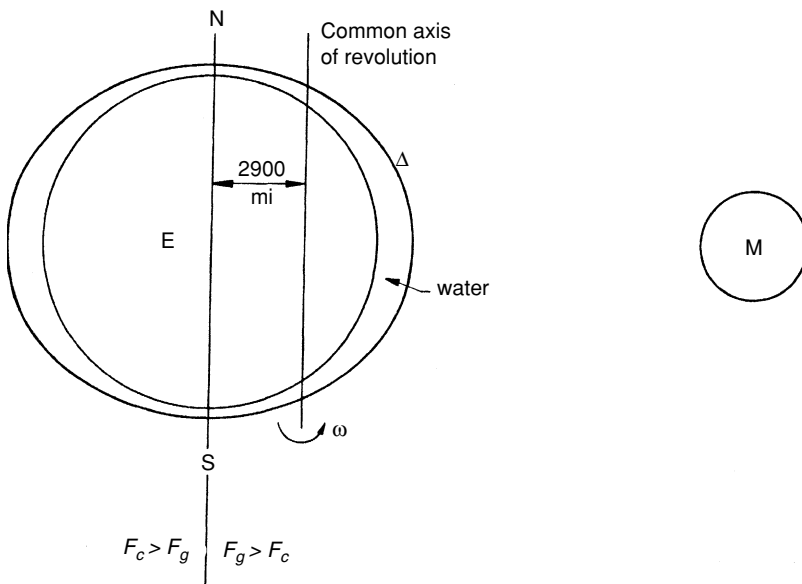


Figure 5.3. Tide generation—idealized earth/moon system.

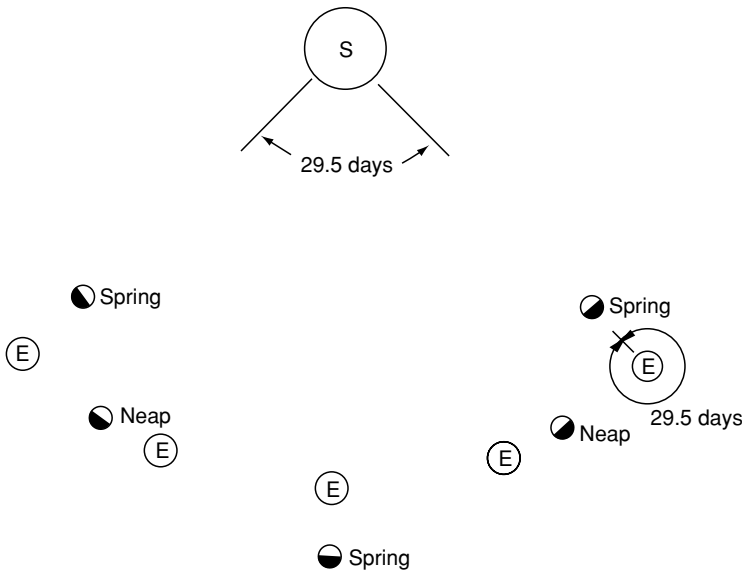


Figure 5.4. Earth, sun, and moon during a lunar month.

net tide generating force very complex. Figure 5.4 shows the approximate orientation of the sun, moon, and earth at the quarter points of the moon's revolution around the earth relative to the position of the sun (29.5 days). At the first position (new moon) and third position (full moon) the solar and lunar tide generating forces reinforce and the highest or spring tides occur. At the second and fourth quarters the lowest or neap tides occur. Each quarter is $29.5/4 = 7.4$ days long, so that spring and neap tides are 14.8 days or about 2 weeks apart. The result of these two principal forces is a water level variation that is similar to the beating effect shown in Figure 2.6, where the lunar component would have a slightly longer period and a greater amplitude than the solar component.

The principal lunar and solar components are just two of over 390 active tidal components having periods ranging from about 8 hours to 18.6 years. Each component has a period that has been determined from astronomical analysis and a phase angle and amplitude that depend on local conditions and are best determined empirically. Most of the 390 components are quite small and can be neglected for practical tide prediction. Eight major components with their common symbol, period, approximate relative strength (depending on location), and description are listed in Table 5.1. The components combine in different ways at each coastal location and are affected by local hydrography, bottom friction, resonance and so on, to produce the local tide.

Table 5.1. Eight Major Tidal Components

Symbol	Period (hours)	Relative Strength	Description
M_2	12.42	100.0	Main lunar semidiurnal component
S_2	12.00	46.6	Main solar semidiurnal component
N_2	12.66	19.1	Lunar component due to monthly variation in moons distance from earth
K_2	11.97	12.7	Soli-lunar component due to changes in declination of sun and moon throughout their orbital cycles
K_1	23.93	58.4	With O_1 and P_1 accounts for lunar and solar diurnal inequalities
O_1	25.82	41.5	Main lunar diurnal component
P_1	24.07	19.3	Main solar diurnal component
M_f	327.86	17.2	Lunar biweekly component

The tidal record at any location can generally be classified as one of three types: semidiurnal, diurnal, or mixed. They are defined as follows:

Semidiurnal: There are two high and two low water levels each tidal day (24.84 hours) with approximately the same vertical variation for each of the two cycles. This is the predominate tidal type throughout the world, including the east coast of North America.

Diurnal: There is only one high and one low water level each tidal day. Diurnal tides predominate on the Gulf coast of the United States, but some Gulf coastal sections have mixed tides.

Mixed: There is a large inequality in the vertical range of the two daily cycles. Typically there is a cyclic transition from mixed to semidiurnal and back, or from mixed to diurnal and back, the former being typical of the tides on the west coast of North America.

Semidiurnal tides occur at a site where the semidiurnal components $M_2 + S_2$ are stronger than the diurnal components $K_1 + O_1$. The reverse occurs where tides are diurnal. The differences are not that great where tides are mixed.

5.3 Tidal Datums and Tide Prediction

Water and land elevations in the coastal zone are referenced to a variety of tidal datums in different regions of the world and for different purposes. Some of these datums are:

Mean sea level (MSL): The average height of all tide elevations (usually on an hourly basis) averaged over a 19-year period

National geodetic vertical datum (NGVD): Mean sea level determined from 19 years of data averaged over 26 North American coastal stations in 1929

Mean low water (MLW): The 19-year arithmetic mean of all low water levels (i.e., low points in tidal elevation cycle). MHW is the average of the high tide levels.

Mean lower low water (MLLW): The 19-year arithmetic mean of only the lower of each pair of low water levels in a mixed tide. MHHW is the average of the higher high tide levels.

Mean tide level (MTL): the level located midway between MLW and MHW.

Sea level is observed to be generally higher on the Pacific coast than on the Atlantic coast and higher in the north than in the south on both coasts. Also, with the passage of time, sea level rise as well as uplift or subsidence of coastal lands causes the true MSL to vary from location to location and as time passes. Thus, NGVD was established as a “fixed” mean sea level reference. The contemporary MSL at any given location will likely differ from NGVD. In 1988 NGVD was refined further to include gravimetric and other anomalies to produce the North American Vertical Datum (NAVD 88). MLW and MLLW are established as datums largely for navigation and related purposes so that depths referenced to these datums are minimums likely to be available throughout the tide cycle. Land elevations are usually referenced to NGVD while depths on coastal hydrographic charts may be referenced to MLW or MLLW so care must be exercised when combining topographic and hydrographic data. The vertical distance between NGVD and say MLLW will vary with location and time.

The mean tide ranges for a number of coastal locations in North America are listed in Table 5.2. The mean tide range is the difference between MLW and MHW for semidiurnal and diurnal tides and between MLLW and MHHW for mixed tides.

Note the wide range of values and the relatively steady progression in values as one moves along the coast. Two sets of values are of particular interest. Grand Manan Island is an island at the entrance to the Bay of Fundy and Burncote Head is located back at the head of the Bay. The relatively large range at the bay entrance is significantly amplified back in the bay owing to resonance. The resonant period of the Bay of Fundy is around the dominant tidal period of 12 hours. Cape May is located at the entrance to the Delaware River while Trenton is over 150 river miles up the river. The larger tide range at Trenton than at Cape May indicates the significant effects of shoaling and shoreline convergence on increasing the amplitude of the tide wave as it propagates up the river. Also note

Table 5.2. Selected Coastal Mean Tide Ranges

Location	Mean Tide Range (m)
Grand Manan Island, New Brunswick	5.24
Burntcoat Head, Nova Scotia	11.70
Boston, MA	2.90
Provincetown, MA	2.77
Sandy Hook, NJ	1.42
Cape May, NJ	1.46
Trenton, NJ	2.46
Ocean City, MD	1.07
Duck, NC	1.00
Folly Island, SC	1.58
Savannah River Entrance, GA	2.10
Cape Canaveral, FL	1.07
Key West, FL	0.40
Pensacola, FL	0.40
Mobile, AL	0.46
Galveston, TX	0.43
La Jolla, CA	1.13
San Francisco, CA	1.25
Crescent City, CA	1.55
Columbia River Entrance, OR	1.71
Juneau, AK	4.18
Anchorage, AK	7.89
Honolulu, HI	0.40

the small tide range at Honolulu which is typical of mid-ocean ranges. This is so because there is not a significant shallow coastal section to increase the tide wave height before it reaches the shore.

A long record, on a continuous or at least hourly basis, of the water level at a given coastal location is required to make future predictions of the tide. Measurements of water level by a device similar to that shown in Figure 5.1 will include short-term wind and atmospheric pressure-induced water level changes, but if the record to be analyzed is of sufficient length these effects can be filtered out. For that reason and considering the range of tidal component periods, the ideal record length would be about 19 years. However, records as short as 370 days can be satisfactory for tide prediction.

The instantaneous tidal elevation η above a selected datum can be given by

$$\eta = A + \sum_{i=1}^N A_i \cos\left(\frac{2\pi t}{T_i} + \Delta_i\right) \quad (5.4)$$

where A is the vertical distance from the selected datum to MSL; A_i , T_i , and Δ_i are the amplitude, period, and phase angle of the particular component (e.g., M_2 , K_1); t is the time elapsed; and N is the number of tidal components being used. Although the eight components listed in Table 5.1 are sufficient to analyze the tide at most locations, the U.S. National Ocean Service considers the 37 most important components in performing this analysis. The measured tide record at a given site is then analyzed by performing an harmonic analysis to determine A_i and Δ_i for each component of period T_i . Once the values of A_i and Δ_i for each component are determined for a given site, Eq. (5.4) can be used to predict future tide elevations at that location. Any changes to the coastal area that would affect propagation of the tide wave to the location of interest will likely affect the empirically determined values of A_i and Δ_i for that location.

The National Ocean Service of the U.S. Department of Commerce annually publishes tide predictions for numerous selected points around the coastlines of the world. (see noaa.gov) The predicted tidal elevations are given in terms of the elevation and time predicted daily highs and lows for a year at several key stations. Corrections on these values are then tabulated for numerous nearby coastal locations. Remember, these are the predicted astronomical tide levels and do not include any meteorological effects that may be active at the time. The National Ocean Service also publishes tables of predicted tidal currents at key coastal locations

The patterns and amplitudes of oceanic tide wave propagation have been modeled using numerical solutions of the long wave equations (e.g., see Hendershott, 1977). The models are driven by a forcing function that includes the desired number of lunar and solar components. The surface stress is omitted and for deep ocean tides the bottom stress term is negligible. The Coriolis term is quite significant and must be included. There are two basic types of oceanic tidal models. One type employs the boundary condition of no flow across the coastal boundaries and attempts to predict tide ranges around the coast and in the ocean interior. The second uses water levels at the coast as a boundary condition and just attempts to predict tides throughout the interior of the ocean. The logic of the second type of model is that coastal tides are known, but there exist little data on the tides throughout the ocean.

One could also model nearshore and river/estuary tide wave propagation using the long wave equations. For example, Reid and Bodine (1968) calibrated a Galveston Bay storm surge numerical model for bottom friction by first modeling the tide without including the surface stress term. The forcing function was based on conditions at the entrance to the bay. Here, the bottom stress term would be significant; but if the lateral extent of the water body is relatively small, the Coriolis term may be neglected.

5.4 Tsunamis

The term “tsunami,” which means “harbor wave” in Japanese, is used to denote the relatively long period waves generated by a variety of underwater disturbances including earthquakes, landslides, and volcanic eruptions. Although tsunami waves have a low amplitude at sea, shoaling, refraction, and resonance can greatly increase the nearshore amplitude and runup of these waves. This has caused severe damage and the loss of many lives in those coastal areas prone to tsunami attack. Thorough discussions of tsunamis are given by Wiegel (1970) and Camfield (1980) and an informative and detailed analysis of the 1964 Alaskan earthquake and resulting tsunami is given by Wilson and Torum (1968).

Tsunamis are generated by a rapid large-scale disturbance of a mass of ocean water that results in the displacement of the ocean surface and the generation of a series of waves that radiate out from the disturbance. While volcano eruptions and underwater landslides have generated waves of local significance, major tsunami events usually are the result of earthquakes that produce significant vertical movement of the sea floor in sufficiently shallow water. These earthquakes typically have a magnitude greater than about 6.5 on the Richter scale and a focal depth of less than 60 kilometers (Iida, 1969). The 1964 Alaskan tsunami was generated by an earthquake of 8.4 to 8.6 magnitude and a 20- to 50-kilometer focal depth that resulted in vertical land movement over an 800-kilometer front in a period of 4 to 5 min (Wilson and Torum, 1968). The sea bed rotated around a hinge line with underwater uplift and subsidence in excess of +8 m and -2 m, respectively. Most tsunamis are generated in the active earthquake regions along the rim of the Pacific Ocean (Aleutian Islands, Japan, New Zealand, and the west coast of South America). Tsunamis have also been generated in the Indian Ocean and the Caribbean and Mediterranean Seas.

A tsunami will typically consist of a group of waves having periods from 5 to 60 min with the most common range of periods being around 20 to 30 min. Wave heights in the deep ocean are believed to typically be a meter or less (Wiegel, 1970). The waves have a very low steepness (see Example 5.4-1) and thus are highly reflective which significantly increases complexity in some coastal areas.

Example 5.4-1

One of the waves in a tsunami has a period of 20 min and a height of 0.6 m at a point in the ocean where the depth is 3800 m (this is the mean depth of the earth's seas). Determine the celerity and length of this wave. Determine its celerity, length, and height in a nearshore depth of 10 m assuming no refraction, diffraction, or reflection effects.

Solution:

Assume that the wave is a shallow water wave so

$$C = \sqrt{gd} = \sqrt{9.81(3800)} = 193 \text{ m/s (695 km/h)}$$

$$L = CT = 193(20)60 = 231,700 \text{ m}$$

$$d/L = 3800/231,700 = 0.016$$

$$H/L = 2/231,700 = 8.6 \times 10^{-6}$$

Thus, the wave is a shallow water wave at a depth of 3800 m (and would be a shallow water wave in the deepest parts of the ocean). Note the large speed and length of the wave, and its very small steepness.

Equating wave power at the two water depths [Eq. (2.40)] leads to

$$(H^2L)_{10} = (H^2L)_{3800}$$

Or, since

$$L = \sqrt{gd}T$$

$$\left(H^2\sqrt{d}\right)_{10} = \left(H^2\sqrt{d}\right)_{3800}$$

So, at a depth of 10 m

$$H = 0.6 \left(\frac{3800}{10}\right)^{0.25} = 2.65 \text{ m}$$

$$C = \sqrt{9.81(10)} = 9.9 \text{ m/s}$$

$$L = 9.9(20)60 = 11,900 \text{ m}$$

Shoaling has increased the wave height by a factor of $2.65/0.6 = 4.4$ times and refraction could cause a much greater increase.

An important concern, once a tsunami has been generated, is to forecast its arrival time at locations that are prone to tsunami wave damage. This can be done by consulting refraction diagrams previously constructed using the basic techniques presented in Sections 4.3 and 4.4 [where wave celerity is given by Eq. (2.19)]. Map projection distortion must be considered and bottom irregularities much shorter than a wave length (see Example 5.4–1) can be smoothed out. Keulegan and Harrison (1970) used numerical techniques to construct tsunami refraction diagrams, including compensation techniques for the distorted picture of the earth's surface found on a Mercator projection, so results could be plotted

on a Mercator map. Refraction diagrams were constructed for tsunamis generated in Alaska; Kamchatka, Russia; and Chile and propagating to Hilo, Hawaii and Crescent City, California. A major objective was to determine nearshore wave crest orientations for use as input to hydraulic model studies of these sites for proposed tsunami barrier projects.

The travel time t_T of a tsunami wave from its source to a point of interest can be predicted by summing the travel times along successive intervals along the wave orthogonal that connects the two points. Thus

$$t_T = \sum \frac{\Delta S}{\sqrt{gd_s}} \quad (5.5)$$

where d_s is the average water depth over the interval having a length ΔS . For places such as Hilo, Hawaii that are frequently attacked by tsunamis, charts of travel time from all possible sources areas have been developed (see Zetler, 1947 and Gilmour, 1961). These charts are applicable for any tsunami since the wave celerity depends only on the water depth.

Example 5.4-1 demonstrates how much the wave height can increase as a tsunami wave approaches the shore. Refraction can cause wave heights to be significantly larger or smaller than this. The spread of wave orthogonals as the waves radiate out from the origin causes a spreading of energy as tsunami waves propagate across the ocean, so regions closer to the tsunami source are generally likely to have higher nearshore wave heights. This will cause an initial wave height reduction which may be reversed if local hydrography refocuses wave energy. Measured tsunami coastal wave heights and runup elevations along an irregular coast line will likely show similar results for different tsunamis approaching the same location, but for the same tsunami results might be quite different from point to point along the coast. This demonstrates the importance of local effects on tsunami nearshore heights and runup elevations.

Figure 5.5 shows a tide gage record from San Francisco Bay, California taken after the 1964 Alaskan earthquake. Tsunami waves having a period around 35 min can be seen superimposed on the tide. It appears that the tsunami set the bay into resonant oscillation to cause noticeable oscillations which continued for over 24 hours.

Tsunami waves still have a very low steepness when they reach the shore (see Example 5.4-1). Primary coastal damage is caused by the surge of water as the tsunami runs up the sloping coast. Although runup elevations of tsunami waves will depend on the land slope and surface conditions as well as the actual tsunami wave steepness, as a rule of thumb (Camfield, 1980) the runup elevation will be equal to or slightly higher than the wave height at the coast. The runup may vary from a rapidly rising water surface to a wave that forms a bore that runs up the coastal slope. The former appears more likely for the longer period waves (e.g., 50 to 60 min) and the latter for the shorter period (e.g., 10 to 20 min) waves. The runup flow velocity can

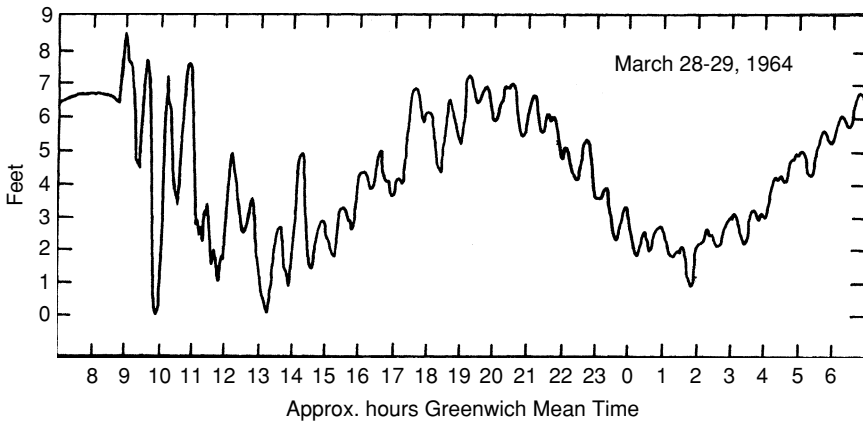


Figure 5.5. Water level gage record, San Francisco Bay.

be significant for some tsunami waves. The 1964 Alaskan tsunami overturned a locomotive engine in nearby Seward. Calculations (Wilson and Torum, 1968) estimated the required flow velocity to overturn the engine to be about 7.5 m/s. Other damage comes from flooding and scour caused by the flowing water.

Certain coastal areas are prone to tsunami damage because of their location (Pacific, Caribbean, Mediterranean) and because of their local topography/hydrography. Hilo, Hawaii for example, is at the head of a funnel-shaped embayment. In general, the best ways to deal with potential tsunami damage are: develop a good early warning system so the damage prone areas can be evacuated, remove structures that are easily damaged by flooding or surge from low coastal areas, design structures that must be in damage-prone areas to withstand the potential flooding and surge, and build barriers that might consist of structures or groves of trees to limit surge damage in key areas.

The best tsunami warning system is the one in place around the rim of the Pacific Ocean and operated by the National Weather Service of the National Oceanic and Atmospheric Administration. Pressure sensors are installed at a number of coastal sites in deep water so that they can only sense long waves (e.g. the tide and tsunamis). When a tsunami passes over the submerged gage its occurrence is signaled to a floating device that transmits the information to a land base, which in turn, notifies an extensive warning system located around the rim of the Pacific.

5.5 Basin Oscillations

There are systems that respond to a disturbing force by developing a restoring force that returns the system to its equilibrium position. But at this equilibrium position the system has inertia which carries the system past the equilibrium

position and a free oscillation at the system's natural period or frequency is established. (A simple example of such a system is a pendulum.) The natural frequency of oscillation of the system depends on the geometry of the system. (For a pendulum the oscillation period depends on the length of the arm.) It is essentially independent of the magnitude of the disturbance, which does, however, establish the magnitude of oscillation of the system. After the initial disturbance has occurred, free oscillations continue at the natural frequency but with exponentially decreasing amplitude due to the effects of friction. These systems can also undergo forced oscillations at frequencies other than the natural frequency owing to a cyclic input of energy at other than the natural frequency. Continuous excitation at frequencies equal or close to the natural frequency will usually cause an amplified system response, the level of amplification depending on the proximity of the excitation frequency to the natural frequency and on the frictional characteristics of the system.

An enclosed or partly open basin of water such as a lake, bay, or harbor can be set into free oscillation at its natural frequency (and harmonic modes) or forced oscillation as described above. The result is a surging or seiche motion of the water mass as a wave propagates back and forth across the basin. The speed and pattern of wave propagation, and the resulting natural frequency of the basin, depend on the basin geometry. Typical sources of excitation energy include:

1. Ambient wave motion if the basin has an opening to permit entry of this energy (e.g., harbor open to the sea from which the energy comes)
2. Atmospheric pressure fluctuations
3. Tilting of the water surface by wind stress and/or a horizontal atmospheric pressure gradient, with subsequent release
4. Local seismic activity
5. Eddies generated by currents moving past the entrance to a harbor

Bay and harbor oscillations are usually of low amplitude and relatively long period. Their importance is due primarily to (1) the large-scale horizontal water motions which can adversely affect moored vessels (mooring lines break, fender systems are damaged, loading/unloading operations are delayed) and (2) the strong reversible currents that can be generated at harbor entrances and other points of flow constriction. The second factor may have positive or negative consequences.

A basin of water, depending on its geometry, can have a variety of resonant modes of oscillation. A resonant mode is established when an integral number of lengths of the wave equals the distance over which the wave is propagating as it reflects repeatedly forward and back. Further insight into the nature of resonance and resonant amplification can be gained from Figure 5.6, a classic

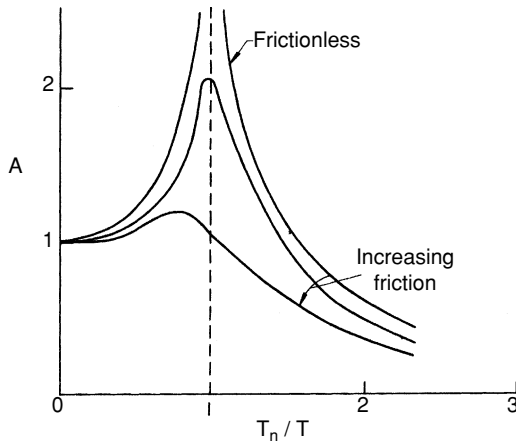


Figure 5.6. Resonant response of an oscillating system.

diagram that demonstrates the resonant response of one of the modes of oscillation of a resonating system. T_n is the natural resonant period for that mode of oscillation—the period of free oscillation that develops when the system has a single disturbance to set up that mode of oscillation. T is the period of the system excitation being considered; it may or may not be at the resonant period. A is the resulting amplification of the oscillating system; that is, the ratio of the amplitude of the system response to the amplitude of excitation of the system. Three curves are shown for the frictionless case, a case with some friction, and a case where the system is heavily damped by friction.

If the system is excited at periods much greater than the natural period (i.e., T_n/T approaching zero) the system response has about the same magnitude as the excitation force. This would be the case, for example, when a small coastal harbor that has a large opening to the ocean responds to the rising and falling water level of the tide. As the excitation period decreases toward the resonant period of the system the response is amplified. The response comes to an equilibrium amplification where the rate at which energy is put into the system equals the rate at which energy is dissipated by the system (A frictionless system would ultimately reach an infinite amplification). Systems with larger rates of dissipation undergo less amplification. When the excitation period equals the resonant period of the system, amplification reaches its peak. Note that frictional effects can slightly shift the period at which peak amplification occurs. At $T > T_n$ the amplification continually diminishes with decreasing excitation period. If the system is excited by a single impulsive force rather than a continuing cyclic force the system oscillates at the natural period. If the system is excited by a spectrum of excitation forces it selectively amplifies those periods at and around the natural period. When the cyclic excitation force is removed, friction causes the response amplitude to decrease exponentially with time.

5.6 Resonant Motion in Two- and Three-Dimensional Basins

When resonant motion is established in a basin a standing wave pattern develops (as briefly discussed in Section 2.7). At antinodal lines there is vertical water particle motion while horizontal particle motion occurs at the nodal lines (see Figure 2.8). Our concerns in analyzing basin resonance are (1) to predict the fundamental and harmonic periods of resonance for the various resonant modes; (2) to predict the pattern of nodal and antinodal lines in the horizontal plane for each of these resonant modes; and (3) to predict, for each resonant mode, the amplitudes and velocities of particle motion, particularly at the nodal lines where motion is essentially horizontal. The first two just depend on the geometry of the basin and can be easily addressed in many cases. The third also depends on the amplitude of the excitation forces and the magnitude of frictional dissipation in the basin. This is difficult to resolve in a quantitative sense.

In this section we present an analysis of resonance in basins where resonant motion is predominantly two-dimensional and in some idealized basin geometries where resonance is three-dimensional. This provides additional insight into the nature of resonance in most basins and provides tools to analyze resonance for many practical situations.

Two-Dimensional Basins

Figure 5.7 shows (in profile view) the fundamental and first two harmonic modes of oscillation for idealized two-dimensional rectangular open and closed basins. For the closed basin the standing wave would have lengths equal to 0.5, 1.0, and 1.5 times the length of the basin. For the basin open to a large water body the standing wave lengths would be 0.25, 0.75, and 1.25 times the basin length. The resonant period for a particular mode of oscillation equals the wave length for that mode divided by the wave celerity. Since most basins of concern to coastal engineers are broad and relatively shallow, the waves are shallow water waves and the resonant periods are given by

$$T_n = \frac{2\Gamma}{(k+1)\sqrt{gd}} \text{ (closed basin)} \quad (5.6)$$

and

$$T_n = \frac{4\Gamma}{(2k+1)\sqrt{gd}} \text{ (open basin)} \quad (5.7)$$

where k depends on the oscillation mode and is equal to 0, 1, 2 etc. for the fundamental, first, and second harmonic modes etc. Γ is the basin length as depicted in Figure 5.7. The fundamental mode of oscillation has the longest

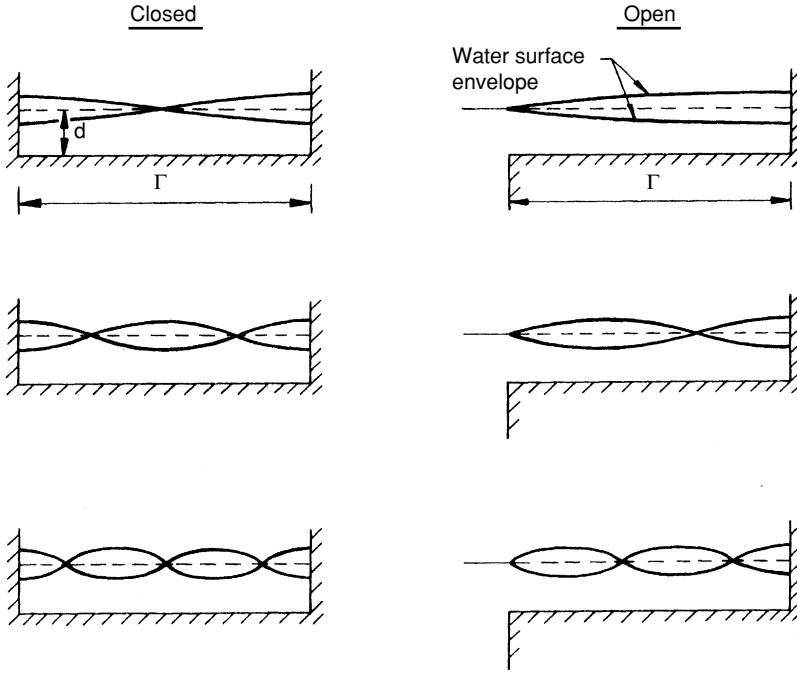


Figure 5.7. Water surface envelope profiles for oscillating two-dimensional idealized basins.

period and the harmonic mode periods decrease by a factor of $1/(k + 1)$ and $1/(2k + 1)$ for closed and open basins, respectively.

For many natural basins that are long and narrow (e.g., Lake Michigan, Bay of Fundy) well established resonance is most likely to involve wave motion along the long axis of the basin. To determine the resonant periods for these water bodies which would have irregular cross-sections and centerline profiles we can rewrite Eqs. (5.6) and (5.7) as follows:

$$T_n = \frac{2}{(k + 1)} \sum_{i=1}^N \frac{\Gamma_i}{\sqrt{gd_i}} \text{ (closed)} \quad (5.8)$$

and

$$T_n = \frac{4}{(2k + 1)} \sum_{i=1}^N \frac{\Gamma_i}{\sqrt{gd_i}} \text{ (open)} \quad (5.9)$$

where the basin length is broken into N segments of length Γ_i each having an average depth d_i .

Equations for estimating the horizontal water excursion and maximum particle velocity, which occur below nodal lines, can be easily developed from the small-amplitude wave theory for shallow water waves. Combining Eqs. (2.28) and (2.57) for the time of peak velocity under the nodal point ($\sin kx \sin \sigma t = 1$) yields

$$u_{\max} = \frac{HL}{2dT} = \frac{HC}{2d} = \frac{H}{2} \sqrt{\frac{g}{d}} \quad (5.10)$$

where T would be the resonant period T_n and u_{\max} is essentially constant over the vertical line extending down from the nodal point. Since water particle motion is sinusoidal, the average particle velocity would be

$$u_{\text{avg}} = u_{\max} \left(\frac{2}{\pi} \right) = \frac{HL}{\pi dT}$$

So, the particle horizontal excursion at the nodal point X during one half period $T/2$ now becomes

$$X = u_{\text{avg}} \left(\frac{T}{2} \right) = \frac{HL}{2\pi d} = \frac{HT}{2\pi} \sqrt{\frac{g}{d}} \quad (5.11)$$

Example 5.6-1

A section of a closed basin has a depth of 8 m and a horizontal length of 1000 m. When resonance occurs in this section at the fundamental period, the height of the standing wave is 0.2 m. Determine the resonant period, the maximum water particle velocity, and the horizontal particle excursion that occurs under the nodal point.

Solution:

From Eq. (5.6) for a closed rectangular basin

$$T_n = \frac{2(1000)}{\sqrt{9.81(8)}} = 226 \text{ s} (3.77 \text{ min})$$

Equation (5.10) then yields the maximum particle velocity

$$u_{\max} = \frac{0.2}{2} \sqrt{\frac{9.81}{8}} = 0.11 \text{ m/s}$$

and Eq. (5.11) yields the horizontal particle excursion

$$X = \frac{0.2(226)}{2\pi} \sqrt{\frac{9.81}{8}} = 7.96 \text{ m}$$

These results typify basin resonance characteristics. The relatively long resonant period indicates that it is a shallow water wave and that the wave motion (0.2 m rise and fall in 3.77 min) would be hardly perceptible to the eye. Water particle velocities are commensurately small. But the horizontal water particle excursion is relatively large. A moored vessel responding to this long period wave motion would oscillate back and forth over a significant distance, tensing and releasing the tension on the mooring line and possible slamming the fender system every 3.77 min.

The preceding discussion assumed that each lateral boundary is either closed, and thus an antinode, or completely open to an infinite sea, and thus a pure node. However, many basin boundaries have partial openings and/or are open to a larger but not effectively infinite body of water. The resulting boundary condition is more complex; it causes resonant behavior at the opening that is somewhat between that of a node and antinode, and the basin resonant periods are commensurately modified.

Three-Dimensional Basins

Basins that have widths and lengths of comparable size can develop more complex patterns of resonant oscillation. The character of these oscillations can be demonstrated by considering a rectangular basin (see Figure 5.8), a form that approximates many basins encountered in practice. The long wave equations can be applied to develop analytical expressions for the periods and water surface oscillation patterns for the various resonant modes [see Sorensen (1993) for more detail].

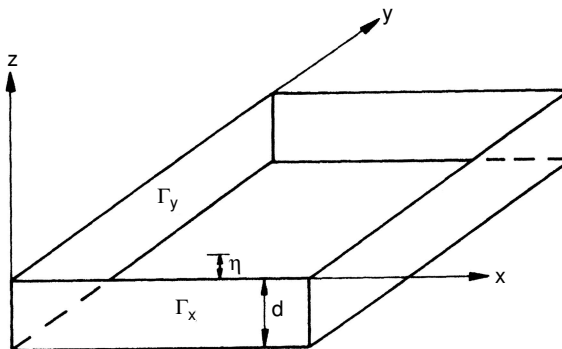


Figure 5.8. Definition sketch for a rectangular basin.

If the basin is relatively small the Coriolis term in the equations of motion [Eqs. (5.3a and b)] can be neglected. For just the patterns of surface oscillation and the resonant periods the surface and bottom stress can also be neglected. In addition, a linearized small amplitude solution allows the two nonlinear convective acceleration terms to be neglected. When these simplified forms of the equations of motion for the two horizontal direction are combined through the continuity equation [Eq. (5.1)] we have

$$gd \left(\frac{\partial^2 \eta}{\partial x^2} + \frac{\partial^2 \eta}{\partial y^2} \right) = \frac{\partial^2 \eta}{\partial t^2} \quad (5.12)$$

A solution to Eq. (5.12) for a standing wave surface form as a function of position (x, y) and time (t) is

$$\eta = H \cos(k_x x) \cos(k_y y) \cos \sigma t \quad (5.13)$$

where the wave numbers k_x and k_y give the standing wave lengths in the x and y directions and σ is the wave angular frequency in terms of the different periods of the various resonant modes. Specific values of k_x , k_y , and σ depend on the basin geometry which establishes the lengths and periods of the standing waves in the basin.

For the rectangular basin shown in Figure 5.8 which has a depth d and horizontal dimensions Γ_x and Γ_y the appropriate wave numbers and angular frequency yield

$$\eta = H \cos\left(\frac{2\pi N x}{\Gamma_x}\right) \cos\left(\frac{2\pi M y}{\Gamma_y}\right) \cos\left(\frac{2\pi t}{T_{NM}}\right) \quad (5.14)$$

from Eq. (5.13). In Eq. (5.14) the various resonant modes are defined by combinations of N and M which can each have values of 0, 0.5, 1.0, 1.5... and T_{NM} is the resonant period of the particular mode. The resonant period is given by

$$T_{NM} = \frac{1}{\sqrt{gd}} \left[\left(\frac{N}{\Gamma_x} \right)^2 + \left(\frac{M}{\Gamma_y} \right)^2 \right]^{-1/2} \quad (5.15)$$

Nodal lines will be located where the water surface elevation is zero at all times. From Eq. (5.14) this would require

$$\cos\left(\frac{2\pi N x}{\Gamma_x}\right) = \cos\left(\frac{2\pi M y}{\Gamma_y}\right) = 0$$

Thus, the coordinates of nodal lines are given by

$$\begin{aligned}
 x &= \frac{\Gamma_x}{4N}, \frac{3\Gamma_x}{4N}, \frac{5\Gamma_x}{4N} \dots \\
 y &= \frac{\Gamma_y}{4M}, \frac{3\Gamma_y}{4M}, \frac{5\Gamma_y}{4M} \dots
 \end{aligned}
 \tag{5.16}$$

for each resonant mode NM . In Eq. (5.16) the number of terms would be truncated at the number of nodal lines which is equal to $2N$ or $2M$ respectively.

Note that when N or M equal zero, Eq. (5.15) reduces to the two-dimensional resonant condition given by Eq. (5.6) with N or M given by $(k + 1)/2$.

Example 5.6–2

A basin has a square planform with side lengths Γ and a water depth d . For the resonant mode having an amplitude H and $N = M = 0.5$ give the equations for the water surface elevation as a function of position and time and the equation for the specified resonant mode. Describe the behavior of the water surface as the oscillations occur.

Solution:

For $N = M = 0.5$ Eq. (5.15) yields

$$T_{11} = \frac{\Gamma}{\sqrt{2gd}}$$

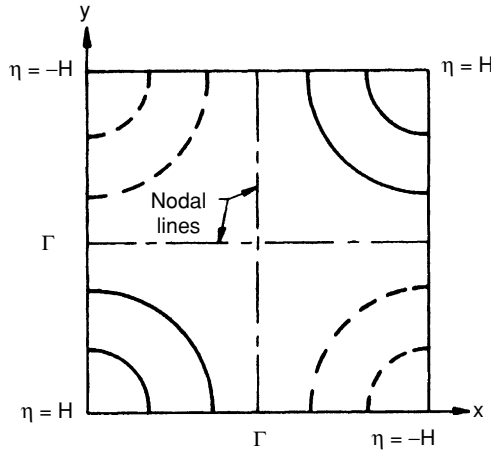
for the period of this resonant mode as a function of the basin dimensions.

The water surface elevation, from Eq. (5.14), is given by

$$\eta = H \cos \frac{\pi x}{\Gamma} \cos \frac{\pi y}{\Gamma} \cos \frac{2\pi t}{T_{11}}$$

Since $2N = 2M = 1$, there will be a pair of nodal lines. From Eq. (5.16), they will be at $x = \Gamma/2$ and $y = \Gamma/2$.

Shown below is a plot of the water surface contours at $t = 0, T_{11}, 2T_{11} \dots$. The solid lines show contours that are above the still water level, increasing from zero at the nodal line to H at the corners $x, y = 0$ and $x, y = \Gamma$. The dashed lines show contours that are below the still water level. A quarter of a period later the water surface is flat. At $t = T_{11}/2$ the contours are reversed and at $t = 3T_{11}/4$ the surface is flat again. At $t = T_{11}$ the surface is the same as at $t = 0$ and the cycle is complete. The maximum standing wave height would be at the corners and would equal $2H$. Maximum horizontal flow velocities would occur at the nodal lines and be perpendicular to the nodal lines.



Equations (5.14) and (5.15) for resonance in a rectangular basin have also been developed using a different approach (Raichlen, 1966). The three-dimensional Laplace equation is solved with the linearized DSBC [Eq. (2.8)], the BBC [Eq. (2.3)], and the boundary conditions at the vertical side walls of the basin, namely that the horizontal component of the flow velocity is zero at the wall. Assuming shallow water this yields the following velocity potential

$$\phi = \frac{Hg}{\sigma} \cos \frac{2N\pi x}{\Gamma_x} \cos \frac{2M\pi y}{\Gamma_y} \sin \sigma t \quad (5.17)$$

With Eq. (5.17), other flow properties including the water particle velocity and displacement patterns can be derived (see Section 2.7).

Helmholtz Resonance

In addition to the standing wave modes of oscillation discussed above, a basin open to the sea through an inlet can resonate in a mode known as the Helmholtz mode. Water motion is analogous to that of a Helmholtz resonator in acoustics. The water surface in the basin uniformly rises and falls while the inlet channel water mass oscillates in and out. For a simple somewhat prismatic basin and channel the resonant period T_H is given by (Carrier et al., 1971)

$$T_H = \sqrt{\frac{(L_c + L'_c)A_b}{gA_c}} \quad (5.18)$$

where A_b is the basin surface area, A_c is the channel cross-section area, L_c is the channel length, and L'_c is an additional length to account for the additional mass

of water at each end of the channel that is involved in the resonant oscillation. L'_c is given by (adapted from Miles, 1948)

$$L'_c = \frac{-W}{\pi} \ln \left(\frac{\pi W}{\sqrt{g d_c T_H}} \right) \quad (5.19)$$

where W and d_c are the channel width and depth, respectively. The Helmholtz mode appears to be important for the response of some ocean harbors to tsunami excitation (Miles, 1974). It is also a significant mode of oscillation for a number of harbors on the Great Lakes (Sorensen and Seelig, 1976) that respond to the storm-generated long wave energy spectrum on the Lakes.

5.7 Resonance Analysis for Complex Basins

Many real basins can be analyzed with sufficient accuracy using the procedures described in the previous section. If the geometry of the basin under investigation is too complex for these procedures to be applied, one can resort to either a physical hydraulic model investigation or analysis by a numerical model procedure.

A hydraulic model for a study of basin resonance would be based on Froude number similarity. If the model to prototype horizontal and vertical scale ratios are the same (undistorted model) this leads to

$$T_r = \sqrt{L_r} \quad (5.20)$$

where T_r , the time ratio, would be the ratio of the resonant period measured in the model to the equivalent prototype period and L_r is the model to prototype scale ratio. To proceed, the harbor and adjacent areas would be modeled to some appropriate scale in a wave basin. Then the model harbor would be exposed to wave attack for a range of periods covering the scaled range of prototype waves expected. The harbor response would typically be measured by wave gages at selected locations of importance and by overhead photography of water movement patterns (using dye or floats). A typical result might show the response amplitude in the harbor versus incident wave period and would produce curves with peaks at the various resonant periods. Since bottom friction and the amplitudes of the incident waves are not typically modeled, the results indicate only expected periods of resonant amplification in the harbor and related patterns of horizontal water motion at these resonant conditions.

If the horizontal and vertical scale ratios are not equal (distorted model), as may be necessary for economic, space availability, or other reasons, Froude number similarity leads to

$$T_r = \frac{L_{rh}}{\sqrt{L_{rv}}} \quad (5.21)$$

where the subscripts h and v refer to the horizontal and vertical scale ratios. For additional discussion on the conduct of basin resonance models see Hudson et al. (1979) and Hughes (1993). Some examples of harbor resonance model studies are presented by U.S. Army Waterways Experiment Station (1975) and Weggel and Sorensen (1980).

The resonant modes in an irregular shaped basin can also be investigated by numerical model analysis. A common approach employs the long wave equations which are solved for the water surface elevation and horizontal velocity components over a grid pattern that covers the basin. This essentially involves dividing the basin with a horizontal grid system and solving the equations of continuity and motion in long wave form at each grid square sequentially through space for successive time intervals. Typically, for harbor-sized basins the Coriolis and convective acceleration terms would be omitted from the equations of motion. The surface stress term would also be omitted but a bottom friction term may be included. A condition of no horizontal flow is specified for the basin solid boundaries. At the opening from the basin to the sea the boundary condition is defined by the input wave condition that sets the basin resonating. The model can be run for a range of periods to see which periods excite the basin. Botes et al. (1984) input a wave spectrum and did a spectral analysis of the water surface response at a point in the harbor to determine the significant resonant periods. The model was then run with a sine wave input at these resonant periods to obtain a detailed look at the resulting water surface oscillation and horizontal flow velocity patterns in the harbor. Wilson (1972) presents a general overview of basin oscillations including a discussion of various numerical modeling approaches.

5.8 Storm Surge and Design Storms

A storm over shallow nearshore coastal waters or shallow inland water bodies can generate large water level fluctuations if the storm is sufficiently strong and the water body is shallow over a large enough area. This is commonly known as storm surge or the meteorological tide. Storm activity can cause both a rise (setup) and fall (setdown) of the water level at different locations and times—with the setup commonly predominating in vertical magnitude, lateral extent, and duration. Specific causes of the water level change include: surface wind stress and the related bottom stress caused by currents generated by the surface wind stress, response to Coriolis acceleration as wind-induced currents develop, atmospheric horizontal pressure gradients, wind wave setup, long wave generation caused by the moving pressure disturbance, and precipitation and surface runoff.

Storm surge is generally not an important factor in water level analysis on the Pacific coast of the United States owing to the narrow continental shelf along this coast. However, on the Gulf and Atlantic coasts where the continental shelf is generally much wider and where hurricanes and extratropical storms are common, storm surge is extremely important. Storm-generated water level fluctuations in the shallower of the Great Lakes (especially at the Buffalo and Toledo ends of Lake Erie) can also be significant.

Hurricane Camille in August 1969 had estimated sustained peak wind speeds of 165 knots as it crossed the Mississippi coast. The storm surge reached a maximum of 6.9 m above MSL at Pass Christian, up to 25 cm of rainfall were measured, and the coastal area in the region of highest winds suffered virtually complete destruction (U.S. Army Engineer District, New Orleans, 1970). Surge levels in excess of 3 m above MSL occurred along the coast from the Mississippi River Delta to the Mississippi–Alabama line, a coastal distance of over 170 km. Estimated storm damage (no major urban areas were hit) was just under a billion dollars.

Storm surge calculations require a knowledge of the spatial and temporal distribution of surface wind speed and direction, and surface air pressure, as well as the forward path and speed of the design storm. The Atlantic coast of the United States experiences extratropical storms that result from the interaction of warm and cold air masses and that can generate a substantial storm surge. However, along most of the Atlantic coast south of Cape Cod and all of the Gulf coast, the worst storm conditions or design storm will usually be a hurricane of tropical origin.

Design wind and pressure field conditions for a site may be established by using the measured conditions from the worst storm of record in the general area. Or, if sufficient data exist, a return period analysis may be conducted to select storm design parameters (e.g., wind speed, pressure drop) having a specified frequency of occurrence for that area. Also, if sufficient historical surge elevation data are available, direct surge elevation–frequency relationships can be developed for a given area. Bodine (1969) did this for the Gulf coast of Texas using data from 19 hurricanes dating from 1900 to 1963.

A hurricane is a cyclonic storm having wind speeds in excess of 63 knots that originates in the tropics near but not at the equator. Those hurricanes that affect the United States typically move north from the region between Africa and South America (often with very irregular paths) into the Gulf of Mexico or up the Atlantic coast, eventually veering east and out over the Atlantic to dissipate. The driving mechanism is warm moist air that flows toward the eye (center) of the hurricane where the pressure is lowest. After rising in the eye the air flows outward at higher altitudes. Coriolis acceleration causes the inward flowing air to have a circular component, counterclockwise (looking down) in the northern hemisphere and clockwise in the southern hemisphere. The diameter of hurricanes usually does not exceed 300 nautical miles. The deficiency of warm moist air and the existence of increased surface friction when the hurricane is over land will cause it to dissipate, as will the deficiency of warm moist air at higher ocean latitudes.

The surface pressure in a hurricane, which decreases from the ambient pressure at the periphery P_a to the lowest pressure at the eye P_e can be estimated by the following empirical equation (see Schwerdt et al., 1979)

$$\frac{P_r - P_e}{P_a - P_e} = e^{-R/r} \quad (5.22)$$

which is based on an analysis of historical hurricane pressure data. In Eq. (5.22), P_r is the pressure at any radius r from the eye of the hurricane and R is the radius from the eye to the point of maximum wind speed. Wind speeds increase from the periphery toward the eye with maximum wind speeds occurring typically at a radius of between 10 and 30 nautical miles from the eye (where the pressure gradient is the largest). Inside this point the wind speeds diminish rapidly to near calm conditions at the eye. The pressure at the periphery may be taken as about the standard atmospheric pressure of 29.92 inches of mercury. The pressure in the eye varies significantly, naturally being lower for stronger hurricanes. A pressure in the eye of the order of 27.5 inches of mercury will occur in a strong hurricane and pressures as low as near 26 inches of mercury having been recorded. The hurricane season in the north Atlantic is from June to November with most hurricanes occurring in the months of August to October.

The U.S. National Weather Service, with support provided by the Nuclear Regulatory Commission and Army Corps of Engineers has developed hypothetical design hurricanes for the U.S. Atlantic and Gulf coasts that are based on a return period analysis of significant hurricane parameters (Schwerdt et al., 1979). They developed a Standard Project Hurricane (SPH) and a Probable Maximum Hurricane (PMH). The SPH has "a severe combination of values of meteorological parameters that will give high sustained wind speeds reasonably characteristic of a specified location." Only a few hurricanes of record for a large region covering the area of concern will exceed the SPH. The combined return period for the total wind field will be several hundred years. The PMH has "a combination of values of meteorological parameters that will give the highest sustained wind speed that can probably occur at a specified coastal location." The PMH was developed largely for use in the design of coastal nuclear power plants. Besides being used for storm surge analysis the SPH and PMH are useful for wave prediction and the analysis of wind loads on coastal structures.

The SPH and PMH are presented in terms of the central pressure in the eye, the peripheral pressure at the outer boundary, the radius to maximum wind speed, the forward speed of the hurricane, the direction of movement as the hurricane approaches the coast, and the inflow angle which is the angle between the wind direction and a circle concentric with the hurricane eye. (The latter typically varies from 10 to 30 degrees at points from the location of maximum wind speed to the hurricane periphery.) Ranges of values for the listed hurricane parameters are given as a function of coastal location from Maine to Texas. With selected values of these parameters the surface (10 m elevation) wind field can be

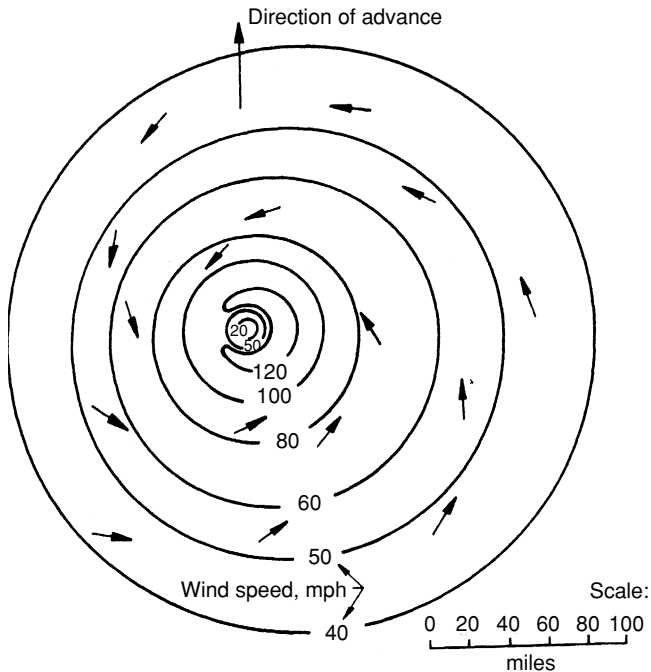


Figure 5.9. Typical surface wind field for a Standard Project Hurricane.

plotted and the pressure field can be calculated from Eq. (5.22). Figure 5.9 shows the surface wind field for a typical SPH.

From economic and other considerations it may be desirable to use a design hurricane other than the SPH and PMH even though the designer has some flexibility in the selection of the parameters for these storms. For example, a wooden pier with a shorter design life or a rubble mound breakwater that can relatively easily be repaired would be designed for a lesser storm than the SPH. North of Cape Cod the design storm is likely to be an extratropical cyclone (known as a Northeaster) rather than a hurricane. Patterson and Goodyear (1964) present the characteristics of Standard Project Northeasters that may be used for storm wind prediction in this region.

5.9 Numerical Analysis of Storm Surge

Several different numerical models have been developed to analyze storm surge along the open coast and in bays and estuaries (e.g., Reid and Bodine, 1968; Butler, 1978; Wanstrath, 1978; Tetra Tech, 1981; Mark and Scheffner, 1993). They are two-dimensional vertically integrated models that apply the long wave

equations [Eqs. (5.1), (5.3a), and (5.3b)] to a grid system that covers the area to be modeled. At each grid point the numerical model calculates the two horizontal flow components and the water surface elevation at the successive time intervals for which the model is operated.

Typically, the area to be modeled is divided into square segments and the three long wave equations are written in finite difference form for application to each square segment in the grid. At the sides of squares that are at the lateral water boundaries the appropriate boundary conditions must be applied to allow for correct computation of flow behavior at these boundaries. Typical boundary conditions might include: water–land boundaries across which there will never be any flow, adjacent low-lying areas that will flood when the water surface level reaches a certain elevation, inflow from rivers and surface runoff, barriers such as barrier islands and dredge spoil dikes that can be overtopped, and offshore boundaries having a specified water level/inflow time history. The computer solution for the unknown values at each grid square (q_x , q_y , η) proceeds sequentially over the successive rows and columns for a given time and then time is advanced and the spatial calculations are repeated.

Several important considerations arise when these models are developed and applied:

1. If the lateral extent of the water body is sufficient for the horizontal atmospheric pressure gradient to be important, the hydrostatic water surface elevation response can be calculated separately as a function of location and time and added to the long wave model result.
2. The bottom stress term must be empirically established from previous experience and by calibration using tide wave propagation analysis for periods of low winds as well as results of previous storms.
3. For complex coastal boundaries the grid mesh shape and size may have to be adjusted to produce adequate surge elevation calculations.
4. Wave setup (see Section 2.6) which occurs inside the surf zone is dependent on the wave conditions generated by the storm. If this is an important component of the total surge level, wave predictions must also be made so the wave setup can be calculated.
5. The wind and pressure fields must be specified in the model. For calibration of models for existing storms there may be adequate information available. For future predictions for storms where adequate measurements are not available, the SPH or PMH may be used or one of the available wind field models may be used (e.g., see Thompson and Cardone, 1996).
6. A wind stress drag coefficient is required to convert the surface wind speed to a resulting surface stress for the equations of motion. A commonly used relationship was developed by Van Dorn (1953). From elementary fluid

mechanics the wind-induced shear stress on a surface is typically written as a product of the drag coefficient times the air density times the wind speed squared. For storm surge analysis it is more useful to write a relationship for surface stress in terms of the water density ρ , i.e.,

$$\tau_s = K_s \rho W^2 \quad (5.23)$$

where K_s is the wind stress drag coefficient and W is the wind speed at the standard 10 m elevation. The relationship given by Van Dorn is

$$K_s = 1.21 \times 10^{-6} + 2.25 \times 10^{-6} \left(1 - \frac{5.6}{W}\right)^2 \quad (5.24)$$

where the wind speed is in meters per second. This is based on a field study that was conducted at a yacht basin along the California coast. For extensive evaluations of the available information on wind stress drag coefficients see Wilson (1960) and Garrett (1977).

7. A storm is a moving pressure disturbance which, given the right conditions, can generate long waves that propagate ahead of the storm and can cause what has been termed an initial setup along the coast (see Sorensen, 1993). This occurs when the forward velocity of the storm is close to the celerity of a shallow water wave for the water depth over which the storm is traveling (i.e., a storm speed Froude number close to unity). It takes time for this wave to develop so the storm must travel over the right water depth for a significant period of time.
8. For detailed and sufficiently accurate analysis of the surge conditions at different locations of the water body a sufficiently fine grid must be established since the water depth is assigned a constant average value over each grid square. But for stability of the model calculations the time interval selected for calculations must fit the grid spacing. Thus, finer grid sizes require shorter time intervals and a commensurately significant increase in computation time.

An early but instructive storm surge model was the one employed by Reid and Bodine (1968) to calculate storm surge in Galveston Bay, Texas. For this application the equations of motion [Eqs. (5.3a) and (5.3b)] were somewhat simplified. The convective acceleration terms were considered negligible owing to the scale of the bay as was the Coriolis acceleration term owing both to the bay scale and the dominance of bottom friction owing to the relatively shallow water depths. The Van Dorn relationship was used to define the wind stress drag coefficient. Flooding of low-lying terrain adjacent to the bay and overtopping of the barrier island that separates the bay from the Gulf of Mexico were

included through the application of the boundary conditions. The boundary condition at the entrance to Galveston Bay from the Gulf was incorporated by extending the model seaward of the bay, specifying a water level condition at this seaward boundary and applying a discharge coefficient for the bay entrance. The area modeled, including the bay, a very small portion of the Gulf, and low-lying land around the bay had a nominal dimension of about 40 miles by 50 miles. This was subdivided into 2 mile square grids and time steps of 3 and 4 min were used. Bottom friction was initially calibrated for a spring astronomical tide propagating into the bay during a period of calm wind conditions. Further calibration of bottom friction and discharge coefficients was carried out for the well-documented Hurricane Carla of 1961. Then the calibrated model was verified by attempting to duplicate the measured surge conditions of Hurricane Cindy of 1963.

5.10 Simplified Analysis of Storm Surge

Occasionally in engineering practice it is not necessary, owing to time and cost limitations and because of lesser required accuracy, to apply the more sophisticated numerical analysis procedures to estimate storm surge at a given site. A simplified approach to storm surge analysis would involve calculating the wind/bottom stress-induced surge, the pressure-induced surge, and possibly the Coriolis-induced surge separately. Each is calculated from a simple hydrostatic balance. Thus, the convective and local acceleration terms as well as continuity requirements are neglected. This basically assumes a static storm that is in position for a sufficient length of time for the water level response to come to equilibrium with sufficient water being available to achieve that equilibrium. Thus, in most cases a conservative setup estimate would be produced. The effects of astronomical tide level variations and wave-induced setup nearshore can also be separately evaluated if necessary.

Each of these components—wind/bottom stress setup, atmospheric pressure gradient setup, and Coriolis setup—is briefly presented below. A few comments on appropriate tide levels and wave-induced setup are also included.

Wind/Bottom Stress Setup

The wind acting on the water surface causes a shear stress given by Eq. (5.23), where the wind stress drag coefficient K_s can be defined by Eq. (5.24) or some other relationship as discussed above. The surface wind stress generates a current that, in turn, develops a bottom stress. Usually, the bottom current velocity is not known nor can it easily be calculated, so the bottom stress cannot be directly calculated. Saville (1952), from field data collected at Lake Okeechobee, FL, suggested that the bottom stress was in the order of 10% of the surface wind stress. Van Dorn (1953), from his field data and the threshold limits on his

equipment for measuring the bottom stress, reported that it was generally less than 10% of the surface stress. Thus, the ratio $\tau_b/\tau_s = 0.1$ can be used for wind-induced setup calculations if no better data are available. If adequate wind, pressure, and resulting setup data are available from a previous storm at a particular site, it is better to determine a local combined surface and bottom stress coefficient $K_{sb}(\tau_s + \tau_b = K_{sb}\rho W^2)$, which then acts as an “all inclusive” calibration factor for subsequent wind/bottom stress setup calculations.

Figure 5.10 shows a section of a nearshore water segment of length Δx in the direction in which setup is being calculated, unit width, and depths d and $d + \Delta S_w$. ΔS_w is the setup owing to wind and bottom stresses acting over the distance Δx . The hydrostatic forces on each end are shown and the bottom stress is drawn in the same direction as the surface wind stress because it is assumed that the wind-generated current causes a reverse flow on the bottom. If the wind is blowing at an angle θ to the x direction, then the component of the wind velocity in the x direction W_x is used. The effective stress then becomes

$$\tau_s + \tau_b = K_{sb}\rho W^2 \cos \theta = K_{sb}\rho W W_x$$

Since the water surface slope $\Delta S_w/\Delta x$ is extremely flat a static balance yields

$$\tau_s \Delta x + \tau_b \Delta x + \frac{1}{2} g \rho d^2 - \frac{1}{2} g \rho (d + \Delta S_w)^2 = 0$$

Inserting the wind/bottom stress relationship, eliminating higher order terms, and solving yields

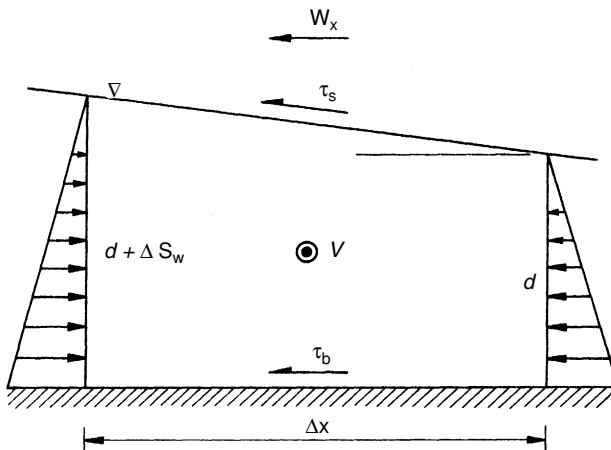


Figure 5.10. Definition sketch for wind/bottom stress and Coriolis setup derivations.

$$\Delta S_w = d \left[\sqrt{\frac{2K_{sb} W W_x \Delta X}{g d^2} + 1} - 1 \right] \quad (5.25)$$

where $K_{sb} = 1.1 K_s$ may be used if no better information is available (as discussed above).

For a shore normal profile on the open coast, wind/bottom stress setup calculations can be made using Eq. (5.25), keeping in mind the assumptions discussed above. The profile would be broken into segments (not necessarily of equal size) of length Δx over which an average depth and wind velocity can be defined. Starting at the offshore point where the wind velocity is sufficiently low and/or the water is sufficiently deep so setup is negligible, the setup for each segment can be calculated and summed to yield the total setup at the shore. As the calculation proceeds, the accumulated setup for the previous segments should be included in determining the water depth for the next segment setup calculation.

Equation (5.25) can be applied (with caution) to enclosed bays that are not too irregular in shape. The depth for a given segment would have to be the average over the length and width of the segment. The volume of water that sets up on the leeward end of the bay must equal that removed from the windward end and the two sections would be divided by a nodal line. For a given wind field, a nodal line position would be assumed and the setup calculations would be carried out up wind and down wind from the nodal line. Then the setup and setdown water volumes would be determined and compared. A balance of the setup and setdown volumes determines the final surface profile and nodal line position.

Atmospheric Pressure Gradient Setup

From hydrostatics, the water level variation or setup S_p owing to a horizontal atmospheric pressure differential Δp between two points on a continuous body of water is

$$S_p = \frac{\Delta p}{\rho g} \quad (5.26)$$

where ρ is the water density.

By combining Eqs. (5.22) and (5.26) one can calculate the static pressure setup that occurs at a point of interest in an SPH. For a pressure differential of say 2.5 inches of mercury (e.g., 29.9 to 27.4) from the periphery to the eye of a hurricane, the static pressure setup at the eye would be 0.86 m.

Example 5.10-1

The bottom profile normal to the shoreline in the area between Galveston and Port Arthur, TX is tabulated below (depths were read in fathoms and converted to meters; 1 fathom = 6 feet = 1.83 m).

<u>Depth (m)</u>	<u>Distance (m)</u>
7.31	2750
10.05	4590
13.72	22930
14.62	45860
20.12	48150
23.97	82550
25.60	100890
27.43	107710
36.57	121530
54.86	144460
73.15	181150
91.43	190320

Seaward of the 91.43 m depth the depth increases relatively rapidly and is sufficiently deep so that little additional setup would occur.

For a 60 knot (30.86 m/s) wind blowing landward along this profile calculate the setup on the shore. If the pressure gradient along this profile is 0.003 inches of mercury per nautical mile what pressure setup would occur?

Solution:

From Eq. (5.24) the drag coefficient is

$$K_s = 1.21 \times 10^{-6} + 2.25 \times 10^{-6} \left[1 - \frac{5.6}{30.86} \right]^2 = 2.72 \times 10^{-6}$$

Then, Eq. (5.25) becomes

$$\Delta S_w = d \left[\sqrt{\frac{2(1.1)(2.72)10^{-6}(30.86)^2 \Delta x}{9.81 d^2}} + 1 - 1 \right]$$

or

$$\Delta S_w = d \left[\sqrt{\frac{0.00058 \Delta x}{d^2}} + 1 - 1 \right]$$

We then break the profile into segments having a length Δx and a depth $d + \Sigma \Delta S_w$ which is the depth below still water for the segment plus the accumulated surge up to that segment. The accumulated surge is then calculated from the above equation, starting at the seaward segment and using the depth plus accumulated surge for d . The results are tabulated below (all values are in meters):

d	Δx	ΔS_w	$d + \Sigma \Delta S_w$
3.66	2750	0.14	5.74
8.68	1840	0.04	10.72
11.88	18340	0.39	13.53
14.17	22930	0.43	15.39
17.37	2290	0.04	18.55
21.95	34400	0.44	22.69
24.79	18340	0.21	25.32
26.51	6820	0.07	26.97
32.00	13820	0.12	32.34
45.72	22930	0.14	45.92
64.00	36690	0.17	64.03
82.29	<u>9170</u>	<u>0.03</u>	82.29
	190320	2.22	

Thus, the total wind-induced setup at the shore would be 2.22 m and the setup profile could be determined by sequentially summing the values in the second and third columns.

The distance from the offshore starting point to the shore is 190320 m = 102.8 nautical miles. Thus, the pressure difference is $(0.003)102.8 = 0.31$ inches of mercury. From hydrostatics

$$S_p = \frac{0.31(13.55)}{12(3.28)} = 0.11 \text{ m}$$

Note how the above calculation relates to Eq. (5.26).

Coriolis Setup

If a current is flowing along a shoreline, Coriolis acceleration will cause the water to deflect to the right in the Northern hemisphere. If the shoreline is on the righthand side of the current the deflection will be restrained, causing a setup of water on the shore. If the shoreline is on the lefthand side there will be a setdown at the shore.

In Figure 5.10 a current of velocity V is coming out of the page and Coriolis acceleration causes a setup as shown. A balance between the hydrostatic forces and the Coriolis acceleration or force per unit mass yields

$$\frac{1}{2} g \rho d^2 + 2 \omega V \sin \phi \rho g d \Delta x - \frac{1}{2} g \rho (d + \Delta S_c)^2 = 0$$

where S_c is the Coriolis set up. Neglecting higher order terms leads to

$$S_c = \frac{2\omega}{g} V \sin \phi \Delta x \quad (5.27)$$

which can be used to calculate the setup over a given horizontal distance at any latitude if the current velocity is known.

Away from the shore, wind-generated currents are free to respond to the Coriolis acceleration; but nearshore this response is restricted and setup or setdown occurs. For simple analyses the resulting wind-generated current velocity is not easily determined. Often, the current velocity is small or in a direction such that the Coriolis setup can be neglected in a simple analysis. The latter is often true in small bays and lakes.

Bretschneider (1967) solved the equation of motion for the alongshore direction, including only the wind and bottom stresses and the local acceleration to obtain an equation for the wind-generated longshore current velocity. For the resulting steady-state condition (i.e., sufficient wind duration)

$$V = Wd^{1/6} \sqrt{\frac{K_s}{14.6n^2}} \sin \theta \quad (5.28)$$

where n is Manning's roughness coefficient (typical value is 0.035), θ is the angle between the wind direction and a line perpendicular to the coast and/or bottom contours, and V is the resulting alongshore current velocity. The derivation of Eq. (5.28) assumes that there is no flow component normal to the shore, limiting its use to the nearshore region. The author has found that results from Eq. (5.28) generally agree with the rule of thumb that wind-generated surface current velocities will be 2% to 3% of the wind speed.

Astronomical Tide and Wave Setup

Storm surge setup calculations should be added to some reasonably expected higher tide for conservative estimates for engineering design. There is a small likelihood that the peak of the storm surge will arrive at exactly the same time as high tide, but assumption of some higher tide level will ensure a conservative estimate of expected water levels. Note also that there is a nonlinear interaction between the wind setup and the astronomical tide level (and arrival time) as both depend on the water depth. When the wind setup is calculated separately and added to the astronomical tide level the result would be a slightly higher water level than the true coupled water level.

Wave-induced setup at the shoreline can be calculated using wind-generated wave predictions (Chapter 6) and the procedures demonstrated in Example 2.6-1. To make these calculations one must know the breaker wave height and water depth as well as the nearshore bottom slope.

5.11 Long-Term Sea Level Change

When the mean sea level is measured at many coastal sites over a long period of time, it is observed that this level is changing relative to the land. The change is due to a general global eustatic rise in the mean sea level superimposed on a possible tectonic uplift or subsidence of the coast. Along most of the U.S. coastline relative sea levels have been rising, except for some coastal regions in Alaska where coastal uplift rates exceed the eustatic sea level rise to produce a lowering of the relative sea level. Hicks and Hickman (1988) report on yearly relative mean sea level trends for 45 U.S. coastal stations based on 50 to over 100 years of tide gage record. The 25 U.S. Atlantic coast relative sea level change values range from +1.79 to +4.33 mm/year, whereas four stations in Alaska had mean sea level changes of -0.09 to -12.4 mm/year.

A sea level rise of 2 to 4 mm/year produces a rise of 0.2 to 0.4 m in a century. This can have some noticeable impacts on the coast as the mean water level rises on the beach face and there is a concurrent retreat of the beach face caused by this sea level rise. It can also have significant impacts on the design of coastal structures. See U.S. National Research Council (1987) and Sorensen (1991) for a discussion of these impacts.

A study conducted by Kyper and Sorensen (1985) well exemplifies the potential impact of the expected rise in mean sea level on a sandy beach backed by a seawall. As mean sea level rises the beach face is flooded by the rising water level. The beach profile also responds by retreating as the raised sea levels causes a net movement of sand on the beach profile to the offshore area. For a coastal structure exposed to the sea, the raised sea level means that the water depth is increased at the toe of the structure. Deeper water typically allows higher waves to reach the structure because the height of a breaking wave is related to the water depth at breaking (see Section 2.8). Recession of the beach profile at the toe of the structure further increases the height of the wave that can attack the structure.

Kyper and Sorensen (1985) studied sea level rise impacts on the beach and stone mound seawall at Sea Bright NJ, for a range of expected sea level rise scenarios. Construction of the seawall commenced in 1898. It was observed that there was increasing damage to the seawall as time progressed through the 1970's and 1980's, by which time much of the seawall had no beach in front of it. Apparently, the lowering of the beach face in front of the seawall combined with the rise in mean sea level at the site allowed waves that exceed the height for which the seawall is stable to cause the damage. It is estimated that the relative rise in mean sea level at the site was of the order of a half meter during the past century. This was exacerbated by the deficiency of sand transport past the structure which caused a further lowering of the beach face.

The primary question addressed by Kyper and Sorensen was to investigate the relative costs of constructing and maintaining an artificial beach in front of the

seawall to protect it from wave attack, versus the cost of adding an additional layer of larger armor stone on the face of the seawall to increase its stability to the increased wave attack. Quantifying the increased shoreline recession and coastal flooding expected from a range of expected future sea level rise scenarios, allowed the authors to quantify the volume of sand necessary to maintain a design beach width with a specified crest elevation. Then the authors determined the increased armor stone size for a refurbished seawall for the same expected sea level rise scenarios. The authors also discuss the impact of no future coastal engineering works being implemented at the site.

The final choice of whether to construct the protecting beach or to upgrade the seawall depends on the material costs (beach fill, stone, etc.) and construction costs at the time the project is to commence. It also depends on other factors such as the economic value of recreational benefits on the expanded beach and the funding available from national and local sources for the competitive projects.

Global eustatic sea level rises that have been observed during the past century are believed to be caused by atmospheric warming which causes sea water to expand and land ice in glaciers to melt, adding water to the seas. There have been a number of forecasts that this rise in global eustatic sea level will accelerate during the coming century (see U.S. National Research Council, 1987). If this happens the effects on the coastline will be significant.

Large mean water level variations are observed on the Great Lakes. These are due primarily to changes in seasonal and longer term rainfall/runoff variations. The lakes can experience mean monthly seasonal fluctuations of 0.3 m or more and longer term fluctuations of 1 to 2 m over a period of several years.

5.12 Summary

This chapter presented the characteristics and, where possible, the techniques for predicting water level fluctuations having a period greater than the periods of waves in the wind wave portion of the wave energy spectrum. The discussion of surface waves to this point considered only the simple monochromatic form of these waves. Chapter 6 considers the complex form of wind-generated waves observed at sea as well as the generation, analysis, and prediction of these waves.

5.13 References

Bodine, B.R. (1969), "Hurricane Surge Frequency Estimated for the Gulf Coast of Texas," Technical Memorandum 26, U.S. Army Coastal Engineering Research Center, Washington, DC.

- Botes, W.A.M., Russell, K.S., and Huizinga, P. (1984), "Model Harbor Seiching Compared to Prototype Data," in *Proceedings, 19th International Conference on Coastal Engineering*, American Society of Civil Engineers, Houston, pp. 846–857.
- Bretschneider, C.L. (1967), "Storm Surges," Vol. 4, *Advances in Hydrosience*, Academic Press, New York, pp. 341–418.
- Butler, H.L. (1978), "Coastal Flood Simulation in Stretched Coordinates," in *Proceedings, 16th Conference on Coastal Engineering*, American Society of Civil Engineers, Hamburg, pp. 1030–1048.
- Camfield, F.E. (1980), "Tsunami Engineering," Special Report No. 6, U.S. Army Coastal Engineering Research Center, Ft. Belvoir, VA.
- Carrier, G.F., Shaw, R.P., and Miyata, M. (1971), "Channel Effects in Harbor Resonance," *Journal, Engineering Mechanics Division, American Society of Civil Engineers*, Dec., pp. 1703–1716.
- Dean, R.G. and Dalrymple, A.T. (1984), *Water Wave Mechanics for Engineers and Scientists*, Prentice-Hall, Englewood Cliffs, NJ.
- Garrett, J.R. (1977), "Review of Drag Coefficients Over Oceans and Continents," *Monthly Weather Review*, Vol. 105, pp. 915–929.
- Gilmour, A.E. (1961), "Tsunami Warning Charts," *New Zealand Journal of Geology and Geophysics*, Vol. 4, pp. 132–135.
- Harris, D.L. (1981), "Tides and Tidal Datums in the United States," Special Report No. 7, U.S. Army Coastal Engineering Research Center, Ft. Belvoir, VA.
- Hendershott, M.C. (1977), "Numerical Models of Ocean Tides," *The Sea*, Vol. 6, John Wiley, New York, pp. 47–96.
- Hicks, S.S. and Hickman, L.E. (1988), "United States Sea Level Variations through 1986," *Shore and Beach*, July, pp. 3–7.
- Hudson, R.L., Hermann, F.A., Sager, R.A., Whalin, R.W., Keulegan, G.H., Chatham, C.E., and Hales, L.Z. (1979), "Coastal Hydraulic Models," Special Report No. 5, U.S. Army Waterways Experiment Station, Vicksburg, MS.
- Hughes, S.A. (1993), *Physical Models and Laboratory Techniques in Coastal Engineering*, World Scientific, Singapore.
- Iida, K. (1969), "The Generation of Tsunamis and the Focal Mechanism of Earthquakes," *Tsunamis in the Pacific Ocean* (W.M. Adams, Editor) East-West Center Press, University of Hawaii, pp. 3–18.
- Keulegan, J.H. and Harrison J. (1970), "Tsunami Refraction Diagrams by Digital Computer," *Journal, Waterways and Harbors Division, American Society of Civil Engineers*, May, pp. 219–233.
- Kyper, T.N. and Sorensen, R.M. (1985), "The Impact of an Accelerated Sea Level Rise on Coastal Works at Sea Bright, New Jersey," Fritz Laboratory Report 200.85.905.1, Lehigh University, Bethlehem, PA.
- Macmillan, D.H. (1966), *Tides*, Elsevier, New York.

- Mark, D.J. and Scheffner, N.W. (1993), "Validation of a Continental Scale Storm Surge Model for the Coast of Delaware," in *Proceedings, Estuarine and Coastal Modeling Conference*, American Society of Civil Engineers, New York, pp. 249–263.
- Miles, J.W. (1948), "Coupling of a Cylindrical Tube to a Half Space," *Journal, Acoustic Society of America*, pp. 652–664.
- Miles, J.W. (1974), "Harbor Seiching," *Annual Review of Fluid Mechanics*, Vol. 6, pp. 17–35.
- Patterson, K.R. and Goodyear, H.V. (1964), "Criteria for a Standard Project Northeast for New England North of Cape Cod," National Hurricane Research Project Report 68, U.S. Department of Commerce, Washington, DC.
- Pugh, D.T. (1987), *Tides, Surges and Mean Sea Level*, John Wiley, New York.
- Raichlen, F.R. (1966), "Harbor Resonance," in *Estuary and Coastline Hydrodynamics* (A.T. Ippen, Editor), McGraw-Hill, New York, pp. 281–340.
- Reid, R.O. and Bodine, B.R. (1968), "Numerical Model for Storm Surges in Galveston Bay," *Journal, Waterways and Harbors Division, American Society of Civil Engineers*, February, pp. 33–57.
- Saville, T. Jr. (1952), "Wind Set-up and Waves in Shallow Water," Technical Memorandum 27, U.S. Army Beach Erosion Board, Washington, DC.
- Schwerdt, R.W., Ho, F.P., and Watkins, R.R. (1979), "Meteorological Criteria for Standard Project Hurricane and Probable Maximum Hurricane Wind Fields, Gulf and East Coasts of the United States," NOAA Technical Report NWS 23, U.S. Department of Commerce, Washington, DC.
- Sorensen, R.M. (1991), "Impact of Expected Climate Change Effects on Coastal Structure Design," in *Proceedings, Coastal Structures and Breakwaters Conference*, Thomas Telford, London, pp. 1–12.
- Sorensen, R.M. (1993), *Basic Wave Mechanics: for Coastal and Ocean Engineers*, John Wiley, New York.
- Sorensen, R.M. and Seelig, W.N. (1976), "Hydraulics of Great Lakes Inlet-Harbor Systems," in *Proceedings, 15th Conference on Coastal Engineering*, American Society of Civil Engineers, Honolulu, pp. 1646–1665.
- Tetra Tech (1981), "Coastal and Flooding Storm Surge Model," Federal Emergency Management Agency, Washington, DC.
- Thompson, E.F. and Cardone, V.J. (1996), "Practical Modeling of Hurricane Surface Wind Fields," *Journal, Waterway, Port, Coastal and Ocean Engineering Division, American Society of Civil Engineers*, July/August, pp. 195–205.
- U.S. Army Engineer District, New Orleans (1970), "Report on Hurricane Camille, 14–22 August 1969."
- U.S. Army Waterways Experiment Station (1975), "Los Angeles and Long Beach Harbors Model Study," Technical Report H-75-4 (series of reports by Hydraulics Laboratory staff), Vicksburg, MS.
- U.S. National Research Council (1987), "Responding to Changes in Sea Level—Engineering Implications," National Academy Press, Washington, DC.

- Van Dorn, W.G. (1953), "Wind Stress on an Artificial Pond," *Journal of Marine Research*, Vol. 12, pp. 249–276.
- Wanstrath, J.J. (1978), "An Open-Coast Mathematical Storm Surge Model with Coastal Flooding for Louisiana," Miscellaneous Paper 78–5, U.S. Army Engineer Waterways Experiment Station, Vicksburg, MS.
- Weggel, J.R. and Sorensen, R.M. (1980), "Surging in the Shark River Boat Basin," in *Proceedings, Ports '80 Conference*, American Society of Civil Engineers, Norfolk, VA.
- Wiegel, R.L. (1970), "Tsunamis," *Earthquake Engineering* (R.L. Wiegel, Editor), Prentice-Hall, Englewood Cliffs, NJ, pp. 253–306.
- Wilson, B.W. (1960), "Note on Surface Wind Stress over Water at Low and High Wind Speeds," *Journal of Geophysical Research*, Vol. 65, pp. 3377–3382.
- Wilson, B.W. (1972), "Seiches," *Advances in Hydrosience*, Vol. 8, Academic Press, New York, pp. 1–94.
- Wilson, B.W. and Torum, A. (1968), "The Tsunami of the Alaskan Earthquake, 1964: Engineering Evaluation," Technical Memorandum 25, U.S. Army Coastal Engineering Research Center, Ft. Belvoir, VA.
- Zetler, B.D. (1947), "Travel Time of Seismic Sea Waves to Honolulu," *Pacific Science*, Vol. 1, pp. 185–188.

5.14 Problems

1. Using the noaa.gov website plot the tide curve for Philadelphia PA and Trenton NJ for the 24 hour period of your birth date this year. Be sure to note the appropriate vertical datum for the tide levels. Is this tide closer to being a spring or a neap tide?
2. Using the noaa.gov website plot the tide at Alcatraz Island and at Sacramento for the 24 hours of your birth date this year. Plot both tides on the same figure and explain the differences.
3. The tide range measured during a single tidal cycle at an offshore tower where the water depth is 100 m is 1.15 m. What maximum water particle velocity at the sea floor would you expect?
4. A tide gage at the end of a pier where the water depth is 6 m measures a tide range of 1.53 m. What tide range would you expect offshore of the pier where the water depth is 110 m? What would the maximum water particle velocity be at the bottom in the 110 m depth? Mention any assumptions made in your analysis.
5. The tide is propagating up a long straight narrow channel (x -direction) from the sea. Write the appropriate linearized form of the long wave equations for this situation. Comment on how you might apply these equations to analyze the tide in this channel, including what information you would need and the possibility of neglecting any terms in the equations you presented.

6. Steady uniform flow occurs in a straight prismatic open channel where bottom and surface friction can be neglected for the sake of our analysis. Starting with the long wave equations develop an equation for predicting the water surface slope normal to the direction of flow along the channel. Mention any required assumptions.

7. Over a great circle route between an earthquake epicenter on the coast of Chile and a coastal location in Hawaii the average depth is 50 fathoms for 150 n.m., 1800 fathoms for 390 n.m., 2200 fathoms for 3870 n.m., and 2800 fathoms for 1260 n.m. Calculate the tsunami travel time between these two points assuming a path along the great circle route.

8. A tsunami wave has a 0.7 m height in water 2000 m deep. If refraction causes orthogonal spacing to decrease by a factor of two at a depth of 20 m, what is the wave energy per foot of crest width at the 20 m depth?

9. Are tsunami waves dispersive? Explain your answer.

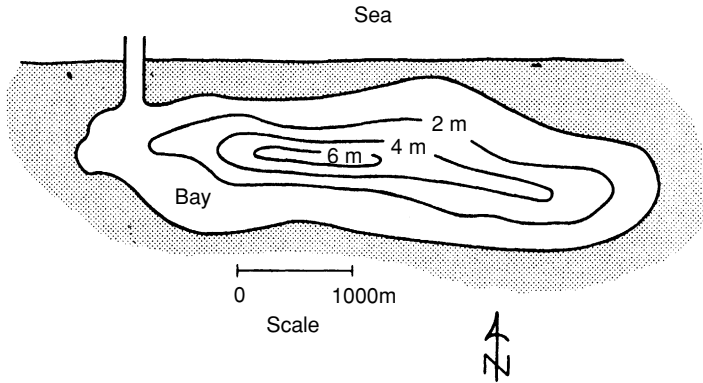
10. The bottom profile at a given coastal site varies linearly from 200 m deep at a distance of 200 km offshore to 10 m deep at a distance of 10 km offshore. If a tsunami wave reaches the offshore point at 6:00 a.m. what time will it arrive at the inshore point? (Note: do not solve this problem by simply assuming an average depth over the travel path of the tsunami.)

11. The U.S. Army Coastal Engineering Research Center had a wave tank that was 193 m long, 4.57 m wide, and 6.1 m deep. If the tank is filled with fresh water to a depth of 4 m, calculate the fundamental periods of longitudinal and lateral resonant oscillations in the tank. Does it appear that these fundamental modes or their harmonics would cause any difficulty to experimenters who wish to operate at full-scale wave periods?

12. A two-dimensional closed basin is 30 m long and the depth varies linearly from 2 m at one end to zero at the other end. Calculate the fundamental period of oscillation for this basin. (Note: do not simply use the average depth of the basin to solve this problem.)

13. A rectangular marina with a small opening to the sea has horizontal dimensions of 100 m by 375 m and a constant depth of 5 m. Estimate the five longest resonant periods and draw plan view diagrams that show the nodal line patterns for these five modes of oscillation. For $H = 0.5$ m for the longest period mode, what is the largest horizontal water velocity that would occur in the marina?

14. A bay has the dimensions and depth contours shown. Estimate the fundamental period of longitudinal free oscillation for this bay. If the jettied entrance is 300 m long, 25 m wide, and 4 m deep, calculate the Helmholtz period.



15. Explain the development of Eqs. (5.20) and (5.21) from basic Froude number similarity requirements.

16. A 50 knot wind blows to the east along the axis of the bay shown in Problem 14. Calculate the wind-induced setup at the down wind end.

17. An SPH with $P_a = 29.9$ inches of mercury, $P_e = 27.5$ inches of mercury, and $R = 15$ n.m. is acting on the bay shown in Problem 14. What is the maximum atmospheric pressure induced setup you would expect to find?

18. Consider a hurricane that travels onshore along a path that is normal to a straight shoreline. The point of maximum wind velocity is just crossing the shoreline.

(a) Sketch the surface wind velocity vector pattern.

(b) Show the expected wind stress-induced setup/-down distribution along the coast.

(c) Show the expected Coriolis-induced setup/-down distribution along the coast.

(d) Show the expected pressure-induced setup/-down along the coast.

19. A flat-bottom trough 400 m long and filled with water to a depth of 0.3 m has a freeboard (clearance above the still water line) of 0.05 m. What is the maximum wind speed along the trough axis that can occur without water spilling out of the trough at the downwind end? Neglect wind waves.

20. The bottom profile normal to the shore off a section of the coast has the following average depths at the given segment distance lengths: 2.7 m (3 n.m.), 3.8 m (7 n.m.), 4 m (10 n.m.), 11 m (20 n.m.), 12.2 m (30 n.m.), 15.5 m (40 n.m.), 27 m (50 n.m.), 48 m (60 n.m.), 73 m (70 n.m.), and 200 m (80 n.m.). There is a sustained wind blowing directly onshore at an average speed of 72 knots. Calculate the wind-induced setup at the shore.

6

Wind-Generated Waves

The most apparent and usually the most important waves in the spectrum of waves at sea (see Figure 5.2) are those generated by the wind. Wind-generated waves are much more complex than the simple monochromatic waves considered to this point. We must briefly look into how these waves are generated by the wind and some of the important characteristics that result. It is important to have a means to quantify wind-generated waves for use in various engineering analyses. It is also important to be able to predict these waves for a given wind condition—both wave hindcasts for historic wind conditions and wave forecasts for predicted impending wind conditions. Finally, we also need to look at procedures for extreme wave analysis, i.e., to predict those extreme wind-generated wave conditions that will be used as the limit for engineering design.

6.1 Waves at Sea

The record of a water surface time history measured at a point in a storm would show an irregular trace somewhat similar to that depicted in Figure 6.3. A wave record taken at the same time at a nearby location would be significantly different but would have similar statistical properties. The records for a particular area may contain locally generated waves from the existing storm superimposed on lower waves having a different range of periods that were generated by earlier winds acting at some distant location.

As the wind velocity, distance or fetch over which the wind blows, and/or duration of the wind increase, the average height and period of the resulting downwind waves will increase (within limits). For a given wind speed and unlimited fetch and duration there is a fixed limit to which the average height and period can grow. At this limiting condition the rate of energy input to the waves from the wind is balanced by the rate of energy dissipation because of wave breaking and surface water turbulence. This condition, which is known as a fully developed sea, is commonly not reached even in large storms.

Waves that are actively being generated have wave crests that are short and poorly defined. These crests are propagating in a range of directions around the dominant wind direction. As the waves propagate through the area where the wind is acting, they grow in average height and period. After leaving the area of active wind generation the surface profiles become smoother and the crests become longer and more easily recognized. These freely propagating waves are commonly called swell. As swell propagate their average height decreases somewhat owing to air resistance and internal friction, but more importantly because of angular spreading of the wave field. Also, period dispersion occurs, causing the longer waves to propagate ahead of the shorter waves in the field of swell.

McClenan and Harris (1975) conducted a study of aerial photographs of swell at sea and in the nearshore zone. They found a high incidence of one or more distinct wave trains having long crests and fairly regular wave periods. In many photographs they could identify as many as four or five distinct wave trains coming from different directions. In the offshore region the shorter and steeper waves were usually most visible. However, the predominant surf zone waves in the same photograph were the longer swell, not as discernible offshore, which undergo the greatest increase in steepness while shoaling. These longer waves tend to dominate surf zone hydraulic and sediment-transport processes. At some nearshore locations the large number of wave trains observed is due partly to reflection and refraction-diffraction effects that cause a wave train to overlap itself.

6.2 Wind-Wave Generation and Decay

Wind blowing over the surface of a water body will transfer energy to the water in the form of a surface current and by generating waves on the water surface. The initial question is, How does a horizontal wind initiate the formation of waves on an initially flat water surface? This process is best explained by a resonance model proposed by Phillips (1957, 1960). There are turbulent eddies in the wind field that exert a fluctuating pressure on the water surface. These pressure fluctuations vary in magnitude and frequency and they move forward at a range of speeds. The pressure fluctuations cause water surface undulations to develop and grow. The key to their growth is that a resonant interaction occurs between the forward moving pressure fluctuations and the free waves that propagate at the same speed as the pressure fluctuations.

Although the Phillips model explains the initiation of wave motion, it is insufficient to explain the continued growth of the waves. This growth is best explained by a shear flow model proposed by Miles (1957). As the wind blows over a forward moving wave a complex air flow pattern develops over the wave. This involves a secondary air circulation that is set up around an axis that is parallel to the wave crest, by the wind velocity profile acting over a moving wave

surface profile. Below a point on the velocity profile where the wind velocity equals the wave celerity, air flow is reversed relative to the forward moving wave profile. Above this point air flow is in the direction of the wave motion. This results in a relative flow circulation in a vertical plane above the wave surface that causes a pressure distribution on the surface that is out of phase with the surface displacement. The result is a momentum transfer to the wave that selectively amplifies the steeper waves.

The resonance and shear flow models both function through pressure forces. There is also a shear force on the water surface that contributes to growth and deformation of the wave profile, but this mechanism is apparently less important than the pressure mechanisms. There are also complex nonlinear interactions between waves of one period and waves of a slightly different period. These wave-wave interactions will cause energy transfer from shorter to longer period waves under certain conditions.

It is desirable to select a single wave height and period to represent a spectrum of wind-waves for use in wave prediction, wave climate analysis, design of coastal structures, and so on. If the wave heights from a wave record are ordered by size one can define a height H_n that is the average of the highest n percent of the wave heights. For example, H_{10} is the average height of the highest 10% of the waves in the record and H_{100} is the average wave height. The most commonly used representative wave height is H_{33} , which is the average height of the highest one-third of the waves. This is commonly called the significant height H_s and it is approximately the height an experienced observer will report when visually estimating the height of waves at sea. The highest waves in a wave record are usually the most significant for coastal design and other concerns. But, as we will see later, these highest waves tend to have periods that are around the middle of the range of periods in a wave spectrum. So we most commonly define a significant period T_s as the average period of the highest one-third of the waves in the record.

The significant wave height and period as well as the resulting spectrum of wind-generated waves depend primarily on the distance over which the wind blows (known as the fetch length F), the wind velocity W (commonly measured at the 10 m elevation), and the duration of the wind t_d . To a lesser (but in some situations possibly a significant) extent other factors that affect the resulting waves generated by a wind field are the fetch width, the water depth and bottom characteristics if the depth is sufficiently shallow, atmospheric stability, and the temporal and spatial variations in the wind field during wave generation.

Waves are generated with propagation directions aligned at a range of oblique angles ($< 90^\circ$) to the direction of the wind. The range of directions decreases with an increase in wave period as waves grow while propagating along the fetch. Thus, the smaller the fetch width the lesser the chance shorter waves have of remaining in the generating area and growing to appreciable size. The water depth affects the wave surface profile form and water particle kinematics and

thus the transfer of energy from the wind to the waves. Water depth also limits the non-breaking wave heights. Bottom friction dissipates wave energy and thus retards the rate of wave growth and the ultimate wave size. Atmospheric stability, which depends on the air/sea temperature ratio, affects the wind velocity profile near the sea surface and the resulting wave generation mechanisms. Wind fields grow in size and average velocity, change shape with time, and ultimately decay. These changes profoundly affect the resulting wave field that is generated. For some simple applications, however, we consider a wave field simply defined by a selected constant wind speed and fetch length having a specified duration.

It is instructive to consider the growth of the significant height and period as a function of distance along a fetch for waves generated by a wind of constant velocity, blowing over a constant fetch and having different durations. This is demonstrated schematically in Figure 6.1. If the wind duration exceeds the time required for waves to propagate the entire fetch length (i.e., $t_d > F/C_g$) the waves will grow along OAB and their characteristics at the end of the fetch will depend on the fetch and the wind velocity. This is known as the “fetch limited” condition. If the duration is less (i.e., $t_d < F/C_g$) wave growth reaches only OAC and wave generation is “duration limited.” If both the fetch and duration are sufficiently large the curve OAB becomes essentially horizontal at the downwind end and a fully developed sea has been generated for that wind velocity. Note that as the waves grow, the component periods and thus the component group celerities continually increase along the fetch so an average group celerity would have to be used to determine if waves are fetch or duration limited.

Outside of the region where the wind is blowing the waves propagate as swell. In this region the significant height will decrease and the significant period will increase. Energy dissipation and lateral spreading of the waves will decrease the

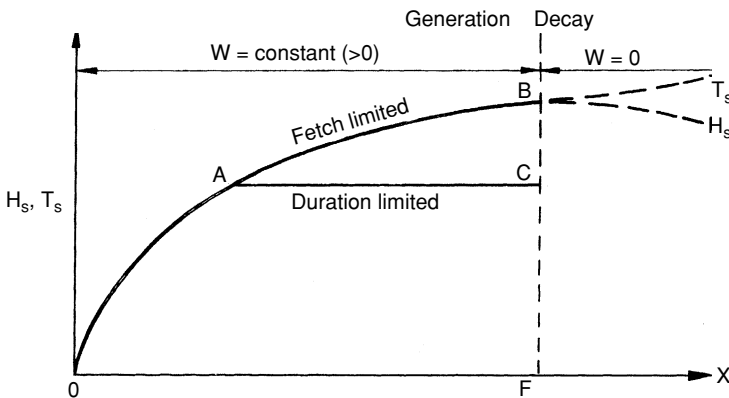


Figure 6.1. Idealized wave growth and decay for a constant wind velocity.

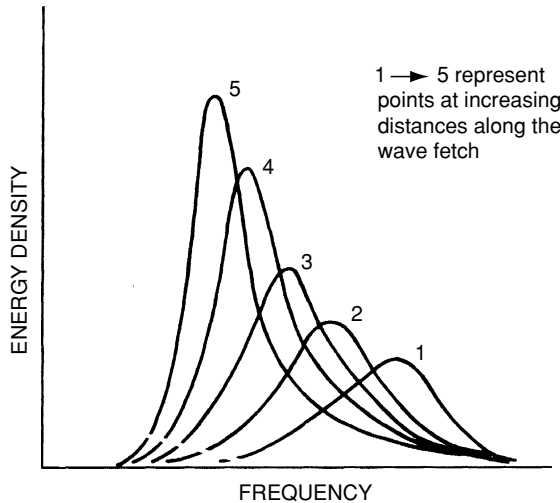


Figure 6.2. Wave spectra growth.

wave height. This effect is greater for the shorter period waves so the significant period will increase.

The characteristics of the waves generated by a given wind condition may also be defined by a wave spectrum. This is a plot of the wave energy density at each component period or frequency versus the range of component periods or frequencies. Figure 6.2 shows a series of typical wave spectra at successive points along a fetch. Note the decrease in the peak frequency (increase in peak period) as the wave spectrum grows along the fetch. The total area under the spectral curve, which is related to the spectral energy and significant wave height, also grows. The higher frequency (lower period) waves on the right side of a spectrum grow to an energy level or wave height that is limited by breaking, so as further growth occurs it must take place at the lower frequencies (higher periods). Also, wave-wave interactions transfer some wave energy from lower to higher wave periods as the spectrum grows. If the wave spectra were measured at a fixed point in the wind field as time elapses, the spectra would exhibit a time-dependent growth that is similar to the growth pattern depicted in Figure 6.2.

6.3 Wave Record Analysis for Height and Period

Our understanding of wind-generated waves at sea comes largely from the analysis of wave records. Most of these wave records are point measurements of the water surface time history for a time period of several minutes. As indicated above, analysis of wave records is commonly carried out in one of

two ways: (1) by identifying individual waves in the record and statistically analyzing the heights and periods of these individual waves and (2) by conducting a Fourier analysis of the wave record to develop the wave spectrum. The former will be discussed in this section and the latter in the next two sections.

Wave Height Distribution

Figure 6.3 shows a short segment of a typical wave record. A question arises as to which undulations of the water surface should be considered as waves and what are the individual heights and periods of these waves. The analysis procedure must be statistically reasonable and consistent. The most commonly used analysis procedure is the zero-upcrossing method (Pierson, 1954). A mean water surface elevation is determined and each point where the water surface crosses this mean elevation in the upward direction is noted (see Figure 6.3). The time elapsed between consecutive points is a wave period and the maximum vertical distance between crest and trough is a wave height. Note that some small surface undulations are not counted as waves so that some higher frequency components in the wave record are filtered out. This is not of major concern, since for engineering purposes our focus is primarily on the larger waves in the spectrum.

A primary concern is the distribution of wave heights in the record. If the wave heights are plotted as a height–frequency distribution the result would typically be like Figure 6.4 where $p(H)$ is the frequency or probability of occurrence of the height H . The shaded area in this figure is the upper third of the wave heights and the related significant wave height is shown.

For engineering purposes it is desirable to have a model for the distribution of wave heights generated by a storm. Longuet-Higgins (1952) demonstrated that this distribution is best defined by a Rayleigh probability distribution. Use of this distribution requires that the wave spectrum has a single narrow band of frequencies and that the individual waves are randomly distributed. Practically, this requires that the waves be from a single storm that preferably is some distance away so that frequency dispersion narrows the band of frequencies recorded. Comparisons of the Rayleigh distribution with measured wave heights by several

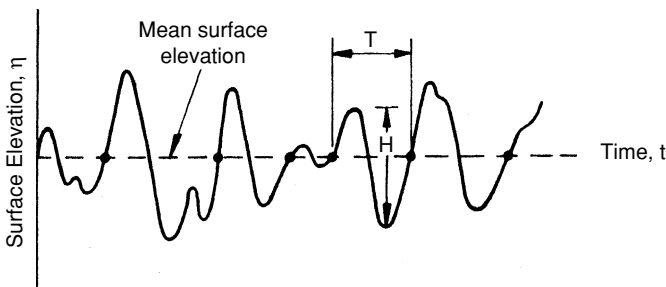


Figure 6.3. Typical water surface elevation versus time record.

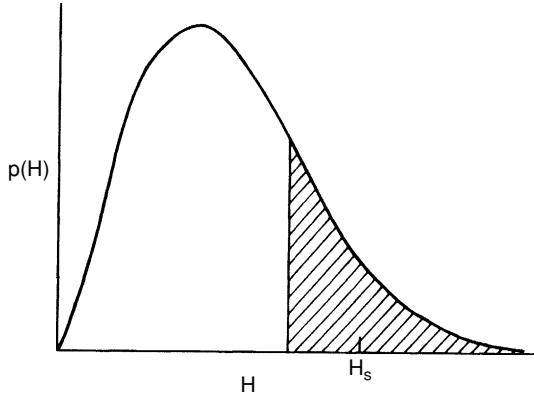


Figure 6.4. Typical wave height–frequency distribution.

authors (e.g., Goodnight and Russell, 1963; Collins, 1967; Chakrabarti and Cooley, 1971; Goda 1974; Earle, 1975) indicate that this distribution yields acceptable results for most storms.

The Rayleigh distribution can be written

$$p(H) = \frac{2H}{(H_{\text{rms}})^2} e^{-(H/H_{\text{rms}})^2} \quad (6.1)$$

where the root mean square height H_{rms} is given by

$$H_{\text{rms}} = \sqrt{\sum \frac{H_i^2}{N}} \quad (6.2)$$

In Eq. (6.2) H_i are the individual wave heights in a record containing N waves.

Employing the Rayleigh distribution leads to the following useful relationships:

$$H_s = 1.416 H_{\text{rms}} \quad (6.3a)$$

$$H_{100} = 0.886 H_{\text{rms}} \quad (6.3b)$$

The cumulative probability distribution $P(H)$ (i.e., the percentage of waves having a height that is equal to or less than H) is

$$P(H) = \int_0^H p(H)dH = 1 - e^{-(H/H_{\text{rms}})^2} \quad (6.4)$$

For our purposes, we are more interested in the percentage of waves that have a height greater than a given height, i.e.,

$$1 - P(H) = e^{-(H/H_{\text{rms}})^2} \quad (6.5)$$

Since $H_s = 1.416H_{\text{rms}}$ [Eq. (6.3a)]

$$1 - P(H_s) = e^{-(1.416)^2} = 0.135$$

so 13.5% of the waves in a storm wave record might have heights that are greater than the significant height.

Figure 6.5, which is adapted from the U.S. Army Coastal Engineering Research Center (1984), is a plot that is useful when applying the Rayleigh distribution. Line *a* in the figure gives the probability *P* that any wave height will exceed the height (H/H_{rms}) and line *b* gives the average height of the *n* highest fraction of the waves.

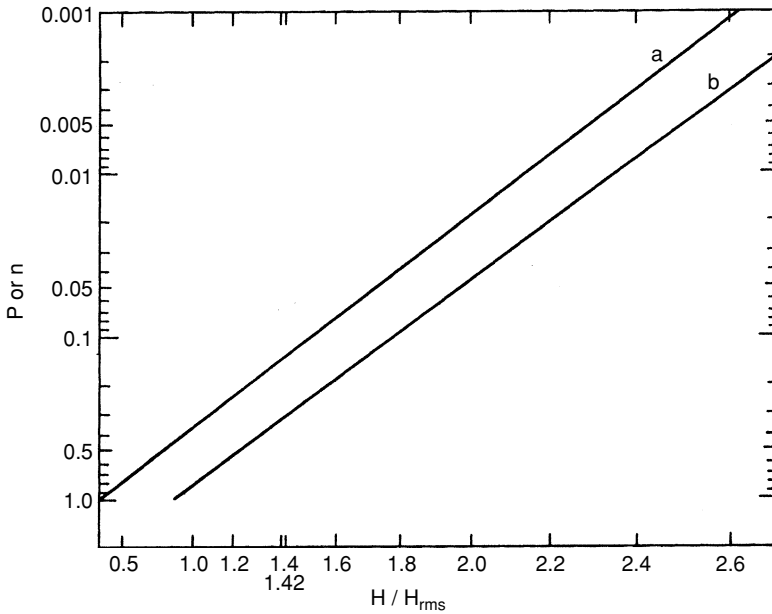


Figure 6.5. Rayleigh distribution for wave heights. (U.S. Army Coastal Engineering Research Center, 1984.)

Example 6.3-1

A wave record taken during a storm is analyzed by the zero-upcrossing method and contains 205 waves. The average wave height in the record is 1.72 m. Estimate H_s , H_5 , and the number of waves in the record that would exceed 2.5 m height.

Solution:

From Eqs. (6.3a) and (6.3b) we have

$$H_{\text{rms}} = \frac{1.72}{0.886} = 1.94 \text{ m}$$

and

$$H_s = 1.416(1.94) = 2.75 \text{ m}$$

From line *b* in Figure 6.5 $H_5/H_{\text{rms}} = 1.98$ so

$$H_5 = 1.98(1.94) = 3.84 \text{ m}$$

From line *a* in Figure 6.5 at

$$\frac{H}{H_{\text{rms}}} = \frac{2.5}{1.94} = 1.29$$

we have $P = 0.19$. So the estimated number of waves exceeding 2.5 m in height is $205(0.19) = 38.95$, or approximately 39 waves.

When a spectrum of waves reaches the shore, wave breaking causes the wave height distribution to be truncated at the higher end. Some authors have modified the Rayleigh distribution to account for nearshore depth-induced wave breaking (see Collins, 1970; Ibrageemov, 1973; Kuo and Kuo, 1974; Goda, 1975; Hughes and Borgman, 1987).

Maximum Wave Height

There is no upper limit to the wave heights defined by the Rayleigh distribution. In a storm, however, the highest wave that might be expected will depend on the length of the storm as well as its strength. Longuet-Higgins (1952) demonstrated that for a storm with a relatively large number of waves N , the expected value of the height of the highest wave H_{max} would be

$$H_{\text{max}} = 0.707 H_s \sqrt{\ln N} \quad (6.6)$$

For example, a storm having a 6 hour duration of high waves having an average period of 8 s would about 2700 waves and H_{max} would be $1.99H_s$. In the nearshore zone, the highest wave might be limited by wave breaking, provided the storm can generate sufficiently high waves for this limit to apply in the water depth of concern. However, in deeper water beyond the depth where waves would break, the value given by Eq. (6.6) should be appropriate.

Wave Period Distribution

It was mentioned previously that the highest waves and the largest energy concentration in a wind wave spectrum are typically found at periods around the middle of the period range of the spectrum. Consequently, for engineering purposes, we are not usually as concerned with the extreme wave periods as we were with the higher wave heights.

The joint wave height–period probability distribution is of some interest. The general shape of this distribution is depicted in Figure 6.6 (see Ochi, 1982). This figure shows the distribution of the wave height versus wave period for each wave in a typical record, nondimensionalized by dividing each height and period value by the average height and average period, respectively. The contour lines are lines of equal probability of occurrence of a height–period combination.

Note, in Figure 6.6, that there is a small range of wave periods for the higher waves and these periods are around the average period of the spectrum of waves. For the lower waves (but not the lowest), there is a much wider distribution of wave periods. The significant period T_s is considered to be more statistically stable than the average period so it is preferred to use the significant period to represent a wave record. If one is using a spectral approach to analyzing a wave record (see the next section) the period of the peak of the spectrum known as the spectral peak period T_p would be used as a representative period. From investigations of numerous wave records the U.S. Army Coastal Engineering Research Center (1984) recommends the relationship $T_s = 0.95 T_p$.

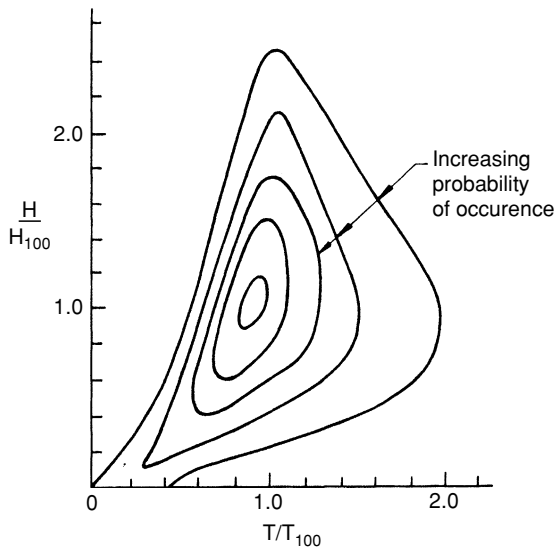


Figure 6.6. Typical dimensionless joint wave height–period distribution.

6.4 Wave Spectral Characteristics

An alternate approach to analyzing a wave record such as that shown in Figure 6.3 is by determining the resulting wave spectrum for that record. A water surface elevation time history can be reconstructed by adding a large number of component sine waves that have different periods, amplitudes, phase positions, and propagation directions. A directional wave spectrum is produced when the sum of the energy density in these component waves at each wave frequency $S(f, \theta)$ is plotted versus wave frequency f and direction θ . Commonly, one-dimensional wave spectra are developed when the energy for all directions at a particular frequency $S(f)$ is plotted as a function of only wave frequency. An alternate form to the above described frequency spectrum is the period spectrum where the wave energy density $S(T)$ is plotted versus the wave period.

From the small-amplitude wave theory, the energy density in a wave is $\rho g H^2 / 8$. Leaving out the product of the fluid density and the acceleration of gravity, as is commonly done, leads to the following expression for a directional wave spectrum:

$$S(f, \theta) df d\theta = \sum_f^{f+df} \sum_\theta^{\theta+d\theta} \frac{H^2}{8} \quad (6.7)$$

where H is the height of the component waves making up the spectrum. This simplifies to

$$S(f) df = \sum_f^{f+df} \frac{H^2}{8} \quad (6.8)$$

for a one-dimensional frequency spectrum. For a one-dimensional period spectrum we have

$$S(T) dT = \sum_T^{T+dT} \frac{H^2}{8} \quad (6.9)$$

It can be shown (see Sorensen, 1993) that the following relationship holds:

$$S(f) = S(T) T^2 \quad (6.10)$$

Equation (6.8) indicates that the dimensions for $S(f)$ would be length squared times time (e.g., m^2s) and from Eq. (6.9) the dimensions of $S(T)$ would be length squared divided by time (e.g., m^2/S). This is consistent with Eq. (6.10).

The exact scale and shape of a wind wave spectrum will depend on the generating factors of wind speed, duration, fetch, etc. as discussed above. However, a general form of a spectral model equation is

$$S(f) = \frac{A}{f^5} e^{-B/f^4} \quad (6.11)$$

where A and B adjust the shape and scale of the spectrum and can be written either as a function of the generating factors or as a function of a representative wave height and period (e.g., H_s and T_s).

Analysis of a wave record to produce the wave spectrum is a complex matter that is beyond the scope of this text. Software packages are available for this task that take a digitized record of the water surface and produce the spectral analysis. Wilson et al. (1974) discuss spectral analysis procedures and give a list of basic references on the subject.

An important way to characterize a wave spectrum is by the moments of a spectrum. The n th moment of a spectrum is defined as

$$m_n = \int_0^\infty S(f) f^n df \quad (6.12)$$

So, for example, the zeroth moment would just be the area under the spectral curve. Since a spectrum plot shows the energy density at each frequency versus the range of frequencies, the area under the spectral curve is equal to the total energy density of the wave spectrum (divided by the product of the fluid density and acceleration of gravity).

As with the analysis procedures discussed in Section 6.3, it would be useful to have a representative wave height and period for the wave spectrum that can be derived from the spectrum. The spectral peak period T_p is a representative period (or one can use its reciprocal, the spectral peak frequency). The spectral moment concept is useful to define a representative wave height.

From the small-amplitude wave theory, the total energy density is twice the potential energy density of a wave. Thus,

$$\bar{E} = 2\bar{E}_p = \frac{2}{T_*} \int_0^{T_*} \rho g \eta \left(\frac{\eta}{2} \right) dt$$

where T_* is the length of wave record being analyzed and the overbar denotes energy density. This can be written

$$\bar{E} = \rho g \bar{\eta}^2 = \frac{\rho g \sum \eta^2}{N_*} \quad (6.13)$$

where the overbar denotes the average of the sum of N_* digitized water surface elevation values from a wave record of length T_* . From our definition of H_{rms} and H_s the energy density can also be written

$$\bar{E} = \frac{\rho g H_{\text{rms}}^2}{8} = \frac{\rho g H_s^2}{16} \quad (6.14)$$

If the zeroth moment of the spectrum equals the energy density divided by ρg , with Eqs. (6.13) and (6.14) we have

$$\bar{E} = \rho g m_o = \rho g \frac{\sum \eta^2}{N_*} \quad (6.15)$$

and

$$\bar{E} = \rho g m_o = \frac{\rho g H_s^2}{16} \quad (6.16)$$

Equation (6.15) provides a useful way to determine the energy density and the zeroth moment of a wave spectrum from digitized water surface elevation values. Equation (6.16) leads to a significant height definition from the wave spectrum energy density or zeroth moment:

$$H_s = 4\sqrt{m_o} \quad (6.17)$$

where the designation H_{mo} will be used for this definition of significant height. Recall that H_s is based on a wave-by-wave analysis from the wave record, but H_{mo} is determined from the energy spectrum or, more basically, from digitized values of the water surface elevation given by the wave record.

Analysis of the same wave records by the wave-by-wave method and by spectral analysis indicates that H_s and H_{mo} are effectively equal for waves in deep water that are not too steep. For steeper waves and waves in intermediate and shallow water H_s will be increasingly larger than H_{mo} so the two terms cannot be interchangeably used. Figure 6.7, which was slightly modified from Thompson and Vincent (1985) and is based on field and laboratory wave records, shows how H_s and H_{mo} compare for different relative water depths. As wave records become more commonly analyzed by computer the second definition of significant height (H_{mo}) is more commonly being used.

6.5 Wave Spectral Models

As the Rayleigh distribution is a useful model for the expected distribution of wave heights from a particular storm, it is also useful to have a model of the expected wave spectrum generated by a storm. Several one-dimensional wave spectra

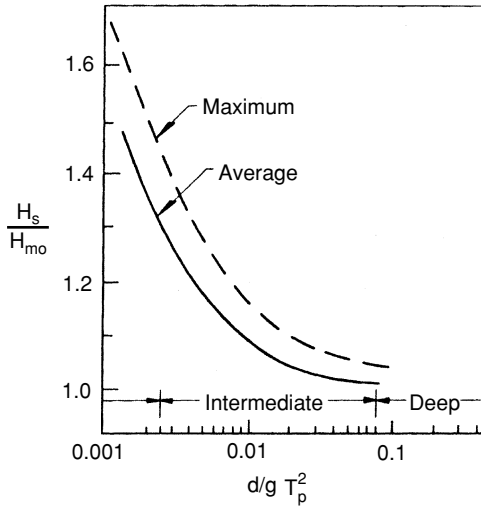


Figure 6.7. Comparison of H_s and H_{mo} versus relative depth. (Thompson and Vincent, 1985.)

models have been proposed. They generally have the form of Eq. (6.11) and are derived from empirical fits to selected sets of wave measurements, supported by dimensional and theoretical reasoning. Four of these spectral models—called the Bretschneider, Pierson–Moskowitz, JONSWAP, and TMA spectra—will be presented. These models are of interest from an historic perspective and because of their common use in coastal engineering practice. The first three models were developed for deep water waves and the last is adjusted for the effects of water depth.

Bretschneider Spectrum (Bretschneider, 1959)

The basic form of this spectrum is

$$S(T) = \frac{\alpha g^2}{(2\pi)^4} T^3 e^{-0.675(gT/2\pi W F_2)^4} \quad (6.18)$$

where W is the wind speed at the 10 m elevation and

$$\alpha = 3.44 \frac{F_1^2}{F_2^2}$$

$$F_1 = \frac{g H_{100}}{W^2} \quad F_2 = \frac{g T_{100}}{2\pi W}$$

H_{100} and T_{100} denote the average wave height and period. The parameters F_1 and F_2 are a dimensionless wave height and dimensionless wave period, respectively.

As will be shown in the next section, Bretschneider empirically related F_1 and F_2 to the wind speed, the fetch, and the wind duration to develop a forecasting relationship for the average wave height and period and, using Eq. (6.18), the wave period spectrum.

Inserting α , F_1 , and F_2 into Eq. (6.18) leads to

$$S(T) = \frac{3.44T^3(H_{100})^2}{(T_{100})^4} e^{-0.675(T/T_{100})^4} \quad (6.19)$$

Employing Eq. (6.10), Eq. (6.19) can be converted to a frequency spectrum that would have the general form of Eq. (6.11). Ochi (1982) recommends the relationship $T_{100} = 0.77T_p$ from empirical data and the average wave height can be related to the significant height through the Rayleigh distribution. Thus, given one of the common representative wave heights and periods the Bretschneider spectrum can be plotted using Eq. (6.19).

Pierson–Moskowitz Spectrum (Pierson and Moskowitz, 1964)

The authors analyzed wave and wind records from British weather ships operating in the north Atlantic. They selected records representing essentially fully developed seas for wind speeds between 20 and 40 knots to produce the following spectrum:

$$S(f) = \frac{\alpha g^2}{(2\pi)^4 f^5} e^{-0.74(g/2\pi Wf)^4} \quad (6.20)$$

In Eq. (6.20) the wind speed W is measured at an elevation of 19.5 m which yields a speed that is typically 5% to 10% higher than the speed measured at the standard elevation of 10 m. The coefficient α has a value of 8.1×10^{-3} . Note that the fetch and wind duration are not included since this spectrum assumes a fully developed sea. At much higher wind speeds than the 20 to 40 knot range it is less likely for a fully developed sea to occur.

The following relationships can be developed from the Pierson–Moskowitz spectrum formulation (see Ochi, 1982):

$$H_{mo} = \frac{0.21 W^2}{g} \quad (6.21)$$

$$f_p = \frac{0.87g}{2\pi W} \quad (6.22)$$

The simple form of the Pierson–Moskowitz spectrum results in it being used in some situations where the sea is not fully developed.

JONSWAP (Hasselmann et al., 1973)

This spectrum results from a Joint North Sea Wave Project operated by laboratories from four countries. Wave and wind measurements were taken with sufficient wind durations to produce a deep water fetch limited model spectrum. If we eliminate the wind speed from Eq. (6.20) by incorporating Eq. (6.22) the Pierson–Moskowitz spectrum can be written

$$S(f) = \frac{\alpha g^2}{(2\pi)^4 f^5} e^{-1.25(f_p/f)^4} \quad (6.23)$$

The JONSWAP spectral form is a modification of Eq. (6.23) by developing relationships for α and f_p in terms of the wind speed and fetch, and enhancing the peak of the spectrum by a factor γ . The resulting spectrum is

$$S(f) = \frac{\alpha g^2}{(2\pi)^4 f^5} e^{-1.25(f_p/f)^4} \gamma^a \quad (6.24)$$

where

$$a = e^{-[(f-f_p)^2/2\sigma^2 f_p^2]}$$

$$\sigma = 0.07 \text{ when } f < f_p$$

$$\sigma = 0.09 \text{ when } f \geq f_p$$

In the JONSWAP spectrum, γ typically has values ranging from 1.6 to 6 but the value of 3.3 is recommended for general usage. The coefficient γ is simply the ratio of $S(f)$ at the peak frequency for the JONSWAP and Pierson–Moskowitz spectra. This is depicted in Figure 6.8, which demonstrates the effect of γ on the spectrum shape.

The coefficient α and the peak frequency f_p for the JONSWAP spectrum are given by

$$\alpha = 0.076 \left(\frac{gF}{W^2} \right)^{-0.22} \quad (6.25)$$

$$f_p = \frac{3.5g}{W} \left(\frac{gF}{W^2} \right)^{-0.33} \quad (6.26)$$

The data used to develop the JONSWAP spectrum were collected for relatively light wind conditions, but data collected at higher wind velocities (see Rye, 1977) compared reasonably well with this spectral formulation. Mitsuyasu et al. (1980), using ocean wave records taken near Japan recommended that a value of γ given by

$$\gamma = 7 \left(\frac{gF}{W^2} \right)^{-0.143} \quad (6.27)$$

might be used. During recent years the JONSWAP spectrum has become the most used spectrum for engineering design and for laboratory irregular wave experiments.

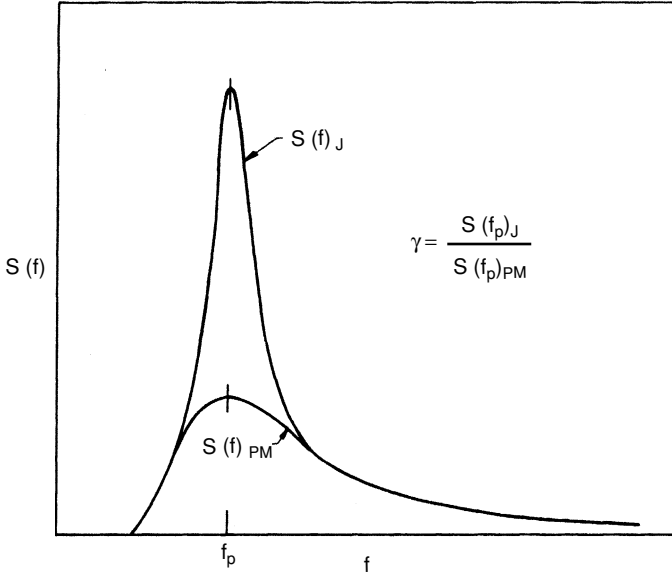


Figure 6.8. JONSWAP and PM spectra comparison.

TMA Spectrum (Bouws et al., 1985)

The previous three models were developed for deep water conditions. As wind waves propagate into intermediate and shallow depths there is a period-dependent change in the shape of the spectrum versus that for deep water. The TMA spectrum is a wave spectrum based on the generation of waves in deep water that then propagate without refracting into intermediate/shallow water depths. The spectral form is a JONSWAP spectrum modified by a depth and frequency dependent factor $\Phi(f, d)$. Thus, $S(f)_{\text{TMA}} = S(f)_J \Phi(f, d)$ where $\Phi(f, d)$ is a relatively complex function defined graphically in Figure 6.9.

Hughes (1984) further proposed that α and γ in the JONSWAP spectral formulation be modified to

$$\alpha = 0.0078 \left(\frac{2\pi W^2}{gL_p} \right)^{0.49} \quad (6.28)$$

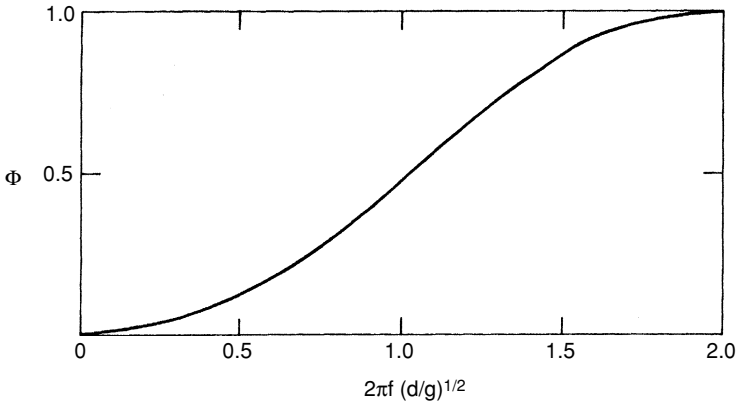


Figure 6.9. Correction factor for TMA spectrum.

for the TMA spectrum. In Eqs. (6.28) and (6.29) L_p is the wave length

$$\gamma = 2.47 \left(\frac{2\pi W^2}{gL_p} \right)^{0.39} \quad (6.29)$$

for the spectral peak frequency and the water depth for which the TMA spectrum is being determined.

Directional Wave Spectra

The components that make up a wave spectrum at a particular location will typically be propagating in a range of directions. A point measurement of the water surface elevation time history will not detect this directional variability, so an analysis of this time history yields a one-dimensional spectrum. But, during recent years, wave gages that can detect the full directionality of the wave field at a given location have come into more common use. Consequently, directional spectral data are becoming available and significant development of directional spectral models has taken place.

The directional spread of wave energy in a wind wave field is frequency dependent. Generally, the short period components of the wave spectrum have a wider range of directions, while the wave energy is more focused on the dominant direction for the frequencies near the spectral peak. Models for directional wave spectra commonly are one-dimensional spectra corrected by a factor that depends on the wave frequency and direction, i.e.,

$$S(f, \theta) = S(f)G(f, \theta) \quad (6.30)$$

where $G(f, \theta)$ is a dimensionless directional spreading function. Since modifying a one-dimensional spectrum to a directional spectrum does not change the total energy density, we have

$$\int_{-\pi}^{\pi} G(f, \theta) d\theta = 1 \quad (6.31)$$

and

$$m_o = \int_0^{\infty} \int_{-\pi}^{\pi} S(f, \theta) d\theta df \quad (6.32)$$

The angle θ is usually measured clockwise starting at zero in the dominant wave direction and has a practical range of $-\pi/2$ to $+\pi/2$.

One of the originally proposed (St. Dennis and Pierson, 1953) directional spreading functions was a simple cosine squared function that is independent of frequency, i.e.,

$$G(f, \theta) = G(\theta) = \frac{2}{\pi} \cos^2 \theta \quad (6.33)$$

where θ varies from $-\pi/2$ to $+\pi/2$. The simplicity of this function makes it appealing for some engineering applications.

A much more complex directional spreading function (Mitsuyasu et al., 1975), which is based on extensive measurements of directional wave spectra, is

$$G(f, \theta) = G(s) \cos^{2s} \left(\frac{\theta}{2} \right) \quad (6.34a)$$

where $G(s)$ is

$$G(s) = \frac{2^{2s-1}}{\pi} \frac{\Gamma^2(s+1)}{\Gamma(2s+1)} \quad (6.34b)$$

In the above equations Γ is the gamma function of the term in parentheses, which is tabulated in some mathematical handbooks. The parameter s was originally given as a function of wave frequency, wave peak frequency, and wind speed. Higher values of s give a more widely spread directional spectrum. Goda and Suzuki (1975) and Goda (1985) give a simpler definition of s that is useful for engineering applications, i.e.,

$$\begin{aligned} s &= S_{\max} (f/f_p)^5 \text{ when } f < f_p \\ &= S_{\max} (f/f_p)^{-2.5} \text{ when } f > f_p \end{aligned} \quad (6.35)$$

For design purposes, Goda (1985) recommends

$$\begin{aligned} S_{\max} &= 10 \text{ Wind waves} \\ S_{\max} &= 25 \text{ Swell with short decay distance} \\ S_{\max} &= 75 \text{ Swell with long decay distance} \end{aligned}$$

As a wind wave spectrum approaches the shore, wave shoaling and refraction tend to reduce the spread of wave directions which would cause some increase in S_{\max} . Mitsuyasu et al. (1975) employed Eq. (6.34) with a JONSWAP one-dimensional spectrum.

Refraction and Diffraction of Directional Spectra

It is common in much of coastal engineering design to select a representative wave height, period and direction (e.g. H_{mo} and T_p having the offshore direction that is dominant in the wave spectrum). This wave is then treated as a monochromatic wave which is shoaled, refracted and diffracted (if necessary) to the point of interest in the nearshore area, employing the methods presented in Chapters 2, 3 and 4. However, shoaling effects depend on the wave period, and refraction and diffraction effects depend on both the wave period and direction. Thus, a more complete analysis of the changes that take place as a directional wave spectrum propagates from offshore to the coast will be dependent on the frequency and direction distribution in the offshore wave spectrum. Each frequency and direction component in the spectrum will shoal, refract and diffract differently. The result will depend on the combination of these components at the point of interest in the coastal zone.

For a directional wave spectrum the combined shoaling/refraction coefficient $(K_r)_s$ is given by

$$(K_r)_s = \left[\frac{1}{(m_0)_s} \sum_0^{\infty} \sum_{-\pi}^{\pi} S(f, \theta) K_s^2 K_r^2 \Delta f \Delta \theta \right]^{1/2}$$

where

$$(m_0)_s = \sum_0^{\infty} \sum_{-\pi}^{\pi} S(f, \theta) K_s^2 \Delta f \Delta \theta$$

In order to apply this equation, the directional spectrum would be broken into directional and frequency segments ($\Delta \theta$ and Δf). Then, a representative value of f and θ from each frequency/direction segment would be used to shoal and refract a monochromatic wave to the coast, yielding the K_s and K_r values for that segment. The results would then be recombined using the above equation to yield a value of $(K_r)_s$ for the directional spectrum. Then,

$$(H_{mo})_c = (K_r)_s (H_{mo})_o$$

Where the subscripts c and o refer to the significant wave height at the coastal point of interest and offshore

This approach is obviously very onerous to apply in practice, especially if a significant number of direction/frequency components are to be used. And, it would have to be repeated *in toto* for a different nearshore hydrography or a different offshore directional wave spectrum.

Goda (1985) employed this procedure to develop results that give some indication of the difference in results for a classic monochromatic wave shoaling/refraction analysis versus a directional spectrum shoaling/refraction analysis. He considered a coastal area with straight shore-parallel bottom contours. This greatly simplified the shoaling/refraction analysis because the refraction coefficient for each frequency/direction component could more easily be calculated from Equations 4.2 and 4.3. Goda employed a modified Bretschneider spectrum with a directional spreading function given by Equation 6.34 and $S_{max} = 10, 25$ and 75 . Dominant offshore directions for the directional spectrum included 0° , 20° , and 40° . The nearshore coastal point selected for analysis was the point where $d/L_o = 0.05$, where L_o is calculated using the peak period for the spectrum.

Goda's results for $(K_r)_s$ as a function of the offshore direction and S_{max} , and the comparative result for $K_r K_s$ for a monochromatic wave are:

S_{max}	0°	20°	40°
10	0.94	0.93	0.87
25	0.97	0.955	0.88
75	0.99	0.97	0.90
Monochromatic	1.00	0.98	0.91

For the results shown in the above table (but not necessarily so for all conditions), the monochromatic refraction/shoaling coefficient is higher than the coefficient for the directional spectrum. The difference is generally less than 5 percent. Considering how well other factors such as the efficacy of the shoaling/refraction analysis and how well the design wave conditions are known, this difference is not exceptional. As expected, the difference between the monochromatic and spectral results diminishes as S_{max} increases (i.e. as the waves more closely resemble a monochromatic wave).

An effective diffraction coefficient for a directional spectrum $(K_d)_s$ is given by

$$(K_d)_s = \left[\frac{1}{(m_0)_s} \sum_0^\infty \sum_{-\pi}^\pi S(f, \theta) K_d^2 \Delta f \Delta \theta \right]^{1/2}$$

where

$$(m_0)_s = \sum_0^{\infty} \sum_{-\pi}^{\pi} S(f, \theta) \Delta f \Delta \theta$$

and K_d is the diffraction coefficient for each frequency/direction component.

Goda (1985) also compared diffraction analyses for a semi-infinite breakwater and a breakwater gap using monochromatic waves versus a directional spectrum using spectral and directional spreading conditions employed in the shoaling/refraction analysis comparison. The above equations were used for the directional spectrum analysis.

At a particular point in the lee of the breakwater there was a shift in the spectral peak frequency away from the incident spectral peak frequency. For monochromatic waves there is no change in the wave frequency as waves diffract to the lee of a breakwater. A shift in the spectral peak frequency should be expected because at a particular point in the lee of the breakwater the value of r/L and thus K_d would be different for the different frequencies in the spectrum. So the recombined components then yield a different peak frequency.

Also, at a particular point in the lee of the breakwater, the monochromatic and spectral diffraction coefficients were different. In many cases these differences were quite significant, with the monochromatic analysis often yielding a much lower wave height than the spectral analysis at a particular point. As might be expected, comparison of calculated results with some available field data on diffracted wave conditions behind a breakwater at a coastal port indicated that the spectral approach gave better results.

6.6 Wave Prediction—Early Methods

Early methods for wave prediction were simple empirical formulations relating the wave height and period to some representative wind speed, fetch, and later duration.

Selection of Wind Conditions

Prediction of wind generated waves by the simple empirical methods or by the use of spectral models requires selection of representative values of wind speed, fetch, and duration. Winds from more than one approach direction may generate waves that must be considered for design analysis at a given coastal site. The fetch may be limited by land boundaries and it may be sufficiently short so that one can assume fetch-limited conditions to make the wave predictions.

The best wind data source would be local speed/direction measurements over a sufficient length of time to do a return period analysis and select a design wind

condition. Typical data sources include airports, Coast Guard stations, and weather ships at sea. If the data are collected inland a correction may be required to adjust for the typically higher wind speeds that occur over water. Often, projects conducted by the Army Corps of Engineers or other government and private organizations have already collected and analyzed available wind data for the area of concern.

Return period analyses of available wind data in the United States have been published by Thom (1960) and the American National Standards Institute (1972). The primary focus of these data analyses is to provide design speeds for wind load determination. Thom, for example, presents 2-, 50-, and 100-year return period isotachs for the continental United States, which allow the selection of a given return period wind speed for a site, but not the wind direction. The stronger winds may predominantly come from a particular direction that is not important for wave generation at a given site. If a wind rose, giving the percentage of higher wind speeds from each compass direction, is available for the area of interest, Thom's return period values can be adjusted for direction (see U.S. Army Coastal Engineering Research Center, 1984).

Wind speed estimates can be made from weather charts showing upper elevation pressure contours, but this requires an extensive effort to develop sufficient data to select a design wind condition. So, even if a sufficient number of historic weather charts are available, this effort is usually not justified for development of design waves for a single project.

Wind speed measurements may be made at some elevation other than the standard 10 m elevation. Also, the recorded wind speed values are averages for a time interval that is typically less than the wind duration required for the waves to travel the length of the generating fetch (F/C_g). Wind speeds are quite irregular over time and average values generally decrease as the time over which the average value is determined increases. Recommended procedures for correcting for elevation and duration of wind measurement are given in U.S. Army Coastal Engineering Research Center (1984) and Sorensen (1993).

When wave predictions are being made for lakes or bays with narrow or irregular shapes, delineation of an effective fetch length can be difficult. Procedures for determining a fetch to be used in wave prediction are also discussed in the two references given in the previous paragraph.

Wave Prediction

Over a century ago simple wave prediction formulas, based on rough observations of wind wave height versus wind speed and fetch, were in use. With the coming of the Second World War and the need for wave forecasts for amphibious landings, Sverdrup and Munk (1947) developed a more rigorous wave prediction procedure. This procedure involved relatively simple wave energy growth concepts with empirical calibration using the small amount of available

data. This procedure was improved by Bretschneider (1952, 1958) over subsequent years by improved calibration using accumulated field data sets. The method is now known as the SMB method after the three authors.

Consider a dimensional analysis of the basic deep water wave prediction relationship

$$H_s, T_s = f(W, F, t_d, g)$$

which leads to

$$\frac{gH_s}{W^2}, \frac{gT_s}{2\pi W} = f\left(\frac{gF}{W^2}, \frac{gt_d}{W}\right) \quad (6.36)$$

Equation (6.36) simply relates the dimensionless significant wave height and period to the dimensionless fetch and duration. Either the fetch or the duration term on the right would control, depending on whether wave generation were fetch or duration limited. Note that the terms on the left are similar to the terms presented in Eq. (6.18). Also, since $C = gT/2\pi$ for deep water waves, the second term on the lefthand side can be written C/W , a parameter known as the wave age and important to the understanding of wind wave growth.

Equation (6.36) has been presented in the form of empirical equations and dimensional plots (see U.S Army coastal Engineering Research Center, 1977). Figure 6.10 presents the relationship as a dimensionless plot as given by

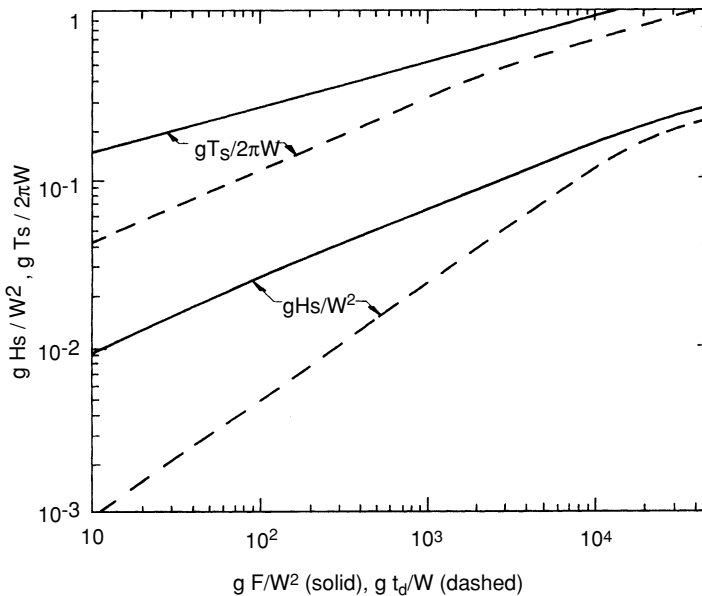


Figure 6.10. SMB wave prediction curves.

Eq. (6.36). The figure is based on a large amount of field data that are not shown. These data show a lot of scatter as would be expected for this simple approach where the wind speed, fetch, and duration are represented by average values. This should be remembered when Figure 6.10 is used.

Given a value for the dimensionless fetch, the solid lines in Figure 6.10 can be used to predict the dimensionless significant height and period. This can also be done using the dimensionless duration and the dashed lines. The smaller sets of values would indicate whether wave generation is fetch or duration limited and would yield the predicted significant height and period. Note that the curves in Figure 6.10 are asymptotic to each other and horizontal lines on the righthand edge; this limit is the fully developed sea condition.

Example 6.6-1

A deep lake has a wind with an average velocity of 30 m/s blowing over it for a period of 2 hours. The fetch in the direction of the wind is 20 km. Using the SMB method, what significant wave height and period will be generated at the downwind end of the lake after two hours?

Solution:

For the given fetch and wind speed

$$\frac{gF}{W^2} = \frac{9.81(20,000)}{(30)^2} = 218$$

Figure 6.10 then yields

$$\frac{gH_s}{W^2} = 0.034 \quad \frac{gT_s}{2\pi W} = 0.33$$

or

$$H_s = \frac{0.034(30)^2}{9.81} = 3.1 \text{ m}$$

$$T_s = \frac{0.33(2)\pi(30)}{9.81} = 6.4 \text{ s}$$

For the given duration and wind speed

$$\frac{gt_d}{W} = \frac{9.81(2)(3600)}{30} = 2354$$

Figure 6.10 then yields

$$\frac{gH_s}{W^2} = 0.043 \quad \frac{gT_s}{2\pi W} = 0.40$$

or

$$H_s = \frac{0.043(30)^2}{9.81} = 3.9 \text{ m}$$

$$T_s = \frac{0.40(2)\pi(30)}{9.81} = 7.7 \text{ s}$$

The smaller values, $H_s = 3.1 \text{ m}$ and $T_s = 6.4 \text{ s}$ control and wave generation is fetch limited.

Note, that for

$$\frac{gH_s}{W^2} = 0.034 \quad \frac{gT_s}{2\pi W} = 0.33$$

Figure 6.10 yields

$$\frac{gt_d}{W} = 1750$$

or

$$t_d = \frac{1750(30)}{9.81} = 5350 \text{ s (1.5 hours)}$$

Thus, after the wind has blown for about 1.5 hours the waves at the downwind end of the lake reach their limiting height and period. During the remaining half hour of wind, wave conditions would remain about the same.

The above discussion applies to deep water wave generation. Occasionally, wave predictions must be made for shallow water bodies where growth of the waves rapidly becomes depth limited. Empirical plots and dimensionless equations using the additional term gd/W^2 (where d is the average water depth) are presented in U.S. Army Coastal Engineering Research Center (1984) and Sørensen (1993), for shallow water wave prediction. Note that these shallow water wave predictions relationships are based on a very limited data set and should be used with some caution.

The circular wind field in a hurricane presents a complex condition for determining the representative wind speed, fetch, and duration. A rough estimate of the peak significant height and period generated by a hurricane can be made from empirical equations presented by Bretschneider (1957).

$$H_s = 16.5e^{0.01R\Delta P} \left[1 + \frac{208\alpha V_F}{\sqrt{W_R}} \right] \quad (6.37)$$

$$T_s = 8.6e^{0.005R\Delta P} \left[1 + \frac{104\alpha V_F}{\sqrt{W_R}} \right] \quad (6.38)$$

In Eqs. (6.37) and (6.38), R is the radius (nautical miles) from the hurricane eye to the point of maximum wind speed W_R (knots), ΔP is the pressure difference from the eye to the periphery of the hurricane (inches of mercury), V_F is the forward speed of the hurricane (knots), and α is a correction factor based on the forward speed which may be taken as unity for slow moving hurricanes. The calculated significant height is in feet. The U.S. Army Coastal Engineering Research Center (1984) has a diagram that predicts the variation of the significant height throughout a hurricane in terms of the peak significant height which occurs in the vicinity of the point of maximum wind speed.

A more sophisticated parametric model for hurricane wave prediction has been developed by Young (1988). Predictions are based on an equivalent fetch and wind speed for a given hurricane that are then used with the JONSWAP model to make significant wave height and period predictions for the hurricane. The Bretschneider model was based on 13 hurricanes off the east coast of the United States; the Young model was based on 43 Australian hurricanes.

6.7 Wave Prediction—Spectral Models

As previously noted, the Bretschneider spectrum is related to the SMB wave prediction method. Given the significant wave height and period determined from SMB, the average wave height and period can be estimated from the relationships discussed earlier, i.e.,

$$\begin{aligned} T_{100} &= 0.77T_p = \frac{0.77}{0.95}T_s = 0.81T_s \\ H_{100} &= 0.886H_{\text{rms}} = \frac{0.886}{1.146}H_s = 0.63H_s \end{aligned}$$

and the Bretschneider spectrum can be computed from Eq. (6.19).

The Pierson–Moskowitz spectrum is written directly in terms of the wind speed. So H_{mo} , f_p , and the spectrum can be directly calculated from Eqs. (6.20) to (6.22). Remember, the wind speed must be corrected to the slightly higher value at an elevation of 19.5 m and the Pierson–Moskowitz spectrum applies only to a fully developed sea condition. [For the 30 m/s wind speed in Example 6.6-1 increased by 10% to give the estimated 19.5 m elevation wind speed, Eq. (6.23) yields $H_{mo} = 23.3$ m and Eq. (6.24) yields $T_p = 24.3$ s. Thus, the condition in Example 6.6-1 is much less than the fully developed sea condition.]

The JONSWAP spectrum is based on fetch-limited conditions. Given the wind speed and fetch length, the wave spectrum peak frequency generated by this wind condition can be calculated from Eq. (6.26) and the spectrum can be calculated from Eq. (6.24). Given the wave spectrum, the significant wave height can be determined using Eq. (6.17) where m_0 is the area under the spectral curve.

In the last edition of the Shore Protection Manual (U.S. Army Coastal Engineering Research Center, 1984), a manual used by the Corps of Engineers for coastal engineering design, a parametric method based on the JONSWAP spectrum is recommended for deep water wave prediction. This replaced the SMB method which was recommended in the previous editions of the manual. The procedure is developed so that it is applicable to both fetch and duration limited conditions.

To apply this wave prediction procedure, first determine the adjusted wind speed W_A given by

$$W_A = 0.71 W^{1.23} \quad (6.39)$$

where W_A and W are both in meters per second. Then the significant height and peak period can be calculated from

$$\frac{gH_{m0}}{W_A^2} = 0.0016 \left(\frac{gF}{W_A^2} \right)^{0.5} \quad (6.40)$$

$$\frac{gT_p}{W_A} = 0.286 \left(\frac{gF}{W_A^2} \right)^{0.33} \quad (6.41)$$

The values determined from Eqs. (6.40) and (6.41) use only the wind speed and fetch and are thus only for the fetch-limited condition. A limiting wind duration would be calculated from

$$\frac{gt_d}{W_A} = 68.8 \left(\frac{gF}{W_A^2} \right)^{0.66} \quad (6.42)$$

If the actual duration is greater than the duration calculated from Eq. (6.42) the wind generation process is fetch limited and the results from Eqs. (6.40) and (6.41) are the predicted significant height and peak period. If the actual duration is less, the process is duration limited. Using the actual duration, calculate a new effective fetch from Eq. (6.42) and, with this new fetch value, calculate the significant height and peak period from Eqs. (6.40) and (6.41).

Example 6.6-2

For the same condition given in Example 6.6-1, calculate the significant height and peak period using the SPM-JONSWAP procedure.

Solution:

The adjusted wind speed is

$$W_A = 0.71(30)^{1.23} = 46.6 \text{ m/s}$$

Then, Eqs. (6.40) to (6.42) yield

$$H_{mo} = 0.0016 \left(\frac{9.81(20,000)}{(46.6)^2} \right)^{0.5} \frac{(46.6)^2}{9.81} = 3.4 \text{ m}$$

$$T_p = 0.286 \left(\frac{9.81(20,000)}{(46.6)^2} \right)^{0.33} \left(\frac{46.6}{9.81} \right) = 6.1 \text{ s}$$

$$t_d = 68.8 \left(\frac{9.81(20,000)}{(46.6)^2} \right)^{0.66} \left(\frac{46.6}{9.81} \right) = 6580 \text{ s (1.82 hours)}$$

Since the actual duration is greater than the calculated duration, the wave generation process is fetch limited and $H_{mo} = 3.4 \text{ m}$, $T_p = 6.1 \text{ s}$. These values are close to the values $H_s = 3.1 \text{ m}$ and $T_s = 6.4 \text{ s}$ given by the SMB method and the process is fetch limited as indicated by that method.

6.8 Numerical Wave Prediction Models

During the past few decades there has been a strong effort to develop numerical computer models for wave prediction; these efforts have recently achieved much success. Generally, these models are based on a numerical integration over a spatial grid of the spectral energy balance equation

$$S_{in} + S_{nl} + S_{ds} = \frac{\partial S(f, \theta)}{\partial t} + C_g \cdot \nabla S(f, \theta) \quad (6.43)$$

where

$$\nabla = i \frac{\partial}{\partial x} + j \frac{\partial}{\partial y}$$

In Eq. (6.43), the lefthand terms give the energy input from the wind S_{in} , the nonlinear transfer of energy from one frequency to another by wave-wave interaction S_{nl} , and the energy dissipation S_{ds} by wave breaking and turbulence as well as bottom effects in shallow water. The righthand terms give the resulting growth of the wave spectrum as a function of time and location. The energy input term includes the Phillips and Miles mechanisms that were briefly discussed in Section 6.2. As the wave field grows, the nonlinear transfer term accounts for the transfer of some energy from the shorter to the longer period components on the growing face of the spectrum (see Figure 6.2). The growing wave field may be given in terms of $S(f, \theta)$ or more simply $S(f)$. In shallower water, propagation of the spectral components from point to point on the grid may include refraction and shoaling effects.

A wide variety of numerical wave prediction models have been developed by various groups around the world (see The SWAMP Group, 1985 and Komen et al., 1994). These models generally involve the solution of Eq. (6.43) in finite difference form throughout a grid placed over the ocean area where active wave generation is taking place. As wave generation proceeds, the model computes the wave spectrum at each grid point and time step. Figure 6.11 shows a typical one-dimensional spectrum at a point in time and space along with the frequency dependent magnitude of each of the terms on the left side of Eq. (6.43). The net input of energy at any frequency would be given by the algebraic sum of $S_{in} + S_{nl} + S_{ds}$.

There are theoretical schemes for computation of each of the three lefthand input terms in Eq. (6.42). But these theoretical schemes are not complete and,

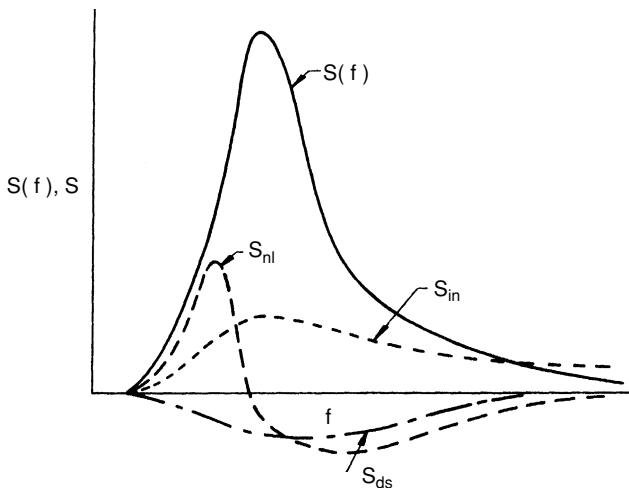


Figure 6.11. Typical energy spectrum and energy input/dissipation distribution at a point in a numerical wave prediction model.

particularly in the case of the nonlinear transfer term, too complex for complete inclusion in a numerical model. So each of the three terms has been strengthened and simplified by empirical calibration using data from field studies. The various wave prediction models differ in the final form of these input terms, in whether the model proceeds from meteorological charts of upper atmospheric isobar patterns or from surface wind fields, in the spectral model used to define $S(f, \theta)$ or $S(f)$ and the related directional spreading term employed, and in the formal model solution procedures.

Typically wave prediction model results for a given storm system might be the directional spectrum or perhaps only H_{mo} , T_p , and the dominant wave propagation direction, at selected coastal grid points. If the model is run for a given design storm, this output may be for sequential times during the storm at each coastal grid point. Or the models may be run from historic weather data to develop longterm wave statistics for a particular coastal region. An example of this is Hubertz et al. (1993), who developed wave statistics for 108 locations along the Atlantic coast of the U.S. and 3 coastal locations in Puerto Rico. Wave predictions were made for each location at a 3-hour interval for 20 years of weather data from 1956 to 1975.

These models are continually being improved with much of the improvement coming from the use of additional field data to calibrate model operations and verify model predictions.

6.9 Extreme Wave Analysis

An investigation of the wave climate for a particular coastal site—by the analysis of wave measurements and/or wave hindcasts from historic weather data—will usually provide a wave data set that is of insufficient length. This record must be extrapolated to a longer time frame to develop design wave conditions for most coastal projects.

Our primary concern is to determine the wave height (i.e., H_s or H_{mo}) at the site that has a particular recurrence interval or return period T_r . We define the return period as the average number of years during which the specified wave height is expected to occur or be exceeded once. For example, a 25-year return period means that the specified wave height will be expected to occur or be exceeded once on the average of every 25 years. It has a 4% chance of occurring any given year. It could happen twice in a given year.

A return period analysis is usually not done for wave period. Extreme wave heights will usually have a relatively well-defined range of wave periods that correlate with the wave heights. The duration of high waves that occur during a design storm may be of concern since the maximum wave height in a storm depends, as discussed above, on the duration of the high waves produced by the storm.

Common return periods for the design of important coastal projects are 50 or 100 years. Different components of a large project may be designed for different return periods. The selected return period for the design of a coastal structure depends on the design life of the structure which, in turn, is based on the economic life and possibly the longer expected physical life of the structure. It may also depend on the importance of the structure—a structure that is critical to the safety of human life along the coast may have a design life of 50 years but may be designed for a much longer return period wave to provide an adequate factor of safety.

Wave Height Return Period Analysis

The data set for a return period analysis might typically be the maximum H_s recorded every 6 hours or daily for a period of a year or a few years. The basic approach to conducting the return period analysis is: (1) tabulate the values by magnitude from the highest value to the lowest, (2) plot the cumulative probability distribution of these heights versus wave height on a graph having a selected probability distribution; the selected distribution should produce an essentially straight line plot, and (3) extrapolate this plot [by eye or some analytical method (see Isaacson and MacKenzie, 1981)] to obtain the wave height value for the probability or related return period desired. This would yield the significant wave height for the desired return period. The Rayleigh distribution can then be used to determine other H_n values for this return period. If a design wave period is desired, a single period or range of periods common to the peak values of the wave spectrum can be selected.

There does not appear to be one probability distribution function that universally fits all long-term wave height data (Ochi, 1982). The usual approach is to try a number of the commonly used distributions and then use the one giving the best fit. The probability distributions in common use are tabulated in Table 6.1 (Isaacson and Mackenzie, 1981). In this table, the general relationship for $P(H)$ versus H is given with coefficients α , β , and γ that are selected by trial to provide

Table 6.1. Common Probability Distributions

Distribution	Cumulative Probability
Log normal	$P(H) = \frac{1}{\sqrt{2\pi}} \int_0^H \frac{1}{\alpha H} \exp \left[-1/2 \left(\frac{\ln(H) - \beta}{\alpha} \right)^2 \right] dH$
Gumbel	$P(H) = \exp \left\{ -\exp \left[-\left(\frac{H-\gamma}{\beta} \right) \right] \right\}$
Frechet	$P(H) = \exp \left[-\left(\frac{H}{\beta} \right)^{-\alpha} \right]$
Weibull	$P(H) = 1 - \exp \left[-\left(\frac{H-\gamma}{\beta} \right)^\alpha \right]$

the best straight line fit to the data. Generally, α is a distribution shape factor, β controls the spread of the distribution along the H axis, and γ locates the central tendency of the distribution along the H axis. Note that some of the distributions use only two of the coefficients.

It is most convenient to plot the data for each of these distributions on graph paper appropriate for the particular distribution. For example, the log normal plot could be done on arithmetic-normal probability paper with the $P(H)$ term plotted on the normal distribution axis and the log of H plotted on the arithmetic axis. For the other distributions, if appropriate paper is not available, arithmetic scale graph paper can be used with the following values being plotted:

$$\begin{aligned} \text{Gumbel: } H \text{ versus } -\ln \{ -\ln [P(H)] \} \\ \text{Frechet: } \ln(H) \text{ versus } -\ln \{ -\ln [P(H)] \} \\ \text{Weibull: } \ln(H - \gamma) \text{ versus } \ln \{ -\ln [1 - P(H)] \} \end{aligned}$$

Note that for the Weibull distribution a value of γ must be assumed before the plot is made. Different γ values can be assumed until the best straight line fit is achieved.

The return period is related to the cumulative probability distribution by

$$\frac{T_r}{r} = \frac{1}{1 - P(H)} \quad (6.44)$$

where r is the time interval in years between successive data points.

In order to plot the data a value of $P(H)$ or T_r has to be assigned to each of the tabulated wave heights. The most common approach is to use the following relationship:

$$P(H) = 1 - \frac{m}{N + 1} \quad (6.45)$$

or

$$\frac{T_r}{r} = \frac{N + 1}{m} \quad (6.46)$$

To use Eq. (6.45) or (6.46), tabulate the N values of wave height in order of decreasing size and assign a sequential value of m to each height where $m = 1$ for the largest height and $m = N$ for the smallest height. Thus, from Eq. (6.46), if data were collected every day for a period of one year, $r = 1/365 = 0.00274$ years and $N = 365$. Then, for the largest wave height in the tabulation of heights, $m = 1$ so

$$P(H) = 1 - \frac{1}{365 + 1} = 0.9973$$

and

$$T_r = \frac{1}{365} \left(\frac{365 + 1}{1} \right) = 1.0027 \text{ years}$$

A useful concept, related to return period, is the encounter probability E . This is the probability that a wave having a return period T_r will be equaled or exceeded during some other period of time T . If $T_r^2/T(r) \gg 1$ as is usually the case,

$$E = 1 - e^{-T/T_r} \quad (6.47)$$

From Eq. (6.47) a wave with a return period of say 100 years has the following probability of occurring or being exceeded in any 50 year period:

$$E = 1 - e^{-50/100} = 0.393$$

Thus, this wave, which has a 2% chance of occurring or being exceeded in any given year, has a 39.3% chance of occurring or being exceeded in the next 50 years (which could be the project design life).

6.10 Summary

This chapter presents basic concepts concerning the nature of wind-generated waves and the analysis and prediction of these waves. This, coupled with the material presented in Chapters 2, 3, 4, and 9 supports the development of the wave climate for a given coastal location. The next chapter is concerned with wave forces on coastal structures and coastal structure stability requirements. The succeeding chapter is concerned with coastal processes and the stability of shorelines. Both chapters rely heavily on a knowledge of the coastal wave climate as well as the expected water level fluctuations that will occur.

6.11 References

- American National Standards Institute (1972), "American National Standard Building Code Requirements for Minimum Design Loads in Buildings and Other Structures," Publication A58.1, New York.
- Bouws, E., Gunther, H., Rosenthal, W., and Vincent, C.L. (1985), "Similarity of the Wind Wave Spectrum in Finite Depth Water, Part I—Spectral Form," *Journal of Geophysical Research*, Vol. 90, pp. 975–986.
- Bretschneider, C.L. (1952), "Revised Wave Forecasting Relationship," in *Proceedings, 2nd Conference on Coastal Engineering*, Council on Wave Research, University of California, Berkeley, pp. 1–5.

- Bretschneider, C.L. (1957), "Hurricane Design Wave Practices," *Journal, Waterways and Harbors Division, American Society of Civil Engineers*, May, pp. 1–33.
- Bretschneider, C.L. (1958), "Revisions in Wave Forecasting: Deep and Shallow Water," in *Proceedings, 6th Conference on Coastal Engineering*, Council on Wave Research, University of California, Berkeley, pp. 1–18.
- Bretschneider, C.L. (1959), "Wave Variability and Wave Spectra for Wind-Generated Gravity Waves," Technical Memorandum 118, U.S. Army Beach Erosion Board, Washington, DC.
- Chakrabarti, S.K. and Cooley, R.P. (1971), "Statistical Distribution of Periods and Heights of Ocean Waves," *Journal of Geophysical Research*, pp. 1361–1368.
- Collins, J.I. (1967), "Wave Statistics from Hurricane Dora," *Journal, Waterways and Harbors Division, American Society of Civil Engineers*, May, pp. 59–77.
- Collins, J.I. (1970), "Probabilities of Breaking Wave Characteristics," in *Proceedings, 12th Conference on Coastal Engineering*, American Society of Civil Engineers, Washington, DC, pp. 399–412.
- Earle, M.D. (1975), "Extreme Wave Conditions During Hurricane Camille," *Journal of Geophysical Research*, pp. 377–379.
- Goda, Y. (1974), "Estimation of Wave Statistics from Spectral Information," in *Proceedings, Ocean Wave Measurement and Analysis Conference*, American Society of Civil Engineers, New Orleans, pp. 320–337.
- Goda, Y. (1975), "Irregular Wave Deformation in the Surf Zone," *Coastal Engineering in Japan*, Vol. 18, pp. 13–26.
- Goda, Y. (1985), *Random Seas and the Design of Maritime Structures*, University of Tokyo Press, Tokyo.
- Goda, Y. and Suzuki, Y. (1975), "Computation of Refraction and Diffraction of Sea Waves with Mitsuyasu's Directional Spectrum," Technical Note, Port and Harbor Research Institute, Japan.
- Goodnight, R.C. and Russell, T.L. (1963), "Investigation of the Statistics of Wave Heights," *Journal, Waterways and Harbors Division, American Society of Civil Engineers*, May, pp. 29–54.
- Hasselmann, K., Barnett, T.P., Bouws, E., Carlson, H., Cartwright, D.E., Enke, K., Ewing, J.A., Gienapp, H., Hasselmann, D.E., Kruseman, P., Meerburg, A., Muller, P., Olbers, D.J., Richter, K., Sell, W., and Walden, H. (1973), "Measurement of Wind-Wave Growth and Swell Decay During the Joint North Sea Wave Project (JONSWAP)," Report, German Hydrographic Institute, Hamburg.
- Hubertz, J.M., Brooks, R.M., Brandom, W.A., and Tracey, B.A. (1993), "Wave Hindcast Information for the US Atlantic Coast," WIS Report 30, U.S. Army Waterways Experiment Station, Vicksburg, MS.
- Hughes, S.A. (1984), "The TMA Shallow-Water Spectrum Description and Applications," Technical Report CERC 84–7, U.S. Army Waterways Experiment Station, Vicksburg, MS.

- Hughes, S.A. and Borgman, L.E. (1987), "Beta-Rayleigh Distribution for Shallow Water Wave Heights," in *Proceedings, Coastal Hydrodynamics 87 Conference*, American Society of Civil Engineers, Newark, DE, pp. 17–31.
- Ibrageemov, A.M. (1973), "Investigation of the Distribution Functions of Wave Parameters During Their Transformation," *Oceanology*, pp. 584–589.
- Isaacson, M. and MacKenzie, N.G. (1981), "Long-term Distributions of Ocean Waves," *Journal, Waterway, Port, Coastal and Ocean Engineering Division, American Society of Civil Engineers*, May, pp. 93–109.
- Komen, G.J., Cavaleri, L., Donelan, M., Hasselmann, K., Hasselmann, S., and Janssen, P.A.E.M. (1994), *The Dynamics and Modeling of Ocean Waves*, Cambridge University Press, Cambridge.
- Kuo, C.T. and Kuo, S.T. (1974), "Effect of Wave Breaking on Statistical Distribution of Wave Heights," in *Proceedings, Civil Engineering in the Oceans III*. American Society of Civil Engineers, San Francisco, pp. 1211–1231.
- Longuet-Higgins, M.S. (1952), "On the Statistical Distribution of the Heights of Sea Waves," *Journal of Marine Research*, Vol. 11, pp. 246–266.
- McClenan, C.M. and Harris, D.L. (1975), "The Use of Aerial Photography in the Study of Wave Characteristics in the Coastal Zone," Technical Memorandum 48, U.S. Army Coastal Engineering Research Center, Ft. Belvoir, VA.
- Miles, J.W. (1957), "On the Generation of Surface Waves by Shear Flows," *Journal of Fluid Mechanics*, Vol. 3, pp. 185–204.
- Mitsuyasu, H., Tsai, F., Subara, T., Mizuno, S., Ohkusu, M., Honda, T., and Rikiishi, K. (1975), "Observation of the Directional Spectrum of Ocean Waves Using a Cloverleaf Buoy," *Journal of Physical Oceanography*, Vol. 5, pp. 750–760.
- Mitsuyasu, H., Tsai, F., Subara, T., Mizuno, S., Ohkusu, M., Honda, T., and Rikiishi, K. (1980), "Observation of the Power Spectrum of Ocean Waves Using a Cloverleaf Buoy," *Journal of Physical Oceanography*, Vol. 10, pp. 286–296.
- Ochi, M.K. (1982), "Stochastic Analysis and Probabilistic Prediction of Random Seas," *Advances in Hydroscience*, Vol. 13, pp. 218–375.
- Phillips, O.M. (1957), "On the Generation of Waves by Turbulent Winds," *Journal of Fluid Mechanics*, Vol. 2, pp. 417–445.
- Phillips, O.M. (1960), "On the Dynamics of Unsteady Gravity Waves of Finite Amplitude, 1. The Elementary Interactions," *Journal of Fluid Mechanics*, Vol. 9, pp. 193–217.
- Pierson, W.J. (1954), "An Interpretation of the Observable Properties of Sea Waves in Terms of the Energy Spectrum of the Gaussian Record," *Transactions of the American Geophysical Union*, Vol. 35, pp. 747–757.
- Pierson, W.J. and Moskowitz, L. (1964), "A Proposed Spectral Form for Fully Developed Wind Seas Based on the Similarity Theory of S.A. Kitaigorodskii," *Journal of Geophysical Research*, Vol. 69, pp. 5181–5190.
- Rye, H. (1977), "The Stability of Some Currently Used Wave Parameters," *Coastal Engineering*, Vol. 1, March, pp. 17–30.

- St. Dennis, M. and Pierson, W.J. (1953), "On the Motions of Ships in Confused Seas," *Transactions, Society of Naval Architects and Marine Engineers*, Vol. 61, pp. 280–357.
- Sorensen, R.M. (1993), *Basic Wave Mechanics for Coastal and Ocean Engineers*, John Wiley, NY.
- Sverdrup, H.U. and Munk, W.H. (1947), "Wind, Sea and Swell: Theory of Relations for Forecasting," Publication 601, U.S. Navy Hydrographic Office, Washington, DC.
- The SWAMP Group, (1985), *Ocean Wave Modeling*, Plenum Press, New York.
- Thom, H.C.S. (1960), "Distributions of Extreme Winds in the United States," *Journal, Structures Division, American Society of Civil Engineers*, April, pp. 11–24.
- Thompson, E.F. and Vincent, C.L. (1985), "Significant Wave Height for Shallow Water Design," *Journal, Waterway Port Coastal and Ocean Engineering Division, American Society of Civil Engineers*, September, pp. 828–842.
- U.S. Army Coastal Engineering Research Center (1977), *Shore Protection Manual*, 3rd Edition, U.S. Government Printing Office, Washington, DC.
- U.S. Army Coastal Engineering Research Center (1984), *Shore Protection Manual*, 4th Edition, U.S. Government Printing Office, Washington, DC.
- Wilson, B.W., Chakrabarti, S.K., and Snider, R.H. (1974), "Spectrum Analysis of Ocean Wave Records," in *Proceedings, Ocean Wave Measurement and Analysis*, American Society of Civil Engineers, New Orleans, pp. 87–106.
- Young, I.R. (1988), "Parametric Hurricane Wave Prediction Model," *Journal, Waterway, Port, Coastal and Ocean Engineering Division, American Society of Civil Engineers*, September, pp. 637–652.

6.12 Problems

1. Plot the Rayleigh distribution [$p(H)$ vs. H] for storm waves having a significant height of 4.75 m. Note H_{100} , H_{rms} , and H_s on the diagram.
2. If the average height in a wave record is 3.5 m and the average period is 6.9 s, how many waves would exceed 4 m height in a wave record that is 30 min long?
3. For the wave record in Problem 2 estimate H_{15} and H_{max} .
4. A wave forecast yields $H_s = 2.7$ m and $T_s = 6.2$ s. In one hour, how many waves will exceed 3 m in height? What will the maximum wave height be?
5. What percentage of the waves in a Rayleigh distribution will exceed the average height, the rms height and H_{10} ?
6. A 50 knot wind blows for 10 hours out of the east toward Milwaukee. Lake Michigan is 80 nautical miles wide at this location.
 - (a) Using the SMB procedure, determine the significant height and period of waves in deep water just offshore of Milwaukee.
 - (b) Plot the Bretschneider spectrum for this wind condition.
 - (c) A tower is located in water 6 m deep just offshore of Milwaukee. What is the highest wave you would expect during the storm at the tower?

7. What is the minimum wind duration that can occur for the wind in Problem 6 and still generate the same wave conditions?

8. For the wind condition in Problem 6, plot the resulting JONSWAP spectrum. From this, determine T_p and H_{mo} .

9. For the wind condition given in Problem 6, plot the Pierson-Moskowitz spectrum. Comment on the results vis-à-vis the wind conditions.

10. For the wind condition in Problem 6, determine the resulting significant height and peak period using the SPM-JONSWAP procedure.

11. For the wave conditions calculated in Problem 6, how long would it take for waves to propagate across Lake Michigan toward the end of the storm?

12. For a water depth of 20 m and the conditions in Problem 6 plot the TMA spectrum.

13. Write the Bretschneider spectrum [Eq. (6.19)] as a frequency spectrum.

14. Swell from the South Pacific arrive at the California coast at the same time as a local storm is taking place. Sketch the frequency spectrum you would expect to see at the coast in deep water. Explain.

15. Sketch a typical period spectrum and, on the same diagram, sketch how the spectrum would look after it passed a submerged barrier. Explain.

16. Consider the L-shaped breakwater given in Problem 4.11. Waves having a typical frequency spectrum propagate from offshore past the breakwater tip to point A. Sketch the spectrum at the tip of the breakwater and at point A on the same diagram. Comment on the difference.

17. Waves from a distant storm are recorded by a wave gage located at the coast. The average period decreases from 9 s to 6 s in 6 hours. How far away from the gage were the waves generated?

18. A wave gage is operated offshore of a potential project site for a period of one year. Owing to gage problems only 47 weeks of data are collected. The gage is run for a 30-min period each day and the highest significant height measured each week is tabulated below (wave heights are in meters):

1.05 1.92 3.72 2.04 2.54 1.47 3.50 0.96 2.54 1.36 1.15 3.05 1.80
1.70 2.05 2.07 2.27 1.39 2.39 2.51 0.82 1.86 2.07 3.07 1.66 3.10
2.94 3.00 1.39 3.11 1.39 1.53 2.37 1.16 2.56 2.84 4.53 3.31 1.58
1.46 2.37 2.26 4.48 1.33 2.53 1.37 3.35

Plot the above data [$P(H)$ versus H] on a Gumbel plot and estimate the 10- and 50-year return period significant wave heights. (Note: Normally all 329 data points would be used in the analysis; the problem was simplified to ease the reader's computation effort.)

19. Given the 50-year return period wave height determined in the previous problem, what is the chance of this wave height occurring in any 5-year period?

Coastal Structures

Structures are constructed along the coast for a variety of purposes. Owing to its nature, there is strong pressure for development of the land and nearshore areas along the coast. There is a commensurate need to protect this development from damage by waves and storm surge. Coastal structures are an important component in any coastal protection scheme. Structures may be designed to act directly to control wave and storm surge action or secondarily to stabilize a beach which, in turn, provides protection to the coast.

Sandy beaches, besides providing for coastal protection, have a significant recreational value. There is a limited amount of sand available in most coastal areas and the sand is usually moving along the shore as well as on- and offshore. Sand may also be artificially placed on the shore to supplement the sand that is there naturally. Often, structures are required to control where this sand remains and to protect the beach from losses caused by waves and storm surge.

Navigation and the moorage of vessels are important components of coastal activities. Coastal structures are important to the establishment of safe and efficient navigation channels across the coastline to interior harbor areas. Structures are also important to the development of safe harbor areas on the outer coast as well as in interior bays and estuaries.

Coastal structures are also constructed for other purposes besides those discussed above. These include pile supported piers that extend seaward from the shore for fishing, research and coastal access, pipelines that cross the shore and nearshore waters for waste disposal and the transport of liquid materials, piles and other structures that support navigation aids, platforms for oil drilling and production, and structures to moor vessels offshore.

There are a variety of structure types that can be constructed to satisfy one or more of the purposes discussed above. These include:

- Long thin cylindrical structures including individual piles and framed structures, pipelines, and cables

- Large single-unit submerged and partially submerged structures

Moored floating structures

Rubble mound structures, both massive structures and rubble mound veneers to protect embankments

Vertical-faced rigid structures

Some structures may combine the types mentioned above. An example would be a vertical faced concrete caisson placed on a submerged rubble mound platform that provides a stable base against wave attack and bottom scour.

There are two primary concerns in the design of any coastal structure. One is the structural aspects which address the stability of the structure when exposed to design hydrodynamic and other loadings. The other is the functional aspects which focus on the geometry of the structure to see that it satisfies the particular design function(s) such as keeping the wave heights in the lee of the structure reduced to an acceptable level or helping to retain a sufficiently wide beach at the desired location. This chapter deals primarily with the first concern, but addresses some aspects of the second concern, which are also covered in the next chapter.

For rigid structures such as piles, vertical-faced walls, and large submerged structures, our focus is on determining the loadings on the structure. This leads to the analysis for design stresses which is a classical civil-structural engineering concern. On the other hand, for a structure such as a rubble mound breakwater, our concern is to determine the stone unit size (and related structure component sizes) required to withstand attack by a given design wave and water level.

7.1 Hydrodynamic Forces in Unsteady Flow

Water particle motion in a wave is continually unsteady flow. When this unsteady flow interacts with a submerged solid body a force is exerted on the body owing both to the particle flow velocity and the flow acceleration.

The flow velocity causes a drag force F_d to act on the submerged body owing to frictional shear stress and normal pressure that is typically given by

$$F_d = \frac{C_d}{2} \rho A u^2 \quad (7.1)$$

For streamlined bodies such as an airfoil, A in Eq. (7.1) would be the surface area, but for a blunter body (e.g., circular and rectangular cross-sections) A is the cross-sectional area projected in the direction of flow. In Eq. (7.1) u is the flow velocity approaching the body, ρ is the fluid density, and C_d is a drag coefficient that depends on the body's shape, orientation to flow, surface roughness, and the flow Reynolds number.

For a circular cylinder the Reynolds number $R = uD/\nu$ where D is the cylinder diameter and ν is the fluid kinematic viscosity. For a given body shape, orientation, and surface roughness the drag coefficient depends primarily on the Reynolds number. This dependence has been determined experimentally for a variety of body shapes and typical values are presented in most fluid mechanics texts. Hoerner (1965) gives a thorough compilation of drag coefficients and related information for various shapes.

When flow accelerates past a body the flow velocity and thus the Reynolds number and to some extent the drag coefficient are continually changing. Thus, since u and C_d are both variable in accelerating flow the drag force (Eq. 7.1) can vary significantly. Consider a wave passing a vertical cylindrical pile. The water particle velocity at any point on the pile continually changes with time and at a given instant the particle velocity varies along the pile. This produces a very complex drag force pattern on the pile.

The accelerating flow causes an additional force on the submerged body beside that given by Eq. (7.1). This acceleration or inertial force has two components. One component arises because an accelerating flow field must have a pressure gradient to cause the flow to accelerate. This pressure gradient causes a variable pressure around the body's surface which produces a net force on the body. Also, when flow accelerates past a body an added mass of fluid is set into motion by the body. (If, for example, a body that is initially at rest in a still fluid is accelerated to some particular velocity, the surrounding fluid that was initially still is also set into motion. A force is required to accelerate that additional mass of fluid. Conversely, when flow accelerates past a still body there is an added mass that produces a force on the body.) This second component of inertial force is a function of the fluid density and acceleration, and the body shape and volume.

Thus, when there is unsteady flow, the total instantaneous hydrodynamic force F on the body can be written

$$F = \frac{C_d}{2} \rho A u^2 + \int_A p_x dA + k \rho V \frac{du}{dt} \quad (7.2)$$

The second term on the right, where p_x is the pressure acting on the body in the flow direction and dA is the differential area on which the pressure acts, is the inertial force owing to the accelerating flow field pressure gradient. The third term on the right is the added mass term. In this term V is the volume of fluid displaced by the body so ρV would be the displaced fluid mass. The dimensionless coefficient k is the ratio of a hypothetical fluid mass having an acceleration du/dt to the actual mass of fluid set in motion (by the body) at its true acceleration.

The pressure field term in Eq. (7.2) can be written in a more usable form by realizing that this pressure field creates a force that is capable of accelerating a mass of fluid having the same volume as the body but at a rate du/dt . Thus,

$$\int_A p_x dA = \rho V \frac{du}{dt}$$

So Eq. (7.2) becomes

$$F = \frac{C_d}{2} \rho A u^2 + (1 + k) \rho V \frac{du}{dt} \quad (7.3)$$

In potential flow, k has the values given below for various shapes and flow orientations:

Sphere	$k = 0.50$
Cube-flow normal to a side	$k = 0.67$
Circular cylinder-flow normal to axis	$k = 1.00$
Square cylinder-flow normal to axis	$k = 1.20$

Additional k values can be obtained from Sarpkaya and Isaacson (1981). In a real fluid, flow patterns past the body and thus the value of k would also depend on the body's surface roughness, the Reynolds number, and the past history of the flow.

Typically, $1 + k$ is called the coefficient of mass or inertia C_m and Eq. (7.3) is written

$$F = \frac{C_d}{2} \rho A u^2 + C_m \rho V \frac{du}{dt} \quad (7.4)$$

Thus, for potential flow past a circular cylinder $C_m = 2.0$, but for real flow past this cylinder C_m values less than 2.0 are common. Equation (7.4), when applied to wave forces on submerged structures, is commonly called the Morison equation after Morison et al. (1950), who first applied it to the study of wave forces on piles. For an in-depth discussion of the Morison equation see Sarpkaya and Isaacson (1981).

It is important to note that the application of Eq. (7.4) to determining wave forces on submerged structures requires that the structure be small compared to the wave particle orbit dimension so that the assumed flow field past the structure is reasonably valid (see Section 7.3). Also, if the submerged structure extends up to near or through the water surface, wave-induced flow past the structure will generate surface waves which cause an additional force on the structure not given by the Morison equation.

7.2 Piles, Pipelines, and Cables

Marine piles, pipelines, and cables constitute a class of long cylindrical structures that must be designed to withstand the unsteady flow forces from wave action. There may also be steady current-induced drag forces on these structures. Electrical cables laid along the sea floor are somewhat similar to underwater pipelines from the stability point of view, but cables are typically less than 15 cm in diameter while some pipelines such as municipal waste outfall lines can be up

to 3 m in diameter. Marine cables are also used to moor ships, buoys, and floating breakwaters. Piles for piers, offshore drilling structures, dolphins, and navigation aids are usually vertical or near vertical, but some of these structures can have horizontal and inclined cylindrical members for cross bracing. Pile diameters can vary from less than a meter for piers up to a few meters for the legs of some deep water oil drilling structures.

For a circular cylinder with its axis oriented in a horizontal y or vertical z direction and wave propagation normal to the axis, the force F_s per elemental length ds of the cylinder can be written

$$F_s = \frac{F}{ds} = \frac{C_d}{2} \rho D u^2 + C_m \rho \left(\frac{\pi D^2}{4} \right) \frac{\partial u}{\partial t} \quad (7.5)$$

The particle velocity u would be given by Eq. (2.21), and the local acceleration $\frac{\partial u}{\partial t}$ given by Eq. (2.23) is used in place of the total acceleration du/dt . Use of the local acceleration yields reasonable results for most cases but particularly for waves of low steepness in deeper water. Note that the u^2 term should be computed as $u|u|$.

The water particle acceleration lags the particle velocity by 90° so the drag F_d and inertia F_i components of F_s at a given point along the cylinder will vary through the wave cycle as shown in Figure 7.1. To construct Figure 7.1 it was assumed that C_d and C_m remain constant through the wave cycle and structure/wave conditions are such as to cause the peak inertia and drag forces to be equal. In any given wave/structure situation the peak total force occurs at some point

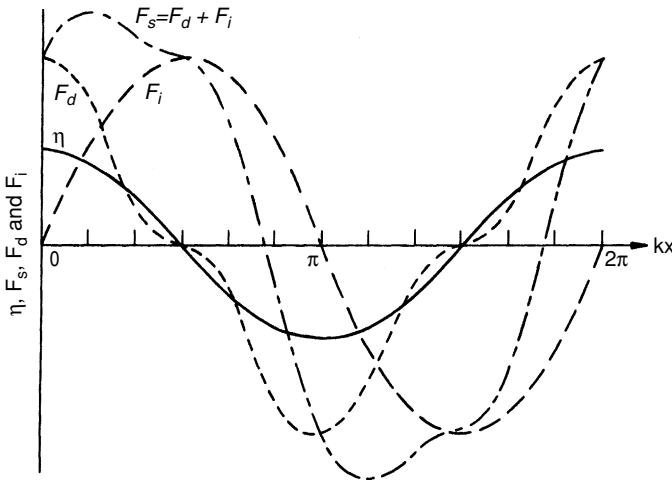


Figure 7.1. Surface elevation and drag, inertia, and total forces versus phase position—for equal peak drag and inertia components.

along the wave between the wave crest or trough and the still water line, the exact position depending on the values of C_d and C_m , the wave height and period, the water depth, and the cylinder diameter. At the wave crest and trough the total force is all drag force and at the still water positions along the wave the total force is all inertia force.

Inserting the relationships for wave particle velocity and acceleration into Eq. (7.4), differentiating F with respect to the phase $(kx - \sigma t)$, and setting the result equal to zero yields

$$\sin(kx)_p = \frac{2C_m V \sinh kd}{C_d A H \cosh k(d+z)} \quad (7.6)$$

where time is set to zero so $(kx)_p$ represents the position along the wave where the peak force occurs.

Equation (7.6) also indicates the relative magnitudes of the drag and inertia components of the total force. If the drag component is larger the total peak force occurs closer to the wave crest and trough, and if the inertia component is larger the total peak force occurs near the still water line position on the wave.

Since the volume of the cylindrical segment is a function of D^2 whereas the projected area of the segment is only a function of D , Eq. (7.6) shows that the ratio D/H indicates where along a wave the peak force will occur and the relative size of the drag and inertia force components. For a given wave, as the structure size increases the inertia force tends to become more dominant and vice versa. For common wave conditions, the total wave force on cables is essentially all drag force whereas the total force on large structures such as submerged oil storage tanks is effectively due solely to inertia effects. For piles either component may dominate, with drag forces being largest at lower D/H ratios and vice versa.

Often, structures are attacked simultaneously by waves and a current moving at some angle to the direction of wave propagation. The total drag force on the structure is due to the combined effects of the current and wave particle velocities. The wave characteristics are somewhat modified by the current, so the exact nature of the resulting force on a cylinder is difficult to determine. The usual design procedure is to vectorally add the current and wave particle velocities and use the resulting velocity component in the drag term of the Morison equation.

It was indicated in the previous section that the drag and inertia coefficients are generally a function of the structure shape, orientation to flow, and surface roughness, as well as the Reynolds number and the prior history of the flow. For cylindrical structures in waves it is common to introduce another independent parameter X/D where X is the distance that a particle moves as it passes the cylinder, i.e., essentially the particle orbit diameter normal to the cylinder axis. This parameter indicates how well the flow field develops around the structure in the wave-induced reversing flow past the structure.

The particle flow velocity in a wave at the structure can be represented by

$$u = u_m \sin\left(\frac{2\pi t}{T}\right)$$

where u_m is the maximum horizontal particle velocity (i.e., u under the wave crest). Then X equals the average flow velocity past the structure times the wave period or

$$X = \left(\frac{u_m}{2\pi}\right)T$$

so

$$\frac{X}{D} = \frac{1}{2\pi} \left(\frac{u_m T}{D}\right)$$

The term in parentheses ($u_m T/D$) is known as the Keulegan–Carpenter number KC , which is proportional to X/D and is also commonly used in defining values of C_d and C_m .

Note that since u_m is proportional to $\pi H/T$, KC is inversely proportional to D/H so either KC or D/H has been used in drag and inertia coefficient investigations. Generally, for $KC > 25$ drag forces dominate and for $KC < 5$ inertia forces dominate.

Most pile and pipeline structures will have several modes of resonant oscillation that may be excited by wave action. This may come about by one of the resonant modes being approximately equal to the incident wave period. Or, if H/D is sufficiently large so flow adequately envelops a structure a vortex field may develop in the lee of the structure and cause oscillatory forces that act normal to the direction of flow. The frequency of the vortices shed by the structure may also excite a resonant mode of the structure. The period of vortex shedding T_e is given by the Strouhal number:

$$S = \frac{D}{T_e u}$$

where u is the flow velocity past the structure having a diameter D . S for the common range of prototype pile Reynolds numbers varies from 0.2 to 0.4. For example, given typical values of $D = 1.0$ m, $u = 1.5$ m/s, and $S = 0.3$, $T_e = 2.2$ s. Thus, with an incident wave period that is significantly greater than 2.2 s, flow past a pile could last long enough for a few cycles of vortex shedding to occur.

Piles

Equation (7.5) gives the force per unit length acting on a cylinder. This can be integrated from the mud line to the water surface to obtain the total force on a vertical circular cylindrical pile as a function of time, i.e.,

$$F = \int_{-d}^{\eta} \left(\frac{C_d}{2} \rho D u^2 + C_m \rho \frac{\pi D^2}{4} \frac{\partial u}{\partial t} \right) dz$$

where dz is a unit length of the pile. If we assume that C_d and C_m are constant, that the water particle velocity and acceleration are given by the small-amplitude wave theory, that the integration is carried out up to the mean water surface elevation, and that the pile location is conveniently taken to be at $x = 0$, the integration yields

$$\begin{aligned} F = & \frac{C_d}{8} \rho g D H^2 n \cos^2(-\sigma t) \\ & + C_m \rho g \frac{\pi D^2}{8} H \tanh kd \sin(-\sigma t) \end{aligned} \quad (7.7)$$

where n is the ratio of the group to phase celerities. Note that $\cos^2(-\sigma t)$ should be computed as $\cos(-\sigma t)|\cos(-\sigma t)|$. This wave-induced force causes a moment on the pile around the mudline given by

$$M = \int_{-d}^{\eta} \left(\frac{C_d}{2} \rho D u^2 + C_m \rho \frac{\pi D^2}{4} \frac{\partial u}{\partial t} \right) (d+z) dz$$

Integration, with the same assumptions yields

$$\begin{aligned} M = & \frac{C_d}{8} \rho g D H^2 n \cos^2(-\sigma t) d \left[\frac{1}{2} + \frac{1}{2n} + \left(\frac{1}{2} + \frac{1 - \cosh 2kd}{2kd \sinh 2kd} \right) \right] \\ & + \frac{C_m}{8} \rho g \pi D^2 H d \tanh kd \sin(-\sigma t) \left[1 + \frac{1 - \cosh kd}{kd \sinh kd} \right] \end{aligned} \quad (7.8)$$

Equations (7.7) and (7.8) yield the force and moment as a function of time. The peak force and moment will occur at some point along the wave depending on the wave and pile characteristics, as discussed above. A procedure for the direct determination of the peak force and moment is given by the U.S. Army Coastal Engineering Research Center (1984). This peak force and moment procedure also employs Dean's stream function wave theory rather than the small-amplitude wave theory because, for most design situations, waves of great height are being employed as the design wave. Note that the drag and inertia terms in the moment equation are simply the drag and inertia forces times the water depth

times the term in brackets. The term in brackets is simply the fraction of the depth up from the mudline at which the force acts.

An important aspect of the calculation of wave forces and moments on a pile is the selection of values for C_d and C_m . One could use the theoretical value of 2.0 for C_m and, after calculating a Reynolds number using some representative water particle velocity, determine C_d from a typical steady flow plot of drag coefficient versus Reynolds number. Remember that C_d and C_m vary both with depth at an instant and with time throughout the wave cycle. The value selected for use in Eqs. (7.7) and (7.8) should provide results that are representative of peak load and moment conditions.

A number of experiments have been conducted both in laboratory wave tanks and in the field to determine design values for the drag and mass coefficients. In the laboratory either monochromatic or spectral waves can be used and wave characteristics can be controlled to yield results for the desired range of wave conditions. Also, the experimental setup, which usually involves a wave gage to measure the incident wave and an instrumented pile to measure the time-dependent wave loading, is easier to install, access, and control. However, a major drawback to laboratory experiments is that they must generally be conducted at reduced scale so Reynolds numbers are usually orders of magnitude smaller than those found in the field. Field experiments are much more difficult and expensive to carry out and there is no control over the incident wave conditions that will occur. Also, particularly for the larger waves, the wave conditions will be quite irregular and currents may also be acting on the pile.

By either approach, when a record of the water surface time history and the resulting time-dependent load on the pile as a wave passes are obtained, a very serious problem arises as to how to evaluate these data to determine drag and mass coefficients. Particle velocities and accelerations are needed to employ the Morison equation to determine C_d and C_m . So a wave theory must be selected to calculate particle velocities and accelerations from the wave record. Different theories, as we have seen, yield different results so the resulting values obtained are dependent on the wave theory used.

Given a wave record, an associated wave load record, and a selected wave theory for calculating particle velocities and accelerations, a variety of approaches have been used to determine C_d and C_m values, i.e.

1. At the wave crest and trough the total force is all drag force (see Figure 7.1) so this value can be used to directly determine a value for the drag coefficient from the drag term in the Morison equation. The measured force, when the wave is at the still water line, is all inertia force so this condition can be used in turn to determine the coefficient of mass from the inertia term in the Morison equation.

2. The Morison equation can be used at any two points along the wave record such as the points of maximum and zero force to solve for C_d and C_m from two simultaneous equations.
3. A least-squares fitting procedure can be employed with the Morison equation serving as the regression relationship. The value

$$\frac{1}{T_*} \int_0^{T_*} \left(F - \frac{C_d}{2} \rho D u^2 - C_m \rho \frac{\pi D^2}{4} \frac{\partial u}{\partial t} \right) dt$$

is minimized where T_* is the length of the wave and wave force records, F is the time-dependent measured wave force, and the particle velocity and acceleration at each point along the record are calculated from the measured wave profile. This would yield best fit values of C_d and C_m for the entire wave and wave force records.

The results of many of these field and laboratory experiments are referenced in Woodward–Clyde Consultants (1980), Sarpkaya and Isaacson (1981), and U.S. Army Coastal Engineering Research Center (1984). These results typically show a great deal of scatter in the resulting drag and mass coefficient values. Based on evaluations of the available laboratory and field experimental results Hogben et al. (1977) and U.S. Army Coastal Engineering Research Center (1984) have recommended design values for C_d and C_m . For the latter, a Reynolds number R is calculated using the maximum water particle velocity in the wave (i.e., at the crest and water surface). Then for:

$$R < 10^5, C_d = 1.2$$

$$R \text{ between } 10^5 \text{ and } 4 \times 10^5, C_d \text{ decreases from } 1.2 \text{ to } 0.6\text{--}0.7$$

$$R > 4 \times 10^5, C_d = 0.6\text{--}0.7$$

$$R < 2.5 \times 10^5, C_m = 2.0$$

$$R \text{ between } 2.5 \times 10^5 \text{ and } 5 \times 10^5, C_m = 2.5 - R/5 \times 10^5$$

$$R > 5 \times 10^5, C_m = 1.5$$

The final values selected for design will also depend on the confidence the designer has in the selected design wave and the related factor of safety desired.

Example 7.2-1

A vertical cylindrical pile having a diameter of 0.3 m is installed in water that is 8 m deep. For an incident wave having a height of 2 m and a period of 7 s, determine the horizontal force on the pile and the moment around the mudline when the pile is situated at the halfway point between the crest and still water line of the passing wave.

Solution:

For $T = 7$ s, $L_o = 9.81(7)^2/2\pi = 76.5$ m. Then, by trial we can solve Eq. (2.18) for the wave length at a water depth of 8 m

$$\frac{L}{76.5} = \tanh \frac{2\pi(8)}{L}$$

yielding $L = 55.2$ m and $k = 2\pi/55.2 = 0.1138$.

Then, from Eq. (2.21) the maximum horizontal particle velocity is

$$u = \frac{\pi(2)}{7} \frac{\cosh(0.1138)(8)}{\sinh(0.1138)(8)}(1) = 1.24 \text{ m/s}$$

and the Reynolds number is

$$R = \frac{1.24(0.3)}{0.93 \times 10^{-6}} = 4 \times 10^5$$

Using the recommended values for C_d and C_m given above yields

$$C_d = 0.72$$

$$C_m = 1.8$$

From Eq. (2.38)

$$n = \frac{1}{2} \left(1 + \frac{2(0.1138)8}{\sinh 2(0.1138)8} \right) = 0.803$$

We can now calculate the force and moment from Eqs. (7.7) and (7.8) where for our point along the wave $\sigma t = 3\pi/4$. From Eq. (7.7)

$$\begin{aligned} F &= \frac{0.72}{8} (9810)(0.3)(2)^2(0.803)(0.707)^2 \\ &+ \frac{1.8(9810)\pi(0.3)^2(2)}{8} (0.7213)(0.707) = 851 + 637 = 1488 \text{ N} \end{aligned}$$

and, from Eq. (7.8)

$$M = 851(8) \left[\frac{1}{2} + \frac{1}{2(0.803)} \left(\frac{1}{2} + \frac{1 - 3.169}{2(0.1138)8(3.007)} \right) \right] \\ + 637(8) \left[1 - \frac{1 - 1.444}{(0.1138)8(1.041)} \right] = 6550 Nm$$

The force calculation shows that the drag and inertia components of the wave force are about equal at the point considered so the plot of forces would be somewhat similar to that shown in Figure 7.1, indicating that the calculated force is approximately the maximum force on the pile. To determine the actual maximum force one would have to calculate the force for several points along the wave and interpolate (or use the procedure given in the U.S. Army Coastal Engineering Research Center (1984)).

The total force at the instant being considered would act at $6550 Nm / 1488 N = 4.40$ m up from the mudline.

Marine growth on a pile will increase the effective diameter of the pile and may significantly increase the surface roughness. Increased surface roughness will affect the drag and inertia coefficients, particularly for the range of Reynolds numbers common to field conditions. There are little data to indicate the expected change in C_d or C_m as a function of surface roughness for field design conditions. Blumberg and Rigg (1961) evaluated C_d for a 3-ft diameter cylinder having varying surface roughnesses and towed through water at a constant velocity. Reynolds numbers for the experiments varied between 1×10^6 and 6×10^6 . C_d was generally independent of Reynolds number as would be expected at these high Reynolds number values, but generally increased from 0.58 for a smooth cylinder to 1.02 for the roughest cylinder having oyster shells and concrete fragments in bitumastic on the surface. This indicates that the drag coefficients recommended above should be increased if excessive marine growth is expected over much of a pile length.

Other concerns that may arise concerning the analysis of wave forces on piles include: expected loadings on pile groups in sufficient proximity to cause flow interactions between the piles, broken wave forces on piles in both deep water and the surf zone, and forces on noncircular cylindrical piles. Discussion of these concerns may be found in Sarpkaya and Isaacson (1981) and the U.S. Army Coastal Engineering Research Center (1984).

Pipelines

If possible, particularly in shallow water and across the surf zone, pipelines should be buried below the ocean bottom to avoid damage from waves and currents as well as from dragging ship anchors, fishing trawls, etc. An alternative

is to lay the pipeline on the bottom and cover it with a layer of stone or one of a variety of commercially available mattresses (see Herbich, 1981). For firm bottoms where it is not economical to bury or cover the pipeline it may be anchored to the bottom with commercially available screw anchors placed at set intervals along the pipeline. Or weights (made of concrete or other materials) may be attached to the pipeline at set intervals to anchor it in place. During storms wave- and current-induced water motion may expose a buried pipeline or scour out the sea floor below a pipeline that is anchored to the bottom.

If a pipeline is carrying a lower density liquid (e.g., fresh water sewage being discharged through a marine outfall into the ocean) or if there is air in the pipeline, it will have a buoyant force that must be overcome by the weight of the pipeline and any anchors. Currents and wave-induced flow normal to the axis of a pipeline will cause a lift force on the pipeline owing to the asymmetry of flow around the pipeline sitting on the bottom. Currents and waves will also cause horizontal drag and inertia forces on the pipeline in the direction of current or wave propagation. Bottom friction between the pipeline and sea floor will resist horizontal forces acting on the pipeline.

The design of a pipeline sitting on the sea floor and relying on weight or screw anchors for stability must include a stability analysis to ensure that the pipeline will be stable for the expected design wave and current conditions and possible bottom scour conditions that may occur. This analysis requires selection of a bottom friction coefficient (Lyons, 1973) and lift, drag, and inertia coefficients for determination of the wave and current-induced forces. The lift force would be determined from an equation similar to the drag equation [Eq. (7.1)] with a lift coefficient C_l in place of C_d . Horizontal wave and current forces would be determined from the Morison equation. A static force analysis will indicate whether the pipeline is prone to sliding along the sea floor for the design wave and current conditions.

If the pipeline is raised from the bottom, the vertical asymmetry of flow decreases as does the resulting lift force. When the clearance between the pipeline and the ocean bottom is about 0.5 diameters, the lift force usually becomes very small.

A variety of studies of the hydrodynamic forces acting on sea floor pipelines have been conducted both for steady flow in flumes and for wave action in wave tanks (Brown, 1967; Beattie et al., 1971; Helfinstine and Shupe, 1972; Brater and Wallace, 1972; Grace and Nicinski, 1976; Parker and Herbich, 1978; Knoll and Herbich, 1980). For summary discussions of these investigations see Grace (1978) and Herbich (1981), who also discuss various other aspects of marine pipeline design. These references allow the selection of C_d , C_l , and C_m for the given pipeline condition. Grace (1971), based on the available literature and wave tank studies, recommends as conservative design values that $C_d = 2.0$, $C_l = 3.0$, and $C_m = 2.5$ for a pipeline on the seafloor. He recommends that C_d remain constant for any spacing between the pipeline and ocean floor, C_l should diminish to about 0.9 as the spacing approaches half the pipe diameter, and C_m should

“drop off” as the spacing increases. These recommendations are quite conservative. Depending on the conservatism desired in the design the reader should consult the above listed references and adjust the coefficient values accordingly.

Example 7.2-2

A 0.61 m outside diameter pipeline is sitting on the sea floor and has fresh water with no air pockets within. The pipe is plastic with an inside diameter of 0.53 m and a weight of 613 N per meter of length in air. Square concrete collar anchors are attached to the pipeline every 3 meters and each collar weighs 10 kN in air. What is the allowable current velocity acting normal to the axis of the pipeline if the pipeline is to be stable against sliding along the sea floor? Assume that the specific gravity of sea water is 1.025 and concrete is 2.40.

Solution:

The total submerged pipe weight in seawater is:

$$\left[613 + \frac{\pi(0.53)^2}{4}(9870) \right] - \frac{\pi(0.61)^2}{4}(9870)(1.025) = -167 \text{ N/m}$$

So, without the collars the pipe would float to the surface.

The submerged weight of the collars is:

$$\frac{10,000}{3} - \frac{10,000(9870)(1.025)}{(2.4)(9870)(3)} = 1910 \text{ N/m}$$

Thus, the submerged weight of the system is $1910 - 167 = 1743 \text{ N/m}$.

From Lyons (1973) for a sandy sea floor we can estimate the static coefficient of friction to be $\mu = 0.8$. This conservatively neglects the possibility of the collars digging into the sea floor, but sizeable bottom undulations could negate some of the bottom sliding resistance.

Thus, a static stability analysis, by summing forces in the horizontal direction yields:

$$F_d - 0.8(1910 - F_l) = 0$$

or

$$\frac{C_d \rho D U^2}{2} - 0.8 \left(1910 - \frac{C_l \rho D U^2}{2} \right) = 0$$

where F_d and F_l are the current-induced drag and lift per meter of pipe length. (The extra drag and possible lift caused by the collar are ignored.) Employing conservative drag and lift coefficients of 1.8 and 2.5, respectively, yields:

$$U = \sqrt{\frac{2(1910)}{1000(0.61)\left(\frac{1.8}{0.8} + 2.5\right)}} = 1.15 \text{ m/s}$$

as the maximum allowable current velocity.

Cables

Rope and woven metal cables are used for ocean towing and the mooring of a variety of floating structures including breakwaters, ships, buoys, and drilling rigs. Design analysis for these structures when exposed to waves and currents focuses primarily on the response of the structure with the cable providing a flexible restraint to the motion of the structure. The loading on the cable may or may not necessarily be included, depending on the characteristics of the structure/cable system.

Cable diameters are typically quite small compared to design incident wave heights. Consequently, D/H values are small or conversely KC values are large (much greater than 25) so essentially all of the wave force on a cable is caused by the drag component. Thus, if the force on a cable is to be determined the Reynolds number for the peak wave-induced particle velocity and the associated drag coefficient can be determined and the force computed from the standard drag equation.

7.3 Large Submerged Structures

A variety of large submerged structures such as oil storage tanks and caissons for the mooring of vessels have been constructed in coastal waters. The lateral dimensions of these structures are typically a significant fraction of the incident wave length. Commonly, D/H ratios are large and KC values are very small—of the order of unity or less. These small KC values indicate that horizontal orbit dimensions are small compared to structure dimensions so that appreciable flow separation will not occur and form drag forces are typically negligible. The total wave force on the structure is due essentially to inertial effects.

An inherent assumption in the Morison equation is that the particle velocity and acceleration are essentially constant over a distance equal to the length of the structure in the direction of wave propagation. This would not be the case for the large submerged structures being considered. Also, these structures cause a large amount of scattering or diffraction of the incident wave. Consequently, it is not appropriate to just employ the inertia term in the Morison equation with an appropriate mass coefficient to determine wave loadings on large submerged structures. Also, it is usually necessary to determine the resulting pressure distribution on these structures for a given design wave condition.

For large submerged structures, viscous effects will generally be confined to relatively thin boundary layers on the structure surface. As a consequence, it is usually possible to assume irrotational flow in the vicinity of the structure and treat the determination of wave-induced pressures and forces as a potential flow problem. Rounder, more streamlined structures will have less flow separation than structures having square corners, for example, but if the KC number is sufficiently small, these effects will be localized and the potential flow solution should still be meaningful.

Physical model studies of the wave-induced force and pressure distribution on large submerged structures are more feasible than model studies of wave loadings on piles, owing to the lesser significance of Reynolds number in the former case. See Garrison and Rao (1971), Chakrabarti and Tam (1973), and Herbich and Shank (1970) for examples of these model studies employing various shaped structures.

Sarpkaya and Isaacson (1981) present a detailed summary of the application of irrotational flow theory to the investigation of wave forces and pressures on large submerged structures. Generally, owing to the complexity of the problem, the small-amplitude wave theory is used. The velocity potential for the flow field is assumed to consist of the incident wave and scattered wave potentials:

$$\phi = \phi_i + \phi_s$$

where the scattered wave potential is due to the interaction of the wave with the structure. The scattered wave will be a normal outgoing wave at some distance from the structure. The boundary condition at the structure surface is that the flow velocity normal to the surface is zero, i.e.

$$\frac{\partial \phi}{\partial n} = 0 \text{ at } S(x, y, z) = 0$$

where n is the surface-normal direction and $S(x, y, z) = 0$ defines the surface geometry. A solution is then obtained for ϕ_s (see Sarpkaya and Isaacson, 1981) to yield $\phi = \phi_i + \phi_s$.

Then, the linearized equation of motion

$$p = -\rho g z - \rho \frac{\partial \phi}{\partial t}$$

yields the time- and space-dependent pressure distribution in the flow field and particularly on the structure. This can be integrated to determine the horizontal and vertical force components acting on the structure.

7.4 Floating Breakwaters

A breakwater is a structure that protects the area in its lee from wave attack. Most breakwaters are stone mound or rigid concrete structures. In recent years there has been an increase in the use of floating breakwaters—a floating structure that penetrates the upper part of the water depth and is moored to the bottom by cables and an anchor.

Floating breakwaters function by reflecting wave energy and dissipating the kinetic energy in the incident wave. This dissipation is primarily accomplished by the generation of turbulence in flow separation as wave-induced flow passes the structure and by the breaking of waves over the top of structure. If the incident wave period is close to one of the resonant periods of the breakwater–mooring line system, the motion response of the breakwater will be amplified which generally causes increased wave energy dissipation.

Floating breakwaters have some distinct advantages: (1) they are easily adaptable to large water level fluctuations as are found, for example, at some recreation/water supply reservoirs; (2) their cost does not rapidly increase with an increase in water depth as is the case for bottom-mounted fixed structures; (3) they are mobile and can relatively easily be relocated; (4) they offer less obstruction to water circulation and fish migration; and (5) they are less dependent on bottom soil conditions.

However, a primary disadvantage is that they are generally limited for use to areas where the design incident wave period is relatively small, e.g., reservoirs, rivers, and other areas having a relatively short wind wave generation distance; or areas where vessel-generated waves are the dominant incident wave. For a given water depth, shorter period waves have most of their energy concentrated near the water surface where the floating breakwater is located, while longer period waves have their energy distributed over a greater portion of the water column and thus are more effective at passing the structure. (For deep water waves over 70% of the kinetic energy is concentrated in the top 20% of the water column, while for shallow water waves the kinetic energy is essentially evenly distributed over the water column.) A secondary, but still important disadvantage, is that they are kinetic structures that are more prone to damage at connecting joints between units and at mooring line connectors. Also, if the mooring lines or anchors fail, a floating breakwater can break loose and damage nearby vessels, piers, and other structures.

A wide variety of floating breakwater types have been constructed (see Kowalski, 1974 and Hales, 1981). The most commonly used floating breakwaters fall into one of three groups demonstrated schematically in Figure 7.2. The prism group typically consists of concrete boxes filled with flotation material and axially connected by flexible connectors. The catamaran group is a variation on the prism group which has greater stability to wave agitation for the same

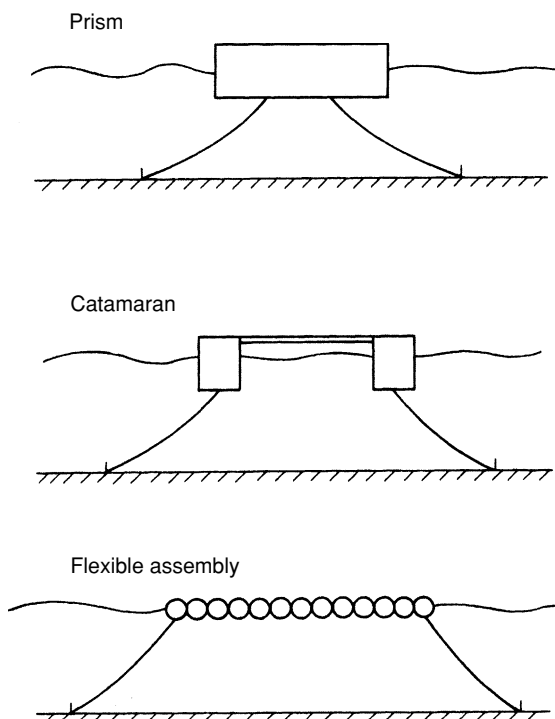


Figure 7.2. Common floating breakwater groups.

breakwater mass. It also has better energy dissipation characteristics owing to flow separation at the structure's additional corners. The most common type of flexible assembly floating breakwater is one made of interconnected scrap tires.

Figure 7.3 shows the transmission coefficient C_t , defined as the height of the transmitted wave in the lee of the breakwater divided by the incident wave height, for selected representatives of the three groups described above. C_t is plotted as a function of the ratio of the breakwater dimension in the direction of wave propagation W divided by the incident wave length. The data for these curves come from wave tank tests with monochromatic waves employing breakwater models for the prism and catamaran and a prototype structure for the tire assembly. Breakwater 1 is a concrete box having a prototype width of 4.87 m and a draft of 1.07 m, tested in water 7.6 m deep (Hales, 1981). Breakwater 2 is a catamaran breakwater having pontoons 1.07 m wide with a 1.42 m draft and a total width of 6.4 m (Hales, 1981). The water depth for the catamaran was also 7.6 m. Breakwater 3 is a tire breakwater consisting of four Goodyear modules for a total width of 12.8 m tested at a water depth of 3.96 m (Giles and Sorensen, 1979). The three breakwaters were moored as depicted in Figure 7.2. Other mooring arrangements or the same arrangements with different mooring line

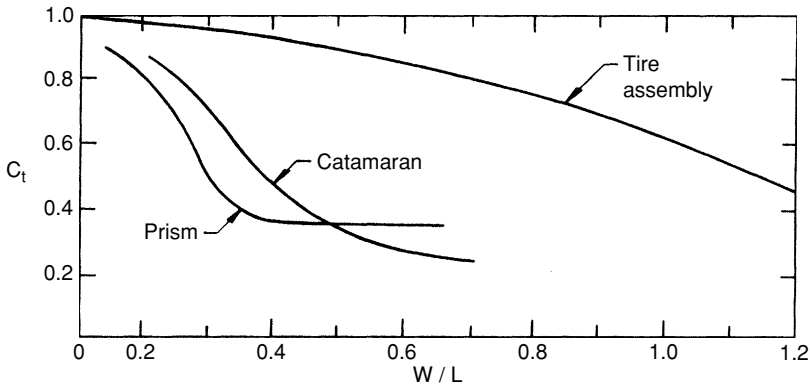


Figure 7.3. Transmission coefficients versus dimensionless size for common floating breakwater groups. (Giles and Sorensen, 1979; Hales, 1981.)

taughtnesses or cable elasticities would somewhat alter the values of the transmission coefficients.

Example 7.4-1

For the catamaran floating breakwater whose transmission characteristics are given by Figure 7.3, determine the transmission coefficient for incident waves having a period of 2, 4, and 6 s.

Solution:

For a water depth of 7.6 m and the three periods of interest Eq. (2.14) yields the following wave lengths:

$T = 2 \text{ s}$	$L = 6.3 \text{ m}$
4 s	24.0 m
6 s	44.4 m

For a breakwater width of 6.4 m the respective W/L values and C_t values from Figure 7.3 are:

$T = 2 \text{ s}$	$W/L = 0.98$	$C_t = 0.24$
4 s	0.27	0.79
6 s	0.14	0.91

The values for 2 and 6 s were determined by a slight extrapolation of the curve in Figure 7.3

The C_t values indicate that the catamaran is very effective for a 2 s wave but quite ineffective for a 4 or 6 s wave. The prism would have about the same general effectiveness and the tire assembly would be similarly but somewhat less effective.

The results from Example 7.4-1 are quite indicative of the behavior of typical floating breakwaters employed in typical water depths. For incident wave periods of 2 to 3 s or less they are useful, but if the incident wave period approaches 4 s or is higher their effectiveness is sharply reduced. For a design wind speed of say 30 m/s (67 miles per hour) and assuming fetch-limited conditions Figure 6.10 indicates that the largest possible fetch for an incident significant wave period to not exceed 3 s is about one kilometer.

Wave-induced loads on floating breakwaters are primarily dependent on the incident wave height. Adequate mooring line-anchor systems must be designed to resist these loads. Hales (1981) and Harmes et al. (1982) provide some wave loading data from wave tank experiments. Harmes et al. (1982) concluded that for the tire breakwaters that they studied, the wave-induced loads increased at a rate generally proportional to the wave height squared.

The most common types of anchors used for a floating breakwater are dead weight anchors such as concrete blocks, screw anchors, and pile anchors that are jettied or driven into the sea floor. The anchor type used depends on the design loads and the sea floor conditions (see Giles and Eckert, 1979 for a brief review of anchor design practice).

7.5 Rubble Mound Structures

Rubble mound structures consisting of interior graded layers of stone and an outer armor layer of stone or specially shaped concrete units are employed in the coastal zone as breakwaters, jetties, groins, and shoreline revetments. An advantage of rubble mound structures is that failure of the armor cover layer is not typically sudden, complete, and due to a few large waves but gradual and usually partial in extent, and spread over the duration of the higher waves that occur in a storm. If damage does occur, the structure usually continues to function and the damage can be repaired after the passage of the storm. In some cases it may be economical to use smaller size armor units, anticipate a certain amount of damage during a design storm, and provide for subsequent repair of the structure.

Armor units must be of sufficient size to resist wave attack. However, if an entire structure were to consist of units of this size, the structure would allow high levels of wave energy transmission and finer material in the foundation or embankment below the structure could easily be removed. Thus, the structure unit sizes are graded in layers, from the large exterior armor units to small quarry-run sizes and finer stone at the core and at the interface with the native soil bed.

Other rubble mound design concerns include: (1) prevention of scour at the seaward toe of the structure caused by wave agitation; (2) spreading of the structure load so that there is no foundation failure owing to excessive loads; (3) raising the crest of the structure to a sufficient height so wave overtopping and transmission are not sufficient to attack the land behind a revetment or regenerate undesirable wave action in the lee of a breakwater, and (4) for breakwaters that tie into the shore or for revetments that are placed along the shore, to be sure that scour at the end of the structure does not damage the structure or diminish its effectiveness.

Figure 7.4 shows a typical breakwater cross-section. Jetties and groins are structures built normal to the shore, the former to protect navigation entrances and the latter to stabilize a shoreline that has an alongshore transport of sand. Typically jetties are less massive than breakwaters and groins are less massive than jetties. They are usually less complex than the breakwater depicted in Figure 7.4, often consisting only of an armor layer and a single finer core/sublayer.

There are many variations in the cross-section design of breakwaters depending on the design wave climate, breakwater orientation, water depth, stone availability, foundation conditions, and degree of protection required of the structure. A concrete cap is most commonly used with concrete armor units. Two layers of armor units are commonly used. The breakwater crest width may be dictated by the minimum width needed for construction equipment to operate on the crest of the structure; otherwise, a minimum width of three armor unit diameters is usually recommended. Structure face slopes are never steeper than $1.5H:1V$ and somewhat flatter slopes are typically used. If the water depth is sufficient, the seaward armor layer should extend at least 1.5 to 2 times the design wave height below MLW. Note the extension of the C-stone to assist in toe protection. If the armor stone weight is W , the first under layer size might be about $W/10$ to $W/15$ and the second underlayer size might be about $W/200$ (remember that the weight of an armor unit is proportional to the diameter cubed).

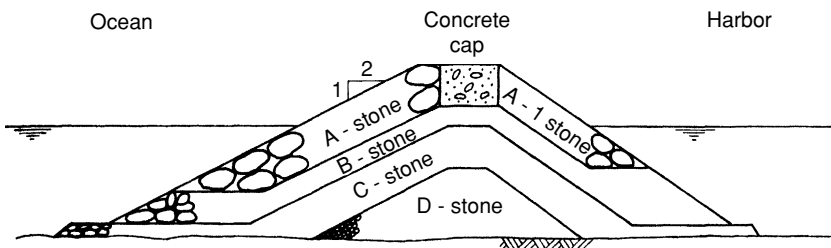


Figure 7.4. Typical rubble mound breakwater cross-section.

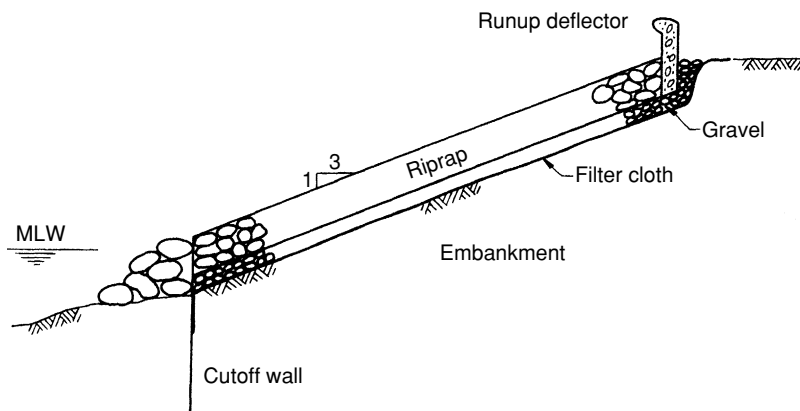


Figure 7.5. Typical revetment cross-section.

The profile of a typical shore revetment is shown in Figure 7.5. The armor layer would be a wider graded stone riprap rather than the well-defined two-layer armor system found in a breakwater. Several varieties of interlocking concrete units have also been used as the armor layer. A finer sublayer will be used under the armor layer and this often is placed over a geosynthetic filter cloth. A cutoff wall of sheet piling and/or a pile of larger stone is commonly placed at the toe of the structure to stabilize the toe against scour. Revetment slopes tend to be flatter than breakwater slopes. Additional design guidance for rubble mound structures is given in the U.S. Army Coastal Engineering Research Center (1984).

Armor Unit Stability

A key element in the design of any rubble mound structure is to determine the required armor unit size. This in turn dictates much of the remaining geometry of the structure (i.e., layer dimensions, sublayer unit sizes, structure slopes, crest width of the structure). The factors affecting the armor unit size, usually specified as the weight of the unit, are listed below.

Design wave characteristics. The design wave height at the structure is of critical importance. Some designers use the significant height although more conservative heights such as H_{10} have been used. The importance of the structure, how well the design wave height is known, and the desired safety factor will affect this choice. The expected duration of attack by high waves during a design storm is also an important factor. If the water depth at the seaward side of the structure is sufficiently shallow the design wave will break before it reaches the structure. This will limit the wave height attacking the structure and will affect the type of attack that occurs.

Armor unit characteristics. The shape, specific gravity, and range of unit sizes in the armor layer are important. More angular rock will be more stable than rock that is rounded. Artificial concrete armor units are designed to have irregular interlocking shapes while maintaining sufficient layer porosity when in place. Narrower stone size ranges are preferred for armor layers as very fine sizes are easily removed from the structure and finer sizes decrease the layer porosity which decreases its ability to relieve underlayer pressure exerted by wave action. Lower layer porosities will also increase the elevation of wave runup on the structure. However, specifying too narrow of a size range to a quarry operator increases the effort and thus cost of obtaining the rock.

Armor layer slope. The flatter the slope the smaller the size of the armor unit required for stability to wave attack. Smaller sizes yield thinner armor layers but flatter slopes require longer layers.

Trunk versus head. The head or end of a structure is typically exposed to more concentrated wave attack than the trunk or side of the structure. For more complex structures it is common to have flatter slopes and/or larger armor unit sizes at the head to protect against the greater wave attack.

Overtopping. The structure may be designed for moderate or significant wave overtopping depending on the structure purpose and design criteria. For significant overtopping there is less return flow on the seaward face of the structure but greater action on the leeward face. This might allow smaller seaward armor unit sizes and steeper slopes but more attention will have to be placed on the design of the structure crest and lee side.

Placement method. Depending on the construction procedure and care taken as well as the complexity of the structure, the armor unit placement may vary from plain dumping of the units to selective placement of individual units. Selective placement of the units will produce a more stable armor layer.

Layer dimensions. Thicker armor unit layers offer more reserve stability if the armor layer is damaged during a storm. It is imperative that damage during a storm not proceed to the point where underlayers are exposed to wave attack.

Allowable damage. It is difficult to predict the amount of damage that will occur to a given armor unit layer for a given design storm. But some information that is available would allow selection of a smaller armor unit with the related economic benefits in anticipation of repairing the structure after the damage has occurred. Smaller units are easier to obtain from a quarry and easier to transport as well as requiring less total volume, so their cost is less.

Determination of Armor Unit Stability

The hydrodynamic and armor unit interaction forces are very complex so a completely analytical development of an equation for armor unit stability is not practicable. Heavy recourse must be made to experiments. The basic problem is to determine the required weight W of an armor unit having a particular

shape and specific gravity S (in air), when exposed to waves of a given height and when placed on a structure face having a given slope θ . From a rough analysis of the forces involved one can define a stability number for an armor unit

$$N_s = H/(S - 1)(W/\gamma_s)^{1/3} \quad (7.9)$$

where γ_s is the specific weight of the stone or concrete armor unit. The stability number can be thought of as a dimensionless wave height and the term in the denominator that is raised to the one-third power is an effective diameter of the unit. A number of wave tank experiments have been run (Hudson, 1959) to relate N_s to the face slope and the armor unit shape at incipient failure of the armor units on the face. Basically, the experiments involved building an armor unit slope and exposing it to increasing wave heights until failure was observed. This failure point defined the stability number. The result is

$$N_s = (K_D \cot \theta)^{1/3} \quad (7.10)$$

where K_D is a dimensionless coefficient that depends on the armor unit shape, method of placement, location on the structure head or trunk, and whether the incident wave breaks before reaching the structure or on the structure face slope. Combining Eqs. (7.9) and (7.10) yields the classic Hudson equation for armor unit stability.

$$W = \frac{\gamma_s H^3}{K_D (S - 1)^3 \cot \theta} \quad (7.11)$$

Most laboratory studies to evaluate K_D have used waves having a constant period and height. For irregular waves, some designers use the significant height for H in Eq. (7.11). For conservative design, the U.S. Army Coastal Engineering Research Center (1984) recommends use of a higher wave such as H_{10} . Note that the required armor stone weight is proportional to the design wave height cubed. The weight used in Eq. (7.11) for stone armor units having a range of sizes is the median weight (i.e., 50% of the stones would weigh more than W).

Several dozen different shaped artificial armor units have been developed. Three of the most commonly used shapes—the dolos, the tetrapod, and the tribar—are depicted in Figure 7.6. Quarystone is most commonly used. However, for a given design wave height and face slope, an artificial concrete unit will have a smaller required size (weight) than a stone for the same stability level (i.e., larger K_D value). However, concrete armor units are occasionally broken either during placement or when under wave attack. Thus, if the quarries cannot produce a sufficiently large armor stone or transportation and placement restrictions eliminate the possibility of using a sufficiently large stone, artificial concrete units can be used.

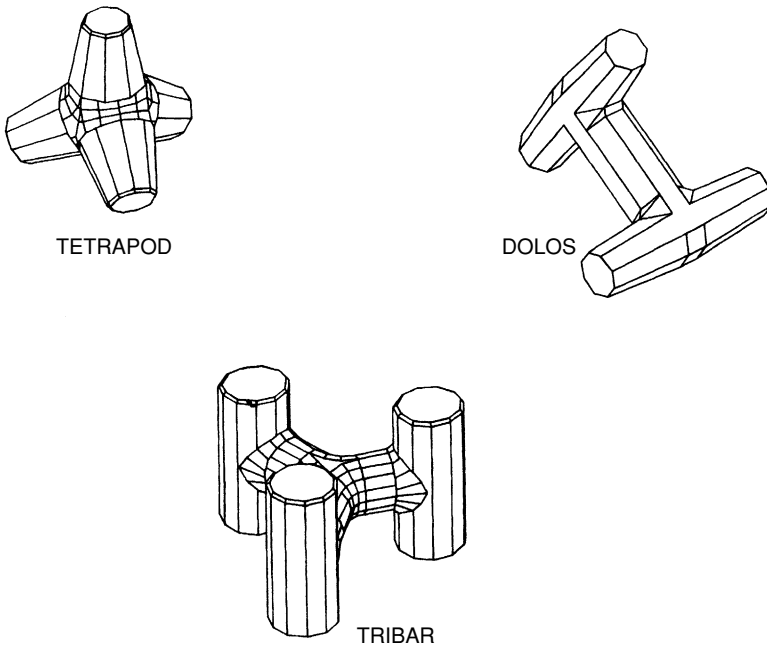


Figure 7.6. Typical concrete armor unit forms.

Selected values of K_D are tabulated in Table 7.1 as a function of unit shape, location on the structure head or trunk, and exposure to breaking or nonbreaking waves (i.e., waves that have or have not broken before they reach the structure). These values, except for the tribar, are for two layers of units, randomly placed, with zero allowable damage, and minor or no overtopping of the structure. The values for the tribar are for a single layer uniformly placed with the three legs perpendicular to the structure face.

Table 7.1. Suggested K_D Values

Unit	Trunk		Head	
	Breaking	Nonbreaking	Breaking	Nonbreaking
Quarrystone—smooth rounded	1.2	2.4	1.1	1.9
Quarrystone—rough angular	2.0	4.0	1.6	2.8
Riprap	2.2	2.5	—	—
Dolos	15.8	31.8	8.0	16.0
Tetrapod	7.0	8.0	4.5	5.5
Tribar	9.0	10.0	7.8	8.5

U.S. Army Coastal Engineering Research Center, 1984.

Table 7.2. H/H (zero damage) as a Function of Percent Damage

Unit	Percent Damage					
	5–10	10–15	15–20	20–30	30–40	40–50
Quarrystone—smooth	1.08	1.14	1.20	1.29	1.41	1.54
Quarrystone—rough	1.08	1.19	1.27	1.37	1.47	1.56
Tetrapods	1.09	1.17	1.24	1.32	1.41	1.50
Tribar	1.11	1.25	1.36	1.50	1.59	1.64
Dolos	1.10	1.14	1.17	1.20	1.24	1.27

Adapted from U.S. Army Coastal Engineering Research Center, 1984.

The stability coefficient can be increased if a certain percent damage is to be allowed for the design wave condition. Modified allowable wave height values can be determined from Table 7.2 which gives the ratio of the wave height allowed to the wave height for zero damage as a function of percent damage allowed. Percent damage is defined as the percent volume of units displaced from a zone on the structure face that extends from the middle of the breakwater crest downward to a depth of one wave height below the still water level.

It should be mentioned that some of the values in Table 7.2 are interpolated or extrapolated from very limited test results. The values generally show the effect one can achieve by allowing a certain level of damage to a rubble mound structure for a given design wave condition. Note also, that the dolos, which has the highest zero damage K_D values, has the lowest reserve stability as indicated by the lower values in Table 7.2 for higher percent damage.

Sensitivity of the Hudson Equation

In order to have a better appreciation of the Hudson equation (Eq. 7.11) for use in the design of stone mound structures, it is helpful to investigate the influence of small changes in each of the key independent parameters in the equation: namely the armor unit specific gravity, the design wave height, the front face slope and the K_D value used.

Considering a typical armor stone specific gravity of 2.6 and salt water, an increase in the armor stone specific gravity of 10% will decrease the armor unit weight required by 30%. Decreasing the specific gravity by 10% increases the necessary weight by 55%. (But, remember that the armor unit nominal diameter and thus the armor layer thickness is a function of the cube root of the unit's weight.). The approximate specific gravity of armor units can vary from concrete (2.25) to granite (2.65) to basalt (2.90). Thus, concrete blocks would need to be about double the weight of basaltic blocks (if the units had about the same shape and thus similar K_D values).

The design wave height used in the Hudson equation is usually only approximately determined owing to the possible variabilities in wave hindcasting and wave measurement, variabilities in extreme wave return period analysis, and the choice of which H_n (e.g. H_s or H_{10}) to use. Given this, an increase in the design wave height by 10% will require an increase in armor unit weight by 33%. A decrease in design wave height by 10% will decrease the required unit's weight by 27%.

Typical front face slopes for stone mound breakwaters vary from about 1:1.5 to 1:2.5 and revetment slopes are usually flatter. Decreasing the front face slope from 1:1.5 to 1:2.5 decreases the armor unit's weight required by 67%. But more volume of stone is required owing to the longer slope.

The K_D values listed in Table 7.1 are those suggested by the U.S. Army Corps of Engineers. They are empirical values based typically on tests of armor unit stability carried out in wave tanks. The given values for a particular armor unit can vary significantly depending on whether the tests were conducted with monochromatic waves or spectral waves (and if spectral waves, the character of the wave spectrum used), the H_n value that is to be used when applying the Hudson equation, and the way armor unit stability is defined in the wave tank tests. Given this background and accepting the values in Table 7.1 for example, the ratio of required armor weight increase in going from dolos to tetrapods (for trunk, breaking waves) would be 2.25.

The above discussion demonstrates the typical uncertainties involved in using the Hudson equation for stone mound structure design. The designer must have a strong sense of the confidence that can be placed in the various factors that influence the calculation of required armor unit weight. From this, and a consideration of the costs of the various breakwater components and related construction costs, choices can be made. Often, especially for fairly major structures and given sufficient time and funds, the designer would be wise to have model tests conducted to further strengthen design decisions that are made.

Example 7.5-1

The head of a rubble mound breakwater that is to be constructed on one of the Great Lakes is to have an armor face slope of 1:2.5. The breakwater head is in water having a design depth (high lake level plus design surge level) of 6.6 m and the bottom slope fronting the structure is 1:30. The deep water design wave significant height and period are 4.0 m and 7.3 s, respectively, and it may be assumed that the refraction coefficient from deep water to the structure is 1.0. Assume that the breakwater will have only minor overtopping for the design condition. Determine the required armor unit size if angular quarrrystones and tetrapods are to be considered. Assume $S = 2.65$ for the stone and $S = 2.40$ for concrete.

Solution:

For conservative design we will use H_{10} as a design wave height. From the Rayleigh distribution (Figure 6.5, line *b*) we can show that

$$H_{10} = 1.27 H_s = 1.27(4) = 5.1 \text{ m}$$

in deep water. From Eq. (2.42) with a refraction coefficient of unity and a wave period of 7.3 s we have $H_{10} = 4.9$ m at a water depth of 6.5 m (i.e., at the breakwater head). From Figure 2.12, for the given bottom slope a wave having a height of 4.9 m will break in water 5.9 m deep. Thus, although H_{10} will not break by the time it reaches the structure (where the depth is 6.5 m), some of the highest waves in the spectrum will break before reaching the structure. This will slightly decrease the value of H_{10} . We will employ a wave height of $H_{10} = 4.9$ m and assume nonbreaking conditions in our analysis.

Thus, from Table 7.1 for the zero damage condition, nonbreaking waves, and structure head, $K_D = 2.8$ for the angular quarrystone and $K_D = 5.5$ for the tetrapods. Then Eq. (7.11) yields

$$W = \frac{(9810)(2.65)(4.9)^3}{2.8(2.65 - 1)^3(2.5)} = 97,300 \text{ N}$$

for the quarrystone unit median weight and

$$W = \frac{(9810)(2.40)(4.9)^3}{5.5(2.40 - 1)^3(2.5)} = 73,400 \text{ N}$$

for the weight of the tetrapod units. Note the combined effect of the higher K_D value for the tetrapods but related lower specific gravity of the concrete used for the tetrapods.

Economic Implications for Design Wave Selection

The common approach to the design of rubble mound structures is to employ a design wave having a certain return period (e.g. 50 years) and use this to calculate the required armor unit size as well as the other related characteristics of the structure. The wave return period is selected based on the design and economic life of the structure and/or local code or common practice dictates. Conceptually, if the waves attacking the structure are lower than the design wave height there would be no damage to the structure. But, higher waves having a longer return period can also be expected to occur with some probability of occurrence and damage to the structure can be expected from these waves.

An alternative approach is to select the design wave based on an optimization of the economics of the structure. For a given design wave height, there will be a related total cost of construction of the structure. As this design wave height is increased the total construction cost of the structure will increase (larger armor units, higher crest elevation, etc.) But, the true cost of a structure must also include the cost of maintenance and repair of any damage during the life of the structure. As the design wave height is increased, the more robust structure can be expected to have lower damage and maintenance costs. Both the construction cost and the maintenance and damage costs can be estimated on an annual basis and summed to give the amortized annual cost of the breakwater over its design life, as a function of the design wave height employed. When this is done, the typical total annual cost of the structure will initially decrease as the design wave height is increased, but up to a point. Beyond this point the total annual cost will typically level off and then begin to increase. The optimum design wave height, then, is the design wave height that yields the lowest combination of annualized construction costs plus annualized maintenance plus damage costs.

Generally, this design approach is conceptually desirable; but, in practice, it is usually quite difficult to employ. Construction costs can be generally well defined, but damage and maintenance costs during the lifetime of the structure are difficult to define with any confidence. Also, one could repeat this entire analysis using different armor units (e.g. dolos vs. tetrapods vs. stone from one quarry vs. stone from another quarry, etc.) Also, one could repeat this analysis for different structure crest elevations to include the cost of damage from wave transmission past the structure for each elevation.

Weggel (1981) presents an analysis employing hypothetical cost data that further demonstrates this approach to design wave selection.

Armor Stone Specification

After the design armor stone size is determined from some equation such as the Hudson equation, additional requirements are typically specified for selection of the specific stone to be used. The stone weight calculated by the Hudson equation is the median weight for a widely graded stone such as that used for a stone-armored revetment. For a breakwater where there is a specific two-layer armor stone section, the range of allowable stone sizes must still be specified. The U.S. Army Corps of Engineers (U.S. Army Coastal Engineering Research Center, 1984) specifies that the armor layer stone weight can vary from $0.75 W$ to $1.25 W$. Since the nominal diameter is a function of the cube root of the weight this is only a 0.93 to 1.09 times the nominal diameter size range. As a practical matter this is probably too restrictive of a requirement. From the author's experience, a broader range of armor stone weights is typically specified. Some stone specifications have given a specific size gradation to be followed (e.g. 20% to be between $1.5W$ and $1.3W$, etc.). This restrictive a specification is probably

too difficult to follow in the field. Stone size range can be checked in the field by having the quarry set aside stone samples of specified weight for the field inspector to visually compare these stones to the delivered stone.

The Hudson equation leads to two other specific stone characteristic requirements. The calculation is based on a given stone specific weight, so a minimum stone specific gravity would typically be specified. The selection of a design K_D is based on the stone shape with smooth rounded stone having a lower K_D value than rough angular stone. A related shape issue is that long thin cylindrical stone are not acceptable. The related specification would specify a maximum to minimum axis length ratio.

Some of the following stone sample analyses may also be specified:

Compressive strength. A minimum stone compressive strength (e.g. 4000 psi) would be specified.

Abrasion. This would specify the percent of stone volume loss allowed after a specified number of revolutions in a tumbler.

Freeze/thaw. For stone in cold regions a test would evaluate the volume of stone lost by spalling for a certain number of cycles of freezing and thawing of wet stone.

Petrographic examination. This simply involves the inspection of stone samples by a knowledgeable person to look for deficient qualities such as layers of weaker stone or significant stone cracks.

The Hudson equation [Eq. (7.11)] is most commonly used for the determination of required armor unit size in the design of rubble mound structures. However, it does not explicitly include such variables as the incident wave period, the type of wave breaking on the structure, the allowable damage level, the duration of storm wave attack (i.e., the number of waves that attack the structure), and the structure (armor and sublayer) permeability. More complex equations that include these parameters and apply to waves breaking on the structure face have been presented by van der Meer (1988, 1995). He presents one equation for plunging breakers and another for surging breakers, with a third equation to define the intersection point between the two equations. The equations were developed only for stone armor units.

Recent Developments

Traditional breakwaters typically contain one or two layers of armor stone with progressively finer layers of stone down to the breakwater core. Where the design wave height is large, large armor units are required. For a variety of reasons these units may be excessively costly. An alternative type of breakwater, commonly known as a berm breakwater (Baird and Hall, 1984; Willis et al., 1988), employs stone that has a smaller median diameter and a wider size range for the armor layer. Figure 7.7 shows a typical profile of a berm breakwater. The “as

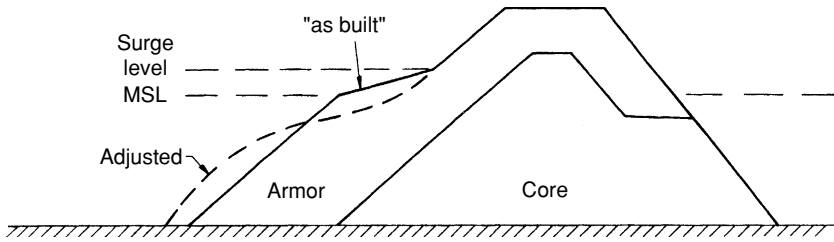


Figure 7.7. Berm breakwater cross-section.

built" profile of the armor layer is expected to adjust as waves attack the structure forming the adjusted profile shown in the figure. The adjusted profile is similar to a beach profile consisting of extremely coarse material (see Chapter 8) where the armor stones move on the slope in response to wave attack.

Baird and Hall (1984) list some of the advantages of berm breakwaters: (1) the armor stones can be less than one-fifth the weight of stones used for conventional armor units which, with the wider allowable size gradation, maximizes the use of available stone from a quarry; (2) stone placement is easier than in conventional breakwaters and construction tolerances and underwater inspection requirements can be relaxed; and (3) the design is much simpler, there being fewer layers and toe scour protection layers are usually not required. Although the total stone volume required may be 10% to 20% greater than for a conventional breakwater, the total cost will usually be significantly less.

Several of these breakwaters have been constructed (see references in the previous two paragraphs). However, at the present time, it is recommended that any design be tested in a model study as no simple formulae similar to the Hudson equation are available to guide the design.

Some laboratory tests (Ward and Ahrens, 1992) have been conducted on a berm revetment concept which is similar to the berm breakwater concept. The revetment would consist of a dumped mass of stone placed in front of an embankment that is to be protected. The stone would have a finer median size and a wider gradation than the armor riprap designed by the Hudson equation. It likewise would adjust its profile in response to wave attack.

During recent years a number of low-crested and submerged crest breakwaters have been constructed. These breakwaters are commonly built parallel to the shore and seaward of the surf zone, with the breakwater crest located around or below MSL. They function to stabilize a beach or assist in the retention of sand artificially placed on a beach. They have also been placed in front of larger structures to increase the stability of these structures. With their low crest they let normal low waves pass through to the beach but cause the breaking of larger storm waves. In recreational areas they are more aesthetically pleasing than structures that extend significantly above MSL. Often they are constructed of a mass of relatively widely graded stone overlying a filter layer on the sea floor.

Failure of submerged crest breakwaters usually involves removal of stones from the breakwater crest as wave-induced reversing flow acts over the crest. A modified stability number N_s^* is used to define structure stability where

$$N_s^* = \frac{H^{2/3} L^{1/3}}{(S-1)(W/\gamma_s)^{1/3}} \quad (7.12)$$

In Eq. (7.12) the wave length L is determined for the water depth at the structure. The wave length is included in the modified stability number because experiments have shown that the wave period is much more significant to the stability of submerged crest breakwaters.

After analyzing the results of a number of laboratory studies of submerged-crest breakwaters van der Meer and Pilarczyk (1990) concluded that the modified stability number is only a function of the damage level and the relative crest height. The damage level S is defined as the area of the structure profile from which stone has been removed divided by the median diameter squared of the stone used to construct the breakwater (van der Meer, 1988). The relative crest height is defined as the height of the structure crest above the sea floor h_c divided by the water depth d at the structure (where $d > h_c$). The resulting relationship for submerged crest breakwater stability is

$$\frac{h_c}{d} = (2.1 + 0.1S)e^{-0.14N_s^*} \quad (7.13)$$

In the modified stability number in Eq. (7.13), T_p is used to calculate the wave length at the structure and H_{mo} is used for the wave height. Thus, employing Eq. (7.13) and given the desired structure cross-section profile one can calculate the required median stone weight as a function of the incident design wave condition and the allowable damage level.

A procedure for determining the size of armor stone required for low-crested stone mound structures ($h_c > d$) has been presented by van der Meer and Pilarczyk (1990). This procedure gives a “reduction factor” for the median nominal stone diameter $(W/\gamma_s)^{1/3}$ based on the median armor stone diameter determined by some armor stone stability formula such as the Hudson equation (Eq. 7.11).

Define R_c as the vertical elevation of the structure crest above the design MWL (i.e. $R_c = h_c - d$). Then a dimensionless structure crest height R_c^* is given by

$$R_c^* = (R_c/H_s)(H_s/gT_p^2)^{0.5}$$

R_c^* can be calculated for a given structure crest elevation and design wave condition. Then the reduction factor (RF) is

$$RF = (1.25 - 4.8R_c^*)^{-1} \quad (7.14)$$

for $0 < R_c^* < 0.052$.

Thus, Eq. (7.14) allows for the calculation of the required armor stone nominal diameter by multiplying RF times the nominal stone diameter calculated by the Hudson equation. RF varies from 0.8 for the structure crest at the design MWL ($h_c = d$) up to unity for a structure crest elevation that allows minor or no wave overtopping.

Tandem Breakwater Concept

Cox and Clark (1992) present the design of a unique breakwater for the marina at Hammond, Indiana that they refer to as a tandem breakwater. A conventional stone mound breakwater for this site, that would control wave transmission by overtopping to within acceptable limits, would have a 4.6 m freeboard above the design lake water level with 1:1.5 side slopes. The armor stone size required for this breakwater ranged up to 8 tons. This breakwater was found to be too costly. Three alternatives were considered, a berm breakwater, a sheet pile wall, and a gravity caisson structure. These alternate structure types for this site all proved to be more expensive than the conventional breakwater design. The least total cost structure for this site turned out to be a tandem breakwater consisting of a smaller conventional stone mound main breakwater fronted by a submerged reef stone breakwater with an open water energy dissipation zone between the conventional and reef breakwaters.

“A reasonable-cost main breakwater could be built if the freeboard could be reduced to 10 ft (3.05 m) and the armor sized down to 3 tons with the same harbor tranquility requirement. This dictated that the transmitted wave from the reef could not exceed 9 ft (2.74m) in the design storm.”

The authors felt that the available published information on wave transmission over a reef structure was insufficient for a thorough design analysis, so they conducted physical model tests to supplement this available information. They investigated reefs of various depths of submergence, crests widths, and reef porosities.

The final design concept had a conventional breakwater with a freeboard of 3.05m and 3 ton armor stones fronted by a reef structure with a crest width of 7m located 0.86 m below the design lake water level. The reef breakwater was constructed of a range of stone sizes from 0 to 1 ton. Both the main and reef breakwaters had 1:1.5 side slopes. The authors conclude that the tandem breakwater may not always be the most economic design, as overall costs are dependent on local material costs and local water depths.

7.6 Rigid Vertical-Faced Structures

Some classes of coastal structures incorporate a rigid vertical face that is exposed to wave action. These include caissons typically consisting of a concrete or steel shell filled with sand and gravel and sitting on a gravel base, and vertical concrete

or wood panels supported at intervals by vertical and batter piles. The latter have been used at marinas and to control wave action at ferry slips. An important aspect of the design of these structures is the determination of the wave loading on the structure. If the wave loading is sufficient, caisson structures can slide off of their base. Vertical panel structures carry the wave-induced force to the supporting piles which can fail if the force is excessive.

If the water is sufficiently deep at the toe of the structure incident waves will reflect from the structure, forming a standing wave system with fluctuating pressures. For shallower water depths the waves will break directly on the structure or they will break seaward of the structure and send a turbulent mass of water forward to impinge on the structure. Each of these conditions is discussed below.

Nonbreaking-Wave Forces

The pressure distribution in a standing wave is given by Eq. (2.59). If the standing wave is formed by the complete reflection from a vertical structure (located at $x = 0$) the crest to trough excursion of the water surface at the structure is $2H$ and the dynamic pressure acting on the structure is

$$p_d = \frac{\rho g H \cosh k(d+z)}{\cosh kd} \cos \sigma t \quad (7.15)$$

Thus, the dynamic pressure at the toe of the structure ($d+z=0$) varies between

$$\pm \frac{\rho g H}{\cosh kd} \quad (7.16)$$

as the standing wave oscillates from the crest to trough position. The dynamic pressure distribution given by Eq. (7.15) is shown in Figure 7.8 for the wave crest and trough positions. These pressure distributions are almost linear from the instantaneous water surface to the bottom and are usually assumed to be linear for simplified conservative calculations of standing wave forces and moments on a vertical structure.

From radiation stress considerations it can be shown that wave reflection causes the mean water level at the structure to rise above the still water level by an amount

$$\Delta z = \frac{\pi H^2}{L} \coth kd \quad (7.17)$$

Wave reflection may not be complete owing to energy losses at the structure (i.e., $C_r = H_r/H_i < 1.0$). Thus

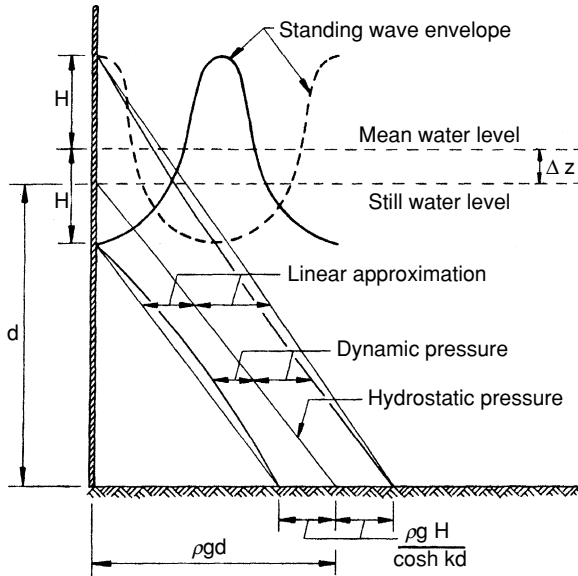


Figure 7.8. Standing wave pressure distributions on a vertical wall. (U.S. Army Coastal Engineering Research Center, 1984.)

$$2H = H_i + H_r = (1 + C_r)H_i$$

or

$$H = \frac{(1 + C_r)H_i}{2} \quad (7.18)$$

which is the value depicted in Figure 7.8 and used in calculations. The U.S. Army Coastal Engineering Research Center (1984) recommends that a minimum value of $C_r = 0.9$ be used for design purposes.

Note that the maximum moment exerted on a thin vertical barrier can occur if there is a wave crest on one side and a wave trough on the other side. Again, for conservative design this condition is often assumed.

If $H + \Delta z$ exceeds the elevation of the structure crest above the still water level, water will spill over the crest. This will relieve some of the pressure acting on the structure just below the crest. Again, for conservative design it is usually assumed that the pressure distribution is the same as if the structure extends up to $H + \Delta z$, with the pressure distribution truncated at the structure crest. The same concept can be applied at the bottom if the structure does not reach to the sea floor.

Example 7.6-1

The breakwater for a small marina is constructed of vertical concrete panels supported by piles. The water depth at the structure is 4 m and the panels have an opening of 0.5 m at the bottom to enhance water circulation in the marina. The panels extend 1.5 m above the still water level (i.e., panel lengths are 5 m). For an incident wave height of 1 m and a period of 4 s determine the maximum wave-induced force and moment on the breakwater per unit length. Assume still water on the lee side.

Solution:

Since the bottom opening will diminish reflection to a small extent we will assume $C_r = 0.9$. Then Eq. (7.18) yields

$$H = \frac{(1 + 0.9)}{2}(1) = 0.95 \text{ m}$$

From Eq. (2.14) with $d = 4$ m and $T = 4$ s, $L = 20.86$ m and $k = 0.3013$. Then Eq. (7.17) yields

$$\Delta z = \frac{\pi(0.95)^2}{20.86} \coth(0.3013)4 = 0.15 \text{ m}$$

and Eq. (7.16) yields a maximum bottom dynamic pressure of

$$p_d = \frac{9810(0.95)}{\cosh(0.3013)4} = 5125 \text{ N/m}^2$$

Then, the pressure on the structure will vary as follows:

$$\begin{aligned} z &= 0.95 + 0.15 = 1.10 \text{ m} & p &= 0 \\ z &= -4.0 \text{ m} & p &= 9810(4) + 5125 = 44,365 \text{ N/m}^2 \\ z &= -3.5 \text{ m} & p &= 44,365 \left[\frac{3.5 + 0.95 + 0.15}{4 + 0.95 + 0.15} \right] = 40,040 \text{ N/m}^2 \end{aligned}$$

Thus, the total force per unit length is

$$\frac{40,040}{2}(3.5 + 0.95 + 0.15)(1) = 92,092 \text{ N/m}$$

This force acts at a distance of

$$0.5 + \frac{(3.5 + 0.95 + .015)}{3} = 2.03 \text{ m}$$

above the sea floor; so the moment per unit length around the sea floor is

$$92,092(2.03) = 187,254 \text{ N m/m}$$

Breaking-Wave Forces

When a wave breaks directly on the face of a vertical structure there is a dynamic impact force on the structure that acts around the still water line. This is superimposed on the normal hydrostatic force. On rare occasions, the breaking wave will have a vertical face that slams against the structure and causes an extremely high intensity, short duration (less than 0.01 s typically) pressure on the structure. Although a high instantaneous force can develop, this force is of very short duration so the effect may not be great, particularly for massive structures that require a sustained force to dislocate them. The force may cause localized damage on a structure face which would be increased by repeated wave attack.

There have been a number of laboratory studies of breaking wave forces on vertical walls, especially caisson structures resting on rubble underlayers (Goda, 1985; Port and Harbor Research Institute, 1994). This has produced some semiempirical formulas for the calculation of wave loadings. Owing to their more common usage in Japan, most of the research on caisson type structures has been carried out there.

Figure 7.9 shows the profile of a typical caisson structure. Goda (1985) gives equations, based on laboratory studies with irregular waves, for determining both the breaking wave pressure distribution on the structure and the related uplift pressure on the caisson base. The pressures are related to the maximum wave height just seaward of the breaker line H_{\max} which is taken as being equal to $1.8 H_s$. The pressure extends up to an elevation given by

$$z = 0.75(1 + \cos \beta)H_{\max}$$

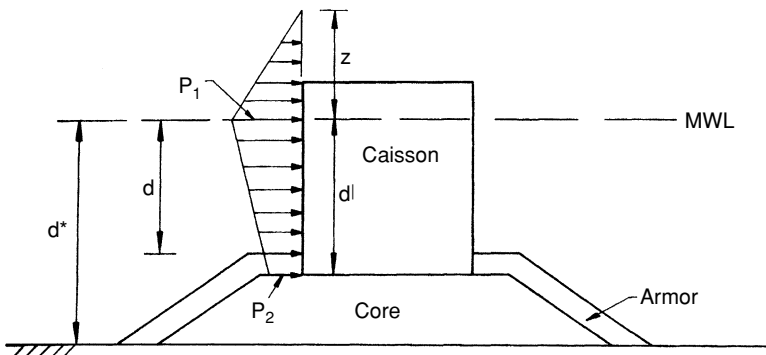


Figure 7.9. Broken wave pressure distribution on a caisson. (From Goda, 1985.).

where β is the angle between the direction of wave approach and a line normal to the caisson face. For force calculations, the pressure distribution would be truncated at the caisson crest. The key pressures are:

$$p_1 = 0.5(1 + \cos \beta)(\alpha_1 + \alpha_2 \cos^2 \beta)\gamma H_{\max}$$

$$p_2 = \alpha_3 p_1$$

$$\alpha_1 = 0.6 + 0.5 \left[\frac{2kd^*}{\sinh 2kd^*} \right]$$

$$\alpha_2 = \left[\frac{d_b - d}{3d_b} \left(\frac{H_{\max}}{d} \right)^2 \right] \text{ or } \left[\frac{2d}{H_{\max}} \right]$$

$$\alpha_3 = 1 - \frac{d'}{d^*} \left[1 - \frac{1}{\cosh kd^*} \right]$$

where, in the term α_2 the larger value is used and where d_b is the water depth at a distance $5 H_s$ seaward of the caisson. This latter term recognizes that the greatest pressures are exerted by waves that break somewhat seaward of the structure and strike it midway through their plunging distance.

The uplift pressure on the base of the caisson varies linearly from a value

$$P_u = 0.5(1 + \cos \beta)\alpha_1\alpha_3\gamma H_{\max}$$

to zero on the lee side of the caisson.

With the wave loading and uplift pressure distributions given above, an analysis of caisson stability against sliding can be carried out. The wave-induced uplift pressure and the buoyant force on the caisson would be included in the determination of structure stability to sliding.

Broken-Wave Forces

When waves break completely seaward of a coastal structure, the structure, which may be located above the still water level, can be subjected to a surge of water that exerts an impact force on the structure. An example of this type of structure would be the runup deflector on the shore revetment shown in Figure 7.5. Another example would be a sheet pile wall located back on a beach face.

This situation has not been thoroughly studied experimentally, but the U.S. Army Coastal Engineering Research Center (1984) presents a method (believed to be conservative) for broken wave force prediction that is based on a number of simplified but reasonable assumptions. It is assumed that when a wave breaks on a slope it causes a mass of water to surge forward with a velocity equal to the wave celerity at breaking, i.e.

$$V = \sqrt{gd_b}$$

The vertical thickness of this water mass is assumed to be equal to the crest amplitude at breaking which is taken as $0.78H_b$. It is then assumed that the water velocity and vertical thickness remain the same until the water reaches the structure or still water line, whichever comes first. If the structure is located landward of the still water line, the water velocity and vertical thickness are assumed to decrease linearly from the value at the still water line to zero at the hypothetical point of maximum wave runup (if there were no structure to interfere with the runup). The kinetic energy of the surging water mass is converted to a dynamic pressure (i.e., the stagnation pressure from the Bernoulli equation) that acts on the structure face to produce the resulting impact force. This is added to the hydrostatic force to predict the resulting force on the structure. This method will give an “order of magnitude” estimate of the broken wave force on the structure, but model tests are recommended if a more accurate force estimate is desired.

7.7 Other Loadings on Coastal Structures

Commonly, along the coast, waves are the dominant phenomenon a designer must consider when designing coastal structures, both because of the loadings they exert on structures and because of their importance in the transport of sediment in the nearshore zone. However, at some coastal locations other forces besides those caused by wave activity can be important to the design of coastal structures. These include forces exerted directly by currents, the wind, and ice; earthquake loadings; and vessel-induced forces on dock and other structures. For more detail on these topics the reader is referred to Bruun (1989), Gaythwaite (1990), Herbich (1990), and Tsinker (1995).

Currents

Coastal currents are generated by a variety of mechanisms: (1) wind-generated waves generate alongshore currents in the surf zone (see Chapter 8); (2) the tide generates reversing currents along the coast and at entrances to harbors, rivers, and estuaries; and (3) the wind generates currents directly by wind-induced stress on the water surface (see Chapter 5). Current-induced drag and lift forces on structures are calculated from the drag equation [Eq. (7.1)] as discussed in Sections 7.1 and 7.2 and in most elementary fluid mechanics texts.

Wind

The wind accompanying major storms, especially hurricanes, can cause significant damage to some coastal structures. For a general references on wind loadings see Simiu and Scanlan (1986). Direct damage is caused primarily to buildings and other lighter structures along the shore and to offshore platforms

particularly during construction and towing to the site. Indirect damage to harbor structures is caused primarily by vessels being torn loose and hitting these structures. Besides the typical drag and lift calculations for fluid forces on structures, the designer must be concerned with wind gusting and flow-induced vibrations owing to eddy shedding at the lee side of structures.

The short-term average wind speed in a wind gust can be significantly higher than the longer term average wind speed. Depending on the structure size and strength, a 5-s long wind gust might be large enough to envelope a structure and cause damage.

As is the case for structures in waves, vortex shedding as the wind blows past a structure can cause a lock-in resonant response if the vortex shedding frequency matches a resonant frequency of the structure. Winds that cannot damage a structure by direct form and friction drag may damage the structure by wind-induced vibrations.

In the coastal zone, the wind will usually have a high concentration of suspended water droplets. This can significantly increase the effective density of the wind and the resulting drag force on a structure.

Ice

In cold regions ice can have a major negative impact on the design of coastal structures and the planning and operation of harbors and navigation channels. It can have a positive impact on some shorelines by protecting them from wave attack during a large portion of the annual cycle.

The tensile and compressive strength of sea ice is quite variable and is dependent on salinity, temperature, depth within the ice sheet, ice growth rate, and the rate at which a load is applied to the ice. Information on such factors as the expected return period for given ice thicknesses, the lateral extent of ice floes that commonly occur, and the tide range and expected speeds and directions of ice floe movement as the ice is driven by the wind and currents is needed for effective design for ice conditions.

There are several ways in which ice can exert forces on coastal structures (see Peyton, 1968) including:

1. Moving sheet ice driven by the wind or currents will exert a horizontal force on a structure at the water line. The force will be caused by the initial impact of the ice or by the cutting of a slot through the ice sheet as moving ice is crushed by a structural member. Ice sheets can be as much as a meter or more thick and, when being crushed, can exert pressures on the order of 200 to 300 N/cm² of frontal projected area. The nature of ice failure by crushing is such that structural loading is often cyclic with a frequency of a cycle/s or more.
2. Inclined structural members will lift an ice sheet and cause ice failure by bending, which results in a much smaller ice force than failure by crushing.

Structural members can often be designed with a sloping section over the expected tide range to cause bending failure of the ice.

3. Ice frozen to a structure at high tide can exert a significant vertical load as the tide drops and similarly, ice frozen to a structure at low tide can exert an uplift force as the water level rises. During a thaw, large ice blocks frozen to structural members can move rapidly and cause damage.
4. Ice sheets resting on a riprap slope and moving with currents and the wind can “pluck out” armor units to seriously degrade a structure.
5. Damage can be caused by freezing and expansion of seawater in cracks and other small openings of structural members.

Earthquakes

Besides the damage caused by earthquake-generated tsunamis that arrive at the coast, earthquakes can cause direct damage to the coast in a variety of ways. Direct ground shaking can cause structural excitation and damage over a broad region surrounding the earthquake epicenter. Near the epicenter, fault displacement can cause uplift or subsidence of the earth’s surface which can have a major impact of coastal projects that survive the shaking. (The 1964 Alaskan earthquake caused uplift of about 2 m at Cordova, Alaska which reduced the water depths in a small boat basin from 4 m to less than 2 m.) Earthquakes can cause underwater and shoreline landslides which can damage structures and modify nearshore hydrography. Also, earthquake-induced vibrations of the ground mass can cause compaction of cohesionless soils to produce settlement or cause the liquefaction of other soils to produce a quick condition resulting in the sinking or overturning of structures.

Vessels

During berthing operations, damage may occur to both the dock fendering systems, dolphins and the vessel being docked. The problem may result from navigation error or the loss of vessel propulsion while docking. Or it may result from movement of a moored vessel caused by harbor seiching. Typically, the forces are absorbed both by the fendering system as well the structure supporting the fenders.

7.8 Wave–Structure Interaction

The primary concern when waves interact with structures is the stability of the structure when it is exposed to wave-induced forces. For breakwaters, seawalls, revetments and, to some extent, jetties there is the additional concern of wave energy passing through or over the structure to cause problems in the lee of the

structure. The transmission of wave energy past floating breakwaters has been discussed in Section 7.4. When waves attack rubble mound breakwaters and jetties, some wave energy is dissipated and some energy is reflected. The remaining energy may pass through the structure or pass over the structure by running up the structure face, overtopping the structure crest, and regenerating waves in the lee of the structure. For seawalls and revetments having land in their lee, wave energy that is not reflected and dissipated will also cause runup and possible overtopping to produce flooding and possible damage to the area behind the structure.

Owing to the nature of the processes involved, quantitative design information on wave reflection, runup, overtopping, and transmission is derived primarily from physical experiments, mostly at reduced scale in wave flumes and basins. Besides the characteristics of the incident waves, the results of these processes are very dependent on the profile geometry, surface roughness, and porosity of the specific structures. Consequently, although a fairly broad range of structures have been investigated, specific information is not available for every type of structure the designer may encounter. The designer must use strong judgement in interpolating and extrapolating the available results, and if the project is of sufficient importance may have to resort to model tests.

Results of wave reflection, runup, overtopping, and transmission tests for the various types of structures investigated are found mainly in the reports from the laboratories that completed the studies as well as journal and conference papers (see Chapter 1) that summarize the experimental results. The best overall summary of results is found in the U.S. Army Coastal Engineering Research Center (1984). Wave reflection and runup were briefly discussed in Sections 2.7 and 2.9, respectively.

Wave Reflection

A good summary of much of the work on wave reflection from structures can be found in Seelig and Ahrens (1981) and Allsop and Hettiarachchi (1988). A general equation for the reflection coefficient for sloped coastal structures may be written

$$C_r = \frac{aI_r^2}{b + I_r^2} \quad (7.19)$$

where a and b depend primarily on the structure surface condition and to a lesser extent on the slope and whether monochromatic or irregular waves are used. I_r is the Iribarren number, defined as

$$I_r = \frac{m}{\sqrt{H/L_o}} \quad (7.20)$$

For stone mound structures and conservative calculations Seelig and Ahrens (1981) recommend that $a = 0.6$ and $b = 6.6$ be used. For structures with concrete armour units Allsop and Hettiarachchi (1988) recommend $a = 0.56$ and $b = 10.0$ for dolos and $a = 0.48$ and $b = 9.62$ for tetrapods.

Wave Runup

Monochromatic wave runup R on a smooth impermeable slope, when the water depth at the toe of the slope is between 1 and 3 times the deep water unrefracted wave height, can be predicted using Figure 2.15. (Similar figures are available for other toe water depths from the U.S. Army Coastal Engineering Research Center, 1984). For a stone mound structure this should be reduced by a factor r having a value of 0.5 to 0.8 (see Table 2.1).

For irregular wave runup it is often assumed that the runup has a Rayleigh distribution so

$$\frac{R_p}{R_s} = \left(\frac{\ln(1/p)}{2} \right)^{1/2} \quad (7.21)$$

where R_p is the runup associated with a particular probability of exceedence p and R_s is the runup of the incident significant wave height as if it were a monochromatic wave. Note that R_p is not the average runup of the upper p fraction; it is the runup exceeded by the upper p fraction of the runups. The latter is most appropriate for determining desired structure crest elevations.

Wave Overtopping

If the elevation of wave runup on the face of a structure sufficiently exceeds the crest elevation, water will flow over the structure crest to the lee of the structure. To evaluate potential flooding conditions in the lee of the structure and to design a system for removal of the water during a storm, it is necessary to predict the wave-induced overtopping flow rate (volume/time/unit length of structure).

No simple relationship is available to predict overtopping rates. The U.S. Army Coastal Engineering Research Center (1984) presents an empirical equation that requires the estimation of two coefficients, with very limited data given on which to base an estimate for these coefficients. Results from the use of this equation are very approximate at best. If determination of overtopping rates is important in a coastal project design, consideration should be given to the conduct of model studies. For some empirical data on overtopping of breakwaters and seawalls see Goda (1985), Ahrens and Heimbaugh (1986), and Aminti and Franco (1988).

Wave Transmission

If an overtopped structure has water in its lee, the overtopping flow will generate waves in the lee of the structure. Also, if the structure is sufficiently permeable,

some wave energy will propagate through the structure. However, for most breakwaters a core is provided so that there is essentially no transmission of windgenerated waves through the structure.

Seelig (1980) conducted a very extensive set of experiments of wave transmission by overtopping of rubble mound structures. He found that most of the transmitted wave energy had the same frequency as the incident waves, but a significant portion of the energy had higher frequencies that were harmonics of the incident frequency.

Seelig presented a simple formula that can be used to estimate the transmission coefficient for rubble mound breakwaters:

$$C_t = C(1 - F/R) \quad (7.22)$$

where F is the freeboard (vertical distance from the MWL to the structure crest), R is the runup that would occur if the structure crest were sufficiently high for no overtopping to occur, B is the structure crest width, d_s is the water depth at the structure toe and

$$C = 0.51 - \frac{0.11B}{d_s + F} \quad (7.23)$$

It is recommended that Eq. (7.22) be applied to the relative depth (d_s/gT^2) range of 0.03 to 0.006 and the range of $B/(d_s + F)$ between 0 and 32 as these are the ranges employed in the data collection.

Madsen and White (1976) developed a numerical procedure for calculating the transmission coefficient for waves transmission through a layered stone structure. As indicated above, this would only likely be important for wave periods significantly greater than those found in the wind wave range.

For low crested stone mound structures, van der Meer and Angremond (1992) presented a wave transmission coefficient curve similar to that shown in Figure 7.10. Given the freeboard (which would be negative for a submerged crest) and the incident wave height one can estimate the transmission coefficient.

7.9 Selection of Design Waves

An important aspect of the design of coastal structures is the selection of design wave conditions for the structure. There are several components to this selection process, most of which have been presented in other chapters of this text. The overall approach is summarized herein. For more detail see Sorensen (1993).

To start, a wave data base for the site must be established. This typically involves the collection of information on the wave significant height and period from the important directions of wave approach and for as long a time period as

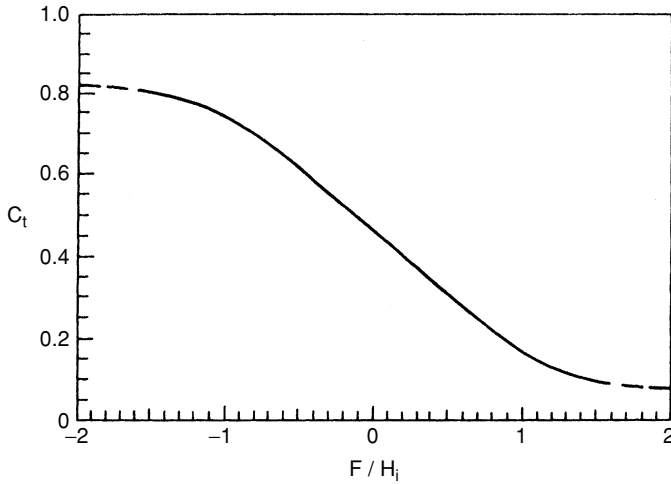


Figure 7.10. Transmission coefficient versus dimensionless freeboard for a low crested breakwater. (Modified from van der Meer and Angremond, 1992.)

is possible. This data base may be derived from wave hindcasts using historic meteorological data (Chapter 6) and/or wave measurements made at the site (Chapter 9). The wave data base is then used to conduct an extreme wave analysis to establish the significant wave height having a particular return period or probability of occurrence (Chapter 6).

This wave height is commonly determined for a deep water point offshore of the structure's location. This height must be transferred by refraction, shoaling, and possibly diffraction analysis (Chapters 2 through 4) to the location of the structure. To do so, the designer must select a design water level (Chapter 5) having a return period related to that of the design wave height.

A design wave period or periods must also be selected. If a sufficient data base is available, a return period analysis can also be done for the significant or spectral peak wave period. Otherwise one can simply select a wave period or range of periods that relate to the selected design wave height. For rubble mound structures this might be just the significant or spectral peak period but, for rigid structures where wave/structure resonance problems are possible, a range of periods bracketing the significant period might be investigated. The lower limit of this range would be set by steepness limits for breaking in deep water. Battjes (1970) recommends that this lower limit be set by

$$T = \left(\frac{32\pi}{g} H_s \right)^{1/2}$$

where H_s is the significant height for the return period of interest.

When the design wave or waves is(are) transferred to the structure location, the Rayleigh distribution can be employed to determine the H_n value to use for the structure design (Chapter 6). Typically rubble mound structures are designed for H_s or H_{10} as discussed above while more rigid structures such as pile structures and vertical walls would employ a higher wave such as H_1 or H_{\max} . The wave height at the structure may be limited by the height of a wave that breaks at some distance (say $0.5 X_p$; Chapter 2) seaward of the structure.

Some Design Wave Examples

Saint John Deep, Canada. As part of the design effort for a proposed deep sea terminal at St. John, New Brunswick, Canada, Khanna and Andru (1974) carried out a wave climate study for the site. St. John Deep is on the Bay of Fundy which opens through the Gulf of Maine to the Atlantic Ocean. Both waves generated locally and waves approaching the site from the Atlantic Ocean were of interest in the determination of expected design extreme wave heights. For a one-year period wind measurements were made at the site and wave measurements (using an accelerometer buoy, see Section 9.2) were made at a point offshore in water about 40 m deep. Owing to instrument malfunctions, wind records were obtained for 61% of the time and the monthly wave data collection varied from 54.2% to 92.4 % of the time. Also, eighteen years of wind records were available from a local airport. A comparison of the wind roses for the 18-year airport record and the one year of measurements from the site, indicated that differences were not large. Thus, the 18 years of airport wind records could be used for local wave hindcasts. They used the SMB method (Section 6.6) for these hindcasts. A third source of wave data was from visual observations made at a weather ship in the Gulf of Maine. Wave refraction analyses, using the dominant range of wave periods, were carried out to transpose the waves from the Gulf of Maine to the site. Extreme wave height projections for the site were then made using Weibull, log normal, and Gumbel probability distributions for the one year of measured wave data. The results of the local hindcasts and the transposed Gulf of Maine wave observations were used to reinforce confidence in the measured wave projections.

Sines, Portugal. The dolos-armoured stone mound breakwater at the Port of Sines in Portugal, is directly exposed to wave attack from the Atlantic Ocean. The breakwater was very seriously damaged by waves from a storm during February 1978 and additional damage was done during storms in December 1978 and February 1979. In order to support an effort to understand the specific causes of the damage that occurred and to provide support for the redesign of the breakwater, extensive studies of the wave climate at the site were carried out by Mynett, et al. (1983).

A numerical wave hindcasting model was employed to hindcast wave conditions for 20 major storms that occurred during the period 1956 to 1980, including

the three storms that did damage to the breakwater. Directional wave spectra were computed at six-hour intervals during the strength of each storm. The hindcast wave spectra and associated significant wave heights were compared, when possible, with ship observations and available wave gage measurements made during the particular storms. This was done to confirm the numerical wave hindcasts. Monochromatic wave numerical calculations and physical model studies were then employed to refract and shoal the waves to the site. Extreme wave predictions were also made from the wave hindcasts for the 20 major storms.

7.10 Summary

A primary focus of this chapter has been the determination of wave loadings on the various types of structures that are constructed in the coastal zone. This leads to the structural analysis of these structures so they may be designed. For rubble mound structures the incident wave conditions lead directly to a selection of the required armor stone size which, in turn, largely dictates the cross-section geometry of the structure. Other factors that enter the design of many structures include the wave reflection, runup, overtopping, and transmission past the structure.

The functional design of coastal structures also requires an analysis of their required length, plan shape, and position. For structures such as breakwaters this largely involves a wave refraction/diffraction analysis to see if the required protection will be achieved. But for structures on the shore such as groins and jetties or seawalls and revetments, and for offshore segmented breakwaters designed to stabilize a beach, the interaction of these structures with coastal zone sediment transport processes is also important. Coastal zone transport processes and the effect of coastal structures are presented in Chapter 8.

7.11 References

- Ahrens, J.P. and Heimbaugh, M.S. (1986), "Irregular Wave Overtopping of Sea Walls," in *Proceedings, Oceans '86 Conference*, Institute of Electronic and Electrical Engineers, Washington, DC, pp. 96–103.
- Allsop, N.W.H. and Hettiarachchi, S.S.L. (1988), "Reflections from Coastal Structures," in *Proceedings, 21st International Conference on Coastal Engineering*, American Society of Civil Engineers, Malaga, Spain, pp. 782–794.
- Aminti, P. and Franco, L. (1988), "Wave Overtopping on Rubble Mound Breakwaters," in *Proceedings, 21st International Conference on Coastal Engineering*, American Society of Civil Engineers, Malaga, Spain, pp. 770–781.
- Baird, W.F. and Hall, K.R. (1984), "The Design of Breakwaters Using Quarried Stones," in *Proceedings, 19th International Conference on Coastal Engineering*, American Society of Civil Engineers, Houston, pp. 2580–2591.

- Battjes, J.A. (1970), "Long-Term Wave Height Distribution at Seven Stations Around the British Isles," National Institute of Oceanography, Report A44, United Kingdom.
- Beattie, J.F., Brown, L.P., and Webb, B. (1971), "Lift and Drag Forces on a Submerged Circular Cylinder," in *Proceedings, Offshore Technology Conference*, Houston, paper 1358.
- Blumberg, R. and Rigg, A.M. (1961), "Hydrodynamic Drag at Supercritical Reynolds Numbers," presented at American Society of Mechanical Engineers meeting, Los Angeles.
- Brater, E.F. and Wallace, R. (1972), "Wave Forces on Submerged Pipelines," in *Proceedings, 13th Conference on Coastal Engineering*, American Society of Civil Engineers, Vancouver, pp. 1703–1722.
- Brown, R.J. (1967), "Hydrodynamic Forces on a Submarine Pipeline," *Journal, Pipeline Division, American Society of Civil Engineers*, March, pp. 9–19.
- Bruun, P. (1989), *Port Engineering*, Fourth Edition, Gulf, Houston.
- Chakrabarti, S.K. and Tam, W.A. (1973), "Gross and Local Wave Loads on a Large Vertical Cylinder—Theory and Experiment," in *Proceedings, Offshore Technology Conference*, Houston, paper 1818.
- Cox, J.C. and Clark, G.R. (1992), "Design Development of a Tandem Breakwater System for Hammond Indiana," in *Proceedings, Coastal Structures and Breakwaters Conference*, Thomas Telford, London, 111–121.
- Garrison, C.J. and Rao, V.S. (1971), "Interaction of Waves with Submerged Objects," *Journal, Waterways, Harbors and Coastal Engineering Division, American Society of Civil Engineers*, May, pp. 259–277.
- Gaythwaite, J.W. (1990), *Design of Marine Facilities*, Van Nostrand Reinhold, New York.
- Giles, M.L. and Eckert, J.W. (1979), "Determination of Mooring Load and Transmitted Wave Height for a Floating Tire Breakwater," Coastal Engineering Technical Aid 79-4, U.S. Army Coastal Engineering Research Center, Ft. Belvoir, VA.
- Giles, M.L. and Sorensen, R.M. (1979), "Determination of Mooring Loads and Wave Transmission for a Floating Tire Breakwater," in *Proceedings, Coastal Structures '79 Conference*, American Society of Civil Engineers, Arlington, VA, pp. 1069–1085.
- Goda, Y. (1985), *Random Seas and Design of Maritime Structures*, University of Tokyo Press, Tokyo.
- Grace, R.A. (1971), "The Effects of Clearance and Orientation on Wave Induced Forces on Pipelines," Look Laboratory Report 15, University of Hawaii, Honolulu.
- Grace, R.A. (1978), *Marine Outfall Systems: Design, Planning and Construction*, Prentice-Hall, Englewood Cliffs, NJ.
- Grace, R.A. and Nicinski, S.A. (1976), "Wave Force Coefficients from Pipeline Research in the Ocean," in *Proceedings, Offshore Technology Conference*, Houston, paper 2767.
- Hales, L.Z. (1981), "Floating Breakwaters: State-of-the-Art Literature Review," Technical Report 81-1, U.S. Army Coastal Engineering Research Center, Ft. Belvoir, VA.
- Harmes, V.W., Westerink, J.J., Sorensen, R.M., and McTamany, J.E. (1982), "Wave Transmission and Mooring Force Characteristics of PipeTire Floating Breakwaters,"

- Technical Paper 82-4, U.S. Army Coastal Engineering Research Center, Ft. Belvoir, VA.
- Helfinstine, R.A. and Shupe, J.W. (1972), "Lift and Drag on a Model Offshore Pipeline," in *Proceedings, Offshore Technology Conference*, Houston, paper 1578.
- Herbich, J.B. (1981), *Offshore Pipeline Design Elements*, Marcel Dekker, New York.
- Herbich, J.B. (1990), *Handbook of Coastal and Ocean Engineering*, Gulf, Houston.
- Herbich, J.B. and Shank, G.E. (1970), "Forces Due to Waves on Submerged Structures: Theory and Experiment," in *Proceedings, Offshore Technology Conference*, Houston, paper 1245.
- Hoerner, S.F. (1965), *Fluid-Dynamic Drag*, Third Edition, published by the author.
- Hogben, N., Miller, B.L., Searle, J.W., and Ward, G. (1977), "Estimation of Fluid Loading on Offshore Structures," Part 2, in *Proceedings of the Institute of Civil Engineers*, London.
- Hudson, R.L. (1959), "Laboratory Investigation of Rubble Mound Breakwaters," *Journal, Waterways and Harbors Division, American Society of Civil Engineers*, September, pp. 93-121.
- Khanna, J. and Andru, P. (1974), "Lifetime Wave Height Curve for Saint John Deep, Canada," in *Proceedings, Conference on Ocean Wave Measurement and Analysis*, American Society of Civil Engineers, New Orleans, pp. 301-319.
- Knoll, D. and Herbich, J.B. (1980), "Simultaneous Wave and Current Forces on a Horizontal Cylinder," in *Proceedings, 17th International Conference on Coastal Engineering*, American Society of Civil Engineers, Sydney, pp. 1743-1760.
- Kowalski, T. (1974), "1974 Floating Breakwater Conference Papers," Marine Technical Report 24, University of Rhode Island, Kingston.
- Lyons, C.G. (1973), "Soil Resistance to Lateral Sliding of Marine Pipelines," in *Proceedings, Offshore Technology Conference*, Houston, paper 1876.
- Madsen, O.S. and White, S.M. (1976), "Reflection and Transmission Characteristics of Porous Rubble-Mound Breakwaters," Miscellaneous Report 76-5, U.S. Army Coastal Engineering Research Center, Ft. Belvoir, VA.
- Morison, J.R., Johnson, J.W., O'Brien, M.P., and Schaaf, S.A. (1950), "The Forces Exerted by Surface Waves on Piles," *Petroleum Transactions, American Institute of Mining Engineers*, Vol. 189, pp. 145-154.
- Mynett, A.E., de Voogt, W.J.P., and Schmeltz, E.J. (1983), "West Breakwater-Sines, Wave Climatology," *Proceedings, Coastal Structures '83 Conference*, American Society of Civil Engineers, Arlington, VA, pp. 17-30.
- Parker, M.E. and Herbich, J.B. (1978), "Drag and Inertia Coefficients for Partially-Buried Offshore Pipelines," in *Proceedings, Offshore Technology Conference*, Houston, paper 3072.
- Peyton, H.R. (1968), "Ice and Marine Structures," *Ocean Industry*, Houston (three articles: March, September, and December).
- Port and Harbor Research Institute (1994), *Proceedings, Wave Barriers in Deep Water Workshop*, Yokosuka, Japan.

- Sarpkaya, T. and Isaacson, M. (1981), *Mechanics of Wave Forces on Offshore Structures*, Van Nostrand Reinhold, New York.
- Seelig, W.N. (1980), "Two-Dimensional Tests of Wave Transmission and Reflection Characteristics of Laboratory Breakwaters," Technical Report 80-1, U.S. Army Coastal Engineering Research Center, Ft. Belvoir, VA.
- Seelig, W.N. and Ahrens, J.P. (1981), "Estimation of Wave Reflection and Energy Dissipation Coefficients for Beaches, Revetments and Breakwaters," Technical Paper 81-1, U.S. Army Coastal Engineering Research Center, Ft. Belvoir, VA.
- Simiu, E. and Scanlan, R.H. (1986), *Wind Effects on Structures*, John Wiley, New York.
- Sorensen, R.M. (1993), *Basic Wave Mechanics for Coastal and Ocean Engineers*, John Wiley, New York.
- Tsinker, G.P. (1995), *Marine Structures Engineering*, Chapman and Hall, New York.
- U.S. Army Coastal Engineering Research Center (1984), *Shore Protection Manual*, U.S. Government Printing Office, Washington, DC.
- van der Meer, J.W. (1988), "Rock Slopes and Gravel Beaches Under Wave Attack," Delft Hydraulics Communication 396, Technical University, Delft, The Netherlands.
- van der Meer, J.W. (1995), "A Review of Stability Formulas for Rock and Riprap Slopes Under Wave Attack," Chapter 13, *River, Coastal and Shoreline Protection* (Thorne, C.R., Abt, S.R., Barends, F.B.J., Maynard, S.T., and Pilarczyk, K.W., Editors), John Wiley, New York.
- van der Meer, J.W. and Angremond, K. (1992), "Wave Transmission at Low-Crested Breakwaters," *Coastal Structures and Breakwaters*, Institution of Civil Engineers, Thomas Telford, London, pp. 25-41.
- van der Meer, J.W. and Pilarczyk, K.W. (1990), "Stability of Low-Crested and Reef Breakwaters," in *Proceedings, 22nd International Conference on Coastal Engineering*, American Society of Civil Engineers, Delft, pp. 1375-1388.
- Ward, D.L. and Ahrens, J.P. (1992), "Laboratory Study of a Dynamic Berm Revetment," Technical Report CERC-92-1, U.S. Army Waterways Experiment Station, Vicksburg, MS.
- Weggel, J.R. (1981), "Some Observations on the Economics of "Overdesigning" Rubble-Mound Structures with Concrete Armor," Coastal Engineering Technical Aid 81-7, U.S. Army Coastal Engineering Research Center, Ft. Belvoir, VA.
- Willis, D.H., Baird, W.F., and Magoon, O.T. (1988), *Berm Breakwaters: Unconventional Rubble-Mound Breakwaters*, Conference Proceedings, American Society of Civil Engineers, Ottawa.
- Woodward—Clyde Consultants (1980), "Assessment of the Morison Equation," Report N68305-80-C-0007 For the U.S. Naval Facilities Engineering Command, Washington, DC.

7.12 Problems

1. The flow velocity of water approaching a 1 m diameter sphere is given by $V = 1.2 + 1.75t^{1.5}$ where V is in m/s and t is in s. Determine the total force on the sphere at $t = 2$ s. Consult an elementary fluid mechanics text for any needed coefficients not given in this text.

2. A sphere having a diameter of 0.7 m is tethered 5 m below the still water level where the water depth is 10 m. A 6 s, 1 m high wave passes the sphere. Determine and plot the horizontal components of the drag, inertia, and total force on the sphere through one wave period. Assume $C_d = 0.6$ and $C_m = 1.5$.

3. A vertical 1 m diameter circular pile standing in water 14 m deep is subjected to a 4 m high, 9 s wave. Calculate and plot the drag, inertia, and total force distributions along the pile at the instant that the wave crest is 20 m seaward of the pile.

4. For the pile and wave condition given in Problem 3, determine the time interval before the arrival of that wave crest at which the maximum force occurs and determine that force. What is the maximum moment around the sea floor acting on the pile?

5. A horizontal cylindrical cross brace on an offshore tower having a 0.8 m diameter and a length of 9 m is located 6 m below the still water level. The water depth is 30 m. For a 12 s, 5 m high wave approaching normal to the axis of the brace, calculate and plot the drag, inertia and total horizontal forces on the brace as a function of time for one wave period.

6. The design wave for a lake has deep water values of $H_s = 2.5$ m and $T_s = 4.6$ s. The wave approaches shore with a $K_r = 0.87$ at the end of a pier located in water 5 m deep. The piles at the end of the pier have a diameter of 0.3 m. Determine the design moment around the sea floor and discuss the basis of the design wave you selected.

7. A 0.8 m diameter submerged pipeline resting on an essentially horizontal sea floor is subjected to a 4 m high, 11 s wave propagating normal to the pipeline axis. The water depth is 14 m. Assume a bottom friction coefficient of 0.8 and $C_d = 1.8$ and $C_t = 2.5$. What minimum weight per meter of length should the pipeline have if it relies on its weight for stability?

8. A floating tire breakwater is installed at a marina where the water depth is 4 m. The breakwater width in the direction of wave propagation is 12 m. If the incident wave height is 1.2 m with a period of 2.1 s what is the wave height in the lee of the breakwater? What is the wave height in the lee if the wave period is 4.1 s?

9. A revetment having a profile similar to that shown in Figure 7.5 is placed on the face of a small earth dam (1:3.5 slope). The toe of the revetment is at a depth of

2 m below the design water level and the bottom slope in front of the revetment is 1:50. For a design wave in deep water having $H_s = 1.9$ m and $T_s = 4.5$ s determine the median size armor stone required for zero damage of the structure. Assume $K_r = 0.78$. Select a desired crest elevation for the revetment.

10. What weight concrete tribars are needed as armor units for a breakwater (cross-section similar to Figure 7.4) if no damage is allowed and minor wave overtopping is assumed? The design water depth at the seaward toe of the breakwater is 6 m and the sea floor in front of the breakwater has a 1:20 slope. A design wave with $H_s = 4.9$ m and $T_s = 8$ s in deep water (assume $K_r = 1.0$) is to be used.

11. A submerged crest stone mound breakwater is constructed in water that is 5.1 m deep with its crest located 1.0 m below the still water level. The incident design wave has a significant height of 1.45 m and a significant period of 4.4 s. What median diameter stone is required for zero damage stability (assume specific gravity of stone is 2.65) if the face slope is 1:1.75?

12. Consider the breakwater in Problem 11; however, the crest is located 1.0 m above the design MWL. What median diameter armor stone is required for a stable structure?

13. A rigid vertical wall has a reflection coefficient of 0.9. The water depth at the toe of the structure is 3 m. For an incident wave having a height of 1.2 m and a period of 4.5 s, plot the total pressure along the wall when the crest of the standing wave is at the wall. Compare this to the linear distribution commonly assumed for design purposes.

14. A rigid vertical wall has a reflection coefficient assumed to be 0.95. The water depth at the toe of the wall is 4.2 m. What is the maximum moment around the toe of the wall for a 1 m, 6 s wave, assuming that a wave trough acts at the back side when a crest acts at the front?

15. A vertical wall is constructed on a beach with a 1:15 slope. The toe of the wall is at an elevation of +0.5 m above the mean water level. For a normally incident 2 m, 7 s design wave estimate the dynamic pressure on the wall. If this pressure is assumed to be constant across the wall, what is the total design force on the wall?

16. For the breakwater in Problem 10, estimate the wave reflection coefficient. If the crest height is located 2.4 m above the design water level and the crest width is 3.5 m, estimate the transmitted wave height owing to wave overtopping.

17. For the breakwater in Problem 10, what height above the design water level must the breakwater crest have if for the given wave condition only 10% of the waves are to run up above the crest elevation?

18. For the submerged breakwater in Problem 11, and the given wave condition, estimate the height of the transmitted wave.

8

Coastal Zone Processes

The zone of interest in this chapter is that segment of the coast located between the offshore point where shoaling waves begin to move sediment and the onshore limit of active marine processes. The latter is usually delineated by a dune field or cliff line, unless a line of structures is constructed along the coast. Most of the world's coastlines consist of sandy beaches. In some locations the beach is covered partially or completely with coarser stone known as shingle. Many shorelines consist of long beaches occasionally interrupted by a river, coastal inlet, or rocky headland. In other locations there are short pocket beaches between large headlands that limit the interchange of sediment between adjacent beaches.

Although sandy beaches predominate, some coastlines are fronted by steep cliffs at the water's edge that may or may not have a small beach at their toe. Where wave and current action is relatively mild and a river provides large deposits of sediment a delta may extend seaward of the line of the coast. The emphasis in this chapter is on those sections of the coast having a sandy beach.

Beach and nearshore sediments are continually responding to direct wave action, wave-induced littoral currents, currents induced by the wind and tide, and the wind directly. However, direct wave action and wave-induced littoral currents are usually the dominant factor in shaping beaches, except near coastal inlets where tide- and river-induced flow will typically dominate.

The stability of a section of sedimentary shoreline depends on a balance between the volume of sediment available to that section and the net onshore-offshore and alongshore sediment transport capacity of waves, wind, and currents in that section. The shoreline may thus be eroding, accreting, or remaining in equilibrium. If equilibrium does exist, it is usually a "dynamic equilibrium" where the shoreline is responding to continuously variable winds, waves, and currents. Also, the supply of sediment to the beach is usually variable in time and space. Dynamic equilibrium usually means that the average shoreline position is relatively stable over a period of months or years while the instantaneous position undergoes short-term oscillations.

Construction of structures, dredging of channels and harbors, beach nourishment with sand, and other projects in the coastal zone have often been carried out to limit or reverse shoreline erosion or accretion. At times, these projects have upset the existing dynamic equilibrium of adjacent shorelines. The result is a continuing shoreline change ultimately to reach a new equilibrium condition that may or may not be desirable.

Coastal developments can affect coastal zone processes by: (1) changing the rate and/or characteristics of sediment supplied to the coast, (2) adjusting the level of wave energy flux to the coast, and (3) directly interfering with coastal sediment transport processes. Two examples of the first effect are the construction of a dam that traps sediment on a river that otherwise would deliver the sediment to the coast, and the periodic placement of sand on a beach, to nourish the beach. Examples of the second and third effects respectively are: construction of a shore parallel offshore breakwater that intercepts waves approaching the shore to, in turn, reduce the wave-induced alongshore sediment transport; and construction of a shore perpendicular groin across the surf zone to directly interrupt wave-induced alongshore sediment transport.

This chapter first considers the characteristics of the sediment on a beach. Then shore normal and alongshore transport processes and resulting beach changes, including those caused by structures, are presented. Numerical models for predicting beach change are discussed. Beach nourishment, sediment bypassing past shoreline obstructions, and dune stabilization are presented. The chapter is concluded with a discussion of the concept of a sediment budget for a coastal segment, a useful tool in understanding beach behavior.

8.1 Beach Sediment Properties and Analysis

Of greatest interest are those physical properties of beach sediments that control their response to wind, wave, and current action and, in turn, are important to the design of engineering works in the coastal zone. We are primarily interested in noncohesive granular sediments. Physical properties of these sediments include:

1. Petrology or chemical constituents of the sediment grains
2. Specific gravity of the grain materials and the bulk specific weight of the granular mass
3. Bulk porosity and permeability of the granular mass
4. Grain shape
5. Representative grain sizes and size distribution

For engineering purposes, the representative grain sizes and size distribution are the most important beach sediment properties and the only properties commonly measured and employed in defining sediment properties.

The common procedures for measuring sediment size and size distribution—namely sieving and settling tube analysis—include the effects of some of the other properties. Sieving incorporates some aspects of grain shape and settling tube analysis incorporates grain shape and specific gravity. In the latter grain shape is incorporated in a better way in that the hydrodynamic behavior, as affected by shape, comes into play.

It can also be shown that the permeability of a granular soil mass is related to the sediment size and size distribution (e.g., see Krumbein and Monk, 1942).

Most beach sands consist predominately of quartz (2.65 specific gravity) with smaller portions of feldspar (2.54 to 2.64 s.g.) and a small content of a variety of heavy minerals (s.g. greater than 2.87). In tropical regions such as Florida and the Caribbean, beach sands are commonly derived from shallow water reefs and are largely calcium carbonate (2.72 s.g.).

Representative Size and Size Distribution

Sediment grains found in the coastal zone will have a wide variety of shapes. Grain sizes are given as a grain diameter. Whether the grain size measurement was done by sieving or settling tube analysis will yield a slightly different grain diameter for a given grain shape. The analysis technique should be considered when comparing grain size analyses.

A full range of sediment sizes from clay (less than one micron diameter) to gravel and boulders (tens of centimeters diameter) may be found in the coastal zone. Except for shingle beaches, most beaches consist of sand with grain diameters typically between 0.1 and 1 mm.

A number of formal sediment size classifications have been proposed; a commonly used classification is that proposed by Wentworth (1922) and given in Table 8.1. Since most sediment sample size distributions are skewed with a preponderance of finer sizes, the Wentworth scale is logarithmic with base 2. This allows a better definition of the finer sizes.

Many physical scientists define grain diameter by the phi unit ϕ proposed by Krumbein (1936) and based on the Wentworth size classification. For a grain diameter d given in mm,

$$\phi = -\log_2 d \quad (8.1)$$

where the minus sign is used so the more common sand grain diameters having $d > 1$ mm will have a positive phi value. Wentworth size class boundaries are thus whole numbers in phi units. However, the phi unit system can cause some confusion because phi units increase with decreasing particle size and each whole number interval represents a different range of particle sizes.

The grain size distribution and representative grain sizes are best defined by standard statistical techniques. Sediment sample size distributions are commonly represented by a cumulative size frequency distribution, which is a plot of the

Table 8.1 Wentworth Size Classification

Class	Particle Diameter	
	mm	phi units
Boulder	256	−8
Cobble	128	−7
	64	−6
Pebble	32	−5
	16	−4
	8	−3
	4	−2
Gravel	2	−1
Very coarse sand	1	0
Coarse sand	1/2	1
Medium sand	1/4	2
Fine sand	1/8	3
Very fine sand	1/16	4
	1/32	5
	1/64	6
	1/128	7
	1/256	8

cumulative percent of the grains having a diameter that is coarser (or finer) than a particular size versus grain size given either in mm or phi units. Figure 8.1 is an example of such a distribution for a beach sand sample.

The important characteristics of a sediment sample cumulative size frequency distribution can generally be defined by three statistical parameters: the central tendency (mean, median, or modal diameter), the dispersion or sorting (standard deviation), and the possible asymmetry (skewness). The median diameter is easiest to determine from a cumulative size frequency diagram and is less affected by a small percentage of extremely large or small sizes than is the mean, so it is usually used to define central tendency. As sediment is transported down a river and deposited at the coast, the coarser sizes often remain behind in the river bed and the finer sizes are usually deposited offshore, so beach sediments are usually well sorted sand (i.e, have a relatively narrow size range). As discussed above, beach sand grain diameters are usually skewed toward the finer sizes.

The most commonly used parameter in engineering practice to define a beach sand sample is the median diameter d_{50} given in mm. For the sample depicted in Figure 8.1 $d_{50} = 0.23$ mm. Several other descriptive measures, based on sediment

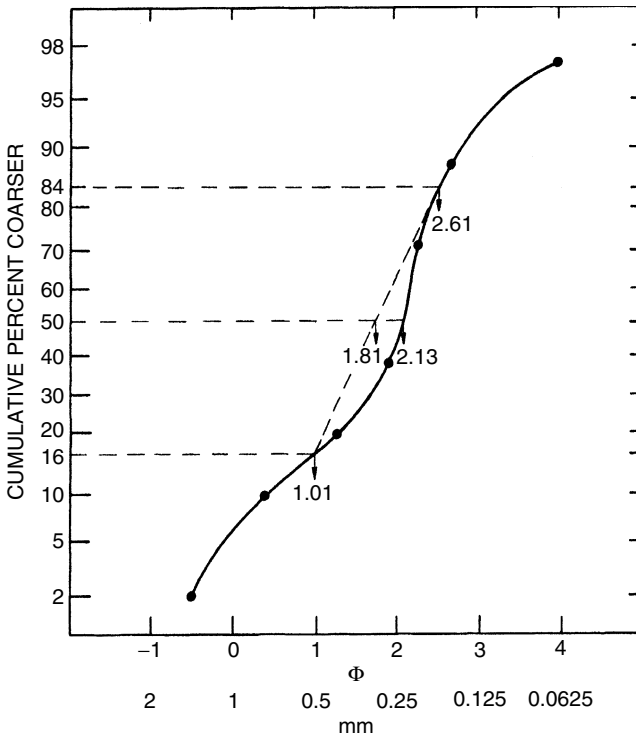


Figure 8.1. Plot of typical sand sample size analysis.

Table 8.2. Sediment Sample Descriptive Measures

Measure	Name	Definition
Central tendency	Phi median diameter	$M_{d\phi} = \phi_{50}$
	Phi mean diameter	$M_{\phi} = \frac{1}{2}(\phi_{16} + \phi_{84})$
Sorting	Phi deviation measure	$\sigma_{\phi} = \frac{1}{2}(\phi_{84} - \phi_{16})$
Skewness	Phi skewness measure	$\alpha_{\phi} = \frac{M_{\phi} - M_{d\phi}}{\sigma_{\phi}}$

after Inman, 1952.

size analyses, have been proposed to define the central tendency, sorting and asymmetry of a sediment sample (see Griffiths, 1967 for a listing and discussion of these parameters). One system commonly used in engineering practice was developed by Inmann (1952). A portion of this system is presented in Table 8.2 where

ϕ_{16} , ϕ_{50} , and ϕ_{84} are the 16, 50, and 84% coarser phi diameters from the cumulative frequency size distribution.

In an arithmetic normal distribution the spacing between the 16th and the 84th percentiles is two standard deviations. This suggests the definition of the phi deviation measure, which indicates the spread or sorting of the sample from the median size. These percentiles are also used to define the phi mean diameter by averaging the phi value at two separated reasonably representative values. The phi skewness measure gives an indication of the displacement of the median value from the mean value and thus indicates the sample skewness. The phi deviation measure is used in the denominator so the phi skewness measure is independent of the actual sediment size.

The descriptive measures defined in Table 8.2, when evaluated for the sample described by Figure 8.1 yield

$$M_{d\phi} = 2.13$$

$$M_{\phi} = (2.61 + 1.01)/2 = 1.81$$

$$\sigma_{\phi} = (2.61 - 1.01)/2 = 0.80$$

$$\alpha_{\phi} = (1.81 - 2.13)/0.80 = -0.40$$

A discussion of beach sediment sampling and grain size analysis is presented in Chapter 9.

8.2 Beach Profiles and Profile Change

Waves that reach a sandy shore, then break and run up on the beach face, will continually reshape the beach. This continuous reshaping occurs because the incident wave characteristics (height, period, and/or approach direction) are seldom constant for any significant time span. Reshaping of the beach is caused by the wave-induced currents that develop in the surf zone and, by the direct action of the waves through turbulence generated by the breaking waves and the surge of water up and down the beach face. Concurrent reshaping of the beach owing to wave-induced sediment transport takes place both in the on-/offshore directions and in the alongshore direction. Although these effects occur together it is easier to consider them separately. This section focuses on the natural beach profile geometry and the wave-induced changes that occur for a typical shore-normal beach profile. Alongshore processes will be considered in the two subsequent sections.

Mechanisms Causing Beach Profile Change

There are a number of mechanisms that can cause the transport of sand across a beach profile. Some of these mechanisms will only transport sand in the offshore direction leading to profile retreat, while others will only transport sand onshore building up the profile. And, there are mechanisms that can cause either profile

buildup or retreat depending on the wave and water level conditions, local beach slope and sand characteristics. These mechanisms are described below.

- As a wave propagates shoreward in the nearshore zone there is an asymmetry in the horizontal water particle velocities at the sea floor, with a higher and shorter duration onshore velocity under the wave crest and a lower and longer duration offshore velocity under the wave trough. The resulting shear stress exerted on a bottom sand grain depends on the water particle velocity squared. Consequently, there will be a larger onshore stress followed by a significantly lower offshore stress. The net bottom stress will act in the onshore direction. The resulting onshore transport tendency is increased owing to the fact that a certain threshold stress must be exceeded for a bottom particle to move.
- Beaches typically slope seaward across the entire profile (except for a short segment on the landward face of offshore bars). Thus, a component of gravity will typically act in the offshore direction on a bottom sand grain.
- Wave-induced setup in the surf zone will lead to a bottom return flow in the seaward direction (undertow) that will exert a seaward stress on sand grains. Also, on a long segment of beach where a significant alongshore current develops, there may be spatially periodic seaward flowing rip currents (see Section 8.3) that can transport large volumes of beach sand seaward.
- Turbulence caused by breaking waves in the surf zone will suspend sediment – the suspension being intermittent with the breaking of successive waves. The net transport of sand will be controlled by the net time-integrated horizontal flow velocity during the interval of sediment suspension. This mechanism may transport sediment in either the onshore or offshore direction.
- Onshore winds will exert an onshore stress on the water surface and a consequent return flow at the bottom that can assist in transporting sand seaward.

This summary indicates the complexity of mechanisms that operate to form a beach profile and to establish the grain size distribution across this profile. This complexity is compounded by the fact that the different mechanisms have significantly different strengths and these relative strengths vary as the wave, wind and water level conditions vary.

Beach profiles measured normal to the shoreline over the zone of active coastal processes are of great importance to coastal engineering studies. This active zone normally extends from the onshore cliff, dune, or structure line to a point offshore where there is little significant wave-induced sediment movement (at a typical depth of about 10 m for the open ocean). Over this active zone a portion of the beach profile can change drastically in a few hours because of a sudden increase in wave activity.

Beach profile data are important for an understanding and quantification of coastal zone processes and the related interaction of coastal structures with these

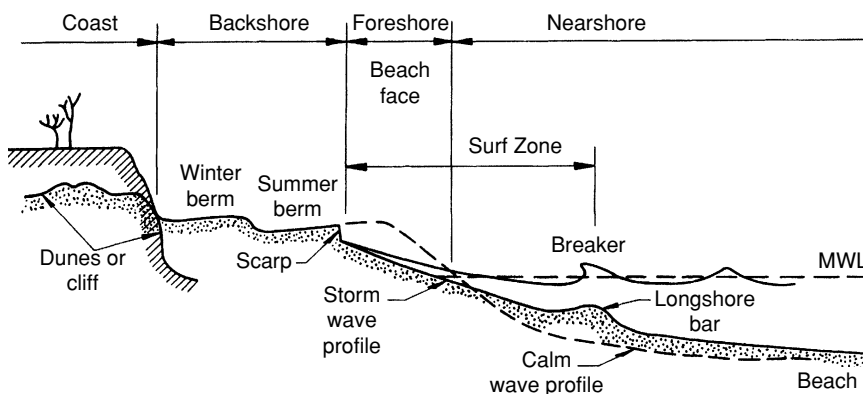


Figure 8.2. Typical beach profiles (vertical scale exaggerated) and terminology.

processes. The total seasonal envelope of profile change must be defined, for example, for the design of such coastal structures as groins, piers, seawalls, and marine pipelines that cross the coastal zone, as well as for the establishment of coastal boundaries and the design of beach nourishment projects.

Figure 8.2 shows typical somewhat idealized beach profiles. Progressing seaward from the dune, cliff, or structure line a beach profile typically includes one or two relatively flat berms that slope landward, a seaward sloping foreshore where the active wave runup on the beach face takes place, and a concave nearshore profile, possibly having one or more breakpoint bars lying approximately parallel to the shore. The above assumes a sufficiently wide beach for these features to develop. If the beach is narrow, the beach face may extend directly to the dune, cliff, or structure line.

The dashed line in Figure 8.2 defines the profile that would be established after a relatively long period of calm wave action. Sand is slowly transported landward to build the beach face in the foreshore zone and to extend the berm seaward, thus causing a steeper beach face profile slope. With the appearance of higher and steeper waves common during a period of storm activity sand is transported seaward so the profile can be expected to adjust to the form shown by the solid line. The beach profile in the vicinity of the mean water level is thus cut back and the slope is flattened. A scarp will form at the edge of the berm. The sand transported offshore will build a larger offshore bar around the point of wave breaking. If the wave attack is severe or after a series of storms the profile may be cut back to the dune or cliff line, causing recession of these features.

At most coastal locations, storm waves predominate during the winter months and calmer waves occur during the summer. Thus, the terms winter and summer profile are often used to define the two types of beach profile. But hurricanes on the Atlantic and Gulf coasts and summer storms in the Pacific southern hemisphere can cause the recession of the beach profile during the summer.

The beach berm is constructed during calm wave periods when waves run up on the beach face and deposit sand. Consequently, the elevation of the crest of the berm is closely tied to the mean elevation of wave runup as the beach face is building.

The beach face slope, which varies with the steepness of the incident waves as discussed above, also depends on the sand size that constitutes the beach face. This is demonstrated in Figure 8.3, which is a plot of the beach face slope as a function of the median sand grain diameter (at the mid-tide elevation on the beach face) for high-energy and low-energy wave exposure. For the same incident wave energy level a beach made of a coarser sand will have a steeper beach face slope. Conversely, for a given sand size, beaches exposed to higher wave energy will have a flatter beach face slope (as discussed above). For example, the beaches of the northern shores of New Jersey have typical average median grain diameters of around 0.4 to 0.5 mm and beach face slopes around 1:10 to 1:15, while the beaches on the southern shore (which have about the same wave exposure) have typical average median grain diameters of around 0.15 to 0.25 mm and, consequently, much flatter slopes around 1:40.

Nearshore bar geometry and spacing closely respond to the predominant wave action. With the occurrence of higher waves a bar will move seaward (as will the wave breaker line), and the size of the bar will grow. With the return of lower waves the bar may be stranded at its seaward position while a new smaller bar is

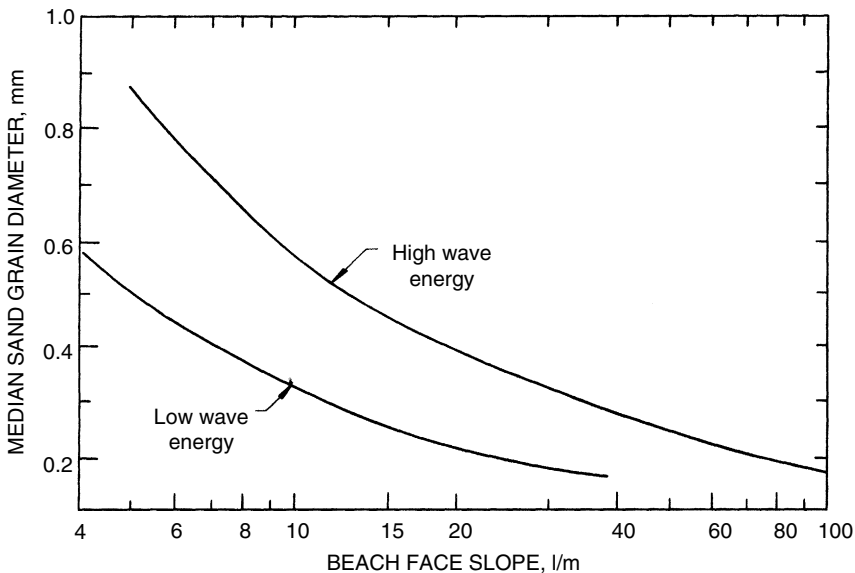


Figure 8.3. Beach face slope versus median sand grain diameter for high and low wave energy exposure. (Modified from Wiegand, 1964.)

formed closer to the shore. During extremely low waves no bars will be built. Shore parallel bars are also less common where the tide range is large.

The occurrence of a calm or storm wave profile depends on the beach sand properties as well as the incident wave characteristics. One relationship, derived from Kriebel et al. (1986), indicates that the parameter $H_0/V_f T$, where V_f is the settling velocity of a sand grain in still water, appears to be a useful indicator of profile characteristics. When the value of this parameter exceeds about 2 to 2.5 an erosive or storm wave profile will develop whereas when the value of this parameter is less than about 2 to 2.5 the beach face accretes.

A beach profile may recede as much as 30 m in the landward direction during a single intense storm. If much of the beach sand is carried too far offshore for subsequent return to the beach face and the nearshore zone by calm waves, and there is insufficient net sand accumulation from alongshore transport processes, permanent recession of the shoreline will result. Seelig and Sorensen (1973) studied shoreline position changes during the past century at 226 points along the 650 km long Texas coast. The MLW shoreline position at 50% of the points showed a small rate of change of less than ± 2 m/year. But at 40% of the points a net shoreline recession in excess of 2 m/year, with extreme rates in excess of 10 m/year, was observed. The remaining 10% of the points, mainly near jettied inlet entrances, showed shoreline net advances in excess of 2 m/year.

The sand size, as indicated by the median grain size for a sample, will vary along the beach profile, particularly for beaches with coarse composite sizes. From a study of samples from several Pacific coast beaches, Bascom (1951) found the sand to be the coarsest at the plunge point in the wave breaker zone where the highest turbulence levels occur. The next coarsest sand was found on the berms, likely because of the winnowing of finer sizes by the wind. Where a dune field exists, the dune sand was progressively finer in the landward direction. Sand grain sizes also progressively decreased in the seaward direction from the surf zone.

In addition to wind wave-induced beach profile changes, there will be a recession of the beach profile if there is a relative rise in mean sea level as has been historically happening along most coastlines of the world. Besides the flooding of a profile caused by a relative rise in MSL, there will be an adjustment of the profile as sand is transported offshore and the MSL position on the beach face is shifted landward to produce a recession of the shoreline. Bruun (1962) discussed this process and presented a procedure to analyze the distance a shoreline will retreat owing to a given small rise in MSL. Weggel (1979) presents techniques for the practical application of the Bruun procedure.

Equilibrium Beach Profiles

As discussed above, as the wave and water level conditions vary, the beach profile will respond by changing. A useful concept, however, is the equilibrium beach profile. This is the mean profile that would occur when profiles are

measured over a period of several years. This concept is useful for a variety of coastal engineering analysis and design purposes including:

- Some numerical models for alongshore morphology change require a representative beach profile.
- When before and after beach profiles are required for the computation of beach nourishment volumes.
- When analyses are to be conducted to define the impact of long term sea level change.
- For analyses of the impact of coastal structures such as seawalls on the resulting beach profile.

For example applications of the equilibrium beach profile concept to the purposes listed above, see Dean (1991).

The most common form of an equation to define the equilibrium beach profile is

$$z = Ax^n$$

where z is the depth below the mean water level for a given distance x offshore. The power n is commonly taken as two-thirds based both on empirical data (Bruun, 1954 and Dean 1987) and on physical reasoning (see Dean and Dalrymple, 2002). The coefficient A is related to the settling velocity of sand grains in water which, in turn, can be related to the sand grain particle diameter D . A useful relationship for A is $A = 0.21 D^{0.48}$ (Dean, 1987) where D is given in mm and A has the units of $m^{1/3}$.

This equilibrium beach profile equation defines a profile that is concave and has an increasing slope at given point for increasing sand grain diameters. However, it also predicts an infinite slope at the shoreline ($x = 0$) so it should not be applied very close to the shoreline. Other more complex profile form equations have been proposed that overcome this problem (see Komar, 1998).

Beach Profile Closure Depth

Seaward of some point along a beach profile in the offshore direction there will be insignificant sand transport for a given wave condition. This point will be further offshore for higher and longer period waves. However, for coastal engineering design, it is desirable to define a profile closure depth at some offshore point where there is negligible profile change for some significant level of wave action. Definition of this profile closure depth is useful, for example, for establishing the seaward limit of the placement of beach sand during a beach nourishment project, deciding at what water depth a pipeline placed across the nearshore zone might no longer need to be buried, or deciding how far seaward to make beach profile measurements for a beach monitoring program.

Hallermeier (1977) defined a closure depth d_c that “gives a seaward limit to extreme surf-related effects, so that significant alongshore transport and intense onshore-offshore transport are restricted to water depths less than d_c .” This depth was developed from laboratory data and limited field data. Birkemeier (1985), using more extensive field data modified Hallermeier’s formulation for closure depth to

$$d_c = 1.75 H_s - 57.9[H_s^2/gT_s^2]$$

where H_s is the extreme nearshore significant wave height in meters exceeded 12 hours per year and T_s is the associated wave period. Birkemeier found that a reasonable fit to the data can also be obtained by the simpler relationship

$$d_c = 1.57H_s$$

where H_s is again defined as that height occurring on average 12 hours per year. It can be shown (U.S. Army Coastal Engineering Research Center, 1985) that this relationship becomes

$$d_c = 6.75H_s$$

where H_s is now the mean average significant wave height. Of course, a better way to determine the closure depth for a given coastal site is to accurately measure the beach profile many times over the period of a year and determine the depth at which there are no significant depth variations over that time period.

8.3 Nearshore Circulation

Sustained winds blowing along the coast will generate an alongshore coastal current. Propagation of the tide along the coast coupled with Coriolis acceleration will generate reversing coastal currents. The tide may also generate strong reversing currents at inlet, harbor, and estuary entrances. The ebb flow of these currents may be supplemented by river and surface runoff. However, away from the immediate influence of tide-generated currents at coastal inlets, the dominant alongshore currents are those in the surf zone generated by waves breaking oblique to the shoreline. These wave-induced longshore currents and the associated surf zone wave-induced turbulence are responsible for most of the alongshore sediment transport in the nearshore zone.

Figure 8.4 is a schematic plan view of a portion of the foreshore–nearshore zone with waves approaching at an angle to the shoreline, breaking and running up on the beach face. Also shown is the resulting longshore current velocity distribution, which extends from a point just seaward of the wave breaking line in to the beach face. The maximum current velocity is typically in the surf zone just inside of the breaker line.

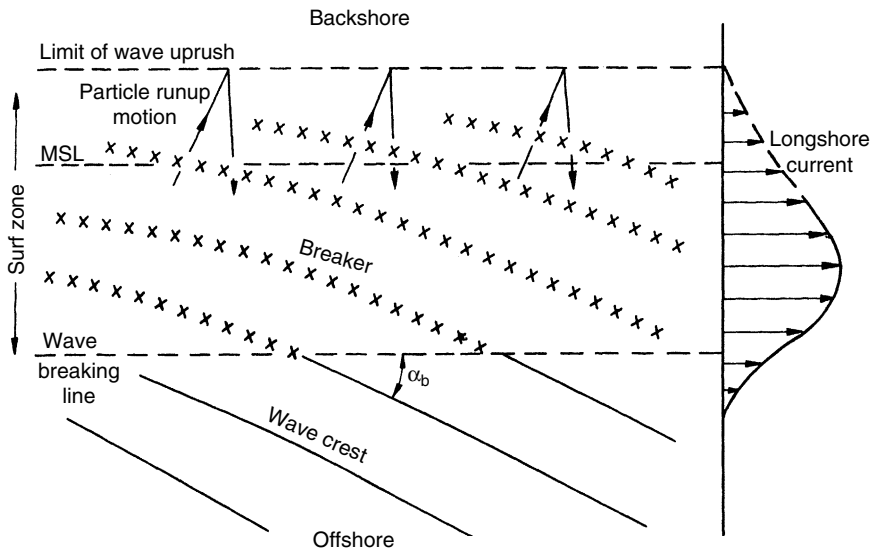


Figure 8.4. Wave-generated longshore current.

Szuwalski (1970) presents the results of nearly 6000 longshore current velocity measurements made at a number of coastal locations in California. The vast majority of the measurements yielded velocities under 0.5 m/s with only occasional velocities reaching a value of 1 m/s. These values are consistent with results presented by Ingle (1966) and Komar (1975). Although these velocities are relatively low, the longshore current's capacity to transport sediment is significantly increased by the turbulence generated in the surf zone by wave breaking.

The mechanism primarily responsible for wave-generated longshore currents is the alongshore component of radiation stress in oblique breaking waves. Also, variations in the alongshore distribution of wave breaker heights will cause alongshore variations in the surf zone wave setup and the generation of currents from areas of high waves to area of low waves. These two mechanisms may support or oppose each other in establishing a longshore current. On most sections of coastline, the former mechanism (oblique wave breaking) will predominate.

Successive waves in a wave train will have different heights and periods. Often the arriving waves consist of alternating groups of higher and lower waves, resulting in pulsating components of radiation stress. Thus, the wave-induced long-shore current often exhibits a pulsating behavior having a period of a few minutes.

The most promising analytical approach to longshore current prediction is based on the work of Longuet-Higgins (1970). He equated the alongshore

component of radiation stress with the bottom frictional resistance developed by the longshore current. A modified form of the Longuett-Higgins equation for longshore current velocity, based on calibration with field data, is given by the U.S. Army Coastal Engineering Research Center (1984) as

$$U = 20.7 m(gH_b)^{1/2} \sin 2\alpha_b \quad (8.2)$$

In Eq. (8.2) U is the average longshore current velocity across the surf zone, m is the bottom slope in the surf zone, H_b is the wave breaker height, and α_b is the wave breaker angle (see Figure 8.4). Although Eq. (8.2) is generally considered to be the best available for longshore current velocity prediction, the difference between predicted and observed velocities can exceed 50%. If there is a sustained alongshore wind, the wind stress acting on the surf zone can accordingly modify the wave-induced current. Likewise, an alongshore current just seaward of the surf zone can, through turbulent momentum exchange, modify the surf zone current.

Example 8.3-1

A train of waves has a height of 1.3 m and an approach angle of 15° at the breaker line. The average beach slope in the surf zone is 1:30 ($m = 0.033$). Estimate the alongshore flow rate in the surf zone.

Solution:

From Eq. (2.68) the water depth at the breaker line will be approximately

$$d_b = H_b/0.9 = 1.3/0.9 = 1.44 \text{ m}$$

This assumes that the wave is a shallow water wave, a reasonable assumption in most cases. The width of the surf zone will then be $1.44(30) = 43.2$ m and the surf zone cross-section area will be $1.44(43.2)(0.5) = 31.1 \text{ m}^2$.

From Eq. (8.2) the average current velocity in the surf zone will be

$$U = 20.7(0.033)(9.82 \times 1.3)^{0.5} \sin 30^\circ = 1.22 \text{ m/s}$$

From continuity, the flow rate will be the average velocity times the cross-section area or $1.22(31.1) = 37.9 \text{ m}^3/\text{s}$.

If a longshore current is intercepted by a headland or a structure (e.g., groin or jetty) oriented normal to the shoreline, it will be deflected seaward as a rip current and dissipated. A new current will develop downcoast of the obstruction. Even on a long, relatively straight, uninterrupted shoreline the longshore current will often be interrupted by a seaward flowing rip current that relieves the

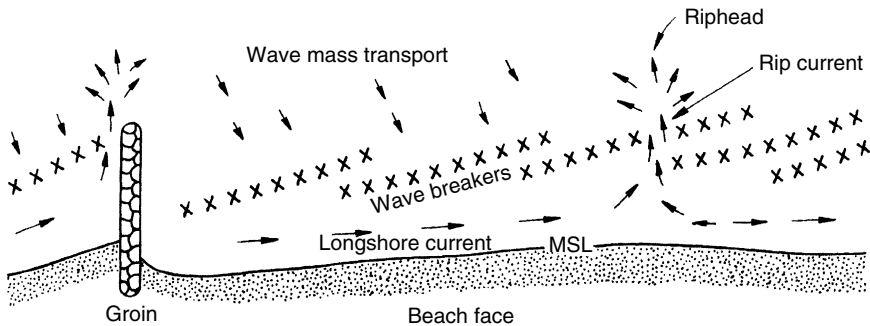


Figure 8.5. Typical wave-generated nearshore circulation.

continuous accumulation of water in the surf zone. This is demonstrated in Figure 8.5. The rip current will likely be situated at a position of lower incident wave heights and will usually scour a seaward trough, helping to stabilize its position. Shorter period incident waves tend to produce more frequent but smaller rip currents.

8.4 Alongshore Sediment Transport Processes and Rates

The wave-induced current in the surf zone and the turbulence induced by wave breaking combine to cause alongshore sediment transport on beaches. Sand is transported both in suspension and along the bed (suspended and bed loads, respectively). The suspended load is relatively high where wave breaking is most active, i.e., near the breaker line for plunging breakers but more evenly spread across the surf zone for spilling breakers. In addition, the oblique wave runup and gravity-induced return flow on the beach face (see Figure 8.4) cause a “zig-zag” sand particle motion on the beach, with a net movement in the downcoast direction.

For both the suspended and bed load transport modes, finer sand sizes will be carried in larger volumes and over longer distances than coarser sizes. A consequence of this is that sediment from a particular point source (e.g., a stream entering the coast) will have successively finer median diameters at greater downcoast distances from the source.

When considering longer term longshore sediment transport rates (volume per time, typically per year), it is important for coastal engineering design to distinguish between the net and gross rates at a particular coastal location. The annual directional distribution of the alongshore component of wave energy flux and the resulting sediment transport rate distribution will commonly be divided in the upcoast and downcoast directions. (The direction of predominant transport

being termed the downcoast direction.) The annual directional distribution of wave energy may cause the transport rate in one direction to be so predominant that the gross transport is just slightly larger than the net transport rate. On the other hand, the transport rates may be approximately equal in both the upcoast and downcoast directions so that a large gross transport rate may produce a net transport rate near zero.

Longshore transport rates are usually given as annual volumes of transported sediment, but it must be remembered that the shorter term rates can be extremely variable, exceeding the average annual rate by several times during a storm and falling to near zero during the periods of low incident waves. Seasonal variations (often summer versus winter) can also be quite variable both in rate and direction. In addition, annual transport rates can be quite variable from year to year owing to fluctuations in the wave climate, modifications to coastal structures that impact the transport rate, and variations in the volume of sediment available from a major source (e.g., a river that has large flood flows only periodically and is nearly dry the remainder of the time).

Longshore Transport Rates

Some average annual net longshore transport rates and directions are listed in Table 8.3 to demonstrate the order of magnitude and variability of transport rates on U.S. beaches. These rates have been obtained from Army Corps of Engineers project reports and U.S. Congress House Documents, and were summarized in the U.S. Army Coastal Engineering Research Center (1984). It should be noted that some of the rates (especially along the New Jersey coast, e.g., see Sorensen, 1990) no longer occur owing to the construction of structures that have limited sediment sources and controlled longshore transport. Some of the variability in rates for nearby locations is due to the fact that the rates were averages determined for different time spans. The net rate of $765,000 \text{ m}^3/\text{year}$ at Oxnard Plain Shore is also essentially the gross rate, as transport is strongly unidirectional. On the other hand, the Gulf shore at Corpus Christi is near a converging nodal point where the net transport is near zero, but the gross transport rate is estimated to be around $550,000 \text{ m}^3/\text{year}$.

Many of the transport rates listed in Table 8.3 were determined primarily by hydrographic surveys of the volume of sand trapped upcoast or eroded downcoast of a groin, jetty, or other structure that creates a barrier to littoral sediment transport. The rate at Sandy Hook was determined by surveys of the rate of growth of Sandy Hook, a terminal spit. Some of the rates may be underestimates because most structures do not act as complete barriers to longshore transport. Transport rate estimates have also been made from periodic dredging records at harbor entrances where a dredged entrance channel crosses the surf zone and is sufficiently wide and deep to act essentially as a sediment trap.

Table 8.3. *Estimated Net Longshore Transport Rates and Directions*

Location	Net Rate(m ³ /yr)	Direction
Sandy Hook, NJ	355,000	N
Asbury Park, NJ	153,000	N
Shark River, NJ	229,000	N
Manasquan, NJ	275,000	N
Barnegat Inlet, NJ	191,000	S
Absecon Inlet, NJ	306,000	S
Cold Spring Inlet, NJ	153,000	S
Ocean City, MD	115,000	S
Atlantic Beach, NC	22,500	E
Hillsboro Inlet, FL	57,000	S
Pinellas County, FL	38,000	S
Perdido Pass, AL	153,000	W
Santa Barbara, CA	214,000	E
Oxnard Plain Shore, CA	765,000	S
Port Hueneme, CA	382,000	S
Santa Monica, CA	206,000	S
El Segundo, CA	124,000	S
Camp Pendleton, CA	76,000	S
Milwaukee County, WI	6,000	S
Racine County, WI	31,000	S
Kenosha, WI	11,000	S

Functional design of many coastal projects requires that estimates of the local net and gross longshore sediment transport rate be made. Examples of these types of projects include the design of a system to mechanically bypass sediment past some obstruction such as a harbor entrance, or estimation of future periodic maintenance dredging requirements for a channel that is to be dredged across the surf zone. These estimates can often be made in one of the following ways:

1. If the longshore transport rate has been established at a nearby location with similar beach characteristics, shoreline orientation, and annual wave climate, this rate can be adapted to the project site with possible modifications to adjust for local conditions. This requires good engineering judgment because the transport rate can change significantly over short distances along the coast as well as with the passage of time. The establishment of a sediment budget for the local coastal area (see Section 8.9) can be helpful in this effort.
2. If there are nearby traps to littoral transport and data defining the induced beach changes that have occurred over a period of time are available or can

be collected, transport estimates can be made. When evaluating these data to estimate the transport rate, due consideration must be given to the effectiveness of the trap and the seasonal and long-term variability of the transport rate that can occur.

3. A number of longshore transport rate formulas have been established that relate the transport rate to the incident wave climate and beach characteristics (see Horikawa, 1988 for a summary). To establish the transport rate at a site using these equations the wave climate (wave height and direction) for at least a year should be determined from wave measurements and/or wave hindcasts.

The best known and easiest to apply longshore transport formula is the CERC formula (U.S. Army Coastal Engineering Research Center, 1984). Also see Bodge and Kraus (1991) for a discussion of this formula. The volumetric longshore sediment transport rate Q is given by

$$Q = K \sqrt{\frac{g}{\gamma}} \frac{H_b^{5/2} \sin 2\alpha_b}{16(s-1)a'} \quad (8.3)$$

where γ is the ratio of wave height to water depth at breaking which may be taken as 0.9, a' is the ratio of solid to total volume for the sediment and may be taken as 0.6 if better information is not available, and s is the sediment specific gravity which may be taken as 2.65 if better information is not available. H_b is the wave breaker height, commonly taken as the significant wave height at breaking. K is a coefficient commonly taken as 0.32 for typical beach sands. For much coarser shingle beaches the appropriate value of K would be much smaller (possibly by a factor of 10 to 20).

It should be noted that the transport rate given by Eq. (8.3) is the potential transport rate, meaning that it is the transport rate if sand is available across the entire surf zone to be transported. For example, at some Caribbean beaches that consist of a narrow beach fronted by fringing coral reefs over a portion of the surf zone, the actual transport rate is often much smaller than the rate given by Eq. (8.3). There is also some indication that the coefficient K varies with the wave breaker type and beach slope (see Bodge and Kraus, 1991).

Example 8.4-1

During the peak of a storm, waves approach a beach with their crests oriented at an angle of 12° with the shoreline and a significant wave height of 2.1 m at the breaker line. Estimate the hourly potential longshore transport rate at this site during the storm peak.

Solution:

Using Eq. (8.3) with the suggested values for the various coefficients and other parameters yields

$$Q = \frac{0.32}{16} \sqrt{\frac{9.81}{0.9}} \frac{(2.1)^{5/2} \sin 24^\circ}{(2.65 - 1)0.6}$$

$$= 0.173 \text{ m}^3/\text{s} (623 \text{ m}^3/\text{hour})$$

8.5 Shore Response to Coastal Structures

Structures are constructed in the coastal zone primarily to stabilize or expand a segment of the beach, to protect the coastline in the lee of the structure from wave-induced damage and flooding, to protect and stabilize navigable entrance channels, and to provide a sheltered area for moored vessels. In essentially all cases these structures interact with the active wave, current, and resulting sediment transport processes in the vicinity of the structure.

For discussion purposes most of these structures can be grouped into three classes: (1) structures constructed essentially perpendicular to the shoreline and attached to the shore, (2) structures constructed essentially parallel to the shore on the beach face or berm, and (3) structures constructed offshore essentially parallel to the shoreline, and commonly segmented.

Shore-Perpendicular Structures

This class of structures includes groins that trap sediment being transported along the coast in the surf zone or sediment that has been mechanically placed on the beach where there is a potential for longshore transport and jetties, which are typically more massive than groins, extend further seaward, and are constructed to stabilize and protect a navigable channel across the coastline.

Figure 8.6 shows, in plan view, the shoreline response to a single shore perpendicular structure exposed to waves arriving from the dominant direction shown. Depending on the width of the surf zone the structure may trap some or most of the longshore sediment transport. This will cause an upcoast accumulation of sediment (A) plus the deposition of sediment at (B) owing to the rip current that will develop along the upcoast face of the structure. Downcoast of the structure (C) the beach will erode to satisfy the potential sediment transport capacity of the waves at that point. Both upcoast and downcoast of the structure, the shoreline will adjust so that it will parallel the incoming wave crest positions as affected by refraction and diffraction. Some sediment will be transported past the structure as the upcoast segment of the beach is filling, particularly if the crest

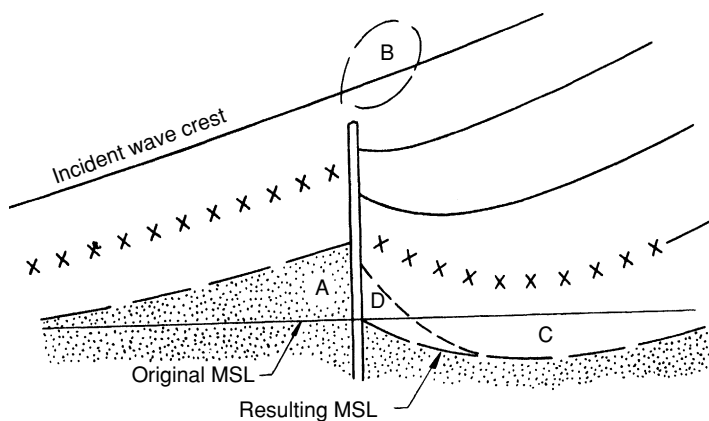


Figure 8.6. Shore response to placement of a shore-perpendicular structure.

of the structure is not too high and/or the structure is somewhat permeable to sand movement. After the upcoast beach segment is full all of the longshore transport will pass either through, over, or around the structure, some of it being deposited offshore downcoast of the structure and the remainder of the sediment being transported to and along the shore.

Usually, the wave direction and breaker height are continually changing so complete equilibrium between the incident wave crest and the shoreline orientation is never completely achieved. The beach is continually adjusting to the changing wave characteristics. However, if the waves come from one predominant direction with only occasional reverses, the resulting shoreline will closely approximate that shown in Figure 8.6. Waves from the other direction would transport sediment back toward the structure to form the fillet at D which would be difficult to remove when the waves return to the predominant direction.

The amount of sediment that passes a filled structure and returns to the downcoast shore depends on how much sediment moves over and through the filled structure and how long the structure is compared to the width of the surf zone (which varies with the incident wave height and tide range). The recommended design profile for a groin consists of a horizontal crest across the beach berm to the seaward extent to which it is desired to retain sand, followed by an intermediate downward sloping section paralleling the beach face to a second horizontal section out to the end of the groin and set at MLW or MLLW (U.S. Army Coastal Engineering Research Center, 1984). The groin essentially acts as a template for the desired beach profile just upcoast of the groin.

A shoreline response similar to that shown in Figure 8.6 would also develop at a pair of jetties constructed at the entrance to a harbor or interior bay. A portion of the sediment that moves past the offshore end of the upcoast jetty would be transported further offshore if there is a sufficiently strong tidal ebb current.

A tidal flood current will transport some of the bypassing sediment into the harbor or bay. Since the purpose of a jetty system is not to trap longshore sediment transport and jetties are typically much longer than groins, a mechanical sediment bypassing system may be necessary.

A common method of preventing beach erosion or rebuilding eroded beaches is to construct a series of groins along the shore to trap and hold existing longshore transport and/or to be artificially filled with sand (Figure 8.7). A system of groins can be constructed one section at a time by beginning at the downcoast end and adding new groins as the spaces between the older groins are filled with sand. If the entire system is constructed at one time, the updrift groins will fill first, and the shoreline between the remaining groins will adjust to the incident waves and subsequently fill as sediment begins to bypass the upcoast groins. Remember, erosion will occur downcoast of the groin system at a rate approximately equal to the rate of sediment deposition in the system (in addition to any natural net erosion that was occurring at the site prior to groin construction). Because of this downcoast erosion it may be desirable to artificially fill the groin system with sand (see Section 8.7). A groin system will not interfere with the on-/offshore transport of sand that occurs with the arrival of calm/storm wave conditions and that may produce a net longer term erosion or accretion.

The common ratio of groin spacing to length (MSL shoreline to seaward end) is between 1.5:1 and 4:1, the ratio depending on the resulting shoreline orientation which in turn depends on the angle of incidence of the dominant waves. A design engineer must consider the annual range of incident wave conditions and, from this, anticipate the resulting range of shoreline positions that will develop. It is important that the groins not be flanked by erosion at the landward end, particularly when newly constructed upcoast groins temporarily deny littoral drift to a downcoast segment or when extensive erosion occurs downcoast of the last groin in a system.

Shore-Parallel Onshore Structures

Seawalls, revetments, and bulkheads constitute this class of coastal structures. Seawalls are massive structures that primarily rely on their mass for stability. Examples are stone mounds and monolithic concrete structures similar to the seawall at Galveston, Texas. Revetments (see Figure 7.5) are an armoring veneer

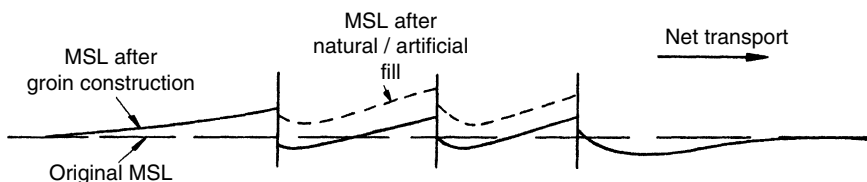


Figure 8.7. Shore response to a series of shore-perpendicular structures.

on a beach face or sloping bluff and are typically installed where the wave climate is milder than where seawalls are employed. Bulkheads are a vertical wall with tiebacks into the soil placed behind the bulkhead. They function more as an earth retaining structure than as a structure designed primarily to withstand wave attack. See the U.S. Army Coastal Engineering Research Center (1984) for examples of these structures.

This class of structures is designed primarily to protect the shore landward of the structure and typically will have little effect on the adjacent upcoast and downcoast areas. However, if they are built to maintain a section of shoreline in an advanced position, this outward jutting section of the shoreline will act as a headland and may trap some portion of the longshore sediment transport. The upcoast and downcoast ends of these structures must tie into a noneroding portion of the shore or must be protected by end walls so the structure is not flanked by the erosion of adjacent beaches.

When storm waves arrive, the beach profile in front of these structures will be cut back as depicted in Figure 8.2 with the wave agitation caused by the structure often increasing the amount of profile cutback over that which would occur at a nonstructured profile. The amount of beach face profile cutting that occurs would likely be greater at a vertical-faced solid structure than at a sloped stone mound structure owing to the higher wave reflection of the former. For this reason, the toe of these structures must be placed sufficiently deep into the beach face or stabilized by placing a stone mat or vertical cutoff wall at the toe. When calm waves return the beach in front of the structure will usually rebuild to its prestorm condition.

A shore parallel onshore structure will impact littoral processes in two ways. By preventing erosion of the shore it limits this section of the shore as a possible source of sediment for longshore transport. If the structure is built seaward of the water line it will reduce the size and transporting capacity of the surf zone, unless the increased surf zone wave agitation due to the structure counteracts this effect.

Shore-Parallel Offshore Structures

Figure 8.8 shows, in plan view, a shore-parallel offshore breakwater and the refraction/diffraction pattern that develops in the lee of the structure for oblique incident waves. Also shown are the original shoreline and the resulting shoreline caused by the modified wave pattern. The oblique waves produce longshore transport from the readers left to right. The reduced wave energy in the lee of the structure diminishes the longshore transport capacity of the waves causing a shoreline bulge (salient) in the lee of the structure. The waves shape the salient to parallel the dominant incoming wave crests. A sediment budget for the vicinity of the structure requires that the sand deposited to form the salient be made up for by downcoast erosion. The volume of sand trapped by the structure depends on the length of the structure, its distance offshore compared to the width of the surf zone, and whether energy is transmitted over or through the structure.

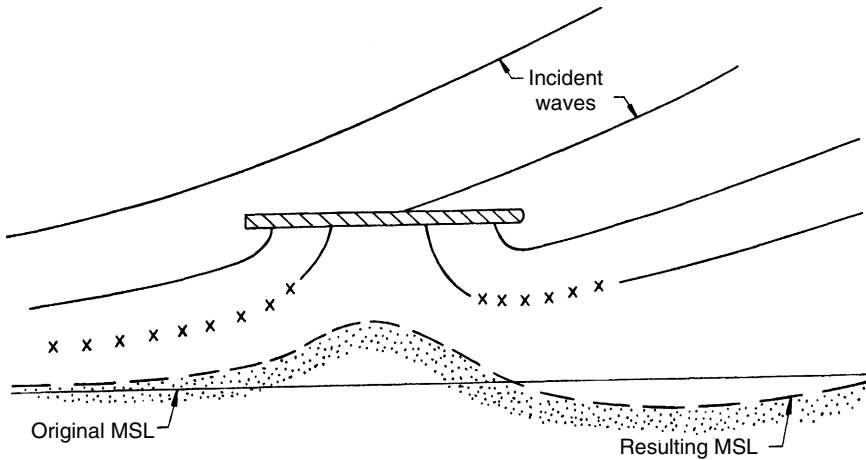


Figure 8.8. Shore response to a shore-parallel offshore structure.

Offshore breakwaters have been constructed for beach stabilization, both for nourished and unnourished beaches. This may typically involve the construction of a series of breakwaters with intervening gaps having a length about equal to the length of the breakwaters. Often offshore breakwaters are constructed with their crest at or below MLW. These structures are less expensive and more aesthetic to the environment. Low waves propagate over the structure but the higher storm waves break at the structure so their capacity to erode a beach or damage shore facilities is greatly reduced. For additional guidance on the functional design of offshore breakwaters see Rosati and Truitt (1990) and Rosati (1990).

8.6 Numerical Models of Shoreline Change

Figure 8.9 shows an idealized short section of the active portion of a sandy beach from the berm down to the offshore point at which longshore transport processes are no longer active. The volume of the segment would be $h(dx) dy$. An equation of continuity for the sediment in the beach section can be written that equates the net longshore transport into and out of the section with the change in beach section volume. This is

$$Q - \left(Q + \frac{\partial Q}{\partial x} dx \right) = \frac{h dx dy}{dt}$$

or

$$\frac{dQ}{dx} + h \frac{dy}{dt} = 0 \quad (8.4)$$

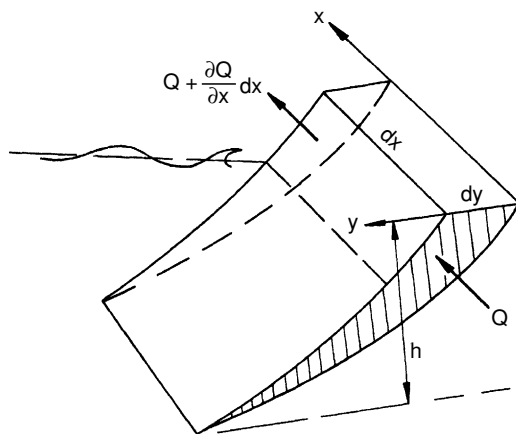


Figure 8.9. Shore segment for sediment continuity equation development.

Equation (8.4) simply says that the advance or retreat of the shoreline (dy/dt) is related to the net change in longshore transport (dQ/dx) across that section.

The longshore transport rate at any point along a beach can be determined from Eq. (8.3). The change in transport rate across the beach section could be caused by a change in the breaker wave height or by a change in the wave breaker angle relative to the shoreline orientation. The latter could arise because of a change in the approaching wave direction across the beach section and/or because of a change in the shoreline orientation from one end to the other end of the section.

Equations (8.3) and (8.4) have been used as a basis for simple numerical models of shoreline change (see Hanson, 1989 and Hanson and Kraus, 1989 for a commonly used model). The shoreline in question is divided into numerous short segments (dx) which may include structures such as groins. With the offshore wave climate (average wave height, period, direction for a time interval) and nearshore hydrographic data the waves can be refracted to the shoreline. From this, the longshore transport rate at the boundary of each segment can be calculated. Then Eq. (8.4) yields the resulting advance or retreat of the shoreline in that segment over the time interval dt . With the new shoreline position at all segments at the end of the time interval, the process is repeated.

These shoreline change models are typically run to investigate shoreline change over distances of from one to tens of kilometers and for time intervals of months to longer than 10 years. These models, which are commonly referred to as one-line models, do not consider onshore/offshore sediment transport across the beach profile. More sophisticated N-line models which also attempt to account for across-shore processes have been developed (see Perlin and Dean, 1983, for example). In these models the beach profile is divided into N segments

and the continuity of sediment transport equation is written for transport in both the x and y directions. A transport prediction equation is required for both alongshore and onshore/offshore to operate the model. The model output is the change in the shoreline with time at each of the N profile segments along the entire alongshore section of shoreline being studied.

A wide variety of more sophisticated numerical models for beach processes and resulting shoreline change are continuously being developed and used in design analysis. They find particular application for smaller spatial and time scales (e.g. for evaluating shoreline response over a few hundred meters to a few kilometers during one storm or a few weeks time interval).

The most sophisticated models are three-dimensional beach evolution models. An example is the model employed by Shimzu, et al. (1990). First, the model calculates the nearshore distribution of wave heights and directions including the effects of refraction, shoaling, diffraction, and breaking. Then, the spatial distribution of radiation stresses is determined from the wave field in order to predict the current field including that in the vicinity of structures. Finally, bottom elevation changes are determined by computing the sediment transport spatial distribution owing to the wave- and current-induced bottom shear stress.

A variety of quasi-three dimensional models have also been developed that simplify computational requirements by employing some two-dimensional aspects. Examples are Briand and Kamphius (1990) and Larson et al. (1990).

Another useful class of numerical models for shoreline change are those that define just the wave-induced change in a beach profile at a point along the shore (see Larson et al., 1988, Hedegaard, et al., 1991 and Nairn and Southgate, 1993, for example). These models are particularly valuable in predicting the retreat of a beach/dune profile and the related offshore bar development owing to storm wave attack and the related rise in mean water level due to storm surge. They are based on a shore-normal sediment transport mechanism due to wave attack coupled with a mass conservation relationship for beach sand on the profile. The models are typically calibrated with beach profile data taken before, during (in wave tanks), and after periods of storm wave activity.

8.7 Beach Nourishment and Sediment Bypassing

An important component of many beach expansion projects for recreation and/or shore protection involves the mechanical placement of sand on the beach. Beach nourishment involves the transfer of sand from some source to the beach that is to be nourished. If the sand source is a deposit of longshore drift and the transfer involves placement of this sand at some point downcoast of the obstruction that caused the deposition, this form of beach nourishment is commonly called sediment bypassing. Both beach nourishment and sediment bypassing projects often involve the construction of structures to improve the efficiency of the project.

Sand bypassing and beach nourishment, particularly when extensive structures are not constructed to hold the sand at the point of placement, must usually be carried out periodically for the life of the project. This may still be the most economical solution to a problem. The bottom line is to achieve the lowest cost per meter of nourished beach per year over the project life.

Beach Nourishment

The primary sources of sand for beach nourishment are: offshore deposits, deposits in bays and estuaries, land quarries, and deposits at navigation entrances. Often, sand borrowed from bays and estuaries is very fine and thus not sufficiently stable for placement on a beach with ocean wave exposure. The last source involves removal of sand deposited in the navigation channel or upcoast of jetties constructed to stabilize the channel. Placement of sand would be on a downcoast beach that is eroded owing to the sand being removed from the littoral zone by the navigation entrance.

The types of structures most commonly employed with a beach nourishment project are groins or, to a lesser extent, segmented offshore breakwaters. When these structures are constructed to stabilize a beach, it was noted above that as they are naturally filled by longshore transport of sand, the downcoast area may seriously erode until natural bypassing of the structures commences. This can be alleviated by the immediate nourishment of the beach in the areas where natural deposition is expected.

A cost-effective source of borrow material for beach nourishment must have a suitable particle size distribution for the wave climate and beach slope at the nourishment location. The coarser the borrow material the more stable it will be, and thus the more cost effective it will be. Coarser sand will form a steeper profile, and if too coarse may be undesirable for recreational beaches. The sand must not contain undesirable contaminants and, for recreational beaches the color of the sand may be important. Removal of the sand should not cause environmental or ecological problems at the borrow site.

The most common sand transfer procedure is to remove the sand by a dredge and transport it by pipeline or barge to the nourishment site. Shorter transport distances will decrease costs, as will borrow sites where a dredge can operate without significant down time owing to high wave action. Borrow areas in deeper water may involve larger unit costs owing to limitations on the dredges that are available for sand removal.

The design beach fill profile at the nourishment site usually includes extension of the berm to achieve the desired beach width and then a seaward slope to below MLW that is typically steeper than the natural slope at the site. Allowance must be made for the subsequent natural reshaping of the beach profile by wave action. And, if structures are not in place to control longshore transport of sand, the beach area at the ends of the fill area will lose sand to downcoast

beaches, which may be a desirable process. Some beach fill projects, where there is a strong net littoral drift in a particular direction, will include the placement of excess sand at the updrift end to act as a sand supply reservoir.

To quantify the volume of sand needed for a nourishment site, besides the design fill profile, one must define the overfill required to allow for subsequent removal of the finer sizes of the fill material owing to winnowing by wave action. A model for predicting an overfill factor was developed by James (1975) and is presented in the U.S. Army Coastal Engineering Research Center (1984). This factor is the estimated number of cubic meters of fill material required to produce one cubic meter of beach material when the filled beach has come to equilibrium. The model is based on the sediment size distributions of the samples from the borrow area and the natural beach where the fill is to be placed. Although this model is used in practice it is based on some somewhat arbitrary assumptions on the behavior of the fill material and it has not been well evaluated in practice.

As noted above, it is commonly necessary to maintain a beach nourishment project by subsequent periodic renourishment of the beach. In order to evaluate the performance of the initial beach nourishment effort and to guide the timing, location and required sediment volumes for the periodic renourishment, a beach monitoring program should be established. This would, at a minimum, require periodic surveys of the beach topography and hydrography (see Section 9.4). Additional monitoring activities might include nearshore wave measurements, sand sample analysis, and aerial photographs.

For additional discussion on the technical as well as the economic and political aspects of beach nourishment the reader is referred to the U.S. Army Coastal Engineering Research Center (1984), Marine Board, National Research Council (1995), Simm et al. (1996), and Dean (2002).

Sediment Bypassing

Often a shoreline harbor or a jettied navigation channel entrance will, as a consequence of structures and a channel being constructed across the surf zone, trap sediment that otherwise would be transported downcoast. To alleviate the resulting downcoast erosion and/or the unwanted sediment deposition in the harbor or entrance channel, it becomes necessary to mechanically bypass sediment past the harbor or channel entrance.

Sediment bypassing is most often accomplished on either an intermittent or continuous basis with a floating hydraulic dredge and a discharge pipeline that extends to the downcoast sediment discharge point. Bypassing has also been accomplished by trucking the sediment past a channel entrance and by a permanently installed pumpout system that can reach the deposited sediment and pass it through a pipeline to the discharge point.

Often the design of a project, where a need for sediment bypassing is anticipated, will include structures that force the sediment to deposit in a well-defined

deposition basin and protect the dredge from wave attack. Most hydraulic dredges become much less efficient when exposed to even moderate wave action which causes the intake line to lift off of the sea floor.

There will be some natural bypassing of most obstructions. It is important to locate and size the deposition basin so as much natural bypassing as possible takes place and so that there is no undesired deposition in the adjacent harbor or entrance channel. When the gross longshore transport rate greatly exceeds the net transport rate it is most desirable, but not always possible, that the bypassing system be designed to only bypass the net rate.

The design of a sediment bypassing system requires that the following basic information be determined:

1. The incident wave climate must be established. This is important for the functional and structural design of any structures. And it is important for the establishment of annual net and gross longshore sediment transport rates. It is also desirable to establish whether transport direction reversals are short term in duration or longer term like seasonal reversals. In addition, the volumes of sand that might be deposited in a deposition basin during a single major storm should be estimated.
2. The surf zone dimensions and position must be determined as this is where the longshore transport takes place. This will depend on the beach slope, the distribution of incident wave breaker heights, and the tide range.
3. Any tidal or other current flow patterns in the vicinity of the deposition basin must be determined.
4. If a dredge is to be used, the capacities of available dredges must be established.

Figure 8.10 illustrates the more common types of sand bypassing systems in use. For a more detailed discussion of these various systems including some examples of each, see the U.S. Army Coastal Engineering Research Center (1984).

Figure 8.10 (upper left) illustrates the classic example of an updrift fillet forming and growing until sediment moves past the channel entrance. Some of this sediment is carried into the entrance channel on flood tide and some is lost to the littoral zone when it is transported offshore on the ebb tide. Simple bypassing operations including trucking, a dredge that cuts its way into the fillet from the lee side, or a fixed pumping plant have been used to bypass sand to the down-coast side of the entrance.

For this condition, if the channel entrance geometry permits, it is best to allow the sediment to deposit in the channel where a dredge can safely operate to transport the sediment to the discharge area. This allows as much natural bypassing as possible but sand jetted offshore by an ebb tide is not trapped for bypassing.

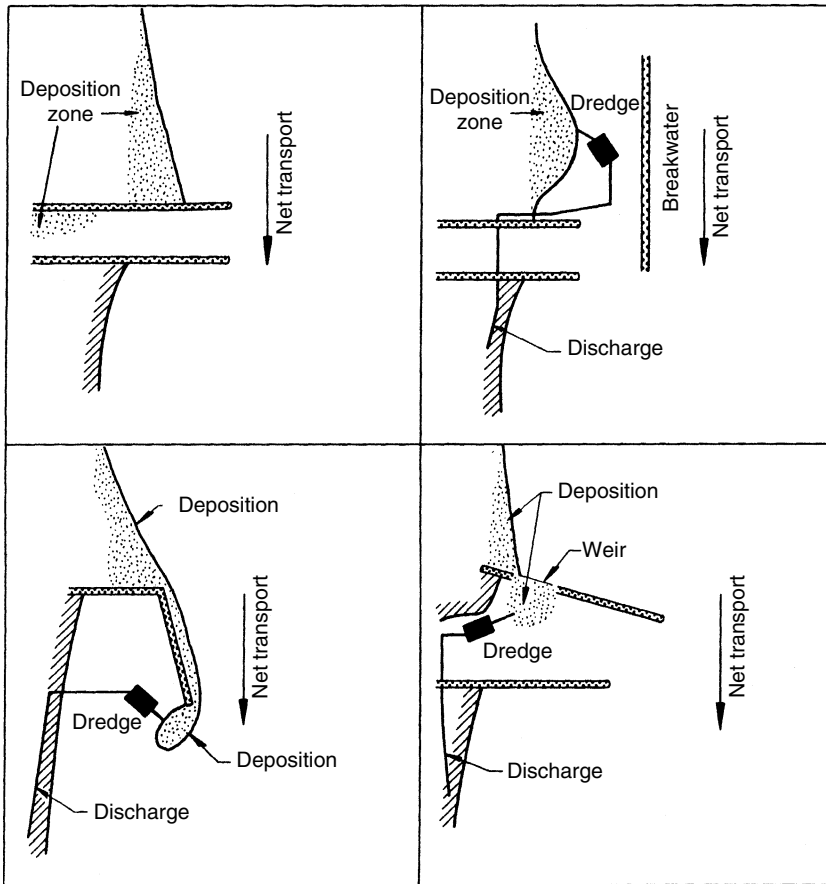


Figure 8.10. Typical sand bypassing systems. (Modified from U.S. Army Coastal Engineering Research Center, 1984.)

At a harbor with a shore-connected breakwater (Figure 8.10 lower left), the longshore drift will eventually move into the harbor entrance to form a depositional spit at the end of the breakwater. The breakwater and spit will protect a dredge operating in their lee to maintain the harbor entrance and mooring areas.

Figure 8.10 (upper right) shows an effective but capital expensive bypassing system in which an offshore breakwater causes a sediment deposition zone and provides a sheltered area for a dredge to operate. The breakwater can also be placed to provide additional shelter from wave attack for the channel entrance and interior.

The system depicted in Figure 8.10 (lower right) consists of a weir (with a crest elevation at or near MSL) at the shoreward end of the upcoast jetty, which, in

turn, is oriented to create a protected deposition basin in the lee of the weir and jetty. The weir is positioned to cross the surf zone so much of the sand reaching it moves over the weir into the deposition basin. It is important that tidal/river flow not cause the dredged navigation channel to migrate into the deposition basin.

8.8 Wind Transport and Dune Stabilization

In addition to the sand transported by waves and littoral currents, significant volumes of sand from the beach face and backshore can be transported by the wind. Where there is a wide beach, a predominant onshore wind as is common in many areas, and low coastal topography, wind transported sand can develop a major dune system extending landward from the beach berm. (see Figure 8.1). The dunes, called foredunes, are continuous irregular mounds of sand situated adjacent and parallel to the beach. A well-established dune system functions as a reservoir that can nourish a beach when the dunes are attacked by waves at higher water levels, and as a shore protection and flooding prevention structure as they yield to wave attack during a storm.

Field and laboratory studies indicate that there are three mechanisms responsible for the transport of sediment by wind:

1. *Saltation.* Particles rise from the bed surface at a nearly vertical (slightly downwind) angle, travel forward in an arc, and land at a flat (10° to 15°) angle at a point 6 to 10 times the arc height downwind. Upon landing, they may jump or saltate again, or they may dislodge other particles that then saltate. The maximum elevation particles achieve is usually less than 0.5 m but may reach 1 m. Saltation is usually the predominant mode of sand transport by wind, often accounting for up to 80% of the total transport load.
2. *Surface creep.* About 25% or less of the wind load is transported by surface sliding or rolling of the particles in essentially continuous contact with the bed. This involves the larger sand grains and the driving forces are wind shear stress and the impact of saltating particles.
3. *Suspension.* Owing to the low relative density of air, a negligible volume of sand size particles is carried by turbulent suspension. Dust and other fine particle sizes not commonly found on a beach can be transported long distances at relatively high altitudes by turbulent suspension.

There is a threshold wind velocity below which sand will not be transported by the wind. This threshold velocity and subsequent sand transport rate depend on the grain size distribution, moisture content of the sand bed, wind vertical velocity profile, wind gustiness, sand bed slope, and the existence of vegetation.

Several semi-empirical predictor equations for the wind transport rate have been developed (see Horikawa, 1988 for a summary and discussion of these

equations). These equations generally relate the transport rate to a representative grain diameter and the wind shear velocity (square root of the wind-induced shear stress divided by the air density), and contain empirical coefficients that relate to the grain size distribution and other factors. These equations are based on field and lab measurements, generally with dry sand and not-too-irregular topography. Often, high wind speeds at the coast occur during storms when there is accompanying precipitation. Given this and the approximate nature of the results given by the available transport formulas, it is generally difficult to calculate long-term wind transport rates at the coast.

The development of a strong and continuous foredune system immediately adjacent to the beach is very desirable where space permits and an adequate supply of sand is being transported landward by the wind. This can be assisted by the installation of semiporous fencing (highway snow fencing) or by the planting of vegetation (particularly beach grasses) to trap sand. Both are particularly effective because of the saltation and surface creep transport mechanisms, which limit sand transport to a region of a meter or less from the beach surface. Recommended practices for fence construction and grass selection, planting, and care are presented in the U.S. Army Coastal Engineering Research Center (1984).

When planted in sufficient quantity and cared for (e.g., prohibit walking on dunes), grasses will continuously trap sand as they grow and the dunes increase in size. Profile data taken at several beaches show dune crest elevations growing at an average rate of about a half meter per year for several years to reach elevations of 3 to 8 m. Fences are less desirable because fencing must be added as dunes grow and the fences deteriorate and become aesthetically less pleasing. In some locations, where a protective dune field must rapidly be established, the dunes were built with earth moving equipment and then stabilized by planting vegetation.

8.9 Sediment Budget Concept and Analysis

In some coastal areas continuous longshore transport of sand can take place over very great distances. However, in many areas sand is transported only short distances alongshore from its source or sources before being deposited at one or more semipermanent locations known as sinks. An improved qualitative, and often quantitative, understanding of the littoral processes in a coastal area can often be accomplished by constructing a sediment budget for that area. This involves defining and quantifying, as well as possible, all of the sediment sources and sinks within the study area for the sand being transported alongshore and relating these to the transport into and out of the area at the area boundaries. If these sources, sinks, and transport rates can be adequately quantified (e.g., cubic meters of sand per year) then a quantitative sediment budget can be developed.

Common sand sources include:

1. *Rivers.* Many rivers discharge sediment to the coast on a regular basis, but some rivers are ephemeral and deposit sediment only during periods of heavy precipitation. Much of the sediment load from a river may be finer than the sand size range and will remain in suspension until deposited offshore. Rivers that discharge into estuaries or large bays may have most of the sand size particles deposited before reaching the shore. Dams and erosion control projects on a river watershed may greatly diminish the amount of beach sand contributed to the coast.
2. *Beach and cliff erosion.* In many areas the main source of sand in the littoral zone is a section of the beach and/or cliffs that is eroding. Cliff erosion usually occurs during storms when any fronting beach is cut back so waves can attack the toe of the cliff. Only a portion of the sediment contributed by the eroding cliffs may be in the beach sand size range.
3. *Artificial beach nourishment.* Periodic nourishment of the beach in a study area may be the primary source of sand in an area that suffers a deficiency of sand.
4. *Nearshore reefs.* In tropical climates beaches often consist primarily of sand (calcium carbonate) derived from nearshore reefs constructed by marine life. The reefs also act to shelter the beach from wave attack.

Common sinks include:

1. *Tidal entrances.* Harbor, bay, and estuary entrances with tide-generated reversing flows can trap large volumes of sediment on both the landward and seaward ends of the entrance. The flood tide carries sediment through the entrance where it is deposited in quieter waters. The ebb tide jet may carry sediment far enough offshore to be effectively removed from the littoral zone.
2. *Structures.* Structures such as groins, jetties, and breakwaters that purposely or inadvertently trap sand will act as a sink while the upcoast fillet is forming. Natural bypassing of the structure will develop after the structure is filled.
3. *Wind transport.* At most coastal locations the dominant transport of sand by wind is from the beach berm to the dune fields where the sand may be stabilized by vegetation. Dune overwash during a storm may permanently remove sand from the littoral zone.
4. *Offshore deposition.* Storm wave attack on a beach may carry some sand sufficiently far offshore that it is not returned to the beach during calm wave conditions.

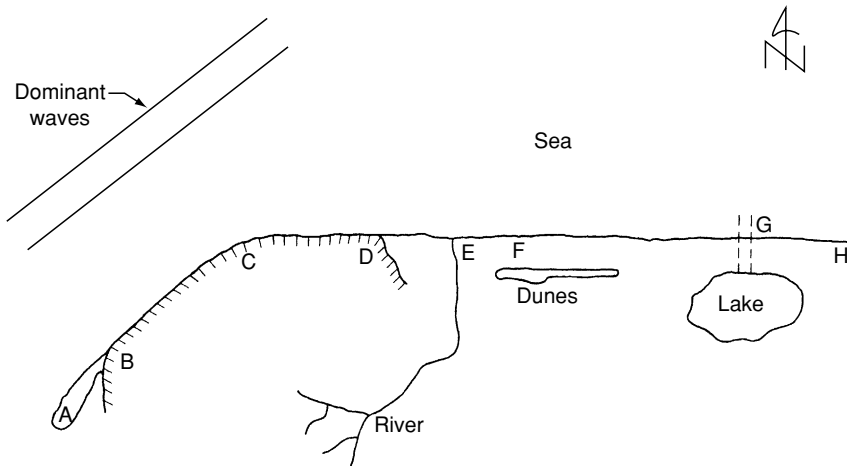


Figure 8.11. Sediment budget example.

5. *Natural formations.* These include depositional features such as spits (A in Figure 8.11) that grow from the shore in the downcoast direction or submarine canyons that lie close to the shore and transport sand offshore.
6. *Beach mining.* Sand is a valuable natural resource in many coastal areas. As a consequence it has been mined from the beach for use elsewhere.

For an illustration of the sediment budget concept consider the hypothetical coastal segment depicted in Figure 8.11. This coastal segment consists of a line of eroding cliffs from B to D, a river discharging to the coast (E), and a straight segment of sandy beach from F to H. The dominant waves approach the coast in the direction shown.

As the cliffs erode, the sand-sized material in the cliffs contributes sand to the littoral zone. Periodic aerial photographs and/or land surveys of the cliffs combined with samples to determine the size distribution of the cliff material would quantify the amount of beach sand being contributed to the littoral zone.

A diverging nodal zone would be located around C with the sand contributed by the cliffs being transported toward A to form the spit and toward D. Eastward from the cliffs sand would be added to the littoral zone from the river. The volume of this material would be estimated from predictions of river transport rates for the sediment size range found in the littoral zone.

The incident waves would produce a potential net longshore transport rate given by Eq. (8.3). Wave measurements and/or hindcasts would be required to make this determination. If the cliffs and river can produce enough sand to satisfy this potential, the beach along F to H would be dynamically stable. If

not, sand would be eroded from the western edge of the beach to satisfy the deficit. Any sand transported by wind to produce the dunes would enter the budget balance by subtracting sand from the beach at F. Dune growth can be estimated from periodic aerial photographs and land surveys

If an inlet with a pair of jetties were to be constructed (G) to open the lake to navigation, this budget analysis would indicate the rate at which sand might be trapped at the inlet and the consequent need for sediment bypassing to maintain the beach at H. A dam constructed on the upper watershed of the river would trap some of the sediment that otherwise reaches the littoral zone. This would diminish the volume of sediment available for transport alongshore and contribute to erosion along the shore from F to H. The same can be said for any effort to stabilize the cliffs between C and D which would diminish the volume of sand available for transport downcoast.

Often, it is difficult to quantify some components of the sediment budget, and rough estimates of these components must be made to balance the budget. The sediment budget is still useful to give an indication of conditions in the study area as well as the potential impact of proposed projects.

8.10 Coastal Entrances

At many coastal locations there are inlets that form waterway passages to the interior. Often they are through barrier islands to the bays that are located behind the barrier island. Their primary purpose is usually for vessel navigation to the interior bay or a harbor. They also function for water exchange to improve water quality in the bay or harbor. And some entrances act as fish passes to allow for fish migration.

Most coastal entrances are constructed by dredging the entrance channel and stabilizing it by a pair of jetties (see Figure 8.10, upper left diagram). Some, however, have been formed naturally when storm surge caused a barrier beach to be overwashed and a natural channel to be formed. To stabilize this naturally formed channel, jetties are then constructed. In either case, the channel would be dredged to the desired design depth and usually out to a point seaward of the ends of the jetties where the design depth bottom contour is reached.

Jetty systems at channel entrances have the following purposes:

- They control the geometry of the channel for secure navigation. This may include keeping the axis of the channel from meandering and limiting the width of the channel so tide-induced flow causes a sufficiently deep channel to be maintained. There will often be a bar located across the entrance to the channel and seaward of the outer ends of the jetties. A well trained ebb flow jet will assist in keeping the channel open across the bar.

- They limit the deposition of sediment in the channel from both the updrift and downdrift sides; and, related to this, they prevent the channel from migrating along the shore (usually in the downdrift direction).
- They provide protection to vessels in the navigation channel from wave attack. This may include temporary protection for a floating dredge as part of a sediment bypassing system.

The required depth for a navigation channel (measured below Mean Lower Low Water) depends primarily on the channel's design vessel; i.e. typically the largest vessel that is to use the channel. This depth is the sum of:

1. The design vessel draft.
2. The amount of vertical motion below MLLW that the vessel undergoes owing to wave action. Since wave action is stronger toward the seaward end of the channel, the channel design depth may be greater at the seaward end than along the inner portion of the channel.
3. An additional depth to provide for safe clearance between the design vessel keel and the channel bed. This allowance depends on the firmness of the channel bottom.
4. An additional depth for overdredging to allow for some sediment deposition before the channel has to be dredged again.

Tobiasson and Kollmeyer (1991) recommend that the channel have a minimum width of 75 feet (22.8m), but if possible, a 100 foot (30.5 m) width is to be preferred. Dredged side slopes plus any clearance space between the dredged channel and the jetty structures would add additional width to the channel. If sailboats not under power are to use the channel, additional width must be allowed for tacking.

The reversing flow through the channel entrance caused by the rising and falling tide plus the seaward flow from river and surface runoff to the bay will assist to keep the channel open. The resulting ebb and flood flow velocities through the channel depend primarily on a relationship between the minimum cross-sectional area of the channel measured below mean sea level (A_c) and the contributing bay or harbor tidal prism for the spring tide range (P). The tidal prism is the volume of water that flows into the bay on flood tide and back out of the bay on ebb tide. O'Brien (1966) gives this relationship for an entrance with two jetties as

$$A_c = 4.69(10^{-4})P^{0.85}$$

Where A_c and P are given in ft^2 and ft^3 respectively. Jarrett (1976) gives similar results based on a much more extensive data base. If the calculated A_c value is

close to the design cross-sectional area based on navigational requirements, then the tide can be counted on to significantly maintain the channel from sand deposition.

Bruun (1978) found that the ratio of the tidal prism volume to the annual gross volume of sediment transported past the channel entrance is also an indicator of potential channel entrance shoaling. If this ratio exceeds 150 there is little entrance shoal formation and good entrance flushing by the tide. As this ratio reduces to around 20 to 50, entrances suffer severe shoaling and require significant maintenance dredging.

8.11 Summary

In this chapter we were concerned with shorelines that consisted of a sandy beach. The focus was those nearshore processes that shaped a beach, both in plan and profile. We also considered the impact of typical coastal structures on beach processes—how to predict these effects and, where there were negative effects, how to overcome these negative effects.

Much of coastal engineering relies on design methods that have a strong empirical component (e.g., wave and water level prediction, wave interaction with structures, analysis of the response of coastal structures to wave attack, and prediction of beach processes and their response to coastal structures). Development of these design methodologies therefore requires physical measurements, either in a laboratory or the field and often both. This is the focus of the remaining chapter in this text.

8.12 References

- Bascom, W.N. (1951), "The Relationship Between Sand Size and Beach-Face Slope," *Transactions, American Geophysical Union*, December, pp. 866–874.
- Birkemeier, W.A. (1985), "Field Data on Seaward Limit of Profile change," *Journal, Waterway, Ports, Coastal and Ocean Division*, American Society of Civil Engineers, Vol. 111, pp. 598–602.
- Bodge, K.R. and Kraus, N.C. (1991), "Critical Examination of Longshore Transport Rate Magnitude," *Proceedings, Coastal Sediments '91 Conference*, American Society of Civil Engineers, Seattle, pp. 139–155.
- Briand, M.H.G. and Kamphius, J.W. (1990), "A Micro Computer Based Quasi 3D Sediment Transport Model," *Proceedings, 22nd International Conference on Coastal Engineering*, American Society of Civil Engineers, Delft, The Netherlands, pp. 2159–2172.
- Bruun, P. (1954), "Coast Erosion and the Development of Beach Profiles," Technical Memorandum 44, U.S. Army Corps of Engineers Beach Erosion Board, Washington, DC.

- Bruun, P. (1962), "Sea Level Rise as a Cause of Erosion," *Journal, Waterways and Harbors Division, American Society of Civil Engineers*, February, pp. 117–133.
- Bruun, P. (1978), *Stability of Tidal Inlets – Theory and Engineering*, Elsevier, Amsterdam.
- Dean, R.G. (1987), "Coastal Sediment Processes: Toward Engineering Solutions," *Proceedings, Coastal Sediments '87*, American Society of Civil Engineers, New York, pp. 1–24.
- Dean, R.G. (1991), "Equilibrium Beach Profiles: Characteristics and Applications," *Journal of Coastal Research*, Vol. 7, pp. 53–84.
- Dean, R.G. and Dalrymple, R.A. (2002), *Coastal Processes with Engineering Applications*, Cambridge University Press, New York.
- Dean, R.G. (2002), *Beach Nourishment Theory and Practice*, World Scientific, Singapore.
- Griffiths, J.C. (1967), *Scientific Method in Analysis of Sediments*, McGraw-Hill, New York.
- Hallermeier, R.J. (1981), "A Profile Zonation for Seasonal Sand Beaches from Wave Climate," *Coastal Engineering*, Vol. 4, pp. 253–277.
- Hanson, H. (1989), "GENESIS—A Generalized Shoreline Change Numerical Model," *Journal of Coastal Research*, Vol. 5, No. 1, pp. 1–27.
- Hanson, H. and Kraus, N.C. (1989), "Genesis: Generalized Model for Simulating Shoreline Change," Technical Report CERC-89–19, U.S. Army Waterways Experiment Station, Vicksburg, MS.
- Hedegaard, I.B., Diegaard, R. and Fredsoe, J. (1991), "Offshore/Onshore Sediment Transport and Morphological Modelling of Coastal Profiles," *Proceedings, Coastal Sediments '91*, American Society of Civil Engineers, Seattle, pp. 643–657.
- Horikawa, K. (1988), *Nearshore Dynamics and Coastal Processes—Theory. Measurement and Predictive Models*, University of Tokyo Press, Tokyo.
- Ingle, J.C. (1966), *The Movement of Beach Sand*, Elsevier, New York.
- Inmann, D.L. (1952), "Measures for Describing the Size Distribution of Sediments," *Journal, Sedimentary Petrology*, September, pp. 125–145.
- James, W.R. (1975), "Techniques in Evaluating Suitability of Borrow Material for Beach Nourishment," Technical Memorandum 60, U.S. Army Coastal Engineering Research Center, Ft. Belvoir, VA.
- Jarrett, J.T. (1976), "Tidal Prism – Inlet Area Relationships," General Investigation of Tidal Inlets Report 3, U.S. Army Coastal Engineering Research Center, Ft. Belvoir, VA.
- Komar, P.D. (1975), "Nearshore Currents: Generation by Obliquely Incident Waves and Longshore Variations in Breaker Height," in *Nearshore Sediment Dynamics and Sedimentation*, (J. Hails and A. Carr, editors), John Wiley, New York.
- Komar, P.D. (1998), *Beach Processes and Sedimentation*, Second Edition, Prentice-Hall, Upper Saddle River, NJ.
- Kriebel, D.L., Dally, W.R., and Dean, R.G. (1986), "Undistorted Froude Model for Surf Zone Sediment Transport," in *Proceedings, 20th International Conference on Coastal Engineering*, American Society of Civil Engineers, Taipei, Taiwan, pp. 1296–1310.

- Krumbein, W.C. (1936), "Application of Logarithmic Moments to Size Frequency Distribution of Sediments," *Journal, Sedimentary Petrology*, pp. 35–47.
- Krumbein, W.C. and Monk, G.D. (1942), "Permeability as a Function of the Size Parameters of Sand," Technical Publication 1492, *Petroleum Technology*, July, pp. 1–11.
- Larson, M., Kraus, N.C. and Hanson, H. (1990), "Decoupled Numerical Model of 3D Beach Change," *Proceedings, 22nd International Conference on Coastal Engineering*, American Society of Civil Engineers, Delft, The Netherlands, pp. 2173–2185.
- Larson, M., Kraus, N.C., and Sunamura, T. (1988), "Beach Profile Change: Morphology, Transport Rate and Numerical Simulation," in *Proceedings, 21st International Conference on Coastal Engineering*, American Society of Civil Engineers, Malaga, Spain, pp. 1295–1309.
- Longuet-Higgins, M.S. (1970), "Longshore Currents Generated by Obliquely Incident Sea Waves," *Journal, Geophysical Research*, Vol. 75, pp. 6778–6789, 6790–6801.
- Marine Board, National Research Council (1995), *Beach Nourishment and Protection*, National Academy Press, Washington, DC.
- Nairn, R.B. and Southgate, H.N. (1993), Deterministic Profile Modelling of Nearshore Processes. Part 2, Sediment Transport and Beach Profile Development," *Coastal Engineering*, Vol. 19, pp. 57–96.
- O'Brien, M.P. (1966), "Equilibrium Flow Areas of Tidal Inlets on Sandy Coasts," *Proceedings, 10th International Conference on Coastal Engineering*, American Society of Civil Engineers, New York, pp. 676–686.
- Perlin, M. and Dean, R.G. (1983), "A Numerical Model to Simulate Sediment Transport in the Vicinity of Coastal Structures," Miscellaneous Report 83–10, U.S. Army Coastal Engineering Research Center, Ft. Belvoir, VA.
- Rosati, J.D. (1990), "Functional Design of Breakwaters for Shore Protection," Technical Report CERC-90–15, U.S. Army Waterways Experiment Station, Vicksburg, MS.
- Rosati, J.D. and Truitt, C.L. (1990), "An Alternative Design Approach for Detached Breakwater Projects," Technical Report CERC-90–7, U.S. Army Waterways Experiment Station, Vicksburg, MS.
- Seelig, W.N. and Sorensen, R.M. (1973), "Texas Shoreline Changes," *Journal, American Shore and Beach Preservation Association*, October, pp. 23–25.
- Shimzu, T., Hitoshi, N. and Kosuke, K. (1990), "Practical Application of the Three-Dimensional Beach Evolution Model," *Proceedings, 22nd International Conference on Coastal Engineering*, American Society of Civil Engineers, Delft, the Netherlands, pp. 2481–2494.
- Simm, J.D., Brampton, A.H., Beech, N.M., and Brooke, J.S. (1996), *Beach Management Manual*, Report 153, Construction Industry Research and Information Association, London.
- Sorensen, R.M. (1990), "Beach Behavior and Effect of Coastal Structures, Bradley Beach, New Jersey," *Journal, American Shore and Beach Preservation Association*, January, pp. 25–29.

- Szuwalski, A. (1970), "Littoral Environment Observation Program in California—Preliminary Report," Miscellaneous Publication 2-70, U.S. Army Coastal Engineering Research Center, Washington, DC.
- Tobiasson, B.O. and Kollmeyer, R.C. (1991), *Marinas and Small Craft Harbors*, Van Nostrand and Reinhold, New York.
- U.S. Army Coastal Engineering Research Center (1984), *Shore Protection Manual*, U.S. Government Printing Office, Washington, DC.
- U.S. Army Coastal Engineering Research Center (1995), "Beach-Fill Volume Required to Produce Specified Beach Width," Coastal Engineering Technical Note II-32, U.S. Army Waterways Experiment Station, Vicksburg MS.
- Weggel, J.R. (1979), "A Method for Estimating Long-Term Erosion Rates from a Long-Term Rise in Water Level," Coastal Engineering Technical Aid 79-2, U.S. Army Coastal Engineering Research Center, Ft. Belvoir, VA.
- Wentworth, C.K. (1922), "A Scale of Grade and Class Terms for Clastic Sediments," *Journal, Geology*, pp. 377-392.
- Wiegel, R.L. (1964), *Oceanographical Engineering*, Prentice-Hall. Englewood Cliffs, NJ.

8.13 Problems

1. A sieve analysis of a beach sample yields the following results:

Opening Size (mm)	Weight Retained (grams)
2.000	0
1.414	0
1.000	0.3
0.707	1.7
0.500	6.2
0.353	27.8
0.250	24.1
0.177	17.7
0.125	15.3
0.088	5.0
0.062	1.9

Plot the cumulative frequency distribution on log-normal graph paper and determine the median diameter, the phi median diameter, the phi mean diameter, the phi deviation measure, and the phi skewness measure. If the sample were collected on the beach face of a beach directly exposed to ocean waves, estimate the beach face slope.

2. Estimate the beach face slope for the sample analysis shown in Figure 8.1 which is for a beach on a small lake.

3. A beach consists of quartz sand particles having an average median settling diameter of 0.27 mm. Assume Stokes law is valid to define particle settling velocity. Plot, on a graph of wave height H_0 versus period T , the line (band) separating eroding and accreting beach profiles. Use a range of H_0 and T values common to the ocean environment. Discuss the practical significance of the results indicated by this plot. After a storm, what slope might the beach face have?

4. Waves approach a sand beach and break in water 1.1 m deep, with the wave crests forming an angle of 12° with the shoreline. Estimate the volume of sand that is transported alongshore in one hour.

5. A wave train has a deep water height of 2.5 m and a period of 7 s. It propagates toward the shore across essentially shore parallel bottom contours. In deep water the wave crests lie at an angle of 36° to the bottom contours and shoreline. What is the potential longshore sediment transport volume in a period of one hour?

6. An essentially straight sand beach has a north—south orientation. The net littoral transport is from north to south and owing to sea level rise and a slight deficiency of sediment available for transport the beach suffers continuing erosion. A series of four groins is simultaneously constructed on the upper end of the beach. With a sketch describe the shoreline response. What might you do to overcome any negative impacts on the shoreline?

7. At a tidal inlet on a north—south oriented coastline, the average annual longshore transport is $300,000 \text{ m}^3$ to the south mostly during the winter and $130,000 \text{ m}^3$ to the north mostly during the summer. The average nearshore beach slope is 1:40 and visual estimates throughout the year yield an average breaker height of 1.1 m. A 100 m wide navigation channel is to be dredged to a depth of -4 m MSL and protected by shore-normal parallel jetties. The mean tide range is 0.9 m. Show, with drawings, and explain the suggested layout of the jetties including a sediment bypassing system.

8. Discuss in detail where it is appropriate to use groins for shore stabilization. For these uses, what precautions must be taken?

9. Explain what information you would need and how you would proceed to predict the plan shape of the beach behind a newly constructed shore parallel offshore breakwater.

10. From a study of the details of the coastal hydrographic chart provided by your instructor, discuss the features observed and the active coastal zone processes.

Field and Laboratory Investigations

The coastal zone—where the land, sea, and air meet—is one of the most complex areas for conducting civil engineering analysis and design. Owing to the nature of the coastal zone, most coastal engineering analysis and design procedures have a partial or complete empirical basis. This empirical basis must be developed and continually improved through extensive field, and in some cases, laboratory investigations.

Our understanding of most coastal processes has been developed largely through field measurements and laboratory experiments. Numerical models for predicting wind waves, storm surge, and beach response all require substantial calibration and verification using extensive experimental data sets. The conditions at a given coastal site must be adequately defined to complete a project design. In addition, the performance of completed coastal projects should be evaluated for a significant post construction period in order to provide adequate maintenance and a better understanding of the effectiveness of the project design and construction. This is particularly true for projects that have not achieved the success desired by the designer.

Most coastal processes occur over relatively long time spans and have large spatial extents. They also involve or are impacted by a variety of coastal factors (e.g., waves, wind, the tide and storm surge, currents, and beach sediment properties). Consequently, the cost of field data collection can be quite high. But continued advancement of coastal engineering requires that these costs be anticipated and met.

To function as a coastal engineer, one must have a basic understanding of the types of field and laboratory investigations that are commonly employed. This chapter gives an overview of the common types of measurements made and, where appropriate, the typical equipment used.

9.1 Field Investigations

For discussion purposes field investigations can be classified into three primary categories: (1) measurement of wind-generated waves and other hydrodynamic measurements, (2) measurement of beach sediment properties and morphology as well as sediment transport processes, and (3) investigation of the behavior of coastal structures.

The first category includes the measurement of water surface time histories to define the various components of the wave energy spectrum defined in Figure 5.2. The measurement of the wind wave portion of the spectrum is usually done directly while the longer period components of the spectrum require that the wind wave frequencies be filtered out so the longer period components are more easily discerned. Other hydrodynamic measurements include the wind and coastal currents.

Beach morphology can be measured by standard surveying techniques. However, owing to the dynamic nature of the coastal zone where large areas across the surf and nearshore zones must be rapidly measured, some unique techniques for hydrographic measurement have been developed. In addition it is often desirable to measure the actual transport of sediment as well as the resulting hydrographic changes. This presents some significant tactical problems that have not been completely mastered.

Most coastal structures are designed to remain in place and suffer little deterioration during their design life. Periodic visual inspection of the structures throughout their lifetime will guide the possible need for maintenance and repair. However, to develop improved design procedures it is often desirable to make in-place measurements of the loads and/or resulting stresses exerted by waves and currents on structural members. For stone-mound structures it may be desirable to measure the wave-induced movement of individual armor units.

9.2 Wind-Wave Measurements

Visual Observations

Wind-wave measurements can be made by the simpler and less expensive approach of an observer visually estimating the height, period, and direction of the waves. The estimated wave height is assumed to be the significant height and the estimated period is assumed to be the average, spectral peak, or significant period. Reasonable results require an observer with some experience at making wave observations. Some scaled object in view might be used to estimate wave height and a watch is used to time a given number of waves to estimate the wave period.

Studies to compare visual estimates of wave height with measured values have concluded that individual wave height estimates can significantly differ from

measured values, but longer term compilations of wave height estimates are more representative of measured values (see Schneider and Weggel, 1980, Soares, 1986). Schneider and Weggel (1980) found that visually estimated wave periods were on average higher than the peak period of the measured spectrum, primarily because the observers failed to include smaller waves in their estimate.

An example of a coastal visual wave observation program is the Littoral Environment Observation program of the U.S. Army Corps of Engineers (Schneider, 1981). Volunteers at over 200 coastal locations estimate wave breaker height, period, and direction as well as other nearshore phenomena such as longshore current velocity and beach face slope.

Weather ships stationed at fixed positions at sea and observers on cruising maritime vessels also make periodic wave height, period, and direction estimates as well as meteorological observations including wind speed and direction. These data have been collected and published. For the United States data are published by the National Climate Data Center (U.S. Naval Weather Service Command, 1976).

Instrumental Wave Measurements

Wave measurements, yielding a one-dimensional water surface time history or, recently with more frequency, directional wave data are made with a wide variety of instrument types. The nature of these instruments dictates that most wave measurements be made in coastal areas. The cost in physical effort and money to maintain an operating wave gage is relatively large. For a variety of reasons, the percentage of time that worthwhile data are obtained is commonly much less than 100%. Most of the common types of instruments in use are briefly discussed below. For a more detailed coverage of instruments and procedures for wave measurement see National Research Council (1982), Ribe and Russin (1974), and Tucker (1991).

The common types of one-dimensional wave gages include:

Staff gages. This is a vertical staff that penetrates the water surface and is capable of electronically detecting the variation of the water surface elevation with time by a change in resistance, capacitance, or inductance. Staff gages usually must be mounted on a rigid structure that does not interfere with the water motion in the vicinity of the gage. Depending on the type and mounting of the gage some of the following difficulties may be encountered: marine fouling or ice may prevent the probe from detecting the water surface movement, lightning may disrupt system electronics, gage-induced and other surface disturbances may cause erroneous readings, and human tampering or floating objects may damage the gage.

A variation on the electronic staff gage is the photo-pole gage, which consists of a vertical pole with a scale marked on it that is photographed by a movie or video camera. The resulting photographs are analyzed frame-by-frame to produce

the surface record time history. This requires a lot of effort, but the photo-pole gage requires no electrical power, is self-calibrating, and has no nonlinearity problems. It is most useful for special studies rather than synoptic measurement of wave climate.

Pressure gages. In Section 2.4 it was noted that a submerged pressure sensor can serve as a wave gage if it is sufficiently close to the surface to adequately detect the wave-induced dynamic pressure variation. These gages are typically mounted on a stable base placed on the sea floor in the nearshore area or on the leg of a pile-supported structure. Pressure gages avoid the free surface so they are not exposed to ice, tampering, or damage from floating objects, but they may suffer marine fouling and damage from dragging anchors and fish trawls.

For relatively low-amplitude swell Eq. (2.32) can be used to determine the wave height and period. For higher amplitude waves some nonlinear theory must be used (see Grace, 1978 and Hsiang et al., 1986) and the analysis becomes more complex. For wave spectra, the measured pressure spectrum can be computed and converted to the surface wave spectrum using the dynamic pressure variation in Eq. (2.32).

Accelerometer buoy gages. A moored floating buoy containing a device to measure the time-dependent vertical acceleration of the buoy can be employed as a wave gage. If the vertical acceleration is electronically integrated twice a signal that represents the time-dependent surface elevation is produced. This signal is then transmitted directly or by satellite link to a shore receiver. Commercially available accelerometer buoy gages are typically spheres about a meter or less in diameter and have been moored in water up to 200 m deep. Since they operate on the surface, they are prone to damage by ice, floating objects, or vandalism.

It is becoming more common to include wave direction in a wave measurement program. This is typically done by one of the following types of instrumentation:

Point-array gages. A horizontal array of one-dimensional wave gages operating simultaneously can produce data that will yield the directional wave spectrum. This typically involves three to six gages along a line or on a two-dimensional grid, with a gage spacing that depends on the anticipated range of wave frequencies to be measured.

Bottom-mounted combination gages. A bottom-mounted pressure gage to measure the surface elevation time history combined with a device such as a sphere with orthogonal strain gages that measures the wave-induced drag force in horizontal orthogonal components will function as a directional wave gage. Orthogonal current meters may also be used to detect wave directionality.

Heave-pitch-roll buoy gages. This is a moored buoy that simultaneously measures vertical acceleration and the local water surface slope in orthogonal directions as a function of time.

9.3 Other Hydrodynamic Measurements

Water Level Fluctuations

Time-dependent mean water level changes having periods greater than those common to the wind wave portion of the wave energy spectrum—particularly the astronomical and meteorological tides—must be measured for many coastal projects and for a synoptic understanding of a coastal area. These water level fluctuations can be determined from most periodic wind wave measurements by analyzing the record using a procedure that filters out the wind wave frequencies in the record. Instruments for directly measuring water level fluctuations achieve the same result by mechanically filtering out the higher frequency components in the measured water surface time history.

One simple device for mean water level measurements is the stilling well-float system depicted in Figure 5.1 and discussed in that section. The higher frequency component damping achieved by frictional dissipation at the orifice and by the stilling well to orifice area ratio may be insufficient for the accuracy of water level measurement desired. Also, wave nonlinear effects can cause a net displacement of the mean water level inside the well relative to the mean water level outside the well (Cross, 1968). To eliminate these problems some investigators have used stilling wells with long narrow diameter tubes attached to the orifice to provide additional linear damping (see Seelig, 1977).

A submerged pressure measuring device can be used to measure water level fluctuations if suitable high-frequency damping is achieved. This can also be achieved by a long narrow tube leading from the water to the pressure transducer. A variation on this system is to lay a long tube from the shore to a point offshore where the water level is to be measured and to drive air through the tube out the open end located underwater. The pressure gage is connected to the landward end of the tube and, since the hydrostatic pressure of the air in the tube can be neglected, measures the pressure at the seaward end of the tube. The air in the tube dampens the higher frequency components.

Coastal Currents

The coastal currents of interest include nearshore currents seaward of the surf zone and in channel entrances, as well as the longshore current in the surf zone. Currents in the surf zone are much more difficult to measure because of wave breaking and the related higher turbulence level which suspends sand and entrains air, as well as because of the shallower depths with fluctuating water levels that will cause alternate water and air exposure at some locations.

Current measurements can best be grouped into two classes: Eulerian, which involve measurements at fixed points with current meters, and Lagrangian, which involve the measurement of water paths and speeds with floats or dye

that follow the water motion and are tracked by some surveying procedure. For some studies such as determining the current velocity in an inlet during a tidal cycle the Eulerian approach is appropriate, whereas to determine the fate of wastes discharged from a marine outfall the Lagrangian approach is better. In many studies a combination of the two classes is best.

The following types of current meters are in common use:

Propeller and rotor current meters. Current meters, which measure current speed with a propeller or rotor whose speed of angular rotation is related to the passing flow velocity and that may have a vane to measure flow direction, are in common use in oceanographic studies. They are also useful for applications outside the surf zone and in channel entrances.

Electromagnetic current meters. A relatively small sensor (sphere or cylindrical slice) with internal electronic components measures the flow speed and direction past the meter. It functions by electronically setting up a magnetic field that is modified as water flows past the sensor. This in turn modifies a current voltage in a separate pair of orthogonal electrodes in the sensor. The meter has no moving parts and can be strongly constructed and supported for measurements in the surf zone.

Ultrasonic current meter. This meter consists of piezoelectric transducers which act both as transmitter and receiver of ultrasonic waves. The water flow velocity past the unit is detected either by measuring the modified speed of the ultrasonic pulse or by measuring the modified frequency of the pulse as it moves with and then against the flow. Orthogonal units allow the determination of flow direction too. Although it has no moving parts this type of meter has seen much less use in the surf zone.

Bottom-mounted combination wave gages that contain a sphere with orthogonal strain gages to measure wave direction will also yield current information if the data are appropriately analyzed.

The common applications of float or dye tracers include:

Floats. A tracking float must be buoyant but not extend above the surface so much that it is affected by the wind. A brightly painted plastic bottle almost filled with water makes an inexpensive but useful float. If it is desired to measure the flow velocity at a particular distance below the surface a float with little drag can be tethered to and support a submerged drogue that has a higher drag and indicates the flow conditions at that submerged point. Floats may be tracked by a pair of transits employing triangulation or by sequential photographs taken at fixed time intervals from a helicopter or balloon. Sequential timed determinations of position allow sequential velocity determinations to be made.

A point velocity determination can be made by releasing a float on a short tether of known length and measuring the time required for the tether to become fully extended.

Dye. Any type of concentrated dye that is very visible and not harmful to the environment may be used. Dye tracing has been used for easy estimates of

current speeds in the surfzone by measuring the time it takes the dye to travel a measured alongshore distance. Dye patches diffuse so they cannot be used for long distances like floats.

Wind

Wind speed and direction data are often available from local airports and other meteorological stations. The standard elevation for wind measurements is 10 m above the ground surface and there should be no nearby obstructions to distort the measurements. For wind stress determinations (e.g., for wind transport of sand studies) a series of at least four velocity measurements should be made over a vertical distance within close proximity to the ground.

Recording anemometers which consist of a propeller or rotating cups are commonly used. The propeller anemometer also has a vane to direct the propeller into the wind and to record the wind direction. Ultrasonic sound anemometers have also been used. A simple hand held anemometer which has a ball in a calibrated tube of increasing diameter with an open end that is to be exposed to the wind (like a float flow meter for pipe flow measurement) is useful for easy field estimates of wind speed.

9.4 Coastal Morphology and Sedimentary Processes

Many coastal engineering activities are concerned with the interaction of coastal sedimentary processes and coastal works such as the construction of structures for shore protection and stabilization, dredging at channel entrances and harbors, and beach nourishment. To understand these processes and to monitor effects of coastal works it is important to be able to measure shoreline topography/hydrography, sediment properties, and sediment transport processes and rates.

Coastal Morphology

The above-water topography and submerged hydrography where coastal processes are active must periodically be measured for many types of coastal investigations. Since the beach face and nearshore zone are often undergoing relatively rapid change, large areas must often be surveyed quite rapidly. For example, an investigation of the impact of a seawall on the storm wave-induced scour and natural rebuilding in front of the seawall may require surveys to be carried out just before the storm arrives, immediately after the storm abates, and periodically thereafter until significant changes have ceased. Hydrographic surveys across the surf zone (especially during the arrival of high waves) can be very difficult to carry out.

The most common surveys involve the measurement of a series of beach profiles oriented perpendicular to the shore and extending from the dune, cliff,

or structure line to the offshore point where negligible change in bottom hydrography is occurring. These profiles may be equally spaced or more closely spaced in the area of greatest interest (e.g., up- and downcoast of a new structure) with wider spacing at some distant point to measure background changes that are naturally being caused by the wave/current conditions in the area. To quantify bottom changes at a tidal or harbor entrance channel a series of profile surveys would typically be measured along parallel lines oriented normal to the channel axis.

The spacing of profile lines, the techniques used to determine the position of the measurement points, and the precision of the bottom elevation measurement must all be consistent with the desired accuracy of the survey. For example, an error of 3 cm in depth measurement over an active coastal profile line that is 300 m long and covering a distance of a kilometer along the shoreline represents 9000 m^3 of sediment (if the selected profile lines are fully representative of the beach in between the profiles).

Beach profiles are commonly measured by standard level and taping surveys. Two flags or targets along the profile line at the landward end allow the rod person to maintain the correct orientation. If repetitive surveys are to be made over time at a given shore location it is important to establish a permanent reference benchmark that will survive significant beach erosion. The benchmark must be referenced to some datum such as NGVD. The rod person will work as far seaward as safety and ability to hold the rod steady will allow. Where there is a significant tide range, surveys should be coordinated with low tide conditions. This will allow the wading portion of the profile to be extended to a little more than a meter below the lowest tide level. To extend the profile further seaward the remainder of the profile would be done with a vessel and fathometer or leadline at higher tide levels, being sure to overlap the two portions of the profile survey as a check.

The seaward portion of a profile line, measured from a vessel, will typically be much less accurate than the landward portion of the profile measured by standard surveying techniques. To overcome this problem, other beach profiling techniques have been developed:

Survey sled. The survey sled consists of a pair of parallel sled runners about 5 m long and spaced 2 to 3 m apart that, with guy wires, supports a vertical pole marked with a scale. A vessel pulls the sled to an offshore position from which it is winched back to and on shore along the profile line while a level is used to read bottom elevations from the scale on the pole. The distance offshore along the profile can be determined from a scale on the line that pulls the sled landward (Langley, 1992). Comparative tests (Clausner et al., 1986) indicate that the sea sled technique performs as well as any other procedure and much better than soundings from a vessel.

Diver/stakes. This approach is useful if comparative bottom elevations at selected locations are to be measured over a long period of time and diving

services are available. Semipermanent vertical stakes are securely placed into the sea floor at the points of interest. A diver routinely visits the stakes and measures the distance from the top end of the stake to the sea floor to measure the change that has taken place.

CRAB. The U.S. Army Corps of Engineers (Birkemeier and Mason, 1984) has a Coastal Research Amphibious Buggy (CRAB) that is a 10.6 m high tripod on wheels that can be driven through the surf and nearshore area. The driver and motor sit on a platform on top of the tripod. As the CRAB is driven through the area to be surveyed periodic total station measurements can be made on the reflector prism mounted on the CRAB to establish x - y - z coordinates of successive sea floor positions. The CRAB also serves as a mobile platform to access the surf and nearshore zones to make a variety of other measurements.

Besides the profile surveys discussed above, other coastal morphology measurements of interest to the coastal engineer include:

Aerial photographs. The standard vertical air photographs employed for photogrammetric measurement of land topography are frequently used in coastal engineering studies. Overlapping photographs taken periodically along the coastal section of interest are very valuable in giving a synoptic picture of the characteristics of the coastline and periodic changes in these characteristics. Sequential photographs may also be analyzed to measure shoreline change rates (Anders and Byrnes, 1991).

Laser technology. An airborne laser transmitter and receiver can be used to detect the water and sea floor surface elevations. Systems employing this technology from a helicopter can quickly, and with acceptable accuracy in many shallow water situations, measure the hydrography over broad areas (Irish and White, 1997).

Seismic reflection and side scan sonar. With side scan sonar, acoustical pulses are transmitted to the sea floor and the return signal can be read to detect the surface texture and (with calibration data from occasional bottom samples) the composition of segments of the sea floor surface. Seismic reflection, often used in conjunction with side scan sonar, can be used to detect the geometry of sub-bottom layers (Williams, 1982). These techniques are useful, for example, in finding and quantifying the volume of potential offshore sand borrow areas for beach nourishment.

Sediment Properties

It was noted in Chapter 8 that the beach sediment property of greatest interest to coastal engineers is the representative grain size and size distribution.

The number and type of sediment samples to be collected in a sampling program depends on the intended use of the sample analyses and the time and funding available for the sampling and analysis program. For a potential borrow area for beach nourishment, core samples should be taken throughout the

borrow area. For beaches, samples can be taken from the upper few centimeters of depth.

Beach sand characteristics commonly vary more across the shore-normal profile than alongshore. The U.S. Army Coastal Engineering Research Center (1984) recommends that for reconnaissance surveys a sample be taken from the wetted beach face and from the dunes at points along the shoreline selected from a visual inspection of beach variability. For more thorough sampling programs, samples might be taken at constant spacings along the active beach profile and at set distances alongshore. A quarter of a cup sample is generally adequate for most sample analysis procedures.

A field estimate of the median sand grain size can be made by visual comparison of a sample with different diameter particles glued to a card or contained in vials. Laboratory grain size analyses are either done by sieving or settling tube analysis.

Sieve analysis. U.S. Standard Sieve opening sizes vary from 125 mm down to 0.038 mm, with opening sizes below 5.6 mm decreasing by a constant ratio of the fourth root of 2 ($= 1.19$) or 0.25Φ intervals. For typical beach sands, alternate sieve sizes between 2.0 mm and 0.062 mm (i.e., 0.5Φ intervals) might be used to perform a size analysis.

A dry sample (40 to 60 grams if fine sand, 100 to 150 grams if coarse) is passed through the series of sieves and the percent of total cumulative sample weight collected on successively larger sieves is plotted versus sieve opening size to yield a cumulative size–frequency diagram similar to Figure 8.1.

Settling tube analysis. The terminal settling velocity of a particle in still water depends on the particle size, shape, and specific gravity. Settling tube analysis yields a grain sedimentation diameter which is the diameter of a sphere of the same density as the sediment grain and with the same settling velocity in water at a standard temperature. The sedimentation diameter will be close to but not generally equal to the sieve diameter of a sand grain.

A variety of types of settling tubes are in use. Generally they are a still vertical water column in which a sample settles and is collected at the bottom. The rate of accumulation of the grains at the bottom is then related directly to the grain cumulative size–frequency distribution. The rate of accumulation of sediment grains can be determined by weighing the accumulated grains, by measuring the decreasing water pressure just above the accumulation point, or by a visual procedure.

Settling tube size analyses are faster than sieve analyses and do not require as large a sample. Most settling tube systems are designed to record data electronically and then directly plot the cumulative size–frequency diagram and compute basic sediment size parameters.

Sediment Transport

Longshore sediment transport rates have been measured primarily by conducting periodic topographic/hydrographic surveys at locations where erosion or

deposition is occurring (see Chapter 8). However, there have been some field experiments in which “instantaneous” measurements of sediment transport patterns and rates have been made.

Transport patterns. Field measurements of nearshore sediment transport patterns have been made by tagging a significant volume of sediment grains, returning them to the nearshore area, and sampling to detect where the tagged sediment has been transported. An example of such a study would be to determine the patterns of sand movement around and through a groin that is naturally bypassing sediment.

There has been some use of radioactive tracers, but most tracer studies use a fluorescent dye to color sand particles. The dying technique must produce a coloring that will be resistant to washing off the grains and that will not change grain transport characteristics. After the tagged sand grains have been released, samples are collected in the down-transport direction. When the samples are dried and spread, an ultraviolet light may be used to count the number of tagged particles. Plotted contours of tagged particle concentration will indicate the transport pattern; and if the time of sample release and collection are noted, particle transport velocities may be estimated. Horikawa (1988) discusses these matters in more detail.

Transport rates. Field measurements of sediment transport rate have been made by using both sediment tracers and sediment traps that collect suspended load and bed load material passing the trap.

To determine volumetric sediment transport rates using tagged sand particles requires that beach face core samples be taken and the depth of mixing of tagged particles be determined from these cores. This gives the depth of the transport layer which, when multiplied by the width of the transport layer and the transport velocity (from tracer displacement and elapsed time), yields the volumetric transport rate. Komar and Inman (1970) used this technique to measure long-shore transport rates in the surf zone.

A variety of traps for collecting suspended load and bed load have been used (Horikawa, 1988). Essentially, these are devices that collect moving sediment so that the concentration of suspended sediment load at sampling points or the volume of bed sediment entering a given trap opening width in a given time can be measured. Horikawa (1988) indicates that it is easier to collect suspended load than bed load samples because the suspended load generally has a lower concentration and because bed load samplers tend to disturb the sea floor which affects the accuracy of sample collection.

Suspended load traps include intake pipes facing the flow where the flow is pumped by suction at a pipe entrance velocity that should approximate the oncoming flow velocity, and grab samplers that quickly close to trap a set volume of sand/water mixture. The measured suspended load concentration integrated over a cross-section perpendicular to the flow with the water volumetric transport rate gives the total suspended load transport rate. Bed load

traps include containers with one open side facing the oncoming bed load transport, and larger open containers with the opening facing upward and having its edge at the bed surface. The volume of sediment accumulated in a given time is the bed load transport rate at that point that can be integrated across the width of the transport zone.

9.5 Coastal Structures

Field investigations of coastal structures typically involve the direct measurement of hydrodynamic loadings on rigid structures such as piles and sea walls or measurement of the displacement of armor units on rubble mound structures. The hydrodynamic loadings of greatest interest are those caused by waves, which would be measured at the structure by one of the wave gages discussed above.

For large structures such as seawalls and revetments the loading on a structure is best measured by installing several pressure transducers into the face of the structure, measuring the time-dependent pressures, and integrating the pressure distribution over the face to determine the total force as well as its distribution as a function of time (e.g., see De Girolamo et al., 1995). Commercially available pressure transducers consist of a small diaphragm with a strain gage that measures the pressure on the diaphragm by the pressure-induced bending of the diaphragm. It is important that the pressure transducers be selected with some knowledge of the frequency and maximum magnitude of the expected pressure fluctuations that are to be measured. As discussed in Section 7.6, breaking wave-induced pressures can have a relatively large magnitude for a very short duration.

For thin structures such as cylindrical piles, the loading on a test section of the pile would be measured. This has been done by installing a ring of pressure transducers around the circumference of the pile at the test section or by building a load cell into the test section. The load cell would have interior strain gages mounted so that the measured strain is related to the instantaneous load on the test section.

Failure of rubble mound structures occurs when a significant number of armor units are displaced. Thus, field monitoring of the behavior of a rubble mound structure requires a survey of the position of armor units immediately after construction and before and after major storms. This can be done by marking points on selected units and surveying the position of these points using standard surveying techniques. An innovative improvement on standard surveying has been to employ stereophotogrammetry using photographs taken from the air (Davis and Kendall, 1992). Side scan sonar has been used to investigate the condition of underwater armor units.

Large concrete armor units may fail when wave action causes the units to rock in place and break. There is a related question of whether concrete units should

be reinforced with steel rebar. To address this question some field armor units have been instrumented with strain gages to measure in situ tensile stresses (Howell, 1985).

9.6 Laboratory Investigations

Most laboratory investigations for coastal engineering are concerned with surface waves. There have been a few studies of wind-blown sand and coastal dune processes, and some laboratory investigations of wind-wave generation processes. Also, steady flow currents have been added in some tidal flow model studies and instantaneous tidal current flows have been simulated by steady flow in basins.

But surface wave investigation are by far the most common. They may be grouped into short wave and long wave studies. The former are concerned with the wind wave portion of the wave spectrum and the latter with long wave phenomena including tides, basin oscillations and tsunami propagation and effects.

One major advantage of laboratory wave studies is the control that the investigator has over input wave conditions. Within the limits of the laboratory wave generator being used, any monochromatic or spectral wave condition can be run for any length of time. Owing to their smaller scale and the difficulties involved in field work, laboratory studies can generally be conducted faster and at lower cost.

But laboratory studies can have major drawbacks, namely scale and laboratory effects. Scale effects generally arise over difficulties in maintaining viscous and surface tension similarity where necessary. At smaller scales in the laboratory, Reynolds and Webber numbers are typically smaller than in the prototype. If these forces are important in the prototype they are difficult to simulate in the laboratory, or they may be unimportant in the prototype but significant in the laboratory. For example, there have been numerous wave tank investigations of wave loadings on vertical cylindrical piles but the laboratory Reynolds numbers are several orders of magnitude smaller than found in the field for storm wave conditions. Beach sand grains when scaled down to a laboratory size may be so small that intersurface forces dominate whereas they are not important in the field.

Laboratory effects may also cause unsurmountable difficulties. The wave generator employed in the lab may not be able to fully simulate the field waves that can occur. During the early decades of wave tank research, wave generators could produce only monochromatic waves. Recently, one-dimensional and directional spectral wave generators have come into use. Lateral boundaries on three-dimensional models may affect conditions over a significant portion of the laboratory investigation that is not affected in the field.

Some laboratory investigations are studies of basic phenomena such as measuring the wave loading on a rigid vertical cylinder for a selected range of incident wave conditions and water depths. Other investigations involve scaled model studies of given field sites for selected field conditions, such as an investigation of wave propagation toward the shore and into the lee of a proposed harbor breakwater configuration. Numerical models are increasingly being used in the place of physical models owing to their lower costs and greater flexibility. Some field problems such as coastal storm surge can only reasonably be studied by field-calibrated numerical models.

Much, but not all, of the instrumentation used in laboratory studies is similar to the instrumentation used in the field (modified to smaller laboratory time and spatial scales and less rigorous conditions). For more extensive discussion of coastal engineering laboratory investigations see Hughes (1993) and Hudson et al. (1979).

9.7 Wave Investigation Facilities

Wave investigations have primarily been conducted in flumes and basins—tanks holding water with a wave generator and, if necessary, a wave absorber to prevent waves from reflecting back to the area where the investigation is being conducted. A wide range of size and shape flumes and basins have been used. Flumes having common lengths of 30 to 40 m, widths of a meter or so, and water depths of less than a meter are used for two-dimensional investigations. Basins would be significantly wider and used for three-dimensional studies.

Wave tanks constructed during the early to middle years of the 1900s had only monochromatic wave generators. By 1960–1970 irregular or spectral wave generators became increasingly common. Figure 9.1 schematically depicts various types of monochromatic wave generators (see Sorensen, 1993 for more detailed discussion.). Most common are the piston or flap generators, the former being better for shallow water waves and the latter better for deep water waves. Some more complex wave generators are designed so that they can be modified from piston to flap motion as the desired wave period is changed. The frequency of oscillation of the piston or flap establishes the wave period and the amplitude of piston or paddle motion (for a given wave period) establishes the wave amplitude.

A variety of wave absorbers have been used. The ideal absorber would be a rough porous flat slope, but this requires a large portion of the wave flume or basin, and would not be easy to relocate as studies change. Consequently, modifications of this ideal have been employed (see Sorensen, 1993).

If, for example, the stability of a proposed rubble mound structure is being investigated, the model structure will cause wave reflection, the reflected waves propagating back to the wave generator, reflecting from the generator, etc. to cause

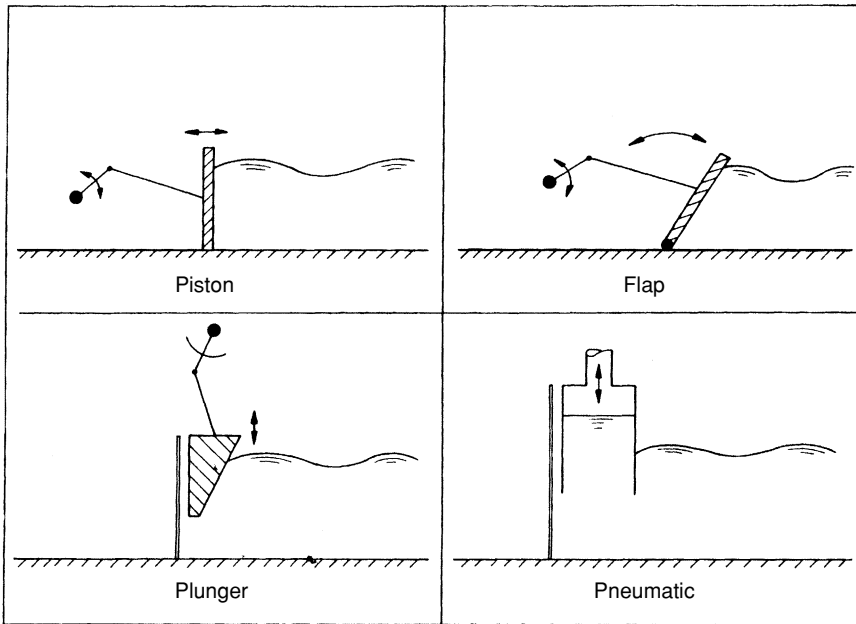


Figure 9.1. Various monochromatic wave generators. (Sorensen, 1993.)

a very different incident wave condition than that desired. In the past this problem was dealt with by using a long wave flume, generating a burst of a few waves, and stopping the generator between bursts to allow the reflected wave energy to dissipate. Recently, wave generators have been designed that detect the reflected waves and adjust the piston or blade motion to cancel out the reflected waves.

During the past few decades irregular wave generators have become common. Figure 9.2 schematically depicts a common type of irregular wave generator. An appropriate electrical input signal is sent to the generator to drive the piston/blade by a hydraulic, pneumatic, or mechanical device. The servo senses the piston motion and sends a proportional voltage feedback to the signal control. The input and feedback signals are continuously compared to adjust the piston motion to the desired form. A monochromatic wave can be generated by inputting a sinusoidal signal. A nonsinusoidal oscillating signal can be input to generate better cnoidal or solitary waves. For spectral waves the input signal is typically produced in one of three ways:

1. By superimposing a large number of sine waves of different periods and amplitudes with random phasing
2. By filtering a white noise electrical signal to form the desired irregular wave input signal spectrum

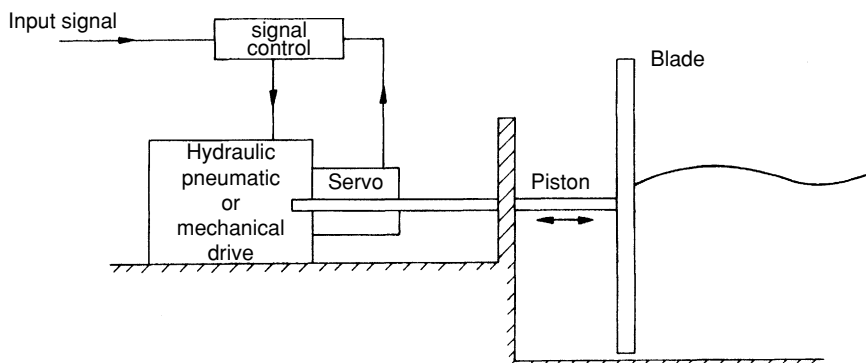


Figure 9.2. Typical irregular wave generator. (Sorensen, 1993.)

3. By creating an input signal that will produce a previously measured or artificially constructed surface elevation time history

There have been some efforts to use wind to generate irregular wave spectra in laboratories. But, because of scaling problems (see Sorensen, 1993) and improved mechanical spectral wave generators, waves generated solely by the wind are no longer used. Wind has been used over mechanically generated irregular waves to more realistically steepen the fronts of waves as would happen during a storm.

For some three-dimensional studies it is desirable to generate directional wave spectra. This has been done by using a series (e.g., 60 to 80) of individually activated wave generators along a line and facing in the same direction. By a very complex operation of driving each of the generators with a different period, amplitude and phasing, a directional wave spectrum can be generated.

9.8 Scaling of Laboratory Investigations

Laboratory investigations are commonly carried out at significantly reduced scale from the prototype. Thus, attention must be paid to appropriate scaling relationships. Wave motion predominantly involves a balance between pressure, gravity, and inertia so Froude similarity dominates. But, as discussed above, viscous and surface tension forces may be important. For Froude similarity the time ratio equals the square root of the length ratio, the pressure ratio equals the length ratio, and the force ratio equals the length ratio to the 2.5 power.

Scale differences are commonly accounted for in experimental results by presenting the results on dimensionless plots (e.g., see Figures 2.11, 2.12, 2.15, 3.5, 4.9, 4.11, 6.10, and 7.3). Consider Figure 2.15, which gives the results from a

wave tank experiment at reduced scale on wave runup on a plane slope. Gravitational effects are included in the H_o'/gT^2 term which is similar to a Froude number. Surface tension and viscous effects are not accounted for—it being implicit that they are negligible or can be accounted for with an additional correction factor.

If the lengths of laboratory waves are greater than about 3 cm surface tension forces will be negligible as they are at prototype scale. Surface tension forces will become important in physical models where the reduced scale causes very shallow depths in some areas of the model. To overcome this potential problem some models employ a distorted scale (i.e., a vertical length ratio that is larger than the horizontal length ratio).

As discussed earlier, it is often impossible to conduct a laboratory investigation at a sufficiently large scale to fully eliminate viscous scale effects in some experiments such as the measurement of wave forces on a vertical pile. The investigator must be aware that these scale effects exist when considering the results from such an experiment, and, when comparable near prototype scale data are available, try to quantitatively account for this effect.

An important facet of coastal engineering is the response of a sandy beach to wave action. At a reduced laboratory scale the prototype sand size is reduced to subsand size so sediment transport processes are not correctly simulated. The usual approach in these experiments is to use a very fine sand or some other granular material of lower density to simulate sand in the laboratory. The conduct of wave-sediment transport investigations then becomes more of an art than a science. Several investigators (e.g., Noda, 1972; Kamphius and Readshaw, 1978; Kamphius, 1985; Kreibel et al., 1986) have developed testing procedures and related scaling guidance for these experiments.

When a three-dimensional investigation such as a study of the refraction and diffraction that occurs as waves propagate from deep water to the shore is conducted, space and cost limitations may require that the investigation be conducted with less than optimum lateral basin dimensions. An undistorted model scale may then lead to very shallow water depths in a portion of the basin—and consequent viscous and surface tension scale effects. Also, wave heights may be so reduced as to be difficult to measure with the required accuracy. Thus, a distorted scale investigation may be necessary.

At a distorted scale, sloped boundaries become steeper which increases their wave reflection characteristics compared to the flatter prototype slope. This problem can be overcome, for example, by increasing the laboratory boundary's roughness and porosity to reduce wave reflection. The impact of a distorted scale on wave refraction and diffraction is more complex.

For shallow water waves wave celerity depends only on the water depth, so refraction patterns are unaffected. For intermediate depth waves refraction is affected by scale distortion. A distorted scale intermediate depth wave investigation can be carried out if appropriate depth ratio and wave length ratios are

used (see Sorensen, 1993). But if significant diffraction also occurs a conflict arises so that it is impossible to correctly scale refraction and diffraction in an intermediate depth wave investigation. For shallow water waves it is possible to correctly scale both refraction and diffraction at the same time (see Sorensen, 1993). Pure diffraction investigations (constant depth) involve no scaling problems when a distorted scale is used.

9.9 Common Types of Investigations

Generally speaking, laboratory investigations are either basic investigations into wave mechanics and the interactions of waves with beaches and structures or model investigations for specific projects. Both are carried out in two-dimensional tanks and/or three-dimensional basins. Some examples are presented below to give a general sense of the important types of studies that have been conducted.

Investigations of basic wave mechanics have included measurement of surface profiles and water particle velocity fields to evaluate the efficacy of various wave theories for different ranges of wave height and period and water depth. Extensive studies of wave breaking, runup, reflection, overtopping rate, and transmission past structures have been conducted—both as basic investigations and as investigations for specific design projects that, in turn, have added to our general knowledge of the phenomena involved. Basic investigations and model studies of short wave refraction, diffraction, and three-dimensional reflection have been conducted. Long wave investigations involving tide and tsunami propagation and basin resonance have been important to our understanding of bay, coastal river, and harbor hydrodynamics.

The design of stable rubble mound structures and the prediction of wave-induced pressure distributions and forces on piles, seawalls, and large submerged structures require the evaluation of empirical coefficients included in the design formulas. Much of the guidance in this area comes from laboratory investigations. This is also true for the dynamic response of floating structures and the wave transmission characteristics of floating breakwaters.

While, as indicated above, there are often serious scaling problems with the investigation of beach response to wave attack, some useful basic investigations and model studies for specific locations have been carried out. This is particularly true for the investigation of wave-induced scour at coastal structures. Some model studies where the bottom geometry is fixed but a granular tracer is used to indicate potential shoaling and scour patterns have been useful.

The vast majority of coastal engineering laboratory investigations focus on the characteristics and effects of short and long period surface gravity waves. But other useful laboratory investigations have been carried out including studies of internal waves, coastal and inlet currents, marine waste diffusion, and wind loadings on structures.

9.10 Summary

Coastal engineering is an atypical branch of civil engineering in that coastal engineering design is less dependent on government or professional society developed design codes (e.g., versus the design of bridges, buildings, highways, and water treatment facilities). It requires a thorough understanding of the complex air/water/land environment at the site where a design is to be carried out, coupled with an understanding of the procedures needed to satisfy design requirements in this complex environment. Both this understanding of the coastal environment and the development of coastal engineering design procedures are strongly dependent on field and laboratory investigations—the subject of this chapter.

9.11 References

- Anders, F.J. and Byrnes, M.B. (1991), “Accuracy of Shoreline Change Rates as Determined from Maps and Aerial Photographs,” *Journal, American Shore and Beach Preservation Association*, January, pp. 17–26.
- Birkemeier, W.A. and Mason, C. (1984), “The CRAB: A Unique Nearshore Surveying Vehicle,” *Journal of Surveying Engineering, American Society of Civil Engineers*, March, pp. 1–7.
- Clausner, J.E., Birkemeier, W.A., and Clark, G.R. (1986), “Field Comparison of Four Nearshore Survey Systems,” Miscellaneous Paper CERC 86–6, U.S. Army Waterways Experiment Station, Vicksburg, MS.
- Cross, R.H. (1968), “Tide Gage Frequency Response,” *Journal, Waterways and Harbors Division, American Society of Civil Engineers*, August, pp. 317–330.
- Davis, R.B. and Kendall, T.R. (1992), “Application of Extremely Low Altitude Photogrammetry for Monitoring Coastal Structures,” *Proceedings, Coastal Engineering Practice '92*, American Society of Civil Engineers, Long Beach, pp. 892–897.
- De Girolamo, P., Noli, A., and Spina, D. (1995), “Field Measurement of Loads Acting On Smooth and Perforated Vertical Walls,” *Proceedings, Advances in Coastal Structures and Breakwaters Conference* (J.E. Clifford, Editor) Thomas Telford, London, pp. 64–76.
- Grace, R.A. (1978), “Surface Wave Heights from Pressure Records,” *Coastal Engineering*, Vol. 2, pp. 55–68.
- Horikawa, K. (1988), *Nearshore Dynamics and Coastal Processes—Theory, Measurement and Predictive Model*, University of Tokyo Press, Tokyo.
- Howell, G.L. (1985), “Crescent City Prototype Dolos Study,” *Proceedings, Workshop on Measurement and Analysis of Structural Response in Concrete Armor Units*, U.S. Army Waterways Experiment Station, Vicksburg, MS.
- Hsiang, W., Dong-Young, L., and Garcia, A. (1986), “Time Series Surface-Wave Recovery from Pressure Gage,” *Coastal Engineering*, Vol. 10, pp. 379–393.

- Hudson, R.L., Herrmann, F.A., Sager, R.A., Whalin, R.W., Keulegan, G.H., Chatham, C.E., and Hales, L.Z. (1979), "Coastal Hydraulic Models," Special Report No. 5, U.S. Army Waterways Experiment Station, Vicksburg, MS.
- Hughes, S.A. (1993), *Physical Models and Laboratory Techniques in Coastal Engineering*, World Scientific, Singapore.
- Irish J.L. and White, T.E. (1997), "Coastal Engineering Applications of Higher-resolution Lidar Bathymetry," *Coastal Engineering* (in press).
- Kamphius, J.W. (1985), "On Understanding Scale Effects in Coastal Mobile Bed Models," *Physical Modelling in Coastal Engineering*, (R.A. Dalrymple, Editor), A.A. Balkema, Rotterdam, pp. 141–162.
- Kamphius, J.W. and Readshaw, J.S. (1978), "A Model Study of Alongshore Sediment Transport Rate" in *Proceedings, 16th International Conference on Coastal Engineering*, American Society of Civil Engineers, Hamburg, pp. 1656–1674.
- Komar, P.D. and Inman, D.L. (1970), "Longshore Sand Transport on Beaches," *Journal of Geophysical Research*, Vol. 75, pp. 5914–5927.
- Kreibel, D.L., Dally, W.R., and Dean, R.G. (1986), "An Undistorted Froude Model for Surf Zone Sediment Transport," in *Proceedings, 20th International Conference on Coastal Engineering*, American Society of Civil Engineers, Taipei, Taiwan, pp. 1296–1310.
- Langley, T.B. (1992), "Sea Sled Survey Through the Surf Zone," *Journal, American Shore and Beach Preservation Association*, April, pp. 15–19.
- National Research Council (1982), "Proceedings, Workshop on Wave Measurement Technology," NRC Marine Board, Washington, DC.
- Noda, E.K. (1972), "Equilibrium Beach Profile Scale-Model Relationships," *Journal, Waterways and Harbors Division, American Society of Civil Engineers*, November, pp. 511–528.
- Ribe, R.L. and Russin, E.M. (1974), "Ocean Wave Measuring Instrumentation," *Proceedings, Conference on Ocean Wave Measurement and Analysis*, American Society of Civil Engineers, New Orleans, pp. 396–416.
- Schneider, C. (1981), "The Littoral Environment Observation (LEO) Data collection Program," Coastal Engineering Technical Aid 81–5, U.S. Army Coastal Engineering Research Center, Ft. Belvoir, VA.
- Schneider, C. and Weggel, J.R. (1980), "Visually Observed Wave Data at Pt. Mugu, California," in *Proceedings, 17th International Conference on Coastal Engineering*, American Society of Civil Engineers, Sydney, pp. 381–393.
- Seelig, W.N. (1977), "Stilling Well Design for Accurate Water Level Measurement," Technical Paper 77–2, U.S. Army Coastal Engineering Research Center, Ft. Belvoir, VA.
- Soares, C.G. (1986), "Assessment of the Uncertainty in Visual Observations of Wave Heights," *Ocean Engineering*, Vol. 13, pp. 37–56.
- Sorensen, R.M. (1993), *Basic Wave Mechanics for Coastal and Ocean Engineers*, John Wiley, New York.

- Tucker, M.J. (1991), *Waves in Ocean Engineering—Measurement, Analysis, Interpretation*, Ellis Horwood, New York.
- U.S. Army Coastal Engineering Research Center (1984), *Shore Protection Manual*, U.S. Government Printing Office, Washington, DC.
- U.S. Naval Weather Service Command (1976), “Summary of Synoptic Meteorological Observations,” National Climate Data Center, Ashville, NC.
- Williams, S.J. (1982), “Use of High Resolution Seismic Reflection and Side-Scan Sonar Equipment for Offshore Surveys,” Coastal Engineering Technical Aid 82–5, U.S. Army Coastal Engineering Research Center, Ft. Belvoir, VA.

Appendices

A. Notation and Dimensions

A	L^2	bay surface and channel cross-section area, structure projected area
A_c	—	channel cross section area
A_i	L	tidal component amplitude
a'	—	sediment porosity
a_c, a_t	L	wave crest amplitude; trough amplitude
a_x, a_z	L/T^2	horizontal and vertical components of acceleration
B	L	wave orthogonal spacing, structure crest width
B_o	L	wave orthogonal spacing in deep water
C	L/T	wave celerity
C_d	—	drag coefficient
C_g	L/T	wave group celerity
C_l	—	lift coefficient
C_m	—	coefficient of mass
C_o	L/T	wave celerity in deep water
C_r	—	wave reflection coefficient
C_t	—	wave transmission coefficient
d	L	water depth, sediment grain diameter
d'	L	setup, setdown of mean water level
d_b	L	water depth at point of wave breaking
d_c	L	channel depth
d_s	L	water depth at structure toe
d_{50}	L	median grain diameter
D	L	cylinder diameter
E, E_k, E_p	F	total, kinetic, potential energy per unit crest width
\bar{E}	F/L	<i>average energy per unit surface area</i>
F	$L, F, —$	wind fetch length, freeboard, force acting on a body, Froude number
F_1, F_2	—	dimensionless coefficients in Bretschneider spectrum
F_c	F	centrifugal force
F_d	F	drag force
F_g	F	gravitational force
F_i	F	inertia force

F_s	F/L	force per unit length
f	$1/T$	Coriolis parameter
f_p	$1/T$	wave frequency at spectral peak
$G(f, \theta)$	—	directional spectrum spreading function
g	L/T^2	acceleration of gravity
H	L	wave height
H_b	L	breaking wave height
H_d	L	diffracted wave height
H_i	L	incident wave height
H_{\max}	L	maximum wave height
H_{mo}	L	significant wave height based on spectral energy
H_n	L	average height of highest n percent of waves
H_o	L	wave height in deep water
H_r	L	reflected wave height
H_{rms}	L	root mean square wave height
H_s	L	significant wave height based on individual wave analysis
h	L	vertical distance from berm crest to depth at which wave transport of sediment vanishes
h_c	L	structure crest height above the sea floor
I_r	—	Iribarren number
K	—	coefficient in sediment transport equation
K_D	—	armor unit stability coefficient
K_d	—	diffraction coefficient
K_r	—	refraction coefficient
K_s	—	shoaling coefficient, wind stress drag coefficient
K_{sb}	—	wind/bottom stress coefficient
k	$1/L, \text{—}$	wave number, inertia coefficient
k^2	—	parameter in cnoidal wave theory
KC	—	Keulegan–Carpenter number
L	L	wave length
L_c	L	channel length
L_o	L	wave length in deep water
L_p	L	wave length for f_p at water depth of interest
L_r	—	model/prototype length ratio
M, N	—	solitary wave theory coefficients, resonance modes
M	FL	moment acting on a structure
$M_{d\Phi}$	—	phi median diameter
M_Φ	—	phi mean diameter
m	—	beach slope
m_n	L^2/T^n	n th moment of a wave spectrum
m_o	L^2	zeroth moment of a wave spectrum

N	—	number of waves in a wave record, number of data points in a return period analysis
N_s	—	armor unit stability number
N_s^*	—	modified armor unit stability number
N_*	—	number of digitized values from a wave record
n	—	ratio of wave group to phase celerity
P	F/T	wave power per unit crest width, tidal prism
$P(H)$	—	cummulative probability of H
p	F/L^2	pressure
$p(H)$	—	probability of H
Q	$L^2/T^2, L^3/T$	Bernoulli constant, potential volumetric sediment transport rate
q_x, q_y	L^2/T	flow rate per unit width
R	$L, —$	vertical elevation of wave runup above SWL, radial distance to point of maximum hurricane wind speeds, Reynolds number
R_p	L	runup exceeded by p percent of waves
R_s	L	runup of significant wave
r	—, L, T	wave runup correction factor, radial distance in the lee of a barrier, radial distance from hurricane eye, time interval between data points
S	—	Strouhal number, structure damage level, fluid specific gravity
S_c	L	Coriolis setup
S_{ds}	L^2/T^2	spectral energy dissipation rate
S_{in}	L^2/T^2	spectral energy input rate from the wind
S_{nl}	L^2/T^2	spectral energy transfer rate by nonlinear interaction
S_p	L	atmospheric pressure setup
S_w	L	wind stress setup
S_{xx}, S_{yy}, S_{xy}	F/L	radiation stress components
$S(f)$	L^2T	frequency spectrum energy density
$S(f, \theta)$	L^2T	directional spectrum energy density
$S(T)$	L^2/T	period spectrum energy density
T	T	wave period
T_e	T	eddy shedding period
T_H	T	Helmholtz resonant period
T_I	T	tidal component period
T_n, T_{NM}	T	resonant periods of basin oscillation
T_p	T	wave period at spectral peak
T_r	—, T	model/prototype time ratio, return period
T_s	T	significant period
T_*	T	wave record length

T_{100}	T	average wave period
t	T	time
t_d	T	wind duration
t_T	T	tsunami wave travel time
U	L/T	current velocity
U_r	—	Ursell parameter
\bar{u}	L/T	mass transport velocity
u, v, w	L/T	velocity components
V	$L^2, L/T, L^3$	volume of mass transport per unit crest width in a solitary wave, current velocity normal to x -direction, volume of a body, vessel speed
V_F	L/T	hurricane forward speed
V_f	L/T	particle settling velocity
W	$L/T, L, F$	wind velocity, floating breakwater width, channel width, armor unit weight
W_A	L/T	adjusted wind speed for SPM-JONSWAP method
W_R	L/T	wind speed at R in a hurricane
X	L	particle travel distance
X_P	L	wave breaker plunge distance
x, y, z	L	coordinate distances
α	—	beach slope angle, angle between wave crest line and bottom contour line
α_b	—	wave breaker angle with the shoreline
α_ϕ	—	phi skewness measure
β	—	angle between barrier and line to point of interest
Γ	L	basin horizontal dimension
γ	—	ratio of breaker height to water depth at breaking, JONSWAP peak enhancement factor
γ_s	F/L^3	specific weight of stone
Δ_i	—	tidal component phase lag
ΔP	F/L^2	difference between central and ambient pressures in a hurricane
ε	L	vertical component of particle displacement
ζ	L	horizontal component of particle displacement
η	L	surface elevation above still water level
η_t	L	trough distance below still water line
θ	—	angle between wave orthogonal and x -axis, angle of wave approach to a barrier, angle between wind and coordinate direction, rubble structure face slope
μ	—	coefficient of static friction
ν	L^2/T	fluid kinematic viscosity
ρ	FT^2/L^4	fluid density

σ	$1/T$	wave angular frequency
σ_Φ	—	phi deviation measure
τ	F/L^2	horizontal shear stress
$\Phi(f, d)$	—	TMA spectrum function
Φ	L^2/T ;—	velocity potential; latitude; phi grain size measure
ψ	L^2/T	stream function
ψ_s	L^2/T	stream function at water surface
ω	$1/T$	speed of earth's rotation

B. Selected Conversion Factors

Multiply	By	To obtain
feet	0.3048	meters
fathoms	6.0	feet
	1.829	meters
statute miles	5280	feet
	1.609	kilometers
nautical miles	6076.115	feet
	1.852	kilometers
acres	43,560	square feet
cubic yards	0.765	cubic meters
cubic meters	1.309	cubic yards
cubic feet	7.48	gallons (U.S.)
slugs	14.594	kilograms
pounds	4.448	Newtons
short tons	2000	pounds
metric tons	2205	pounds
long tons	2240	pounds
statute miles/hour	1.47	feet/second
knots	1.151	statute miles/hour
	1.692	feet/second
pounds/square inch	0.0680	atmospheres
	2.036	inches of mercury
	6985	Newtons/square meter
	2.307	feet of water
cubic feet/second	448.8	gallons/minute
	0.0283	cubic meters/second
horse power	550	foot pounds/second
	745.7	Watts (Newton meters/second)
foot pounds	1.356	Joules (Newton meters)

C. Glossary of Selected Terms

Selected terms encountered in the text or common to U.S. coastal engineering practice are defined below. Most of these definitions are taken (many with modification) from: Allen, R.H. (1972), "A Glossary of Coastal Engineering Terms," U.S. Army Coastal Engineering Research Center, Ft. Belvoir, VA.

Accretion The buildup of a beach owing to natural processes which may be supplemented by the interference of a structure with littoral processes.

Armor unit Stone or precast concrete unit placed on a stone mound coastal structure as the primary protection against wave attack.

Artificial nourishment The replenishment of a beach with material (usually sand) obtained from another location.

Bar A submerged embankment of sand or other natural material built on the sea floor in shallow water by the action of currents and waves.

Bay A recess in the shore or an inlet of a sea between two headlands, not as large as a gulf but larger than a cove.

Beach berm A nearly horizontal part of a beach or backshore formed by the deposit of material by wave and wind action. Some beaches have no berms; others have more than one.

Beach face The section of the beach normally exposed to wave uprush.

Breakwater A structure that protects a shore area, harbor anchorage, or basin from waves.

Bulkhead A structure (usually vertical) that prevents sliding or collapsing of a soil embankment. A secondary purpose is to protect the embankment against damage by wave action.

Bypassing Hydraulic or mechanical movement of beach material from the accreting updrift side to the eroding downdrift side of an inlet or harbor entrance.

Celerity The propagation speed of the wave form.

Coast That area of land and water that borders the shoreline and extends sufficiently landward and seaward to encompass the area where processes important to the shore area are active.

Decay distance The distance waves travel as swell from the generating area. As they travel through this region of relatively calm winds the significant height decreases and the significant period increases. Dispersion of the spectral components also occurs.

Deep water waves Waves propagating across water depths that are greater than half the wave length.

Diffraction (of waves) The phenomena by which energy is transferred laterally along the wave crest. When a train of waves is interrupted by a barrier diffraction causes energy to be transmitted into the lee of the barrier.

Diurnal tide A tide having only one high and one low water level in a tidal day.

Duration, minimum The time necessary for steady-state wave conditions to develop for a given wind velocity and fetch length.

Ebb Tide The interval between high water and the following low tide.

Fetch The surface area of the sea over which wind blows to generate waves.

Flood tide The interval between low water and the following high tide.

Forecasting, wave The prediction of future wave conditions for existing or future wind or weather conditions.

Foreshore The part of the shore lying between the crest of the seaward berm (or upper limit of wave runup at high tide) and the ordinary low water mark.

Fully developed sea The ultimate wind-generated wave condition that can be reached for a given wind speed.

Groin A structure built generally perpendicular to the shoreline to trap littoral drift and/or hold artificial nourishment.

Group celerity The speed at which a group of waves propagates.

Hindcasting, wave The prediction of wave conditions for historic wind or weather conditions.

Inlet A short, narrow waterway connecting a bay, lagoon, or similar water body to a larger body of water and often maintained by tidal and river flow.

Jetty A structure built generally perpendicular to the shoreline to prevent shoaling of a channel by littoral materials, and to direct and control flow in the channel.

Knot A term for speed equalling one nautical mile per hour.

Littoral current A current in the surf zone generated by incident wave action.

Littoral drift The sedimentary material in and near the surf zone moved by waves and currents.

Littoral transport The movement of littoral drift.

Littoral zone The zone extending seaward from the shoreline to just beyond the wave breaker line.

Longshore transport rate The volume of sedimentary material per unit time being transported parallel to the shore.

Mean higher high water The average height of the higher high tide levels averaged over a 19-year period.

Mean high water The average height of all the high tide levels averaged over a 19-year period.

Mean lower low water The average height of the lower low tide levels averaged over a 19-year period.

Mean low water The average height of all of the low tide levels averaged over a 19-year period.

Mean sea level The average height of all tide levels (usually on an hourly basis) averaged over a 19-year period.

Mean tide level An elevation that is midway between mean high water and mean low water.

Monochromatic waves A train of waves each having the same wave height and period.

National Geodetic Vertical Datum 1929 (NGVD 1929) Mean sea level from data at 26 North American coastal stations averaged over 19 years up to 1929.

Nautical mile The length of a minute of arc, generally one minute of latitude. Accepted in the United States as 6076.115 ft or 1852 m.

Neap tide The tide occurring near the time when the sun and moon are most out of phase producing the two lower tide ranges during the monthly tidal cycle.

Nodal zone A shore location where the net direction of longshore transport of sediment changes.

North American Vertical Datum 1988 (NAVD 1988) Adjustment of NGVD 1929 to 1988 including gravimetric and other anomalies.

Orthogonal A line drawn perpendicular to successive wave crests.

Phi sediment size The negative logarithm to the base two of the sediment particle diameter.

Pier A structure, usually of open construction (e.g., on piles), extending out into the water from shore, to serve as a vessel landing place, a recreational facility, etc.

Quay A section of paved stabilized bank along a navigable waterway or in a harbor, used to load and unload vessels.

Radiation stress The excess flux of momentum owing to the existence of a wave.

Recession The retreat of a beach or other coastal section owing to natural processes and/or the effects of structure interference with littoral processes.

Refraction (of waves) The process by which intermediate or shallow water waves have their direction changed because the bottom contour is not parallel to the wave crest. May also be caused by currents.

Relative depth The ratio of water depth to wave height.

Revetment A facing or veneer of stone, concrete blocks, etc. placed on a sloping embankment to protect against erosion by waves or currents.

Rip current A strong relatively narrow current flowing seaward through and beyond the surf zone owing to the piling up of water in the surf zone by waves.

Riprap A protective layer of stone typically having a wide size gradation and placed to protect an embankment from erosion.

Rubble mound structure A structure built of a mound of stones typically with an outer layer of large stone sizes (armor stone) and one or more interior layers of smaller stone.

Runup The surge of water up a slope (beach or structure) from the breaking of a wave. Quantified as the highest elevation above mean sea level reached by the water.

Scarp, beach An almost vertical surface on the beach caused by erosion of the beach material from just in front of the scarp.

Sea breeze A light onshore directed wind resulting from the unequal temperature of the sea and land.

Seas Waves in the fetch being actively generated by the wind.

Seawall A structure, usually massive in nature (rubble mound or concrete) designed to prevent flooding and wave damage to the land in its lee.

Seiche A resonant oscillation in a body of water.

Semidiurnal tide A tide with two relatively equal high and low water levels in a tidal day.

Setup (setdown) The wave-induced rise (fall) of the mean water level above (below) the still water level.

Shallow water waves Waves in water sufficiently shallow that the water depth is less than one-twentieth of the wave length.

Shingle Granular beach material coarser than ordinary gravel.

Shoal (noun) An especially shallow section of the nearshore area, often caused by sediment deposition.

Shoal (verb) To become shallow; to cause to become shallow; or, for waves, to propagate from deep in to shallower water.

Shoreline The boundary between the land surface and the surface of a water body such as an ocean, sea, or lake.

Significant wave height The average height of the highest one-third of the waves in a given wave record.

Significant wave period The average period of the highest one-third of the waves in a given wave record.

Solitary wave A wave having a crest but no trough (so the wave length is infinite).

Spring tide The tide occurring near the time when the sun and moon are most in phase producing the two higher tide ranges during the monthly tidal cycle.

Standing wave A wave produced by the propagation in opposite directions of two identical wave trains. The resulting water surface oscillates only in the vertical direction with alternating nodal and antinodal points.

Storm surge The buildup of the water level along the coast owing to wind-induced shear and pressure forces.

Surf beat Irregular oscillations of the nearshore water level with periods of the order of minutes.

Surf zone The area between the outermost breaker and the limit of wave runup.

Swell Freely propagating wind-generated waves that have propagated out from the area of generation.

Tidal prism The total volume of water that enters into or flows out of a harbor or estuary in one tidal cycle, excluding river flow and surface runoff.

Tide range The difference in height between successive high and low tides.

Tombolo A segment of deposited material in the lee of an offshore structure that connects the structure to the land.

Transitional (or intermediate) water wave A wave propagating in water having a depth between one-half and one-twentieth of the wave length.

Tsunami A long period wave generated by an underwater disturbance.

Wave steepness The ratio of wave height to wave length.

Wave train A series of waves traveling in the same direction.

Index

- Armor unit, per cent damage, 214, 217
 - shape, 215–218
 - stability, 216–217
 - stability coefficient, 217–218
 - weight, 215, 220–221
- Armor stone specification, 223–224
- Basin oscillations, 113–138
 - Helmholtz resonance, 136–137
 - resonant patterns, 117, 133, 201
 - resonant period, 114
- Beach, berm, 224
 - dynamic equilibrium, 247–248
 - measurements, 269
 - nourishment, 256, 272
 - profile, 224–225
 - slope, 254
- Beach profile closure depth, 257–258
- Bernoulli equation, 15, 32, 233
- Bottom stress, 115–116, 123, 134, 138, 142, 144
 - coefficient, 145
- Boundary conditions, 10–11, 13, 53, 69, 136, 142, 144
- Breakwater, berm, 224–225, 234
 - floating, 199, 209, 211–212
 - low-crested, 215
 - offshore, 79, 214
 - rubble mound, 196, 215, 221, 225
- Bretschneider wave spectrum, 149, 170, 177, 182–183
- Cables, 195, 198–200, 209
- Coastal engineering, definition, 3
 - literature, 3–4, 6
 - recent trends, 5
- Coastal entrances, 280–282
- Coastal environment, 1–2, 305
- Coriolis acceleration, 115–117, 134, 138–139, 143, 148–149, 258
 - parameter, 116
- Currents longshore, 149, 258–260
 - measurement, 288
 - rip, 253, 261
 - wind-generated, 247
- Design storm, 138–141, 187, 214, 216–217, 227
- Design wave, 79, 99, 177–179, 187–188, 196, 202, 204, 207, 209, 215–216, 218, 220–222, 224, 226, 238–241
- Design wave selection
 - economic implications of, 222–223
- Diffraction, analysis, 92–104
 - coefficient, 93
 - diagrams, 97–98
 - laboratory studies, 93
 - phenomenon, 80
- Dispersion equation, 15, 17, 21, 47
- Drag, coefficient of, 196–197, 203–206
- Dune, characteristics, 247, 254
 - stabilization, 248, 276–277
- Duration limited condition, 160, 184
- Equilibrium beach profiles, 256–257
- Equivalent deep water wave height, 45, 82
- Extreme wave height analysis, 157, 187, 240
- Fetch limited condition, 160, 178, 184, 214
- Force, current-induced, 198
 - drag, 196–197, 199–201
 - ice-induced, 234–235
 - inertia, 197, 199–201, 203
 - lift, 207
 - measurement, 203–206
 - pressure-induced, 228–230

- Force, current-induced, 198 (*Continued*)
 - vessel-induced, 233
 - wind-induced, 276
- Freeboard, 227, 238–239
- Froude number, 105, 137, 143, 156, 303
- Fully developed sea, 157, 160, 171, 181, 183
- Groin, 214–215, 241, 248, 254, 260, 265–267
- Hudson equation, 218, 220–221, 223–227
 - sensitivity of, 220
- Hurricane, characteristics, 139, 182
 - probable maximum, 140, 183
 - standard project, 140–141
 - waves, 183
- Inertia, coefficient of, 198, 199–201, 206–207
 - Inman's size description parameters, 251–252
 - Iribarren number, 236
- Jetty, 260, 262, 266–267, 275–276, 280–281
- JONSWAP wave spectrum, 170, 172–173, 176, 183
- Keulegan-Carpenter parameter, 201
- Laplace equation, 11, 13, 53, 69–70, 136
- Large submerged structures, 196, 209–210, 304
- Lift, coefficient of, 207
- Longshore bar, 254
- Long wave equations, 114–115, 123, 133, 138, 142
- Mass, coefficient of, 66, 197, 198, 203–204, 206, 209
 - transport, 58–60, 66, 261–262
- Morison equation, 198, 200, 203–204, 207, 209
- Nodal point, longshore transport, 262
 - water surface, 9, 35, 114, 116, 132–133, 136, 174, 288
- Particle, acceleration, 18–19, 21, 199
 - orbit, 12, 15–16, 19–22, 38, 58, 65, 118, 120, 198, 201, 209
 - velocity, 12–13, 15, 18–24, 27, 31, 37, 48, 64, 66–71, 132, 197, 199–205, 209, 253, 304
- Phi unit, 249–250
- Pierson-Moskowitz wave spectrum, 171–172, 183
- Piles, 195, 198, 202, 206, 228, 230, 298–299, 304
- Pipelines, 4, 195, 198–199, 206–207, 254
- Probability distribution, 162–163, 188–189, 240
 - wave height, 24–27, 33–34, 37–39, 47, 54, 61–62, 72, 79–85, 88, 93, 96, 99, 105, 125–126, 135, 159–165, 168, 170, 176, 187, 215, 221, 261, 264, 290
 - sediment size, 249–252, 273, 279, 296
- Radiation stress, 30–35, 228, 259–260, 271
- Rayleigh distribution, 162–166, 169, 171, 188, 222, 237, 240
- Refraction, analysis, 71, 80–82, 90, 99–100, 177, 240
 - caustic, 88–89
 - coefficient, 82, 85, 90, 177, 221–222
 - current-induced, 91, 198, 207, 209, 233, 271
 - diagrams, 82–83, 86–88, 125–126
 - manual analysis, 82
 - numerical computation, 89, 186–187, 257
 - phenomenon, 79–80, 91, 233
 - template, 82, 86–88, 266
- Refraction and diffraction of directional spectra, 176–178
- Relative depth, 12, 15–17, 26, 47–48, 54, 58, 61, 71–72, 79, 86, 173, 238
- Resonance, 117, 119, 122, 124, 128, 130–133, 136–138, 158–159, 239, 304
- Return period, 71, 139–140, 178–179, 187–190, 221–222, 234, 239
- Revetment, 4, 45, 102, 214–216, 221, 223, 225, 232, 235–236, 241, 267, 298

- Reynolds number, 196–198, 200–201, 203–206, 209–210, 299
- Sea level change, 150–151, 257
- Sediment, properties, 248–252, 287–288, 293
 - sampling, 252, 295–298
 - size analysis, 252, 296
 - size distribution, 248–249, 295
 - Wentworth size classification, 249–250
- Sediment budget, 248, 263, 268, 277–280
- Sediment bypassing, 248, 267, 271, 273–276, 280–281, 286
- Sediment transport, interaction with
 - structures, 265–269
 - longshore rate, 262–265
 - measurement, 249–252
 - processes, 293
- Shoaling coefficient, 81, 177
- Shoreline, numerical models, 248, 257, 269–271
- Sink, sediment, 277–278
- SMB wave prediction method, 183
- Snell's law, 83–84, 86
- Source, sediment, 261–262, 268, 277
- Spectral energy balance equation, 185
- Spit, 262, 275, 279
- Standing wave, 35, 37–38, 51, 130, 132–136, 228, 246
- Storm surge, characteristics, 105
 - numerical analysis, 141, 144
 - simplified analysis, 144
- Strouhal number, 201
- Surf beat, 114–115
- Swell, 158, 160, 176, 290
- Tide, classification, 120,
 - components, 119–120
 - datums, 120–121
 - gage, 126, 150, 154
 - generation, 117–120
 - prediction, 119–120, 122–123
 - range, 122–123, 154
- TMA wave spectrum, 170, 173–174
- Transmission coefficient, 212–213, 238
- Tsunami, defense against, 126–127, 304
 - generation, 124
 - runup, 124, 126
 - travel time, 126, 155
- Ursell number, 62–63
- Velocity potential, 11, 13–14, 18, 21, 35, 53–55, 69, 136, 210
- Vessel-generated waves, 10, 80, 102–105, 211
- Visual wave observation, 289
- Wave breaking, 11, 32, 34, 38–44, 65, 68, 89, 157, 165, 186, 224, 254, 258–259, 261, 291, 304
 - breaker classification, 40–41
- Wave celerity, 11, 14–17, 28, 39, 53, 56, 59–62, 65, 67–69, 79, 82–83, 87, 89–91, 105, 114, 159, 232, 303
- Wave classification, 15–17
- Wave, design, 79, 216, 222, 238–240
- Wave direction, 91–93, 98, 175–176, 266, 270, 290, 292
- Wave energy, 11, 22–25, 28–32, 67, 79–80, 88, 92–93, 99, 117, 126
 - energy density, 24
 - energy dissipation, 33–34
 - kinetic, 22–23, 35
 - potential, 22–23, 35
 - spectrum, 80, 92, 114, 137, 151, 167–176
- Wave frequency, 167, 174–175, 178
 - angular, 12, 14, 134
 - spectral peak, 168, 174, 178, 239
- Wave gage, accelerometer buoy, 290
 - directional, 290
 - photo-pole, 289–290
 - pressure, 290
 - staff, 289
- Wave generation, 158–161, 179–180
- Wave group celerity, 28–30
- Wave height, distribution, 162–165
 - significant, 160, 162
 - maximum, 165

- Wave length, 11–12, 14–16, 21–24, 29–30, 37–38, 40, 53, 56, 59, 61–65, 70, 80–82, 86, 93, 96–98, 104, 125, 130, 174, 209, 212, 226, 303
- Wave measurement, 288–290
- Wave number, 12, 14, 70, 90, 134
- Wave orthogonal, 79, 83, 89–90, 126
- Wave overtopping, 4, 215, 217, 227, 237
- Wave period, average, 166
 - distribution, 166
 - significant, 161, 164
 - spectral peak, 166
- Wave power, 24–27, 67, 72, 125
- Wave prediction, empirical, 179–183
 - hurricane, 182–183
 - numerical, 185–187
 - spectral models, 169–178
- Wave-induced pressure force, 210
- Wave reflection, coefficient, 37–38, 101–102
 - three-dimensional, 101
 - two-dimensional, 37–38
- Wave record analysis, 161–166
- Wave runup, 5, 42, 44–47, 217, 233, 237, 254–255, 261, 303
- Wave setup and setdown, 30–35
- Wave, shallow water, 17, 34, 40, 53–54, 64, 91, 114–115, 117–118, 125, 130, 132–133, 143, 182, 211, 260, 300, 303–304
- Wave spectrum, characteristics, 161, 167–169
 - directional, 174–176
 - models, 169–174
 - moments, 168–169
- Wave steepness, 12, 19, 41–42, 46, 55–59, 61, 71–72, 92, 126
- Wave surface profile, 12, 14, 63
- Wave theory, cnoidal, 61–64
 - numerical, 68–69
 - range of application, 71–72
 - small-amplitude, 10–15, 67
 - solitary, 64–65
 - Stokes, 54–61
- Wave transformation, 5, 54, 79–80
- Wave transmission, 99, 223, 227, 237–238, 304
- Wave-wave interaction, 159, 161, 186
- Wind, duration, 149
 - fetch, 160, 171
 - force, 276
 - measurement, 172, 179, 240, 293
 - sediment transport by, 261–264
 - stress, 128, 138, 142–145, 260, 293
 - stress coefficient, 145